THE EXPERIENCE OF PETROBRAS WITH CHARACTERIZATION AND CLASSIFICATION OF DEPOSITED MATERIALS FOUND IN OIL PRODUCTION

Marco Antonio Gomes Teixeira, Fátima Regina Dutra Faria and Maria Luísa Aleixo Gonçalves
PETROBRAS Research & Development Center-Division of Chemistry
Av. Um, Quadra 7, Cidade Universitária, Rio de Janeiro, Brazil - CEP:21949-900
E-Mail: marco@cenpes.petrobras.com.br

Keywords: PARAFFIN WAX, ASPHALTENES, CHARACTERIZATION

ABSTRACT

Experimental characterization of some deposited materials collected in Brazilian oil fields and transportation pipelines are presented, to point out limitations of data generated by fractional solubilization, which is normally employed for classification of deposits into paraffin waxes or asphaltenes. Gas chromatography, which is a reference technique for paraffinic materials, has its data campared to molecular weight by VPO, being clearly characterized the difficulties of elution for heavy fractions. It is also shown that most characteristical compositional properties for asphaltenes, like elemental analyses and aromaticity, are not conclusive for the definition of deposits as asphaltenic materials.

So, it is proposed that chemical analysis of deposited materials should aim ready classification of deposited material, since all of the techniques have limitations and yield information that should be considered qualitative and for comparison purposes. And since classification should be a way to provide quick responses to field problems, another concept was sought.

A classification technique based on thermogravimetry has been proposed to improve the capacity of PETROBRAS to determine the nature of some deposits verified in production equipment. It is based on the fact that asphaltenes yield considerable amounts of coke by pyrolysis, while paraffinic material do not. The method has been validated with several reference samples, and it is being used successfully in various field situatuions in Brazil

INTRODUCTION

Concerning to deposition problems, analytical techniques employed for characterization yield data to provide information about chemical nature of deposited material, which are also used to feed mathematical simulators of deposition used by production engineers. These computer programs support operational decisions that try to minimize or avoid deposition phenomena. Of course, due to the economical magnitude of problems brought by deposition, much is expected of these simulators, and therefore much is charged of analytical data. However, usual analytical techniques have some limitations, and careful interpretation of results is necessary.

Of course, it is normally easy to tell inorganic and organic (main focus of interest of this work) materials apart. And operational culture may be frequently employed for a successful pre-classification of organic ones into the two main classes normally recognized, i. e., paraffinic or asphaltenic deposits. In these cases, simulators may need some temperature or pressure dependent measurements, being a minimum characterization required. Sometimes, however, it is not possible to affirm anything previously. Our work has been showing this is the case of deposits found in production columns. Past experience shows that asphaltene precipitation frequently happens in pressure disturbance zones, mainly in bubble point regions of oils in production columns, as observed for example by IZQUIERDO and RIVAS (1995). Differently, paraffin deposition may possibly be observed in almost all pipes and tanks used in petroleum industry. So column deposits are an application of particular interest for any work on characterization, because both classes are possibly found. When the nature of deposited material is an uncertainness, its definition is the first necessary input. It should be remarked that, for analytical purposes, an operational definition for paraffin waxes or asphaltenes is based on solubility. It is normally accepted that paraffin waxes are a fraction insoluble in ketones at low temperatures (according for example to Shell SMS 1769) and asphaltenes are a fraction insoluble in light n-alkanes and soluble in aromatic solvents (according for example to IP-143). This definition may be used for classification of deposited material, being normally employed a sequential solubilization with a light alkane (which would solve paraffinic components) and an aromatic (which would solve asphaltenic components), as performed by ABUL FAZAL et al. (1995).

If further characterization is required, analytical techniques employed for deposited material are normally gas chromatography and nuclear magnetic resonance. Since they are both well known by analytical chemists, there is no need for considerations about their fundamentals. Interpretation of results from these two techniques are normally supported by other information, like elemental analyses or infrared spectra. It is impossible, however, to achieve a complete characterization, *stricto sensu*, of all components of deposits because there is an uncountable number of heavy components from

petroleum, and chemical analysis can not resolve heavy components.

Careful investigation of results obtained, shown below, indicates that these data may be inadequate for non equivocal conclusions about the nature of deposits. So, a new approach has been proposed, based on the fact that asphaltenes have large aromatic nuclei (BESTOUGEFF e BYRAMJEE, 1994). Those nuclei yield coke when pyrolysed, and this may be detected by thermogravimetry. This approach has been employed successfully for several field cases in Brazil.

EXPERIMENTAL

Sequential solubilization experiments were performed in a Soxhlet apparatus, and solvents chosen were n-heptane and toluene. After extraction, solvents were evaporated and weighed. All the procedure was repeated to constant weight with each solvent. Number molecular weights were determined by vapor pressure osmometry (VPO; a Wescan model 233 apparatus was employed), in toluene solutions at 88°C, with benzyl as a calibration standard. GC chromatograms were obtained in an HP 5890-2, with the following analytical conditions: 0.53 mm i. d. methyl silicon column (5 m length), programation for inlet temperature from 60 to 430°C at 70°/min, for the oven -20 to 430°C at 10°/min, then 5 min at final temperature, flame ionization detector at 430°C. TG curves were obtained in a DuPont 951 thermal balance with TA Instruments 2100 control system: 10 mg of sample heated firstly at 10°C/min up to 700°C under a 60 mL/min nitrogen flow, then at 10°C/min up to 1000°C under a 60 mL/min air flow.

RESULTS AND DISCUSSION

Sequential solubilization

To determine and follow the nature of deposited material found in the column production of a Brazilian off-shore well throughout 3 months in 1996, sequential solubilization was firstly employed. Samples were obtained on different days. Some samples demanded a 72 h reflux to constant weight, showing that even if the result is very conclusive, that procedure could not be considered practical. However, abundant insoluble material in both solvents was obtained, what makes impossible a classification by this approach. The presence of inorganics was considered, but low ash yields after burning did not confirm this possibility. Table 1 shows these results, which stress the need of further work in some cases.

Some possibilities were sought for a cconclusive characterization. However, since deposits are normally complex mixtures, average parameters obtained by NMR, like amount of aromatic carbons (the most relevant one), are frequently found in intermediate values, which do not assign a clear classification, and the same happens to the C/H ratio from ultimate analysis. Fractionated precipitation and liquid chromatography (LC) show in some cases poor resolution of fractions obtained, and for LC fractions (normally saturates, aromatics, resins and asphaltenes) there is also loss of polar compounds that stay strongly adsorbed onto the stationary phase.

Gas chromatography and vapour pressure osmometry

An alternative that is very useful for several characterizations in petroleum industry is gas chromatography. So, the possibility of determination of paraffinic material by this technique was considered. Since one can accept two classes of materials in deposits, low contents of paraffins would charaterize asphaltenic deposition.

Typically, a gas chromatogram of paraffinic material is similar to the picture presented in figure 1, for a paraffin wax obtained from a Brazilian oil by Shell SMS 1769/88. This oil was chosen for the study because it has deposition of paraffin wax proved by field experience. Clear separation is achieved for lighter linear alkanes, and peaks between them are attributed to other sarturated hydrocarbons. In high temperature GC, this task is easily done up to 40 carbon atom alkanes, normally. After that, the number of carbon atoms after which no resolution is obtained (called in this work C^*) is a subjective parameter. If eluted material represented the whole sample, the distribution of linear alkanes and other components would be an important characteristic, since linear molecules have more ease to overlap their chains, propiciating deposition.

Table 2 shows main interpretation data for the chromatogram in figure 1, and, for comparison, for the GC analysis of a natural deposit. Naturally, one should expect that deposits would have longer components than laboratory precipitated paraffin wax, since this material was stable in oil before intervention, while the components of deposits were not. However, that is not what was found in the comparison, since the chromatogram of deposited material could be resolved up to 50 carbon atoms, while the other one coul be up to 45, only, being also the amount of material up to C^* larger for the deposit. The non resolved fraction (from figure 1, one can consider after 60 carbon

atoms) was larger for the laboratorial wax. The only information that agreed with previous expectance was the ratio of linear alkanes to other components, which was slightly superior in natural deposit. The possibility of components of the oil that could be ocluded in the natural deposit and would not be in the laboratorial one, because of washing by the ketone used as precipitant, was considered but not confirmed, since the first hydrocarbon present in both samples had the same carbon number, 16. These results are better explained in a comparison to molecular weight data by VPO. This technique, itself, yielded values of 554 and 506 for the number molecular weights of the laboratorial and natural waxes, respectively, leading to the same trend given by GC. However, from compositional distribution in the chromatogram, it is possible to obtain the molecular weight and thus a carbon number for a pseudo-alkane component that would represent the C_{60}+ fraction (#C_{60}+). The equation for that is readily deduced:

$$M_n=100/\Sigma(\%_i/M_i) \qquad \text{(Eq.1)}$$

where M_n stands for the average molecular weight of the whole deposit, and $\%_i$ and M_i for the weight fraction in the material and the molecular weight of each individual component, respectively. Using equation 1, one gets a value for #C_{60}+ of 76 for the laboratorial wax, while for the natural deposit even an infinite carbon numbered pseudo component would yield the value from VPO. After substitution of all $\%_i$'s and M_i's from the chromatogram of this sample, the value of M_n by equation 1 has a limit of 498 as the M_nC_{60}+ increases. One can deduce that non eluted material is much more representative for the natural deposit than it is for the laboratorial wax, and that evidences the limitation of GC for the analysis of field material. Qualitative analysis of eluted material does not help very much either, since it has been found that asphaltenes yield chromatograms similar to other petroleum fractions (AQUINO NETO et al., 1995).

Approach proposed - use of thermogravimetry

Based on the need of an appoach that would not have all limitations detected by other techniques, we have conceived a quick experiment by thermogravimetry (TEIXEIRA and GONÇALVES, 1977). Basically the sample is heated under inert atmosphere, for distillation and pyrolisis of some constituents, then under oxidative atmosphere, which allows the burning of remaining material.

Behaviours of paraffins and asphaltenes submitted to those conditions were evaluated. Asphaltenes have as a remarkable characteristic relatively large alkyl side chains and aromatic nuclei (BESTOUGEFF e BYRAMJEE, 1994). We believe that branches may be thermally eliminated from the major structure, but aromatic nuclei will be thermally stable under inert atmosphere, maybe by the generation of coke. Paraffins should be either distilled or pyrolised, so their TG would show different profiles in relation to asphaltenes, which would be enough since only classification of the predominant class of constituents of the sample is aimed. Inorganics would yield stable material at 1000°C under air, so they would be also evaluated.

TG would also have the advantage of analysis of the whole deposit without any pre-treatment, since water and excess ocluded oil would be distilled before the temperatures of interest. It should be emphasized, however, that classification by the methodology studied necessarily presuposes that there are only the three possible classes cited above in deposited material, but that assumption is normally good for classification purposes.

Figure 2 shows a TG curve of a standard paraffin. It can be seen that before 700°C the distillation (or maybe pyrolysis) of the materials is already complete. In these TG curves, and in all the other ones in this work, mass loss is indicated by the monotonically decreasing curve, while the other curve is its first derivative. Figure 3 shows a TG curve of an asphaltene sample obtained by a standard method (IP-143), from which a typical profile of this class of material may be determined. There is effectively mass loss before air introduction, but the main remark, which will make possible the differenciation from paraffinic material, is mass loss after air introduction that is clearly seen. From these facts a classification scheme is proposed: paraffins are characterized by complete volatilization under inert atmosphere up to 700°C, asphaltenes by burning with air injection from 700°C, and inorganics by the burning residue at 1000°C.

The methodology has been employed for the classification of several real field deposits. Examples that prove consistency of the proposed approach are its applications to column deposits. Figures 4 and 5 show TG curves of two ones, from different wells from Brazilian fields, whose nature was found to be very distinct by the methodology proposed here.

CONCLUSIONS

Thermogravimetry may be used successfully to overcome a major problem in the study of

depositions, which is to reach a clear qualitative definition of the nature of deposited material. It does not yield properties of the deposits that are necessary inputs for simulation work, but it provides the ways to determine which fenomenum is to be modeled in each case.

REFERENCES

ABUL FAZAL, S.; ZARAPKAR, S. S.; JOSHI, G. C. (1995) "Studies on Sludge from Waxy Crude Oil Storage Tank.II.Solvent Fractionation", Fuel Science and Technology Int'l., vol. **13**(10), 1239-49

AQUINO NETO, F. R. et al. (1995) "High Temperature - High Resolution Gas Chromatography (HT-HRGC) of Paraffinic and Asphaltenic Crudes and Related Deposits", *Proceedings of the First International Symposium on Colloid Chemistry in Oil Production*-ISCOP'95 (Rio de Janeiro), pp. 63-7

BESTOUGEFF, M. A. & BYRAMJEE, R. J. (1994) "Chemical Constitution of Asphaltenes" *in* YEN, T. F. & CHILINGARIAN, G.V. (Editors), *Asphaltenes and Asphalts, 1. Developments in Petroleum Science, 40*, pp. 67-93

IP Standard Methods for Petroleum and its Products, The Institute of Petroleum, London (1965), Part I, Section 2, Standard 143, p. 596

IZQUIERDO, A. & RIVAS, O. (1995) "INTEVEP's Overall Approach to Asphaltenes Deposition Problem", *Proceedings of the First International Symposium on Colloid Chemistry in Oil Production*-ISCOP'95, pp. 155-8

SHELL. "Wax contains of petroleum and its products", SMS 1769/88 (1988), 7 p.

TEIXEIRA, M. A. G. & GONÇALVES, M. L. A. (1997) "Use of Thermogravimetry for Classification of Chemical Nature of Deposits of Petroleum Industry", *Petroleum Science & Technology International*, submitted

Table 1. Characterization of deposits of the same well (weight %)

Sample collected on	n-heptane solubles	toluene solubles	burning residue
January 11th	28.01	1.25	13.25
January 16th	2.85	6.31	11.65
February 9th	23.73	0.68	9.81
March 9th	24.39	1.16	5.62

Table 2. Comparison of a laboratorial paraffin wax of a Brazilian oil and a natural deposit

Sample	*C**	*%up to C**	*%C_{60}+*	*%linear up to C* / % other up to C**	*#C_{60}+*
Paraffin wax by Shell SMS 1769/88	*45*	*55.53*	*27.53*	*1.83*	*76*
Natural paraffinic deposit	*50*	*69.01*	*11.90*	*1.93*	*∞*

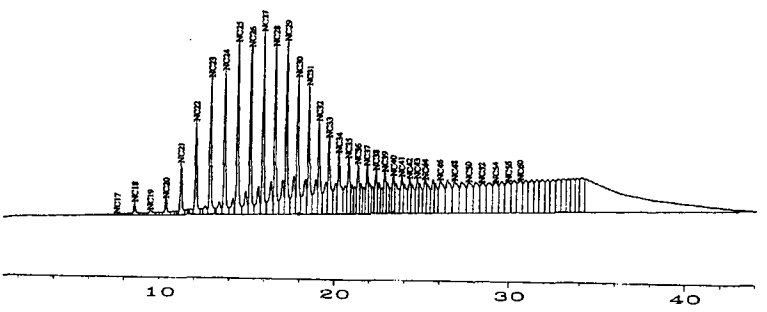

Figure 1. Gas chromatogram of a sample of laboratorial paraffin wax of a Brazilian oil

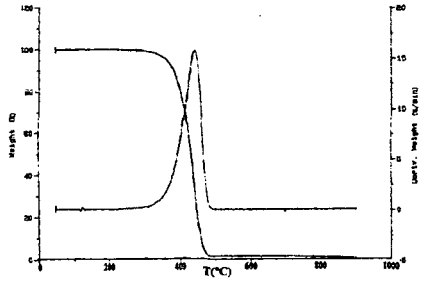

Figure 2. TG curve of a standard paraffin of average molecular weight 1000

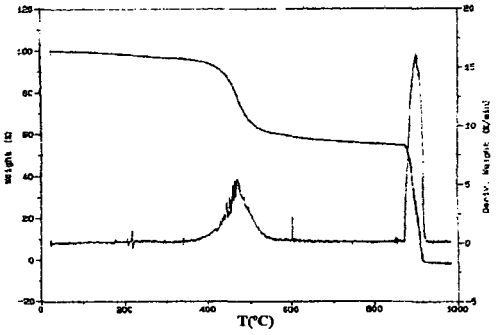

Figure 3. TG curve of asphaltenes from light arabian oil

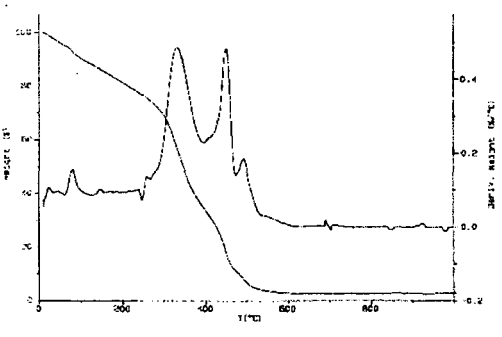

Figure 4. TG curve of a paraffinic production column deposit

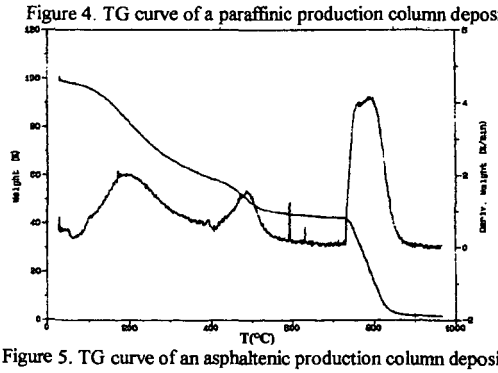

Figure 5. TG curve of an asphaltenic production column deposit

PARAFFIN AND ASPHALTENE DEPOSITION RESULTING FROM COMMINGLING OF OILS DURING PIPELINE TRANSPORTATION AND STORAGE.

N. Thanh, M. Hsieh, J. Allen, and R. P. Philp, School of Geology and Geophysics, University of Oklahoma, Norman, OK. 73019.

ABSTRACT

Commingling of oils from different reservoirs and different sources is a common process during production and transportation. In certain situations, this may lead to the precipitation of solid residues and cause serious production problems. The question arises as to the nature of the solid residues produced in this manner. Are they waxes or asphaltenes or mixtures? In this paper we will describe a recent study of such a problem. Using recently developed processes in our laboratory the characterization of such a residue in a storage tank in terms of its asphaltene and paraffin content will be described. In addition high temperature gas chromatography has been used to document high concentrations of hydrocarbons up to C_{80} in the wax despite their relatively low concentration of these components in the original sample. Laboratory mixing experiments have also been undertaken in an effort to simulate the production of such residues in the storage tanks to determine whether or not such problems could have been avoided by adjusting the relative proportions of the two oils prior to mixing in the pipeline.

INTRODUCTION

In many cases crude oils produced from different wells in the same field have to be commingled during production or in pipelines to storage facilities prior to shipping. In certain situations oils, which when transported independently may not produce any problems, may have significant problems resulting from paraffin or asphaltene deposition when commingled with other oils with slightly different properties but produced from the same field. In a recent study we had the opportunity to examine such a situation from a geochemical perspective. In this study, two oils being produced from a certain field had to be commingled and transported via pipeline to a storage tank prior to shipping. Neither of these oils showed any signs of paraffin or asphaltene deposition when transported individually. However when commingled, it was observed that within a relatively short period of time, the storage tank containing the commingled oils was filled to about 30% of its capacity with a black residue. Characterization of this residue demonstrated that it consisted of predominantly paraffins with a small amount of asphaltenes. In this paper it is proposed to discuss the characteristics of the original oils, particularly in terms of their wax contents as determined by high temperature gas chromatography, as well as the characteristics of the black residue and the liquid oil in the storage tank. It is also anticipated that by the time of the meeting additional laboratory data will be available to show the nature of the residues formed as a result of mixing various proportions of these two oils in the laboratory and permitting them to stand for different periods of time.

DISCUSSION

In the initial part of this study oils from the two sources were characterized by high temperature gas chromatography. The resulting chromatograms obtained in this way suggested that the oils contained some high molecular weight hydrocarbons above C_{35}, although the concentrations of these compounds were relatively low. In order to get a better indication of the distribution of hydrocarbons in these samples a wax concentrate was isolated from each sample and using a method developed in our laboratory the asphaltenes were quantitatively separated from the wax components. HTGC analysis of the asphaltene fraction clearly showed that there were no hydrocarbons in the wax fraction. HTGC analysis of the wax concentrate gave a clearer picture of the HMWHC distribution but clearly the relative concentrations of these compounds was still relatively low in the individual oils.

As mentioned above mixing of the two oils in question did not produce any paraffin deposition problems in the pipeline transporting the mixture to the storage tanks. IN Fig. 1 the top chromatogram shows the oil mixture from the pipeline and the relatively low concentration of HMWHCs present in this mixture. However in the storage tanks a considerable quantity of a heavy black residue accumulated over a relatively short period

of time. This residue was treated in the same way as the oils, with the separation of a wax concentrate and removal of the small quantity of asphaltenes in the sample. The wax content in this sample was around 34%, asphaltenes 0.5% and the remaining part of the sample was low molecular weight hydrocarbons. Fig. 1c shows the HTGC chromatogram for the residue and it can be seen very clearly that there has been significant concentration of the hydrocarbons in the region above C_{40}, and in view of the relatively low concentrations of these compounds in the original oils this clearly represents the accumulation from several filling episodes of the tank. Quantitation of individual components in this wax concentrate and comparison with their concentrations in the original sample should permit one to determine the volumes of oils necessary to produce this amount of residue.

Fig. 1b shows the HTGC chromatograms of the oil produced from the storage tank. A comparison of the chromatogram for the pipeline mixture and the produced oil from the storage tank shows that the difference in the envelope of these two chromatograms represents the wax material that has precipitated in the storage tank. Over time significantly higher concentrations of the compounds above C_{40} have accumulated.

SUMMARY

Whilst HTGC could not prevent this type of wax accumulation it does provide us with the ability to quantitatively assess what is happening in this particular situation and determine the amount of material that is basically being lost as a result of mixing these two oil samples. Furthermore it is anticipated that careful and detailed laboratory mixing studies should permit one to determine the optimum mixture of these two oils which will minimize the amount of wax precipitation occurring in the storage tank as a result of mixing the two oils. Finally it is also suggested that no wax problems are observed in the pipeline transporting the mixture of these two oils simply because of the turbulence and shearing effects in the pipeline preventing such deposition. The wax crystals in this particular case are of a microcrystalline nature and relatively fine. Hence it is only when the oil has reached the storage tank that these crystals can finally undergo separation as a result of gravitational segregation. The use of HTGC is also vitally important in these types of studies since it permits one to clearly differentiate between the waxes and asphaltenes and also on the purity of these different fractions which can have a significant impact in any purification or remedial steps that may be used at a later stage of the process.

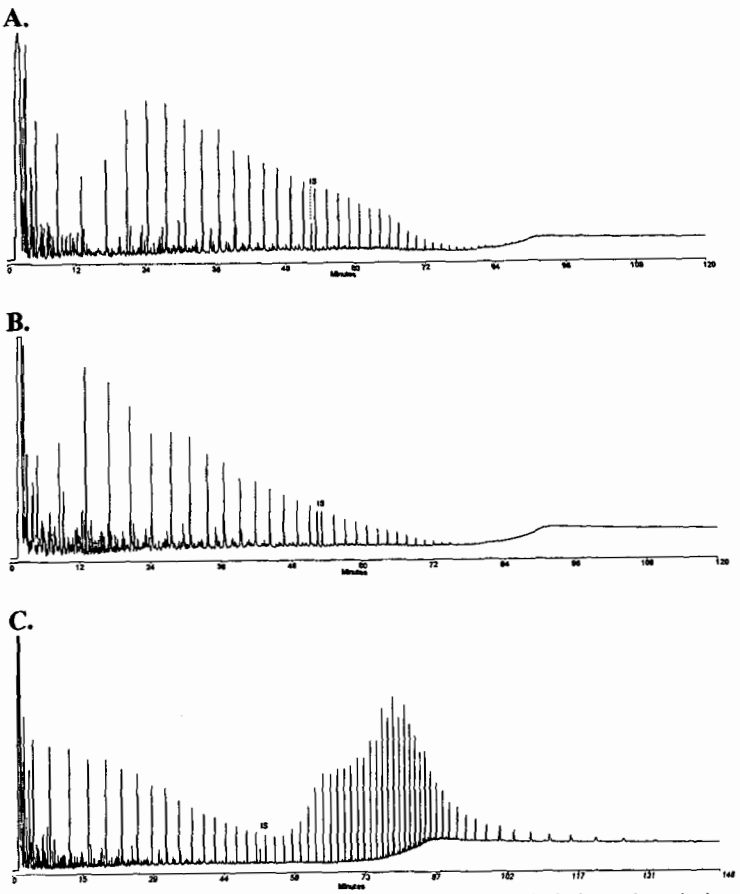

Fig. 1. Chromatograms showing (a)the pipeline mixture (note-IS is the internal standard and is $C_{24}D_{50}$); (b) the liquid crude in the tank; and (c)the solid residue in the tank (note also that the top two chromatograms have total run times of 120 mins and the bottom chromatogram has a run time of 146mins).

A STUDY OF MAGNETIC EFFECTS ON THE PHYSICOCHEMICAL PROPERTIES OF INDIVIDUAL HYDROCARBONS

Hejun Guo, Zhizhong Liu, Yunchao Chen, Rujie Yao
Logistical Engineering College, Chongqing 400042, P.R.China

Keywords: magnetic treatment, hydrocarbon, IR and UV spectra

INTRODUCTION

There have occurred a great number of experimental studies which present evidences of the benefits of magnetic treatment on many occasions. Some eye-catching proto-industrial examples ever reported include: the enhancement of oil recovery[1] and prevention of wax deposition[2-4] in petroleum production, transportation and refining; the improvement of fluidity of crude oils[5-7], and the demulsification of oil-water mixtures[1,8]. Even for motor vehicles and industrial boilers, much fuel economy and noticeable soot suppressions could be approached when the magnetic treatment was introduced[9-11]. Over the last decade or so, the magnetic treatment, as a novel technique with great economic potentiality, has been strenuously exploited and widely adopted in the domain of petroleum chemical engineering. However, there remain some blurring issues waiting eagerly for early answers, with the core of the uncertainties being the unfolding of the molecular interaction mechanism(s) governing the macro-behaviors of the magnetically treated hydrocarbons and fuels. In our study, focus has been laid on the understanding of magnetic action modes which have led to the fuel economy and soot abatement in engine applications.

In the present research, measurement was made about the properties of some typical individual hydrocarbons such as viscosity, surface tension and maximum smokeless flame height(MSFH) after they have been treated in the magnetic fields of different intensities. The IR and UV spectra of the magnetized hydrocarbons were employed to elucidate the property changes in terms of molecular structures.

EXPERIMENTAL

An electromagnet of double yokes was devised and utilized. Each of its two poles is 80mm in diameter and the distance between the poles is 11mm. The intensity of the magnetic field was displayed by a Tesla gauge of CT3 type and could be adjusted from 0 T to 1.0 T.

An L-type quartz glass tube of 10mm in diameter was positioned in the center of the magnetic field. The tube had a rotatable piston in one end just like that of the acid buret to be used to control the flowing rate of liquid samples. In the experiment, the liquid samples of individual hydrocarbons were conducted into the glass tube and flowed transversly through the magnetic field to be magnetized at the rate of 7.5 ~ 10.0ml per minute .

The individual hydrocarbons selected were as follows: n-heptane,n-hendecane, n-hexadecane, cyclohexane, methylcyclohexane, toluene, m-xylene, n-butylbenzene and isopropylbenzene.All of them were in analytical pure. The UV analytical samples were the n-heptane solution of individual aromatic hydarocarbon .

After being magnetized the sample was immediately tested at room temperature in strict accordance with China National Standard Test Method of Petroleum Products. For comparison, measurements were also made on the same untreated samples. Of the tests, the viscosity was determined with a capillary viscosimeter, and the surface tension with the DuNouy ring method described in previous studies[12,14]. The MSFH was measured on an apparatus specified by GB5539-86. In data processing, suspected data were judged with the statistic method of t-check test.

The HITACHI 260-50 type IR spectrometer was employed; its sample cell was KBr crystal. The UV spectra were measured on a UV spectrometer of LAMBDA-Q type, and the sample cell was 1cm in width. In the analysis procedure, blank tests were conducted to adjust the absorbance of n-heptane in UV region to be equal to zero for measurement of the real absorbances of each of the tested individual hydrocarbons.

RESULTS AND DISCUSSION

In Figure 1 is listed the changes of the viscosities of three magnetized normal paraffinic hydrocarbons. As is easily seen, there occur slight decreases of the viscosity of the magnetized normal hydrocarbons.The magnitude of the change becomes larger as strength of the magnetic field increases, with more obvious change pace below 0.3T than above 0.3T. Such a phenomenon is very similar to those of the magnetized petroleum fuels[13]. It can also be noticed that, approximately below 0.2T, the viscosity decreases of the studied normal paraffinic hydrocarbons

are almost the same while above 0.2T, they are different and follow the order of n-hexadecane > n-hendecane >n-heptane. In other words, the more the carbon numbers of the normal paraffinic hydrocarbons, the more obvious of the decrease rate of their viscosity after magnetized.

Figure 2 shows the viscosity decrease of the magnetized methylcyclohexane and cyclohexane. It is apparent that the viscosity decrease of the magnetized cycloalkanes also becomes bigger with the increase of the applied magnetic field. Comparatively, the viscosity decreases more rapidly below 0.2T than above it, a very resemblance to those identified for the nomal paraffins stated above.

Figure 3 displays the viscosity decreases of aromatics such as n-butylbenzene and m-xylene. Evidently, similar features to those of normal paraffins and cycloalkanes have been demonstrated between their viscosity decrease rates and the strength of the applied magnetic fields. It can be observed that there occur rapid decreases of viscosity below 0.5T ,while above 0.5T the decrease of the viscosity becomes more and more slowly with the increase of the magnetic field strength.This indicates that the decrease of the viscosity of the magnetized individual hydrocarbons is not directly proportional to the strength of the applied magnetic field.

Figure 4 displays the relationship between the decrease rates of the surface tension of magnetized n-octane and the applied magnetic intensities, and Table 1 lists the decrease magnitudes of the surface tensions of n-hexadecane, cyclohexane and isopropylbenzene. The results show that, after magnetized, the surface tension of the individual hydrocarbons decreases. However, the decrease rates or the decrease magnitudes do not increase accordingly very well as the strength of the magnetic field increases. At some certain magnetic fields, the surface tension decreases comparatively considerably while at others it decreases comparatively unnoticeably. So, it can be easily concluded that the surface tension of the individual hydrocarbons decreases fluctuately with the increase of the magnetic field strength.

The value of surface tension is determined not only by molecular attraction force but also by molecular orientation state on the liquid surface[15]. It is suggested that the oriented distribution state of hydrocarbon molecules on the liquid surface must have changed after they have been magnetized, and that the oriented distribution state must have changed differently at different magnetic field strength. This can result in high decrease rate of surface tension compared with that of viscosity, and the fluctuation of the decrease of surface tension .

Table 4 exhibits the changes of the MSFH of magnetized toluene and its mixture with n-heptane and methylcyclohexane. It is shown that, after being magnetized, the MSFH of the individual hydrocarbons rises with the increase of the magnetic field strength. This indicates that soot formation has been suppressed after the hydrocarbons are magnetized, implying that the combustion efficiency of the hydrocarbons has been improved.

Theoretical researches have been done to unfold the magnetization mechanism of hydrocarbons. It is proposed that the magnetic treament can depolimerize molecular aggregates of hydrocarbons in normal conditions[16,17].In the present study, the molecular structure changes of the magnetized hydrocarbons were analyzed which could reveal the mechanism of the changes of the above phisico-chemical properties in terms of microstructure.

From Figure 5 it can be easily seen that, after 1,3,5-trimethyl benzene is magnetized at 1.0T, the absorption peaks of its methyl stretching vibration ($2860cm^{-1}$ ~ $2920cm^{-1}$), skeleton vibration of aromatic ring($1456cm^{-1}$ ~ $1616cm^{-1}$), methyl symmetrical deformation vibration($1384cm^{-1}$), in-plane bending vibration of C=CH($1035cm^{-1}$), out-of-plane bending vibration of C=CH($840cm^{-1}$) and out-of-plane vibration of aromatic ring($685cm^{-1}$) all shift toward higher wavenumber regions. Also, the peaks of the overtone and combination bands in the region of $2000cm^{-1}$ ~ $1660cm^{-1}$ due to the C-H out-of-plane deformation vibrations are clearly observed in the higher wavenumber regions. Since the frequency is determined by the energy difference between the excited vibration state and the ground vibration state, the vibrational energy levels of above groups must have changed. Because the molecular attraction energy(Vl) of nonpolar hydrocarbon is determined by group vibrational frequency(ν) according to the formula of $Vl = -3/4 \cdot (h \nu e^4) / (K^2 R^6)$ (where $\nu = 1/(2\pi) \cdot (K/\mu)^{1/2}$), so a conclusion can be easily reached that the higher the frequency the lower the absolute value of Vl, or, the lower the group attraction energy. Thus, it can be deduced that the molecular attraction force among hydrocarbons decreases after they are magnetized.This is why the property indices of hydrocarbons, such as vicosity and surface tension which are influenced by the molecular attraction force, decline after the hydrocarbons flow through magnetic field.

Table 2 and Table 3 list the changes of the UV absoptions of toluene and n-butylbenzene respectively. Figure 6 shows the UV absoption spectra of the magnetized and unmagnetized naphthalene. It is evident that the UV absorption strength increases remarkably after the aromatic hydrocarbons have been magnetized.This means that the transition probability of electrons in the π-bond conjugated system among different energy levels has become higher. Since the transition of the bond electrons from the ground level to the excited level is the main process of molecule

radicalization. This may enhance the splitting of the C=C bonds in the aromatic rings in the course of combustion under intense actions of light and heat, and therefore the oxidation of the aromatic rings can be accelerated and easily completed thoroughly. As a result, the combustion efficiency of aromatic hydrocarbons could be boosted, which gives rise to the noticeable increase of their MSFH.

CONCLUSION

(1) After individual hydrocarbons are magnetized , viscosity and surface tension decrease slightly and weakly respectively, MSFH rises noticeablely. The decrease rate of viscosity increases more and more slowly accompanying the increase of the magnetic field strength,and also increases with molecular carbon atom number increasing,while surface tension decreases fluctuately.

(2) IR absorption peaks shift toward higher wavenumber regions, and UV absorptions of aromatics increase remarkablely in strength,which grants the explanations to the changes of above phsico-chemical properties .

REFERENCES

1. Yu Zhaoxian et al, "The Application of Intense Magnetic Technique in Petrochemical Industry," Physics(China), 1992,21(3).
2. JAY, "Magnets Utilized for Paraffin Control Appear to Be Effective," Amoco Oil Company Newsletter, Dec.1981.
3. Chen Lidian et al, "Magnetic Treatment for Scale and Paraffin Deposits Prevention --- An Promising Technique," Oil-Field Chemistry(China) , 1986,6(3).
4. Ye Yazhong, "The Applied Test of Wax Protection by Intensive Magnetism," Oil & Gas Storage and Transportation(China) , 1990,9(2).
5. Liang Changqing et al, "Experimental Study of the Effect of Magnetic Treatment on Crude Oil in Pipeline," Oil & Gas Storage and Transportiou(China), 1990,9(1).
6. Zhang Yuxian, "The Applicable Research of Magnetic Technology in the Pipeline Transportation of Crude Oil," Oil & Gas Storage and Transportation(China), 1989,8(1).
7. Cao Yujuan et al, "Reduction of Viscosity of Crude Oil by A Strong Magnetic Field and Its Application," Acta Petrolei Sinica , 1989,10(1).
8. Liu Wenping et al, "The Effect of Magnetic Treatment on the Breaking of Heavy Oil Emulsions," Oil-field Chemitry(China), 1990,7(3).
9. 吉村克郎, "The Effect of Fuel Oil Combustion through Magnetic Treatment Device," Fuel and Combustion (Japan),49(3).
10. 藤田越丈, "The Combustion Efficiency Improving of Magnetized Fuel Oil," Fuel and Combustion, 45(1) .
11. Sun Mingdong et al, "Study on the Combustion Efficiency of Magnetized Petroleum Fuels," Chinese Science Bulletin, 1984. 3.
12. Zhao Yang et al, "Effect of Magnetic Fields on Physico-chemical Properties of Surfactant Solutions," Oil-field Chemistry(China), 1989,6(3).
13. Guo Hejun et al, "Discussion on Energy Saving Mechanism of Magnetized Fuel Oil, Energy Conservation(China),1997.4.
14. Zhao Liang et al, "Effect of Magnetic Field on the Surface Tension of Alkanes and Alcohols," Chemistry(China), 1989. 1.
15. A.W.Adamson,Phsical chemistry of Surfaces, VOL ONE (Chinese Version),Science Publishing House of China, 1983, P63.
16. Tong Jingshan et al, "The Molecular Thermodynamics Model of Magnetized Fluid and the Study of Combustion Performance of Magnetized Oil Fuels," Energy Conservation Technology(China), 1989.9 .
17. Chen Guoxian, Yi Zhiying, "Microscopical Analyses of Magnetically Treated Fuel Oil, " Physics(China), 1992,21(3).

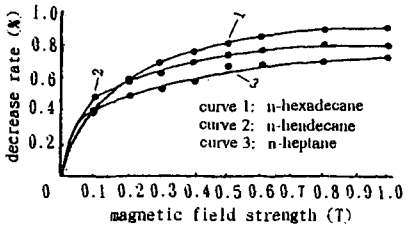

Figure 1. Viscosity decrease rate of normal paraffin versus magnetic field strength

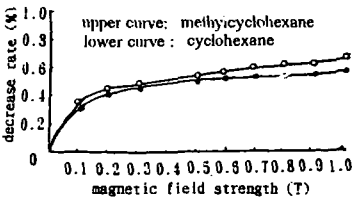

Figure 2. Viscosity decrease rate of cycloalkane versus magnetic field strength

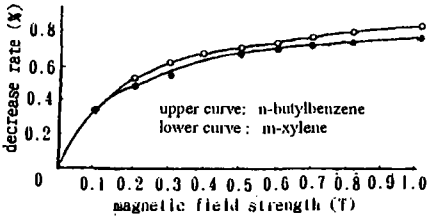

Figure 3. Viscosity decrease rate of aromatics versus magnetic field strength

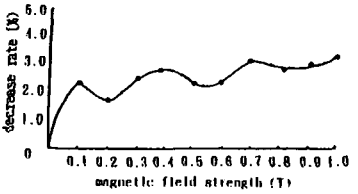

Figure 4. Surface tension decrease rate of n-octane versus magnetic field strength

Table1 The Surface Tension Changes of Magnetized Individual Hydrocarbons ($\triangle \gamma$, dyn/cm)

B(T) / sample	0.1	0.2	0.3	0.4	0.5	0.6	0.7	0.8	1.0
n-hexadeane	-0.5	-0.4	-0.6	-0.5	-0.6	-0.7	-0.8	-0.9	-1.1
cyclohexane	-0.2	-0.4	-0.4	-0.4	-0.5	-0.5	-0.7	-0.5	-0.6
isopropylbenzene	-0.4	-0.6	-0.6	-0.7	-0.8	-0.5	-0.5	-0.6	-1.0

Table 2 The MSFH Increases of Magnetized Toluene and Its Mixture($\triangle$h)

B / sample	1.8 T	5.0 T	1.0 T
toluene	1.2mm	1.6mm	1.9mm
toluene + methylcyclohexane + n-heptane(1:1:1, vol)	1.7mm	2.1mm	2.5mm

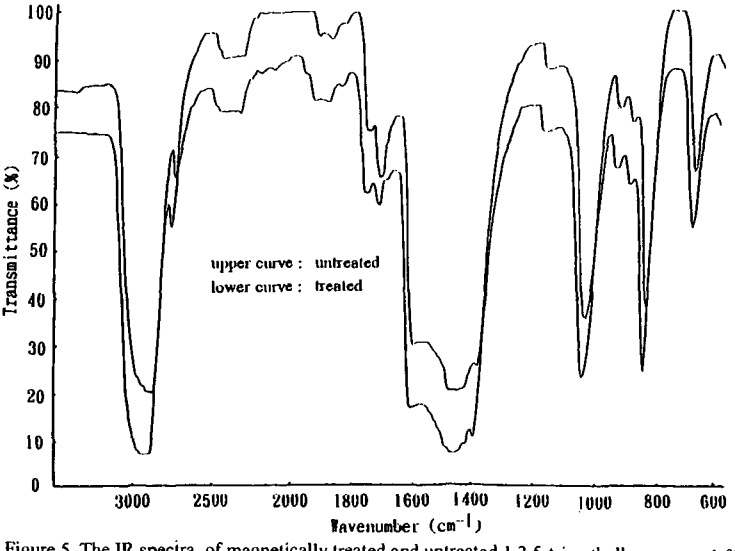

Figure 5. The IR specira of magnetically treated and untreated 1,3,5-trimethylbenzene at 1.0T

Table 3 The absorbance increase rates of magnetized toluene UV absorption

B \ wavelength	220.4 nm	257.2 nm	263.0 nm
1.0 T	18.1%	6.4%	6.0%
0.3 T	21.1%	5.0%	5.0%

Table 4 The absorbance increase rates of magnetized n-butylbenzene UV absorption

B \ wavelength	220.6 nm	253.0 nm	259.2 nm
1.0 T	16.6%	6.1%	6.8%
0.3 T	11.6%	4.2%	5.6%

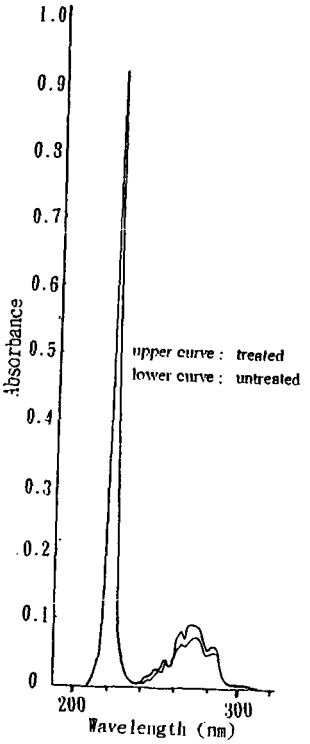

Figure 5. The UV spectra of magnetically treated and untreated naphthalene at the strength of 1.0 T

notes: sample concentration: 1.5 μ g/ml . The very similar graph was also achieved at the conditions of 3 cm in width of sample cell and 0.5 μ g/ml in sample concentration

COMPOSITIONAL MODELLING OF GENERATION AND MIGRATION OF PETROLEUM COMPOUNDS IN A HIGH PRESSURE/ HIGH TEMPERATURE ZONE IN THE CENTRAL GRABEN (NORTH SEA): INFLUENCE OF THE THERMAL STABILITY OF CHEMICAL CLASSES ON THE OIL PREDICTION.

M. Vandenbroucke, F. Behar, J.L Rudkiewicz, J. Wendebourg, J.M. Gaulier, IFP 92500 Rueil-Malmaison, FRANCE; A. Vear, N. Beveridge, BP Sunbury TW16 7LN, U.K.; S. Düppenbecker, BP Houston TX77079, U.S.A; F. Brigaud, EEP 64018 Pau, FRANCE, D. Grauls, EEP 64018 Pau, FRANCE.

Keywords: petroleum system modelling, compositional kinetics, high pressure/ high temperature reservoirs, Temispack.

INTRODUCTION

Basin simulators that predict oil and gas generation and migration in petroleum systems use kinetic schemes of oil and gas production based on pyrolysis of source rock samples for simulating their natural maturation. The organic matter decomposition with increasing temperature due to burial in geological conditions is governed by kinetics, the thermodynamically stable ends being methane and almost pure carbon. As millions of reactions occur in source rocks, a number of product groupings and assumptions have to be done for modelling cracking kinetics, and several models have been described in the literature (1-7). The present study is a part of an European Union sponsored project associating BP, EEP and IFP. In this paper we simulate the generation, migration and cracking of fluids until present on the high pressure (1100 bars) high temperature (190°C) Elgin field in the North sea with the 2D simulator Temispack . We compared in the same 2D cross section a kinetic model 1 calibrated on pyrolysis and field data, describing kerogen cracking into two classes, oil and gas, and another kinetic model 2 calibrated on pyrolysis data only, based on various chemical classes with different thermal stabilities. Oil cracking is calibrated on pyrolysis data, giving gas and coke in model 1 and a chemical class distribution in model 2. The two models compute the genesis and secondary cracking of hydrocarbons in the source rocks, their expulsion, migration and secondary cracking in carriers and reservoirs, the saturations and number of phases in each element of the section. The present hydrocarbon composition observed in Elgin Fulmar sands reservoirs is compared with the corresponding results of these models and thus accounts for their difference in kinetic modelling.

EXPERIMENTAL AND MODEL SETTINGS

Geological context modelling

The studied zone is located in the 'four corners' high pressure high temperature area in the North Sea Central Graben. The choice of this zone was guided by the will to test the models in an unusual geological setting where present day conditions may seem a priori unfavorable to oil preservation, leading to question the kinetic schemes currently used in basin simulators. A 2D cross section intersecting the structural crest of the Elgin field as well as the relevant kitchen areas was reconstructed through time, the geological history of sediment deposition being described by a series of 31 events corresponding to stratigraphic markers. To each formation is associated during burial a lithology describing the compaction (porosity vs. depth), the conductivity and the permeability of the rock. The stratigraphic and lithologic parameters of the 2D cross section are given in Table 1. The parameters of lithologies and the thermal boundary conditions were calibrated on present day temperatures and pressures coming from well data, and on vitrinite reflectance measurements. The present day geometry and source rock position as reconstructed by Temispack is shown on Fig. 1.

Geochemical parameters

a) source rock distribution

Pertinent information on the sedimentology of source rocks is crucial for a good prediction of oil and gas potentials. Previous geochemical studies in the Elgin area showed that main source rocks are within the Kimmeridge and Heather formations and contain marine organic matter (Type II of Tissot and Welte (8); organofacies B of Pepper and Corvi (6)). A second source rock can be found in the Pentland formation (Middle Jurassic). However its organofacies varies according to the studied zone from algal lacustrine (Type I/organofacies C) to coaly (Type III/organofacies F), making difficult to estimate at a regional scale the amount and petroleum potential of the formation. In the Elgin area, the Pentland source rock is considered as Type III organic matter bearing.

b) kerogen cracking parameters

As primary cracking of kerogen consists mainly in breaking of functional bonds, the kinetic parameters depend on the kerogen type. Both models describe kerogen and oil cracking by a set of parallel reactions, assuming that the order of all reactions is one and the rate constants follow the Arrhenius law. The distribution of partial potentials according to activation energies is Gaussian in model 1, thus defined by its mean and standard deviation and one preexponential factor; it is calibrated on pyrolysis experiments and field data. Oil (C_6) and gas (C_1-C_5) generation are modelled separately. For model 2, a discrete distribution of partial potentials for increasing activation energies is calculated by an optimization procedure (9) to account for the Rock Eval

pyrolysis curve obtained with different heating rates; the preexponential factor is the same for all reactions and a reactive fraction of the total hydrogen index is calculated for each activation energy.
In order to simulate hydrocarbon generation and migration, once geochemical types and amounts of possible source rocks are mapped, two options can be chosen. Either default cracking parameters are used on the basis of known geochemical data on the modelled area, or cracking parameters are adjusted on the pyrolysis study of representative samples. The first option is the only one possible for model 1. For using the second option, samples at the beginning of the catagenesis zone (oil generation) have to be recovered in sufficient amount. Their organic matter must be isolated from minerals to avoid undesirable catalytic effects due to the increase in temperature necessary for compensating geological time during the pyrolysis procedure. For calibration of the Kimmeridge and Heather source rock in model 2, an immature Kimmeridge clay from the Yorkshire coast was used for pyrolysis experiments. The immature equivalent of the Pentland Type III was not available, thus default kinetic parameters were used for this source rock.
The complete methodology for determining the kinetic parameters of reference kerogens is defined in (10). The derived procedure used here for Type II kerogen in model 2 is summarized hereunder.
A first step is to perform compositional Rock Eval according to the method described by Espitalié et al. (11). Briefly, kinetic parameters are derived from pyrolyses at various heating rates in open system using an optimization procedure which determines for each kerogen an unique frequency factor and a weight distribution, for a discrete series of activation energies, of C_1, C_2-C_5, C_6-C_{14} and C_{15+} classes, using various cold traps. This step allows to compare the primary cracking of the type II kerogen into gas (C_1-C_5) and oil (C_{6+}) between models 1 and 2. Model 1 is centered on E = 51 Kcal/mol with a preexponential factor A =8.14 10^{13} s-1 for oil and on E = 67 Kcal/mol with a preexponential factor A =2.17 10^{18} s-1 for gas. Model 2 is strongly asymetrical and maximizes on E = 52-54 Kcal/mol for oil and on E = 54 Kcal/mol for gas with a same preexponential factor A =1.6 10^{14} s-1 for oil and gas. Although these models give very close generation curves in the laboratory conditions, it can be seen on Fig. 2 that it is no longer true in basin conditions, where the proportion of gas and oil are calculated for a constant sediment burial of 50 m/My and a geothermal gradient of 25 °C/km.
The second step consists in running preparative pyrolysis as decribed in (10), in order to quantify by gas chromatography the C_6-C_{14} fraction into saturates and aromatics, and by weighing the C_{15+} compounds after fractionation by liquid chromatography into C_{15+} saturates, C_{15+} aromatics and NSO compounds. These proportions are applied evenly to the C_6-C_{14} and C_{15+} classes obtained in the first step whatever the activation energy, as it was shown (10) that the pyrolysate composition does not change during open system pyrolysis.
A third step is to run gas chromatography on the C_{15+} saturates and to measure in the same carbon interval the total area of the chromatogram once the blank is substracted, and the total area of *n*-alkanes and 1*n*-alkenes. The ratio of these areas gives the proportions of *n*-alkanes and *iso-/cyclo-* alkanes in the C_{15+} saturates. Separation of these compounds in the kinetic scheme results from a recent study (12) on the effect of pressure on cracking of pure *n*- C_{25}, showing that pressure in the range 100-800 bars has little influence on cracking kinetics compared to temperature. The influence of pressure was assumed to be small for all chemical classes. Absolute kinetic parameters were obtained, showing that *n*-alkanes are more stable than *iso-/cyclo-* alkanes. These kinetic parameters are used for all C_{15+} *n*-alkanes. Because using pure compounds does not automatically take into account the mixture effect (hydrogen donors/acceptors), another study was performed to test this parameter (13), indicating that this effect does not change significantly the kinetic parameters and tends to delay cracking.
The final step is to perform an isothermal pyrolysis in closed system at 550°C during 24 hours on a kerogen at the beginning of the metagenesis stage. It was in fact shown (10) that open and closed system pyrolyses give fairly similar results for stoichiometric coefficients of primary cracking except for methane. In the open system the final pyrolysis temperature is higher than in the closed system and results in a competition between C-C and C-H bond cracking in the kerogen. The molecular hydrogen that is generated lowers the amount of methane. The kerogen at the beginning of the metagenesis stage may be either prepared on a natural sample, or preferably by performing a first pyrolysis on the immature sample at 350°C during 48 hours to generate all the oil from primary cracking, then extracting the remaining kerogen. The C_1 and C_2 gases being stable in geological conditions can be quantified after the second pyrolysis, allowing to split the gas into C_1, C_2 and C_3-C_5.
This methodology results in a complete compositional description of the products of kerogen cracking into chemical classes of compounds. Even if these chemical classes represent the lumping of a great number of compounds, they behave similarly during secondary cracking because of similar chemical structures and bonds. The kinetic scheme for secondary cracking can thus be better constrained. In basins where source rocks do not experience a strong secondary cracking, this kinetic model can be highly simplified.
c) oil cracking parameters
Secondary cracking of oil consists mainly in breaking of C-C bonds, hence it does not depend on the kerogen type. In our work, we used standard secondary cracking schemes that were calibrated on pyrolysis experiments on isolated oils and mixtures of kerogen and its cracking products.
Model 1 uses as for kerogen a Gaussian distribution of activation energies, thus secondary cracking is defined by three parameters, the mean energy E = 58 Kcal/mol and its standard deviation and a preexponential factor A = 10^{14} s-1 (7). Oil cracks into gas and coke. Model 2,

presented in detail in (5), describes cracking of each chemical class defined previously by a reaction producing other chemical classes. The kinetic parameters, E, A and the stoichiometric coefficients are fitted on experimental pyrolysis values, and constrained by mass and atomic balances; the model is simplified by chosing the same preexponential factor for all reactions. This kinetic scheme (5) was modified in the present study by adding the cracking reaction of *n*-alkanes with its own E and A (12).

RESULTS AND DISCUSSION

Once the 2D cross section was calibrated to match the pressure and temperature data, several compositional runs tested the influence of geochemical parameters on the saturation and composition of fluids in possible reservoirs. Typically, runs with model 1 need 10 hours and runs with model 2 need 25 hours of CPU on a Sun Spark Ultra 1 workstation. This difference is linked to the number of unknowns that have to be computed.

Geological events

As shown on Fig. 1, during the Quaternary (1.64 My), over 1000 meters of silty shales were deposited. This large input of sediments resulted in a very rapid burial of the petroleum system. Fig. 3 shows the thermal history of the Fulmar sands, the reservoir of the Elgin field located just under the Kimmeridge and Heather source rocks. In this reservoir, the temperature increased from 160 to more than 180°C in the last million years. Due to the very low permeability of the carbonates in the Hod formation, the fluid expulsion was not quick enough to accomodate the rapid burial, enabling fluid pressures close to lithostatic pressure in the underlying sediments.

Saturations and phase behaviour

The petroleum system modelling through time indicates that the Elgin reservoir filling begins around - 50 My. The petroleum fluid is monophasic during migration, thus all hydrocarbons, either C_{6+} or C_1-C_5, move with the same speed.

Primary cracking

The separate contribution of each source rock to the reservoir filling was tested. The results show that primary cracking is completed whatever the source rock considered, hence the oil composition does not depend much on the kerogen type. However as *n*-alkanes are fairly stable, their characteristic carbon distribution according to the source rock contribution, particularly in the Type I Pentland in other zones of the study, can still be recognized in the oil analyses.

Secondary cracking

Its kinetic parameters determine the hydrocarbon composition in the Elgin reservoir. Model 1 predicts only gas; model 2 predicts both oil and gas. The oil composition predicted by model 2 and observed in the Elgin oil is shown on Fig 4. The prediction is fairly good for all chemical classes except for methane which is underestimated, and condensed aromatics which are overestimated.

The reason why model 1 overestimates secondary cracking can be found in the way it is mathematically expressed and calibrated. The Gaussian distribution of activation energies may be a reason as in many oils, saturates are both the most abundant and the most stable compounds. The calibration of cracking experiments is done by pyrolysis-gas chromatography. This technique allows the analysis of small amounts of hydrocarbon compounds to be performed but no mass balance can be made: only compounds able to cross the chromatographic column are detected. Heavy fractions are thus not taken into account, and this may bias the description of cracking, thus the mean activation energy, towards the light ends.

The methane underestimation of model 2 could be due in part to its quantification in primary cracking. Although the Rock Eval value has been corrected using the result of a closed system pyrolysis at 550°C/24h, a currently performed research shows that this correction represents only 60% of the total methane potential of the kerogen. Condensed aromatics are probably the least constrained chemical class in the secondary cracking scheme (6). Their definition was based on elemental analysis but the low amounts obtained during pyrolyses made it difficult to calibrate correctly the stoichiometric coefficients, and the activation energy may be too high, as already noticed in (6): 59.1 Kcal/mol for type II and III kerogens as compared with 57.1 for Boscan oil.

Evolution of the petroleum system

The petroleum system modelling shows that the occurrence of oil in Elgin despite the presently high temperature is due to its very recent increase from 160 to 190°C in the last million years. This situation evolves rapidly as shown both by the model and by optical studies on reservoir cores proving that pyrobitumen due to the oil cracking is currently forming.

CONCLUSION

Simulating generation, migration and entrapment of hydrocarbons in a petroleum system is the only way to handle its numerous variables and to be able to test the influence of selected parameters. Many of them depend upon assumptions which are sometimes uncertain; however the simulation allows us to check the current hypotheses, to measure the sensitivity to parameter changes and to calibrate the entry parameters against field data.

In this respect the present study shows that in a petroleum system where high temperature causes a large amount of secondary cracking both in source rocks and in reservoirs, it seems difficult to predict the occurrence of oil or gas without taking into account the detailed chemical composition of products, linked to their thermal stability, as done in model 2. It shows also that in this latter, the calibration of secondary cracking should be improved to better account for a higher proportion of

methane and a lower proportion of condensed aromatics. Future work will be performed in two directions: one is to run new pyrolyses on the oil constituents generating condensed aromatics, such as NSO compounds; it seems also necessary to check again the database and the optimisation procedure used to establish the secondary cracking scheme. The second consists in adjusting modified cracking parameters to the present study and then checking whether they are able to account for observed compositions in reservoirs from various sedimentary basins.

REFERENCES

1. LOPATIN N.V. (1971) Temperature and geologic time as factors in coalification. Akad. Nauk SSSR Izv. Ser. Geol.,3,95-106 (in Russian).

2. TISSOT B.P. and ESPITALIE J. (1975) L'evolution de la matiere organique des sediments: application d'une simulation mathématique. Rev. Inst. Fr. Petrol., 30, 743-777.

3. QUIGLEY T.M., MACKENZIE A.S. and GRAY J.R. (1987) Kinetic theory of petroleum generation In: "Migration of hydrocarbons in sedimentary basins" (Ed. B. Doligez). Editions Technip, Paris, 649-665.

4. BURNHAM A.K. and BRAUN R. L.(1990) Developement of a detailed model of petroleum formation, destruction and expulsion from lacustrine and marine source rocks. Org. Geochem., 16, 1-3, 27-39.

5. BEHAR F., KRESSMANN S., RUDKIEWICZ J.L. and VANDENBROUCKE M. (1991) Experimental simulation in a confined system and kinetic modelling of kerogen and oil cracking. Org. Geochem., 19, 1-3, 173-189.

6. PEPPER A.S and P.J. CORVI (1995) Simple kinetic models of petroleum formation. part 1: oil and gas generation from kerogen. Marine and Petroleum Geology, 12, 3 , 291-319.

7. PEPPER A.S and T.A. DODD (1995) Simple kinetic models of petroleum formation. part 2: oil - gas cracking. Marine and Petroleum Geology, 12, 3 , 321-340.

8. TISSOT B.P. et WELTE D.H. (1984) Petroleum formation and occurrence. Springer Verlag, Berlin

9. UNGERER P. and R. PELET (1987) Extrapolation of the kinetics of oil and gas formation from laboratory experiments to sedimentary basins. Nature, 327, 6117, 52-54.

10. BEHAR F., VANDENBROUCKE M., TANG Y., MARQUIS F. and ESPITALIE J. (1997) Thermal cracking of kerogen in open and closed systems: determination of kinetic parameters and stoichiometric coefficients for oil and gas generation. Org. Geochem., 26,321-339.

11. ESPITALIE J., UNGERER P., IRWIN H. and MARQUIS F. (1988) Primary cracking of kerogens. Experimenting and modelling C_1, C_2-C_5, C_6-C_{15} and C_{15+} classes of hydrocarbons formed. Org. Geochem., 13, 893-899.

12. BEHAR F. and VANDENBROUCKE M. (1996) Experimental determination of the rate constants of the n-C25 thermal cracking at 120. 400. and 800 bar: implications for high-pressure/high-temperature prospects. Energy Fuels, 10, 932-940.

13. MCKINNEY D.E., BEHAR F. and HATCHER P.G. (1998) Reaction kinetics and product distribution of ^{13}C labeled n-C_{25} in Arabian Light marine oil as determined by SIM/GC/MS: are mixture effects important? Submitted to Energy Fuels.

n°	stratigr. markers	Age (My)	Stratigraphy	Lithology
		(Top)		
1	Seabed	0	Quaternary	Shale_silty
2	T_Plio	1.64	Pliocene	Shale_silty
3	TE_Plio	3.4	Pliocene	Shale_silty
4	T_Miocene	5.2	Miocene	Shale_silty
5	T_Mid_Mio	10.4	Miocene	Shale_silty
6	T_Oligoc	23.3	Oligocene	Shale_silty
7	TMid_Eocene	38.6	Eocene	Shale_silty
8	TEar_Eocene	50	Eocene	Shale_silty
9	T_Balder	54.5	Palaeocene	Shale
10	T_Forties sd	57	Palaeocene	Sand
11	T_Maureen	61	Palaeocene	Shale_silty
12	T_Ekofisk	63	Maastricht.	Chalk
13	T_Chalk	65	Campanian	Chalk
14	Intra Chalk	71	Campanian	Chalk
15	T_Hod	78	Turon/Campan.	Arg_Lmst.
16	Intra Hod	81	Turon/Campan.	Hardgrds
17	int_Hod	83	Turon/Campan.	Arg_Lmst.
18	T_Herring	85	Cenom/Turon.	Plns_Marl
19	T_PlensMrl	90.4	Cenom/Turon.	Plns_Marl
20	T_Rodby	97	Albian	Tight_shale
21	T_Sola	112	Aptian	Shale
22	Kim_Clay	145.6	Portland/Berria.	KCF
23	Heather_shly	152	Oxford/Kimmeri.	Heather_src
24	int_Heather	153.5	Oxfordian	Shale_silty
25	Fulmar sdy	155	Callov/Oxford	Sand
26	PentInd-sdy	157	Bathon./Callov.	Shale&Sand
27	PentInd-shly	182	Bathon./Callov.	Pentland_src
28	Tr_Skagerrak	208	U.Triassic	Shale&Sand
29	Tr_Smithbank	222	L.Triassic	Shale_silty
30	Top_Salt	245	Zechstein	Salt
31	Rotliegend	256	M-L.Perm.	

Table 1: Stratigraphic and lithologic parameters of the 2D section

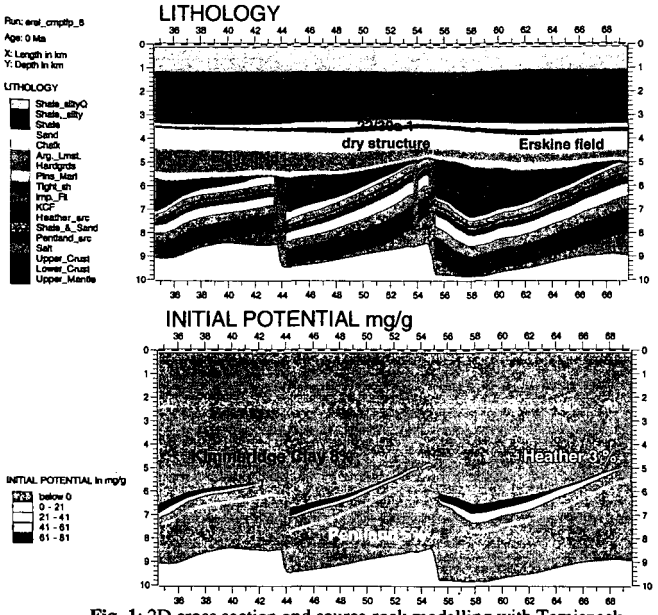

Fig. 1: 2D cross section and source rock modelling with Temispack.

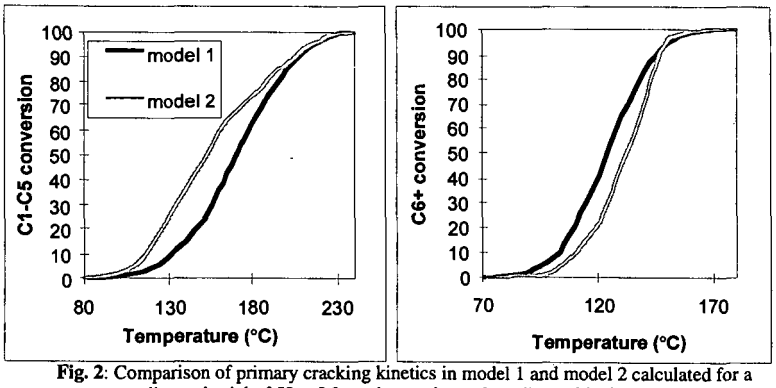

Fig. 2: Comparison of primary cracking kinetics in model 1 and model 2 calculated for a constant sediment burial of 50 m/My and a geothermal gradient of 25 °C/km.

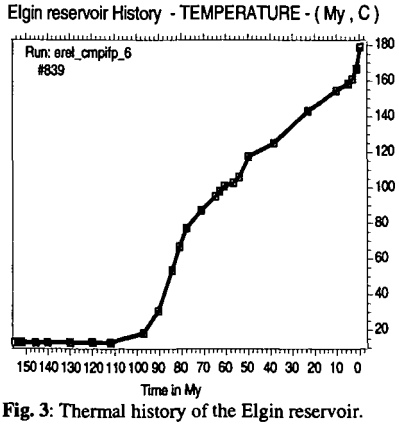

Fig. 3: Thermal history of the Elgin reservoir.

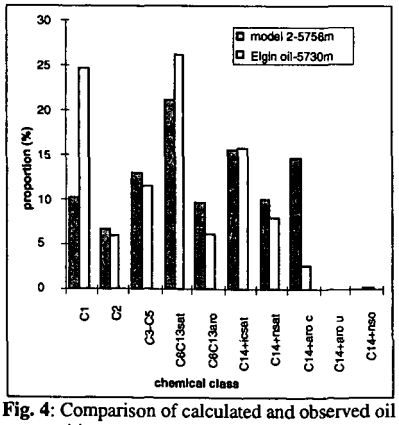

Fig. 4: Comparison of calculated and observed oil composition.

Analysis of High Pressure Samples by Gas Chromatography

Paul A. Peaden

APTI Geosciences, 10450 Stancliff Road, Houston TX 77099

Gas Analysis, Adamantanes, Hydrocarbons

ABSTRACT

High molecular weight compounds dissolved in gases at elevated pressures and temperatures in reservoirs often present production problems. These can range from precipitation of solids which foul chillers and tubing to plasticizing membranes used for gas component separations. Quantitative analysis of such samples is problematic because they are frequently present in sample vessels as two phases (gas and solid or liquid). This paper describes a technique for rendering samples collected at high temperature and pressure single phase and analysis by gas chromatography. Results of this technique to the analysis of gases containing diamondoids and other high molecular weight hydrocarbons are presented.

INTRODUCTION

The analysis of hydrocarbon gases is usually done by gas chromatography. Common analyses performed include a natural gas analysis which provides the hydrocarbon composition through n-pentane, a hexanes plus value, nitrogen, oxygen, and carbon dioxide. The analysis of these hydrocarbon gases by gas chromatography using a flame ionization detector is also often used to provide details about the hydrocarbons present in the C1 to C8 range. If it is necessary to extend the analysis range to C12, or in the extreme to C28, this can be done by careful heating of the sample and sampling lines to the appropriate temperatures to make sure that the higher boiling hydrocarbons are not lost due to adsorption or cold spots. It is possible to get around these sampling problems which lead to discrimination by sampling under supercritical conditions.

EXPERIMENTAL

SFC grade carbon dioxide was obtained from Air Liquid. An Isco syringe pump was used to pressurize samples with the carbon dioxide. A 6 port valve allowing sample pressures up to 6000 psi with a 30µL sample loop was used. The sample inlet line and valve was heated to about 60°C. The restrictor used between the valve and the injection port was between 5 and 10 cm of 50 µm id fused silica tubing. This is similar to the approaches taken in SFE/GC techniques (1). The gas chromatograph was a Hewlett-Packard 5890 equipped with both FID and FPD detectors. A high pressure gauge reading from 0 to 10,000 psi was positioned between the valve and the waste outlet. Flow at the outlet was controlled with a needle valve (see Figure 1). Samples were in stainless steel cylinders ranging from 150 cc to 500 cc.

To do the extended hydrocarbon analysis first a conventional natural gas analysis was obtained. This was done in order to get the concentrations of nitrogen, oxygen, carbon dioxide, and the C1 to C4 hydrocarbons. At this time the sample pressure was also measured along with the cylinder weight. Based on the amount of methane and carbon dioxide present the quantity of carbon dioxide necessary to bring the sample to a reduced density of 1 or greater was calculated. Using the syringe pump this quantity of carbon dioxide was added to the sample and the sample was reweighed. The weighing helped verify that the right amount of carbon dioxide really was added to the cylinder. The sample was then allowed to equilibrate (usually overnight) at 60°C until sampling.

Sampling was done at cylinder pressure and temperature. The sampling line was heat traced along with the valve. Another high pressure line to the valve from the ISCO pump supplied carbon dioxide at or slightly above the cylinder pressure as measured by the pressure gauge. Prior to sampling the sample was allowed to flow through the sampling system for at least 2 to 3 minutes at about 100 mL/min. In order to keep methane through butane on scale a range change from lower to higher sensitivity was done automatically after the elution of n-butane. The magnitude of this change was generally a factor of 512, but for some samples with high concentrations of hydrocarbons it was lower.

RESULTS AND DISCUSSION

The data indicate that reduced densities of at least one are sufficient to give quantitative results for most samples. This is shown by the results in figures 2-4. Most importantly this data indicates that by sampling under the proper conditions it is possible to significantly reduce or eliminate any discrimination between low boiling and high boiling hydrocarbons. Quantitative results for the hydrocarbons are calculated by using the natural gas results for the amount of methane through butanes in the sample. Using this value as an internal standard amount the quantities of other hydrocarbons in the sample can be calculated based on a carbon equivalent response for the FID (2). It is possible to determine adamantanes and other hydrocarbons quantitatively at concentrations of 1 ppm with detection limits around 0.05 ppm. The actual quantitative limits depend on the initial state of the sample. Samples which require the addition of large amounts of carbon dioxide will have higher detection limits, and those requiring little carbon dioxide will have lower detection limits. Obviously this analysis excludes water. If water is present is not expected to significantly impact the results obtained except for its exclusion.

REFERENCES

(1) Lee, M. L.; Markides, K. E. *Analytical Supercritical Fluid Chromatography and Extraction;* Chromatography Conferences, Inc.: Provo, Utah, 1990; PP 335-344.
(2) Scanion, J. T. Willis, D. E. *J. Chromatogr. Sci.* **1985,** *23,* 333.

FIGURES

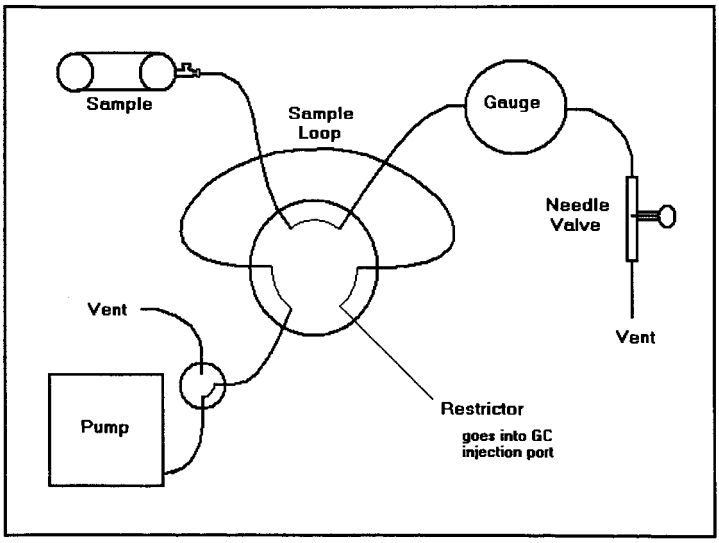

Figure 1. Diagram of the sampling system.

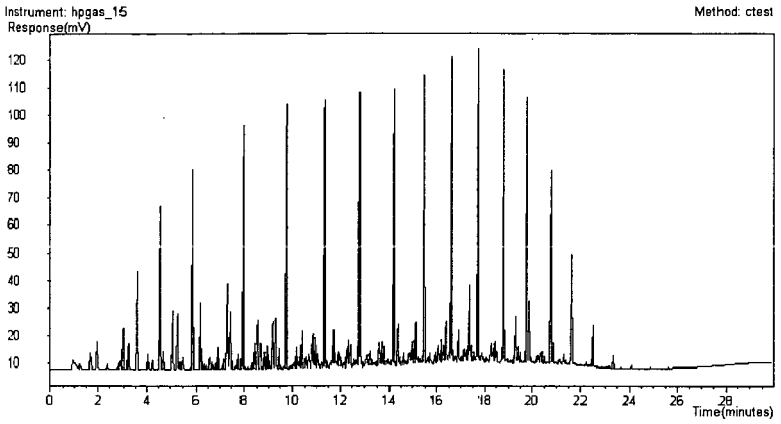

Figure 2. Results at a reduced density of 0.5.

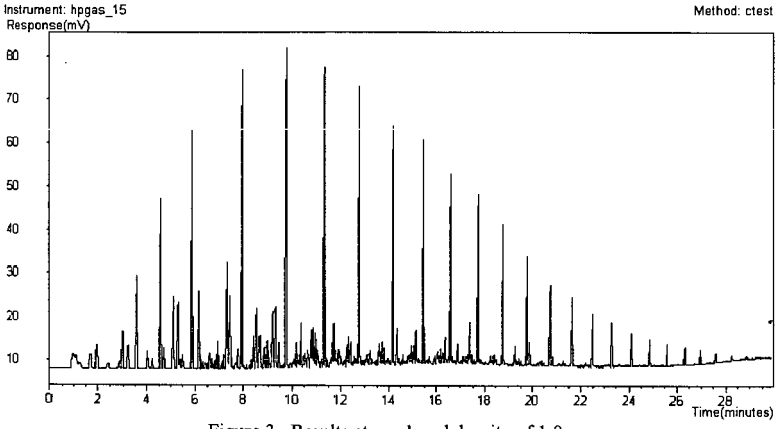

Figure 3. Results at a reduced density of 1.0.

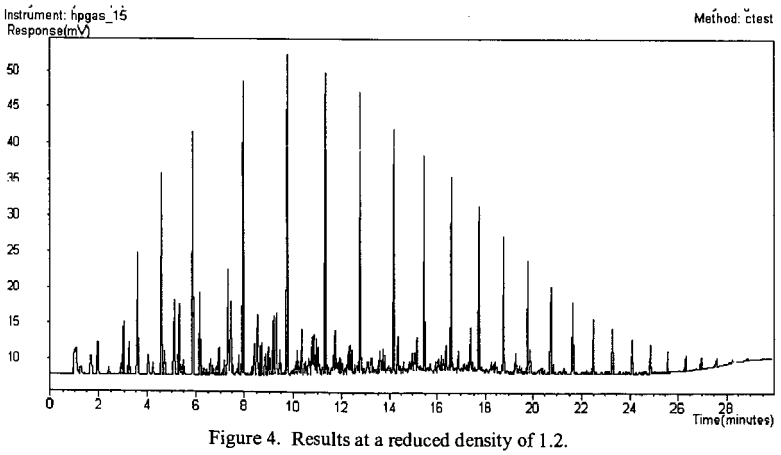

Figure 4. Results at a reduced density of 1.2.

CONCENTRATION OF HYDROCARBONS ADSORBED ON SOIL AND ROCK SAMPLES BY SUPERCRITICAL FLUID CHROMATOGRAPHY

Bruce W. Bromley, Victoria Corona, Paul A. Peaden

APTI Geosciences, 10450 Stancliff Road, Houston, Texas 77099

Extraction, Supercritical Fluid, Drilling Mud

ABSTRACT

A procedure for quantitatively extracting hydrocarbons ranging from C5 to C44 using carbon dioxide at supercritical conditions to yield a concentrated extract suitable for analysis by GC or GC-MS is described. Examples are presented of the application of this technique for the detection of petroleum hydrocarbons in samples from wells drilled with oil based mud and for the characterization of gasoline range contamination in water saturated soils.

INTRODUCTION

Isolation and concentration of hydrocarbons contained in soil and rock matrices by solvent extraction frequently results in the loss of low boiling components. Much of this loss results from the process of solvent removal by evaporation that must be performed in order to concentrate components prior to analysis. Also, presence of high concentrations of water in samples can interfere with the solvent extraction process. Supercritical fluid extraction (SFE) is the process by which a supercritical fluid removes analytes from a matrix and transfers them to a trap where the supercritical fluid is returned to a gaseous state and escapes, leaving the sample components behind. The sample is then rinsed from the trap with a small amount of solvent and transferred to output vials. A SFE procedure that overcomes difficulties of light end retention and water interference is described.

EXPERIMENTAL

A Hewlett Packard Model 7680T Supercritical Fluid Extractor was employed (1) using SFC grade carbon dioxide. The SFE trap was packed with a porous polymer selected to retain hydrocarbons while being inert to CO2. If samples were wet, desiccant was mixed with the sample prior to extraction. Extractions described here were performed in two steps as follows:

Step 1
Density = 0.25 g/cc, sample cell temperature = 40°C
Static (closed cell) extraction time = 1 minute
Dynamic (open cell) extraction time = 5 minutes (5.3 cell volumes)
Rinse trap to collection vial with 500 µl dichloromethane
Step 2
Density = 0.84 g/cc , sample cell temperature = 40°C
Static (closed cell) extraction time = 1 minute
Dynamic (open cell) extraction time = 10 minutes (3.1 cell volumes)
Rinse trap to collection vial with 500 µl dichloromethane

RESULTS AND DISCUSSION

As the use of oil based muds becomes more prevalent in drilling oil wells, detecting oil shows can be problematic. Hydrocarbons ranging from C5 to C44 can be readily extracted from rock samples (conventional cores, sidewall cores , or cuttings) using SFE and examined for non-mud hydrocarbon presence by gas chromatography of the extract.

The restricted boiling range of oil based muds, as shown in Figure 1, allows detection of hydrocarbons boiling at higher or lower temperatures than those of compounds present in the mud. Figure 2 contains expansions of gas chromatograms of supercritical fluid extracts of sidewall cores from a single well; one containing only oil based drilling mud and the other containing mud and hydrocarbons contributed from the core. A profile of the data down this well yielded the results in Figure 3, showing the presence of non-mud hydrocarbons at approximately 11,250 ft. Testing of this well from the interval identified by SFE produced oil with the composition shown in Figure 4. This oil likely could not have been detected using conventional solvent extraction methods as solvent evaporation would likely have resulted in loss of most of this particularly volatile oil.

Hydrocarbon contamination in soils can be very difficult to quantitatively extract and characterize, especially when water or low boiling components are present. Hydrocarbons ranging from C5 to C44 can be readily extracted from soil samples using SFE (even if the soils are wet) and the resulting extract characterized by gas chromatography.

Figure 5 is a chromatogram of a hydrocarbon "free product" collected from a severely contaminated site. The goal of this investigation was to evaluate soil core samples surrounding this free product accumulation to determine the extent of contamination and to ascertain if more than one source may have contributed to the main accumulation.

The character of the soil in this site was sandy with small pebbles. In order to test the effectiveness of the SFE method, a sample of clean sand was soaked with water and then spiked with the free product illustrated in Figure 5. A chromatogram of the resulting SFE extract, shown in Figure 6, is indistinguishable from the original material. Segments from multiple cores were extracted by SFE and analyzed by GC. Sample amounts, SFE and GC conditions were held constant. Figure 7 is an example a chromatogram of an actual core extract. Using the results of these analyses the extent of the contamination was clearly defined and significant differences in origin of material contributing to the free product were observed.

REFERENCES

(1) Hewlett Packard 7680A Supercritical Fluid Extractor Operational Manual: Part Number 07680-90320. Edition 2, November, 1991.

FIGURES

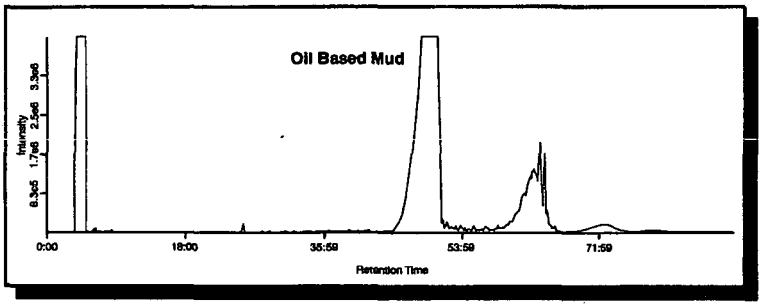

Figure 1 - Oil based Mud, Gulf of Mexico

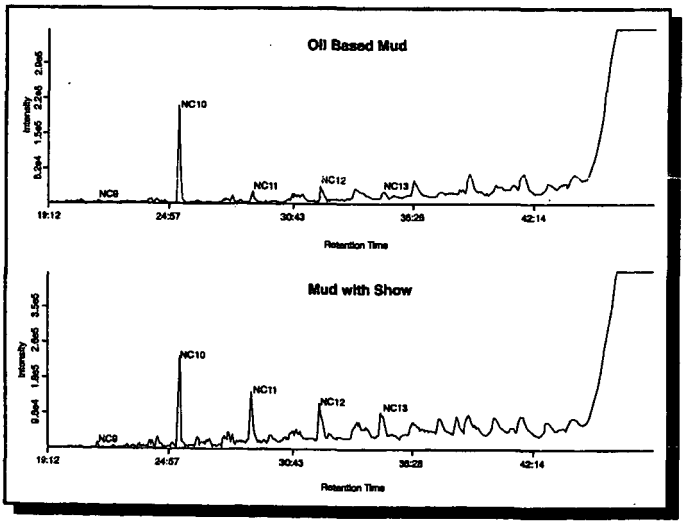

Figure 2 - Oil Based Mud and Mud with Show

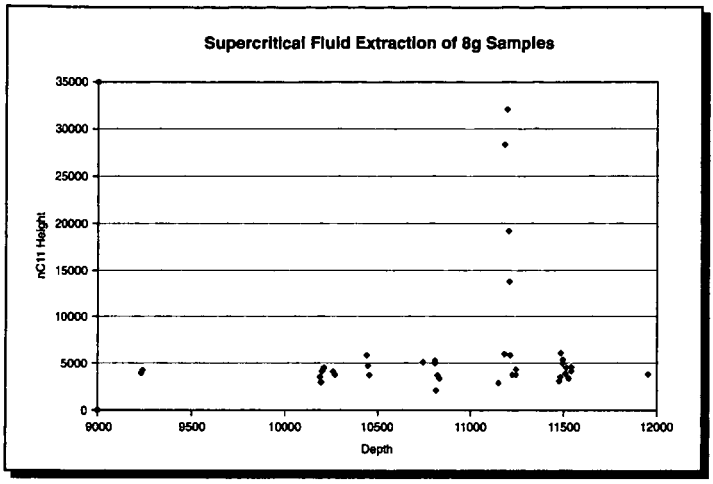

Figure 3 - Supercritical Fluid Extraction of 8 gram Core Samples

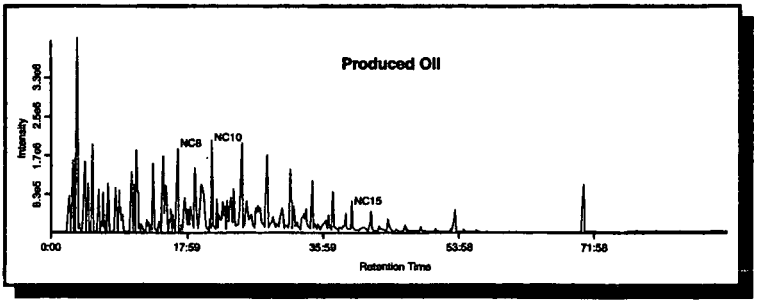

Figure 4 - Produced Oil

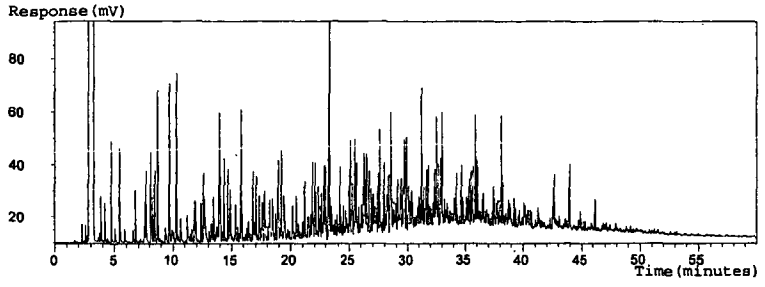

Figure 5 - Free Product

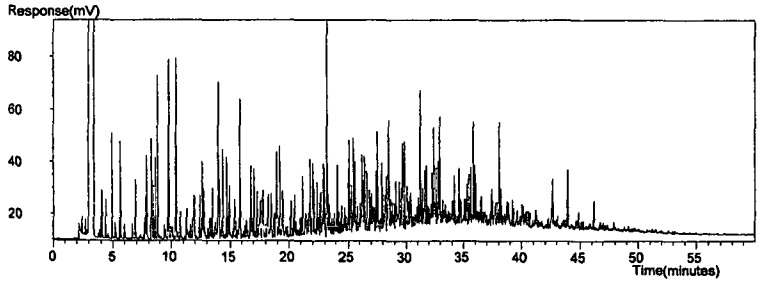

Figure 6 - Test of SFE Method to Remove Free Product From Similar Soil Matrix: 100ul Free Product on Water Saturated Sand

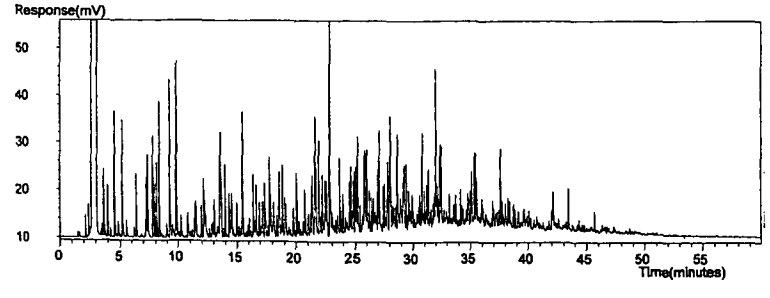

Figure 7 - Core Extract

THE USE OF SYNTHETICS IN WELL DRILLING FLUIDS FOR THE FOR OFFSHORE OIL FIELD

Burney Lee
Amoco Chemicals
Building 503-1330
150 West Warrenville Road
Naperville, IL 60563-8460

KEYWORDS: Synthetic Based Mud, Drilling Mud, Offshore Drilling

ABSTRACT

As Gulf of Mexico offshore drilling moves into deeper water and into more demanding conditions in terms of the depth and type of wells (deviated and horizontal), drilling muds providing higher lubricity and better hole stability are needed. Previously, oil based muds (OBMs) which are primarily based on diesel oil met this need. However, the on site discharge of cuttings from wells drilled using OBMs was banned in the early 1990's. At this time, synthetic based muds (SBMs) were introduced that are prepared using synthetically derived base fluids. SBMs were developed to provide an environmentally safe alternative drilling mud that would meet both the severe drilling mud requirements and the need for cuttings discharge into the ocean. These base fluids are chemically synthesized from the reaction of specific purified chemical feedstocks to give readily characterized products. The synthetic fluids used in the Gulf of Mexico today are linear alpha olefins (LAOs), isomerized olefins (IOs), polyalphaolefins (PAOs) and esters. A description of their chemistry, the benefits they provide and the regulatory issues surrounding their use is discussed.

INTRODUCTION

Oil exploration and production offshore continues at high rates today all around the globe. It is expected to continue at these rates for the next 5 years. In the Gulf of Mexico, this activity has moved out onto the continental slope and beyond to water depths over 6000 feet at locations that are many miles from shore support. These severe conditions coupled with difficult drilling through water sensitive formations push drilling technology to the limit and demand maximum performance in all aspects of the oil exploration process. To minimize difficulties encountered from drilling through water sensitive formations, invert emulsion based drilling muds are often used today.

Drilling muds are materials that are pumped through the rig's drill string and drill bit to remove drill cuttings from the bore hole during drilling operations. They also clean the bit, maintain desired pressure differential between the formation and mud and serve to stabilize the hole. For most drilling, the muds used are prepared by dispersing finely divided clays in water and are called water based muds (WBMs). These solids provide the desired suspending power to assist with cuttings removal and mud density to control pressure. However, WBMs tend to interact with water sensitive formations during drilling operations leading to bit balling and hole stability problems. These conditions can lead to a variety of costly difficulties for operators such as stuck pipe and reduced drilling rates.

To combat these problems when drilling through difficult or unknown formation conditions, an invert emulsion based mud is used. In an invert emulsion mud an organic based fluid forms a continuous outer phase surrounding an internal aqueous phase of finely dispersed droplets (an emulsion). The mud solids and other additives are also suspended in the organic phase. Because the external phase is insoluble in water, interactions with water sensitive formations are reduced. For this reason invert muds reduce sloughing problems, form better filter cakes and produce more stable bore holes. These attributes lead to formation of in-guage holes that provide higher space velocity of the mud and thus better removal of cuttings. Cutting fines are also less likely to disperse in an organic phase, leading to fewer solids control problems. Lubricity, heat transfer and bit wear performance are also improved leading to enhanced drilling rates.

Invert muds are generally based on diesel or mineral oil and called oil base muds (OBMs). In the early 1990's, however, the discharge of drill cuttings into the ocean from wells drilled using

OBMs was prohibited. The inability to discharge cuttings greatly increased cost as they now had to be transported to a safe disposal site. This quickly produced a need for a high performance environmentally safe mud to allow for cuttings discharge. To meet this need, alternative inverse emulsion muds were developed using less toxic synthetic based organic fluids so that drill cuttings discharge would be allowed. These synthetic based muds (SBMs) are produced using synthetic fluids prepared from specific purified starting materials, and they lead to defined products that are essentially free of undesirable polycyclic aromatic hydrocarbons (PAHs). These materials are less toxic and more biodegradable than refined mineral oil products such as diesel oil. Synthetic fluids used today in the Gulf of Mexico to make SBMs include linear alpha-olefins, isomerized olefins, polyalphaolefins, and esters.

EXPERIMENTAL

In this section a brief description is given of the various chemistries used to produce synthetic fluids.

Synthesis of Linear Alpha Olefins (LAOs) and Isomerized Olefins (IOs)

Linear alpha olefins (LAOs) are prepared from the catalytic chain growth of ethylene on triethyl aluminum. After the chain growth step the larger alkyl groups are displaced from the aluminum either simultaneously with the chain growth step or in a separate step to give even numbered linear olefin products with carbon numbers from C4 - C20+ (Figure 1). The olefin double bond is formed between the first and second carbons of the alkyl chain (the alpha position) during the displacement step. Distillation provides clean cuts of the desired olefin products.

Isomerized Olefins (IOs) are produced from LAOs using an isomerization catalyst to move the olefin double bond from the alpha position to an internal position along the carbon chain (Figure 1). The internal double bond is distributed throughout the linear chain. Isomerizing an LAO lowers the pour point of the fluid.

Synthesis of Polyalphaolefins (PAOs)

Polyalphaolefins are prepared by the catalytic oligomerization of LAOs followed by hydrogenation of the material to remove the double bond (Figure 2). The oligomerization reaction produces dimers, trimers, tetramers, ... of the LAO. These oligomers have many different types of branched structures due to olefin rearrangements occurring during the oligomerization reaction. The structure in Figure 2 represents one possibility for a dimer oligomer.

Synthesis of Esters

Esters are prepared from the condensation reaction of alcohols and organic acids generally under acid catalysis conditions (Figure 3). Because the alkyl group associated with the alcohol or acid can be obtained from a variety of sources, many structures of esters are possible. For drilling mud applications the starting materials generally come from vegetable oils.[1]

Refining of Mineral Oils

In contrast to the synthesis of organic fluids for invert emulsions, diesel and mineral oils are refined from crude oil (Figure 4). These traditional fluids are produced solely through physical separation processes and/or minor chemical reactions such as cracking and hydroprocessing. Refining eliminates most of the undesirable components of these mixtures but they still can contain significant amounts of PAHs.

DISCUSSION

The different chemistries available for making SBMs allows the operator choices when using the muds for drilling a well. The properties of synthetic fluids used in the Gulf of Mexico today to make drilling muds are given in Table I. The first generation of synthetic fluids were PAOs and esters. These materials provided technical performance that was equal to or better than that of an OBM, and because of their low toxicity, the drill cuttings could be discharged into the ocean. A second generation of synthetic fluids, LAOs and IOs, are used singularly or as blends with other synthetics. Cuttings produced when using these muds can also be discharged on site.

The lower viscosity of the second generation synthetic fluids leads to better rheological control in the muds and they have become the preferred materials of use. The ability to control low temperature viscosity becomes more important at deeper water depths where temperatures are in the low 30's (°F). Low temperature results in viscosity increases in the mud as it travels through the water column to the surface. IOs have lower pour points than LAOs (Table I) which allows for more rheological flexibility at lower temperatures.

SBMs are invert emulsion muds and thus are less reactive to water sensitive formations providing better hole stability, filter cake formation and drill rates. Enhanced hole stability provides better solids removal because of better mud velocities due to in-guage hole and reduces maintenance time while tripping (moving in and out of the hole), casing and cementing. Stable filter cake provides lower drag and torque and less stuck pipe particularly while drilling deviated wells.

These benefits result in less nonproductive down time during drilling which can lower costs more than the enhanced rate of penetration SBMs provide. Operators choose SBMs to reduce risks and save time when drilling offshore through difficult water sensitive formations. With expensive drill rig day costs for these offshore operations, SBMs have proven themselves to have substantial economic benefits.[2]

The environmental properties of synthetic fluids used in SBMs are excellent because of their low toxicity and biodegradability. This is due to their controlled synthesis from purified feedstocks to provide products that are typically free of PAHs. Removal of these priority pollutants greatly reduces fugitive emissions and worker exposure.

The use of SBMs and cuttings discharge criteria are currently piggy backed onto EPA regulations governing WBMs. Because of this, SBM well drill cuttings can be discharged at the well site provided they pass the mysid shrimp toxicity test and are free of crude and diesel oil contaminates. The EPA has now defined synthetics as materials produced by the reaction of specific purified chemical feedstocks, as opposed to traditional base fluids obtained through refining processes. Also the EPA is working to develop regulations specific to their use.

All synthetic materials used to produce SBMs meet the EPA's current toxicity effluent limit guideline for cuttings disposal with a mysid shrimp LC_{50} of 30,000 ppm suspended particulate phase. Because SBMs are invert emulsions, the organic phase tends to stick to the drill cutting's surface and can be carried to the sea floor. This changes the focus of toxicity concerns to the benthic communities that are exposed to these cuttings. There is currently no test accepted by the EPA to measure benthic toxicity of SBMs in the Gulf of Mexico.

The invert emulsion nature of SBMs also causes a problem measuring crude oil contamination in drilling muds using the current static sheen test developed for WBMs. The synthetic itself is lighter than water and can form a sheen giving a false positive, or stick to the cuttings and carry crude oil contamination to the sea floor producing a false negative. In contaminated SBM lab samples crude levels of up to 20 wt % have passed the sheen test.

The EPA recognizes the problems with the current regulatory toxicity and compliance monitoring tests developed for WBMs do not adequately address SBMs. The EPA is now working with the National Oceans Industry Association and the American Petroleum Institute to develop tests to measure the benthic toxicity for muds and crude oil contamination.

Synthetic fluids are biodegradable as measured by the difficult BODIS marine aerobic assay test. These studies show a trend that generally follows the molecular weight (MW) of the fluids for LAOs and IOs. The order of biodegradability generally increases as the MW decreases from that of PAOs to LAOs and IOs, PAOs<LAOs/IOs<esters (Figure 5). This trend is opposite that for mysid shrimp toxicity where toxicity tends to increase as MW decreases. When choosing a synthetic fluid for preparing a drilling mud a balance between biodegradability and toxicity must be reached. This balance is set by regulations governing the drilling area.

Other trends that follow the MW of synthetic fluids are skin compatibility and flash point, which increase as MW increases, and pour point and viscosity both decrease with decreasing MW.

CONCLUSIONS

Synthetic fluids have excellent physical properties suitable for producing invert emulsion based muds, SBMs. Their low toxicity provides improved worker safety, reduces environmental hazards and lessens fugitive emissions of PAHs The number and type of synthetic fluids available give operators choices of performance when considering the use of SBMs for drilling wells. These materials are also marketed globally to meet drilling needs in the Gulf of Mexico and around the world.

REFERENCES

1. Peresich, R.L., Burrell, B.R. and Prentice, G.M., "Development and Field Trial of a Biodegradable Invert Emulsion Fluid," paper SPE/IADC 21935 presented at the 1991 SPE/IADC Drilling Conference, Amsterdam, Mar. 11-14, 1991.

2. Burke, C. and Veil, J.A.: "Synthetic-based Drilling Fluids have many Environmental Pluses," paper presented at the 1995 SPE/EPA Environmental Conference, Houston, TX, Mar. 27-29.

Figure 1: Synthesis of LAOs and IOs

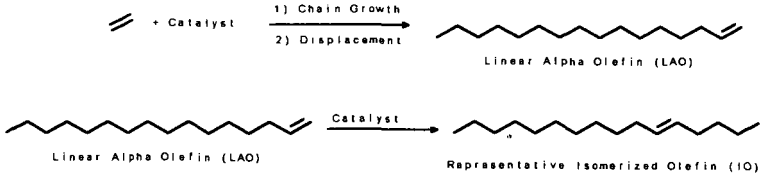

Figure 2: Synthesis of Polyalphaolefins

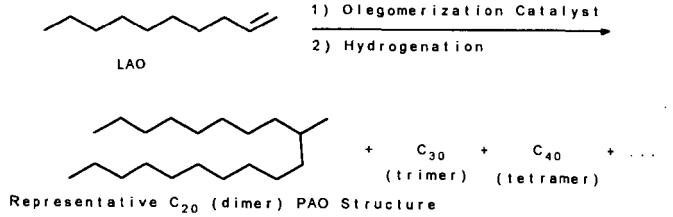

Figure 3: Synthesis of Esters

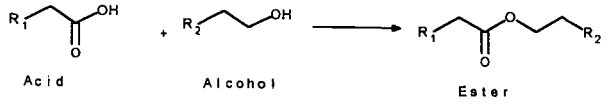

R_1 and R_2 represent different hydrocarbon side chains

Figure 4: Refining of Diesel and Mineral Oils

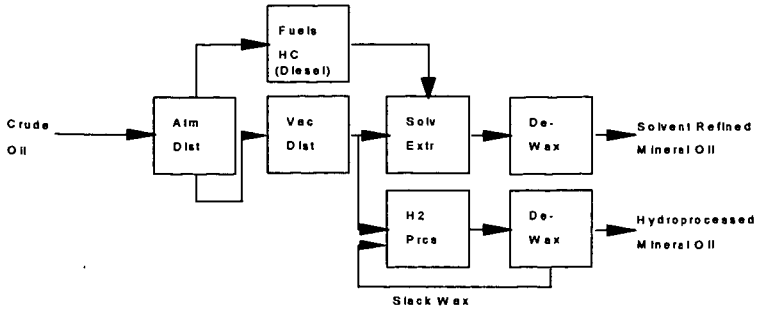

Table I: Physical Properties of Synthetic Fluids

	Viscosity (cSt) @ 40 °C	@ 100 °C	Pour Point (°C)	Flash Point (°C)
2 cSt PAO	5.50	1.80	<-65	155
4 cSt PAO	16.8	3.90	<-65	215
Ester	5.13	1.82	-33	170
C1416 LAO	2.09-2.11	0.97	-12 to -9	114
C1618 IO	3.09-3.37	1.30-1.39	-24 to -14	134-137
C1618 LAO	2.98-3.08	1.27-1.29	3-9	146

Figure 5: Trends in Synthetics for Biodegradability and Toxicity with Carbon Number

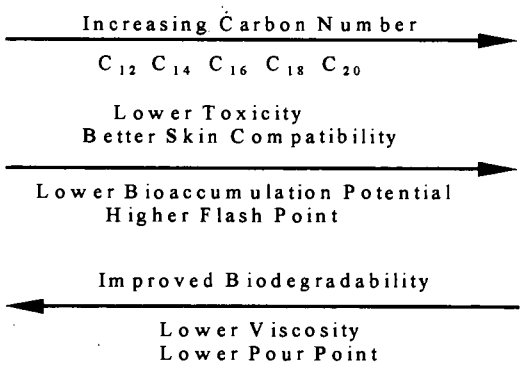

THE DETECTION OF CRUDE OIL CONTAMINATION IN SYNTHETIC BASED DRILLING MUDS

Jim Story
Amoco Corporation
Building 600-2034
150 West Warrenville Road
Naperville, IL 60563-8460

Burney Lee
Amoco Chemicals
Building 503-1330
150 West Warrenville Road
Naperville, IL 60563-8460

KEYWORDS: Synthetic Based Mud, Crude Oil Contamination, Detection

ABSTRACT

In response to a need for a simple compliance monitoring test for crude oil contamination in synthetic drilling muds an inexpensive and rig-worthy ultraviolet (UV)/chromatography method was developed. The method utilizes prepackaged silica gel solid phase extraction columns to separate various mud components from the synthetic base and crude oil contaminates using common organic solvents. The synthetic fluids along with any crude oil are eluted down the column. Observance of any UV induced fluorescence along the column can be attributed to crude oil contamination as synthetic base fluids do not contain fluorescent entities. Detection limits to 0.05 wt% crude oil contamination were found.

INTRODUCTION

The offshore drilling conditions in the Gulf of Mexico are demanding with water depths up to 6,000 feet through reactive clays and around salt formations often using deviated drilling techniques. These severe conditions require the use of inverse emulsion drilling muds or oil based muds (OBMs) that provide optimum drilling performance. In an invert emulsion mud, there is continuous outer organic phase that contains the mud solids and an internal aqueous phase dispersed (emulsified) as separate droplets. The continuous organic outer phase is water insoluble and thus reduces the amount of interaction of the drilling mud with water sensitive formations leading to better solids control, cuttings removal, hole stability and drilling rates.

Traditionally the invert emulsion muds used diesel or mineral oil for the organic phase, OBMs. However, on site discharge of drill cuttings from drilling rigs produced from wells using OBMs was banned in the early 1990's. This created a need and lead to the development of synthetic based muds (SBMs). These drilling muds are also inverse emulsions and provide the same or improved drilling characteristics as an OBM. A key advantage to their use is that the low toxicity of the synthetic fluid resolves many of the environmental issues associated with the use of invert muds and in particular allows for discharge of the drill cuttings. The low toxicity also reduces pollution hazards and worker exposure to diesel oil.

Current EPA regulations do not specifically address SBMs today but the EPA is working with industry groups, the American Petroleum Institute (API) and the National Oceans Industries Association (NOIA), to develop these regulations. An important compliance test needed for WBMs is one to detect crude oil contamination. The static sheen test developed for water based muds (WBMs) is ineffective for SBMs. The synthetic itself is lighter than water and can form a sheen giving a false positive. Also because the mud is an invert emulsion mud with a water insoluble external phase, the mud can stick to the drill cutting's surface and be carried to the seafloor hiding any contamination to produce a false negative. SBMs containing up to 20 wt% crude oil contamination have shown negative static sheen tests in lab tests. A joint API/NOIA analytical work group with EPA participation was formed to find a suitable test to determine crude oil contamination in SBMs. The suggested requirements for the analytical method were:

- comparable detection limits to static sheen test, 1 wt% crude
- suitable for rig site (rig motion, power fluctuations, rugged, small spaces)
- single pass/fail limit
- minimal false positives
- works with a variety of crude oils and synthetic base oils
- easy operation (minimal training required)
- reasonable costs.

Using these criteria, a simple effective chromatographic test method using black light fluorescence detection for crude oils was developed. It uses readily available rugged equipment, prepackaged activated silica solid phase extraction columns, and common solvents. The test meets the detection requirements and is easy to run using minimal space and simple equipment.

EXPERIMENTAL

Determination of Crude Oil Contamination in Drilling Fluids - Field Method

The method is intended for the on-site measurement of total crude oil in new or contaminated drilling fluids. It relies upon fluorescence of the aromatics in the crude oil for detection and measurement of crude oil contamination. Aromatics are visualized by fluorescence on an active silica column during separation from other components of the sample. The liquid portion of the drilling fluid is separated from the mud solids by settling. Centrifugation may be necessary in rare cases to separate the liquid and solids. One drop of the liquid is carefully placed on an active silica solid phase extraction (SPE) column using a pipet or medicine dropper. One half ml. of isopropanol is added and the column is placed under a black (mercury vapor UV) light. The fluorescing aromatics in the sample are observed as they move down the column and the concentration of crude is determined by visual comparison of the sample fluorescence with that of standards prepared in hexadecane solvent from the suspect crude. Alternatively the fluorescence intensity can be compared to a polynuclear aromatic standard reference, such as phenanthrene. This might be done in those cases where no samples of the potential crude contaminant exist, as is the case when drilling through new formations.

The apparatus consists of solid phase extraction (SPE) columns packed with active silica. For this work we used SPE columns manufactured by J.T. Baker and marketed by a number of distributors. They were used as received. These columns will become deactivated if saturated by water, so they should be kept carefully sealed from atmospheric humidity until a few minutes before use. A 300mw black light emitting wavelength 254 nm was used for visualization. Isopropanol was purchased as chromatographic grade. Phenanthrene and hexadecane were reagent grade.

This work was part of a collaborative test study to determine the best ways to identify crude contamination of drilling muds. Sixty samples of muds were prepared from five different crude oils and three different fluids by a drilling company. The fluids used to prepare the samples were enhanced mineral oil fluids (EMO), internal olefin fluids(IO), and linear alpha olefin-ester fluids (LAO). Crude oil concentrations in the prepared samples were 0.5%, 1%, 2% and 5% v/v. Samples of the presumably crude-oil free mud were also provided. The crudes were chosen for variety. Four of the five crudes were fairly typical, fluoresced strongly, and could be easily detected. Most crudes would be expected to behave in this way. The fifth crude, labeled crude D, was extremely light and possessed little aromatic content. Instead of the normal brown to black color it was yellow, suggesting that it was more typical of a condensate than a real crude. Gas chromatographic analysis confirmed that the crude contained only the light fraction, and was thus not typical of what might be encountered while drilling.

In this work the fluorescence intensity was used to determine the presence or absence of crude oil, and to rank the samples in order of crude concentration. Presence of crude was defined as observing a fluorescence intensity equal to or greater than that of a 0.5% solution of the same crude diluted with hexadecane and analyzed in the same way. A sample of the uncontaminated mud was also run to define a blank level.

RESULTS

In order to define a detection limit for the method, a series of dilutions of phenanthrene in hexadecane were run. These experiments showed the limit of detectability for the method to be approximately 50ppmw/v phenanthrene.

As mentioned above, one of the crudes, the crude labeled D, used in preparing the samples was, in actuality, a condensate and not a realistic sample. The aromatics level in this crude was very low and greater difficulty was encountered in detection of this crude than any of the others.

Drilling fluids typically also contain additives which may fluoresce. These additives are often very polar structures. Samples of all three fluids showed varying levels of a fluorescing material which was strongly retained at the top of the silica column and resolved chromatographically in the SPE column from the crude oil aromatics. All twenty spiked samples of the enhanced mineral oil fluids tested positive for at least 0.5% crude oil. All of the samples fluoresced at levels consistent with their crude oil concentration. The blank mud showed no fluorescence, except for the small band at the top of the column, presumably due to the additive fluorescence. Each of the crude oil/mud samples also showed the additive fluorescence band at the top of the column.

When the internal olefin (IO) based mud was analyzed, it was found that the blank mud containing supposedly no crude actually contained a small amount of fluorescing material. Analysis of the mud liquid phase by GC-MS showed that the mud was contaminated with polycyclic aromatics (PAH's). It was later discovered that this mud actually was a field mud. The presence of PAH's created a significant blank fluorescence which had to be considered in evaluating the actual samples. However interference was minimal and analysis of all twenty spiked IO samples showed all samples to test positive for at least 0.5% crude, except for 2 of the 0.5% samples, which were only marginally positive. One of the two samples was the 0.5% sample of the condensate, crude D

The LAO-ester fluid mud samples were also prepared from the same used mud as the IO samples. All spiked LAO samples tested clearly positive again with the exception of the 0.5% sample of crude condensate D.

CONCLUSIONS

All samples correctly tested positive at the required 1.0% level. The test resulted in clear positive results for all but three of the sixty spiked samples at the 0.5% level. Two of the three questionable results were for the atypical crude D, in reality a condensate. Only one of the sixty spiked samples would have been judged erroneously to be below the 0.5% level, and that was the 0.5% LAO sample of crude D. Two of the three supposedly clean muds were found by this method in fact to be contaminated with low levels of crude oil. This was confirmed by GC-MS analysis of the mud fluid and by admission of the preparer that the mud had already been used in a formation. The test is thus very sensitive, sensitive enough to detect ppm levels of crude oil in muds. For accuracy in predicting contamination at or above a certain level, a comparison or reference standard, such as a solution of crude oil or phenanthrene, must be used. Any sample producing fluorescence above that standard is judged to test positive.

This method has several advantages:

- It is capable of being used at the drilling site since it requires minimal equipment and training and uses inexpensive and safe equipment and material
- It is rapid (<5 minutes), simple, and inexpensive
- It works with all synthetic fluids and gives no false positives at the 0.5% level. Polar surfactants which fluoresce do not interfere because they are chromatographically separated from the fluorescing crude components.
- The threshold limit for positive report can be set at any level above about 0.1% crude oil because of the sensitivity of the method.

REVERSE PHASE EXTRACTION METHOD FOR DETECTING OIL CONTAMINATION IN SBM

Jerry L. Sides and Kerry Spilker
Texaco EPTD, Briarpark Technical Facility
Houston, TX

Keywords: synthetic base drilling mud, static sheen test, C_{18} SEP PAK®.

ABSTRACT

Waters Associates SEP PAK® reverse phase cartridges are used to separate and collect crude oil contamination from synthetic base drilling mud (SBM) in a quick and easy procedure for subsequent blacklight (ultraviolet) detection. The method is intended as a positive/negative test to determine the presence of crude oil in SBM prior to dumping drill cuttings overboard in the offshore environment. The test should be comparable to the accepted static sheen test presently used for water base muds.

INTRODUCTION

The regulatory permitting agencies that oversee the offshore oil and gas operations depend on a static sheen test (1) to determine if drill cuttings recovered from the drilling mud are contaminated with crude oil prior to dumping cuttings in the open sea environment. Crude oil contamination can result when an oil bearing geologic formation has been penetrated during the drilling operation. The static sheen test is simple and will indicate if the cuttings contain oil that could cause a sheen on the sea surface. The test is adequate when conventional water based drilling muds (WBM) are used. If the water based mud is replaced with an oil based mud (OBM), the drilling operation is greatly enhanced when drilling certain geologic structures, deviated wells and horizontal wells. Such muds have crude oil or a refined oil as the continuous phase. These OBM's and the cuttings separated from them can not be dumped in the offshore environment because of their toxicity. The industry has found certain synthetic solvents such as internal olefins (IO), esters, linear alpha-olefins (LAO) and enhanced mineral oil (EMO), to be environmentally friendly substitutes for conventional OBM's which are not environmentally acceptable. Industry studies have shown that crude oil contaminated cuttings in SBM systems do not produce a static sheen as normally seen for oil contaminated cuttings from WBM. These synthetic base mud (SBM) systems contain chemical additive packages to stabilize the drilling fluid emulsion and to maintain proper drilling mud properties such as viscosity and gel strength. The emulsifier package interferes with the static sheen test by emulsifying any oil contamination on cuttings from the SBM systems. A test that is similar to the static sheen test for WBM systems is needed by the industry to insure that oil contaminated cuttings from SBM systems are not dumped into the sea.

An industry work group (API-Synthetic Based Mud Analytical Work Group) has determined that the new test should have certain desirable characteristics. The test should work well on an offshore platform; have a detection limit comparable to the static sheen test ($\geq$ 0.5% crude oil contamination); have reasonable cost; be reproducible; use equipment that is easy to operate with a minimum of expertise; work well with a variety of crude oils and SBM's; not be prone to false positives; and have a pass/fail limit.

EXPERIMENTAL

A whole mud sample is taken at the drilling site for this test. It is necessary to have the nonaqueous phase in a polar solvent to pass through the C_{18} SEP PAK® for separation of the emulsifier from the crude oil components. After looking at several solvents, it was found that extraction of the whole mud with isopropyl alcohol (IPA) uniformly extracts the crude oil from the mud system and also has enough polarity to carry the emulsifiers through the C_{18} SEP PAK® while leaving the crude oil behind. IPA also has the added benefit of being a familiar, available and relatively safe solvent for on-site use.

The developed procedure has the following steps for extraction.

1. Transfer 0.10 ml of SBM sample to a large (16x125-mm) test tube and add 10 ml of solvent grade IPA. Stir the solvent and SBM thoroughly (10 sec. on a Vortex mixer) and let stand to allow the solids to separate.
2. Filter about 4 ml of the extract from the test tube through a syringe cartridge filter (PTFE syringe type filter, 25-mm, 0.45-µm) into a second test tube.
3. Precondition a C_{18} SEP PAK® cartridge by attaching to a five-ml syringe and pushing 3 ml of solvent grade IPA via the syringe through the SEP PAK®.
4. Transfer 0.50 ml of the extract (Step 2) to the syringe barrel and add 3 ml of IPA. Push the extract and IPA through the preconditioned C_{18} SEP PAK® cartridge to separate any crude oil contamination from the extract. Push another 2 ml of solvent grade IPA through the SEP PAK®.

5. Place the C_{18} SEP PAK® cartridge under the blacklight and observe the absence or presence of fluorescence as compared to a blank. Presence of fluorescence is a positive test for crude oil.
6. A blank is prepared by carrying out the procedure on a sample of the SBM as sent from the supplier (has not been circulated downhole).

To assure the quality of the IPA and filters, a reagent blank is prepared by passing 5 ml of the IPA through a PTFE cartridge filter and collected in a small test tube. Add 0.5 ml of the filtered IPA and 3 ml of IPA to a syringe and push through a preconditioned SEP PAK® cartridge (step 3 above). Add 2 ml of IPA to the syringe barrel and push it through the cartridge. Check the SEP PAK® cartridge under the black light for fluorescence. No fluorescence should be observed if the IPA and the filter are of good quality.

The procedure was carried through on laboratory prepared SBM drilling fluids that had been spiked with known amounts of crude oil. The laboratory samples were comprised of sets of three SBM types, an EMO, an IO, and a mixed Ester/LAO. Each SBM was spiked with five different crude oils at four different oil concentrations (0.5, 1.0, 2.0, 5.0 % by wt) resulting in 20 spikes and a base mud blank for each of the three SBM sample sets. The sample designations and API gravities for the crude oils are: A, 28°API; B, 31°API; C, 36°API; D, 51°API; E, 24°API. Simulated distillations of the five crude oils by gas chromatography (ASTM D2887) were performed to characterize and compare the relative boiling point and molecular size distributions.

Five observers independently determined the presence or absence of fluorescence by comparing the SEP PAK® cartridges developed for each of the prepared oil spiked SBM's to a blank in a view box with a built in UV light source. The observation was made by placing the test cartridge next to a blank cartridge corresponding to the SBM with no oil spike.

RESULTS AND DISCUSSION

Fluorescence of crude oil by ultra-violet electromagnetic energy is due to molecular excitation of multi-ring aromatic hydrocarbons and heterocyclic compounds. Non-aromatic, but highly conjugated compounds may also fluoresce (2), and such compounds and smaller heterocyclics may exist in the SBM emulsifier packages. The reverse phase extraction method passes these more polar emulsifiers through the SEP PAK® cartridge while retaining the less polar aromatics and heterocyclics found in crude oil. This test assumes that crude oil compounds are retained on the SEP PAK® cartridge, and that the concentration of fluorescent compounds in the crude oil are high enough for detection at about 0.5% or higher concentration of crude oil in the SBM.

The observation of fluorescence by comparing cartridges is somewhat subjective when there is a very low concentration of oil on the developed cartridge. Absence of fluorescence was indicated by a "0" (negative test result) and presence by a "1" (positive test result). Five observers were selected to see if a consensus result would be found in each case. The observers were to report a positive test if the sample cartridge showed "more fluorescence" than the blank. Three of the observers were experienced laboratory experimentalists while two were contract technicians with about one-year laboratory experience. Tables 1 through 3 are summaries of the results of the five observers' readings for each of the three sets of SBM samples. Each sample was given the sum of the five observers' readings. Therefore, a summary value of "0" indicates that the reading was "0" (negative) for all five observers; and a "5" indicates the reading was "1" (positive) by all five observers. Values of 1, 2, 3, and 4 show non-agreement among the observers and indicate the difficulty in determining fluorescence for these samples.

The tabulated results show the test summary by SBM. The IO based mud (Table 2) appears to be slightly more sensitive to crude oil detection than the other two systems (Tables 2 and 3), since fluorescence was more often observed at the 0.5 % concentration.

Crude oil D (51°API) was only detected once at concentrations up to and including 5% in any of the SBM systems. The API gravity and lack of fluorescence leads to the belief that the oil is paraffinic with a low concentration of multi-ring aromatic molecules present. The gas chromatogram (Figure 1) of crude oil D confirms this idea. The chromatogram shows the relative carbon numbers for the straight chain paraffins. The carbon numbers and retention times are consistent in all of the figures. Crude oil D shows very little material after C 24.

Contamination of 2% or higher is consistently detected for crude oils A, B, C, and E in all of the drilling muds. The crude oils A, B, C, and E are similar in fluorescence sensitivity as shown by the split negative and positive readings by the observers at the 0.5% and 1.0% concentrations in the various SBM's. Gas chromatograms (Figures 2-5) for these oils are similar and contain significant amounts of high molecular weight oil (>C 24) that probably contains multi-ring aromatic compounds.

IV. Conclusions

The reverse phase extraction method for determining crude oil contamination in SBM's appears to have merit as a possible field test. The inability to detect the high API gravity paraffinic oil is obvious. Aside from this, the test meets the desirable characteristics determined by the industry

study group. It is comparable to the static sheen test in detection limits, can be performed offshore with reliable equipment by field personnel, is reasonably low cost, and has a single pass/fail end point.

The inconsistency of this test from one crude oil to the next is not unexpected. There is no standard crude oil that can be representative of all crude oils. This field test is to be applied during exploratory drilling where the oil encountered will be unknown. It is important to note that the toxic components in petroleum hydrocarbons are generally thought to be the multi-ring aromatics or polycyclic aromatic hydrocarbons (3). These components produce fluorescence. The paraffinic components do not fluoresce under the blacklight, but the paraffinic compounds are not detrimental to the environment. Effectively, the test could be determining the presence of the components that are environmentally unfriendly. The inability to detect high API gravity oils that are primarily paraffinic may not be a draw back to using this test.

REFERENCES

(1) Weintritt, D. J.; Qaisieh, N. S.; and Otto, G. H. *Oil & Gas Journal* **1993**, 91, No. 18, 77-78, 80, 82, 84.

(2) Guilbault, G.C.; *Practical Fluorescence*; Marcel Dekker, Inc.; New York, 1990.

(3) Neff, J. M.; *Polycyclic Aromatic Hydrocarbons in the Aquatic Environment*; Applied Science Publishers Ltd.; London, 1979.

Table 1: EMO SBM					
Oil	0% Oil	0.5% Oil	1.0% Oil	2.0% Oil	5.0% Oil
A	0	0	4	4	5
B	0	0	0	4	5
C	0	0	2	3	5
D	0	0	0	0	0
E	0	1	3	5	5

Table 2: IO SBM					
Oil	0% Oil	0.5% Oil	1.0% Oil	2.0% Oil	5.0% Oil
A	0	2	1	5	5
B	0	4	2	5	5
C	0	2	5	5	5
D	0	0	0	0	0
E	0	2	5	5	5

Table 3: Ester/LAO SBM					
Oil	0% Oil	0.5% Oil	1.0% Oil	2.0% Oil	5.0% Oil
A	0	0	3	5	5
B	0	0	3	5	5
C	0	2	3	5	5
D	0	0	1	0	0
E	0	1	5	5	5

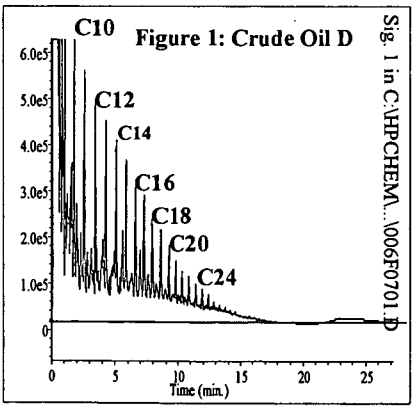

Figure 1: Crude Oil D

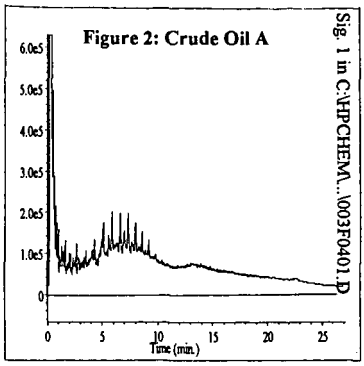
Figure 2: Crude Oil A
Sig. 1 in C:\HPCHEM\..\003F0401.D
6.0e5
5.0e5
4.0e5
3.0e5
2.0e5
1.0e5
0
0 5 10 15 20 25
Time (min.)

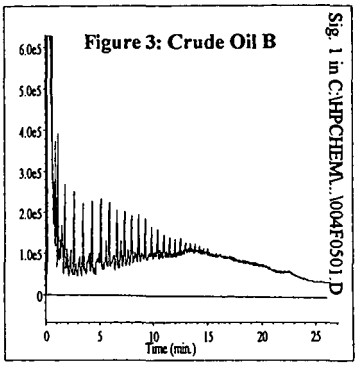
Figure 3: Crude Oil B
Sig. 1 in C:\HPCHEM\..\004F0501.D
6.0e5
5.0e5
4.0e5
3.0e5
2.0e5
1.0e5
0
0 5 10 15 20 25
Time (min.)

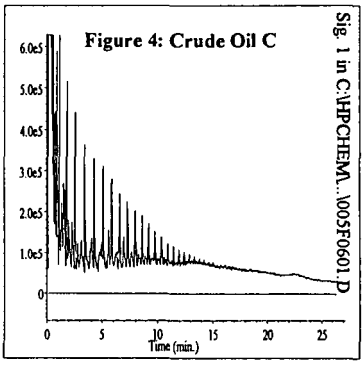
Figure 4: Crude Oil C
Sig. 1 in C:\HPCHEM\..\005F0601.D
6.0e5
5.0e5
4.0e5
3.0e5
2.0e5
1.0e5
0
0 5 10 15 20 25
Time (min.)

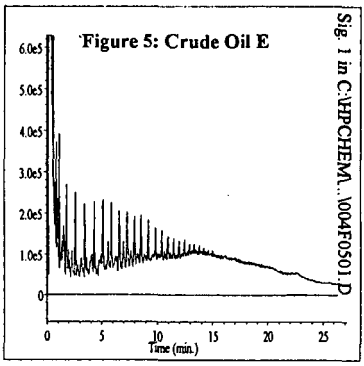
Figure 5: Crude Oil E
Sig. 1 in C:\HPCHEM\..\004F0501.D
6.0e5
5.0e5
4.0e5
3.0e5
2.0e5
1.0e5
0
0 5 10 15 20 25
Time (min.)

THE FATE OF SCALE INHIBITORS IN OIL/GAS PRODUCTION

Jianjun Xiao, Amy T. Kan, Mason B. Tomson
Department of Environmental Science and Engineering, Rice University, Houston, TX 77005

Keywords: Phosphino-polycarboxylic acid (PPCA); Potentiometric titration; Calcium phosphino-polycarboxylate.

ABSTRACT

The thermodynamic properties of the scale inhibitor, phosphino-polycarboxylic acid (PPCA) and of its calcium complexes under conditions of high ionic strength and high temperature have been studied by potentiometric titration. Applying the electrostatic theory for polymers gives dissociation constant K_M for $ML \leftrightarrow M+L$ as $pK_M=pK_{Mint}+zf\theta_u$ where L stands for polymer ions, pK_{Mint} stands for intrinsic constant, z is the charge of the small ion M which can be H^+ and any metal ion, f is a parameter related with polymer characteristics and θ_u stands for the dissociation fraction of the polymer ion. A general equation for f is obtained: $f=2.757-1.056I^{1/2}+0.220I$ where I stands for ionic strength. The intrinsic constant for proton dissociation pK_{Hint} (when M is proton) is assumed to be: $pK_{Hint}=4.798-0.954I^{1/2}+0.246I-187.8/T$ where T stands for temperature in Kelvin. For calcium ion (M is Ca^{2+}), the intrinsic constant is: $pK_{Mint}=3.928-2.631I^{1/2}+0.738I-1099.4/T$. Also investigated are calcium-PPCA precipitation and dissolution. An empirical dissolution reaction is observed as: $Ca_3(A\text{-}A\text{-}A)_{2\,(S)} \leftrightarrow 3Ca^{2+}+2(A\text{-}A\text{-}A)$, of which the solubility product $Ksp=[Ca]^3[A\text{-}A\text{-}A]^2$ can be expressed as: $pKsp=34.02-0.832I^{1/2}+0.762I-6839.5/T$. Here, (A-A-A) stands for an arbitrary unit of three functional groups (A). Therefore, PPCA concentration and its species distribution in any oil/gas production can be predicted by these equations and consequently the efficiency of PPCA as a scale inhibitor for a specific well can be evaluated and can be applied in squeeze design.

INTRODUCTION

Phosphino-polycarboxylic acid (PPCA), $H\text{-}\{CH_2CHCOOH\}_x\text{-}POOH\text{-}\{CH_2CHCOOH\}_y\text{-}H$, is different by only one group (phosphino group) from polyacrylic acid (PAA). It is widely used in oil fields as a scale inhibitor because of its good quality, low cost and environmental acceptability. Chang and Patel (1) have studied PPCA under typical boiler conditions and found that as a scale inhibitor (for $CaCO_3$, calcium hydroxyapatite and iron oxide), PPCA has advantages over PAA and phosphonates in thermal stability, dispersion and iron transport. Some other research (2,3) implies that PPCA or its derivatives have potential to be multifunctional inhibitors in boilers, cooling water formulations and oil wells. Rabaioli and Lockhart (4) have investigated the precipitation conditions and precipitate yield of CaPPCA and its solubility in a brine system. The sharp contrast of high solubility to the observed very low concentration of inhibitors in the return produced water of oil wells was explained as a kinetically controlled dissolution.

Taking into consideration the great potential of application of PPCA in many aspects and the variety of the conditions of those applications, this paper tries to explore the fundamental aspects of the solution chemistry of PPCA under various harsh conditions and to provide basic data for its application. This includes constants of proton dissociation, metal complexation of PPCA, and precipitation/dissolution of CaPPCA. They all together determine the efficiency of PPCA as a scale inhibitor and the lifetime of a squeeze.

In structure, PPCA is similar to PAA which is used as a standard polymer for studying properties of linear polyelectrolytes. For this reason, the basic concept in this study is transplanted from those developed for PAA. On the base of research by Debye and Huckel (5), Falkenhagen (6), Kirkwood and Poirier (7), Hill (8), Hermans and Overbeek (9), Tanford (10,11) et al, applying electrostatic theory to PPCA, one can easily derive the following hypothetical reaction and their constant expressions:

$$ML \leftrightarrow L + M, \quad pK_M \qquad (1)$$

$$pK_M = -\log\frac{[M][L]}{[ML]} = pM - \log\frac{\theta_u}{\theta_M}$$

$$= pK_{M\,int} + zf(R,r,\kappa)\theta_u \qquad (2)$$

where L is an arbitrary combined unit of z functional groups (monoacids, A), L=zA and [L]=[A]/z, and ML is electroneutral. M with charge z represents any cation which can associate with PPCA. For instance, when M stands for proton, H^+, z=1 and L is just one group while for Ca^{2+}, z=2 and L is an arbitrary unit of any two groups. The parameter f is a function of the polymer size R, small cation (M) size r and Debye-Huckel parameter κ which is then related with ionic strength. Of course f is also a function of temperature. pK_{Mint} is the so-called intrinsic constant. θ_u stands for dissociation fraction of PPCA, $\theta_u=z[L]/C_A=[A]/C_A$ while θ_M stands for

the association fraction of PPCA by M, $\theta_M = z[ML]/C_A$ with C_A meaning total PPCA concentration in normality.

The second term in equation 2 represents the electrostatic effect of neighboring dissociated groups on the given group. Under certain conditions, R might be independent of the dissociation fraction so that $zf(R, r, \kappa)$ in the second term of equation 2 might be a constant through a titration. Therefore, pK_M is linear to dissociation fraction θ_u. Applying this to titration data can yield pK_{Mint} and $f(R, r, \kappa)$ from a plot of pK_M versus θ_u.

After pK_Ms are available, precipitation/dissolution of metal polymer precipitates can be analyzed. However, this equilibrium is very complicated and no definition of solubility product for metal polymer precipitates is available from literature. Therefore, a hypothetical precipitate and its dissolution equilibrium are assumed to be:

$$M_mL_{l\,(c)} \leftrightarrow mM + lL\,,\ K_{sp} \qquad (3)$$

$$K_{sp} = [M]^m[L]^l \qquad (4)$$

where L is an arbitrary unit (statistically) of x As (univalent). Therefore, L=xA and [L]=[A]/x. Furthermore, the electroneutrality requires xl=mz. Thus equation (4) becomes:

$$K_{sp} = [M]^m\,[A]^l\,(\frac{1}{mz})^l \qquad (5)$$

or

$$\log[A] = \{\frac{\log(K_{sp})}{l} - \log(\frac{1}{mz})\} - \frac{m}{l}\log[M]$$

$$= \text{constant} - \frac{m}{l}\log[M] \qquad (6)$$

Equation (6) shows that m and l can be obtained from the plot of log[A] vs. log[M]. In this plot, the slope is -m/l. Since m, l and x should be integral, m/l is the common fraction of the slope. For example, if the slope is -m/l=-0.33, take l=3, m=1, and x=0.333z, thus z must be 3; if -m/l=-1.5, then take l=2, m=3, and x=1.5z.

EXPERIMENTAL

Chemicals: Phosphino-polycarboxylic acid (PPCA) was from FMC Co., 50%, MW ~3600. NaCl, used for adjusting ionic strength, was from Fisher Scientific Co., 99.4%. $CaCl_2{\cdot}2H_2O$, used for titration , precipitation and stock solution, was from Fisher Scientific Co., 76.1% ($CaCl_2$). Acid/base titrant of 1.600±0.008 N and 0.1600±0.0007 N NaOH cartridges and EDTA titrant cartridges were from HACH Co. All stock solutions were made with deionized water.

Potentiometric titration: Solutions of different concentration of PPCA with or without Ca^{2+} were titrated by NaOH in a jacketed beaker. The ionic strength of the solutions was adjusted by NaCl and the temperature was monitored by a temperature circulator within ±0.1 °C. Each titration was finished under a fixed condition. pH was measured by an Accumet model 15 pH meter (Fisher Scientific Co.) with a Ross combination pH electrode (Orion Inc.). Before each titration, the pH electrode was refilled with new filling solution (Orion Inc.) and was kept in a storage solution at the same temperature for about 2 hours to be stabilized. Immediately before and after each titration, the stabilized pH electrode was calibrated. All operations relevant to titrations were run under N_2 atmosphere.

Precipitation/solubility product: Precipitation was carried out by slowly titrating PPCA solution [using a syringe pump (Harvard Co.)] into a bulk solution of 1N NaCl-$CaCl_2$-1mM NaAc at pH5.5 and 70°C under stirring. The Ca^{2+} concentration was made so that after equivalent precipitation, the remaining Ca^{2+} concentration in solution was 0.1M. pH was simultaneously monitored at pH 5.5. After the titration precipitation was finished, the slurry was kept stirring about 5 hours and then transferred into an Amicon cell fitted with an Amicon YM 10 membrane to do diafiltration/maturation under 70°C and stirring for a week with an inflow of stock solution of 1N NaCl-0.1M $CaCl_2$-1mM NaAc at pH5.5 and 70°C. The flow was monitored by a pump (Pharmacia LKB) at about 90 ml/hr. After a week, the produced solids-solution mixture was kept in a 70°C oven for static maturation. Samples were taken at different stages to study the evolution of the stoichiometry of the precipitate and its solubility. All solid samples were put through a 0.2 μm microfilter and washed with deionized water many times at the same temperature. Solids collected in this manner were used to study the stoichiometry while the filtrates were collected for quantitative analyses to provide data for the study of thermodynamic properties. Also the samples at different stages were used to explore the relationship between the solubility and other condition variables, such as ionic strength, temperature and different Ca^{2+} concentrations.

RESULTS AND DISCUSSION

The plots of acid/base titration curves (pH vs. dissociation fraction, θ_u) at different ionic strength and temperature in the absence of Ca^{2+} are shown in figures 1 and 2, respectively. As the figures show, with an increase of ionic strength, pH decreases (figure 1)with the same dissociation fraction, implying that the dissociation constant decreases. While temperature has little effect on the PPCA association/dissociation (figure 2). Data treatment shows that pK_H is linear with θ_u in the range of dissociation fraction 0.3 to 0.95, especially at higher ionic strength ([NaCl]>0.05M). This observation is consistent with that by Miyajima et al (12) for PAA and other observations (13,14,15,16). It was also observed that the concentration of polyacid has a slight influence on the dissociation constant but at a higher concentration and higher ionic strength, pK_H has no significant change with concentration, which is consistent with findings for PAA by Nagasawa et al (12), Arnold and Overbeek (17), and Samelson (18). Quantifying all relationships between the dissociation constant and condition variables by the nonlinear regression method, a general equation for proton dissociation of PPCA acid was obtained:

$$pK_H = (4.798 - 0.954\sqrt{I} + 0.245I - \frac{187.8}{T}) + (2.757 - 1.056\sqrt{I} + 0.220I) * \theta_u \qquad (7)$$

From this equation, it is easy to get $pK_{Hint}(I=0,T=298K)=4.17$ for PPCA which is smaller than $pK_{Hint}=4.28$ for PAA by other researchers (13), $pK_H=4.76$ for acetic acid and $pK_{Hint}=4.64$ for glutaric acid under the same conditions.

Figures 3 and 4 show the similar titration curves but at the presence of Ca^{2+}. Applying equation 2 and equation 7 to these titration curves, a general equation was then obtained by least square method:

$$pK_M = (3.928 - 2.631\sqrt{I} + 0.738I - \frac{1099.4}{T}) + 2(2.757 - 1.056\sqrt{I} + 0.220I) * \theta_u \qquad (8)$$

This equation gives $pK_{Mint}(I=0, 298K)=0.24$, comparing with $pK_M=1.06$ for glutaric acid (H_2L)-calcium complexation (19) and 1.16 for succinic acid-calcium (20). But extrapolation to I=0 for both pK_{Hint} and pK_{Mint} should be careful since no titration is carried out at very low ionic strength where constants are extremely sensitive to that.

Once both pK_H and pK_M are set up, solution equilibria analysis can be done for a Ca-PPCA solution system. Sampling the long-time matured precipitates, solubility experiments under wide diverse conditions were carried out. The solid speciation indicated that these long-matured precipitates are composed of only Ca and PPCA and the ratio is: Ca:PPCA=1:1 (in equivalence). The formula can thus be written as: $[Ca(CH_2CHCOO)_2 \cdot xH_2O]_n$ (-POO-). Figure 5 shows the results of the dissolution experiments on these precipitates designed for solubility product at pH 5.5, 70°C and in 1.0m NaCl solution. It implies that the product $[Ca]^{1.5}[A]$ or $[Ca]^3[L]^2$ is constant (A represents free monomer, L represents a unit of certain monomers). Considering electroneutrality and applying equations (5) and (6), we let l=2, m=3, and x=3 and the precipitate of CaPPCA behaves like the simple crystals of calcium-trimer precipitate. Applying this semi-empirical definition of solubility product to solubility data, a plot of pK_{sp} vs. ionic strength at differing temperature was obtained as in figure 6. And further nonlinear regression analyses yield the equation:

$$pK_{sp} = 34.02 - 0.832\sqrt{I} + 0.762I - \frac{6839.5}{T} \qquad (9)$$

It should be pointed out that at a different temperature, the crystalline morphology of the precipitates might be different. This equation might therefore not reflect the real physical details of pK_{sp} but just a mathematical expression. However, the equilibria calculations showed that the calculated solubility of CaPPCA is very close to the experimental result, and more than that, is reasonably consistent with that of CaPAA from literature (21).

The predicted titration curves by these numerical equations also show the very good consistency with titration data, as shown by lines in figures 1 and 3.

With these constants, one can evaluate the feasibility of PPCA as a scale inhibitor in a specific well. Table 1 gives 3 field case studies. In this table, 'equil PPCA' means the equilibrium concentration of PPCA calculated from those equations above under the well condition and 'min PPCA' means the minimum PPCA concentration required for inhibiting scale formation in this specific well and is calculated from the Scalesoft™ (A scale control and treatment software produced by the Brine Chemistry Consortium in Rice University). In well #1,

PPCA can not be applied as an inhibitor in a precipitation squeeze because the equilibrium concentration can not meet the minimun concentration needed. Well #2 doesn't need any inhibitor. PPCA can work well as a scale inhibitor in Well #3. However, further reasearch need to be done at extremely high temperature where the polymer properties might change and extended application of these equations might be inappropriate.

Table 1. The equilibrium concentration (available) and the minimum concentration (required) of PPCA as a scale inhibitor in three oil wells' production assuming precipitation squeeze.

Well	Ca (M)	I (M)	T (K)	pH	equil PPCA, (ppm)	min PPCA, (ppm)
#1	0.240	2.91	424.7	5.5	0.0012	11.15
#2	0.0307	1.20	411.9	6.0	0.10	0
#3	0.0112	0.74	371.9	6.5	3.92	3.51

ACKNOWLEDGEMENTS

The authors are grateful for the financial support of the Brine Chemistry Consortium in Rice University.

REFERENCE

[1]. Kelvin Y. Chang and Suresh Patel. A Mechanistic Study of Phosphinocarboxylic Acid for Boiler Deposit Control. MP/July 1996, p.48-53.

[2]. T. Grchev, M. Cvetkovska and J. W. Schultze. The Electrochemical Testing of Polyacrylic Acid and Its Derivatives as inhibitors of Corrosion. Corrosion Science, Vol 32, No 1, 103-112, 1991.

[3]. S. Patel and A.J. Nicol. Developing a Cooling Water Inhibitor with Multifunctional Deposit Control Properties. MP/June 1996, p.41-47.

[4]. M.R. Rabaioli, Thomas P. Lockhart. Solubility and phase Behavior of Polyacrylate scale inhibitors. J. petroleum Sci and Engin 15(1996) 115-126.

[5]. P. Debye and E. Huckel, Physik. Z., 24, 185 (1923).

[6]. H.S.Harned and B.B. Owen, Physical Chemistry of Electrolytes, 2nd ed., Reinhold Publishing Corp., New York, 1950, Chs2,3.

[7]. J.G. Kirkwood and J.C. Poirie, J. Phys. Chem., 58, 591 (1954).

[8]. T.L. Hill, Arch. Biochem. Biophys., 57, 229 (1955).

[9]. J.J. Hermans and J. Th. G. Overbeek, Rec. trav. chim., 67, 761 (1948).

[10]. C. Tanford, J. Phys. Chem., 57, 229 (1955).

[11]. Charles Tanford, Physical Chemistry of Macromolecules, Joh Wiley & Sons, Inc., 1967.

[12]. Tohru Miyajima, Megumi Mori and Shin-ichi Ishiguro, Journal of Colloid and Interface Science, 187, 259-266 (1997).

[13]. R. Arnold and J.Th.G. Overbeek, Rec. trav. chim., 69,192(1950)

[14]. D.T.F. Pals and J.J.Hermans, Rec. trav. chim., 71, 433 (1952)

[15]. V.Ya. Kabo, L.A. Itskovich and V.P.Budtov, Polym Sci USSR 31,10, 2217(1989)

[16]. K.R.Rogan, Colloid Plym Sci 273: 364-369 (1995)

[17]. R. Arnold and J.Th.G. Overbeek, Rec. trav. chim., 69,192(1950)

[18]. Samelson,H., Columbia Univ. thesis; Univ. Microfilms (Ann Arbor, Michigan), Publ. No. 9531 (1954).

[19]. R.K. Cannan and A. Kibrick, J. Amer. Chem. Soc., 1938, 60, 2314.

[20]. H. morawetz, A.M. Kotliar and H. Mark, J. Phys. Chem., 58, 619 (1954).

[21]. Tsuneo Okubo and Nobuyuki Mohri, The Solubility of Polyelectrolyte Complexes. CalciumPolyacrylate and the Poly(4-Vinyl-N-pentylpiridinium) Salt of Poly(styrenesulfonic Acid). Macromolecules 1988, 21, 2744-2747.

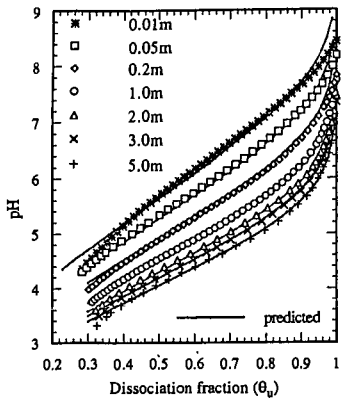

Figure 1. Plot of pH vs θ_u for acid-base titration of 0.0025N PPCA at 70°C and different NaCl concentration

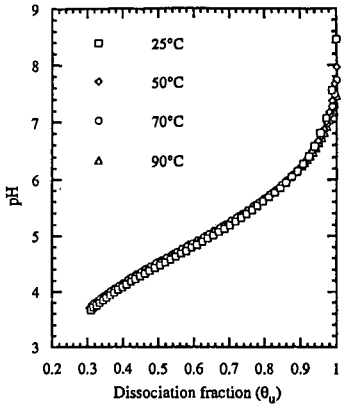

Figure 2. pH vs θ_u for acid-base titration of PPCA solution: 0.0025N PPCA-1.0m NaCl at different temperatures.

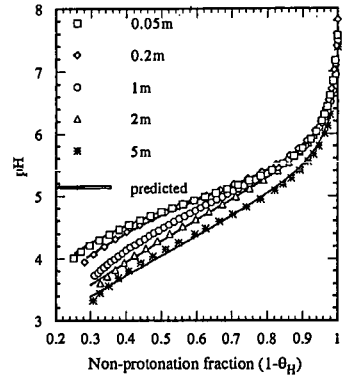

Figure 3. Plot of pH vs ($1-\theta_H$) for the acid-base titration of 0.0025N PPCA-0.005M Ca solution at 70°C and different NaCl concentration.

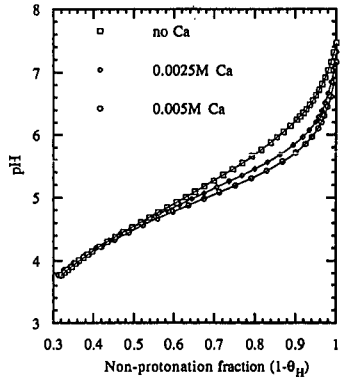

Figure 4. pH vs ($1-\theta_H$) for acid-base titration of 0.0025 N PPCA solution at 90°C and 1m NaCl.

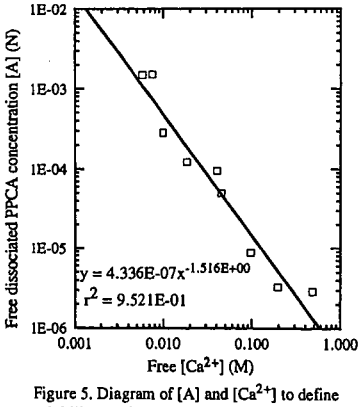

Figure 5. Diagram of [A] and [Ca^{2+}] to define solubility product of Ca-PPCA.

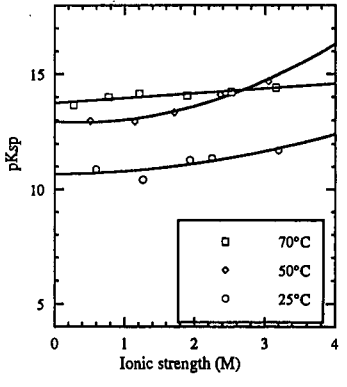

Figure 6. Diagram of pKsp of Ca-PPCA vs. ionic strength at three different temperatures.

SYNTHESIS OF METHYL METHACRYLATE (MMA) VIA C_2-CARBONYLATION AND C_3-CONDENSATION REACTIONS

Makarand R. Gogate[1], James J. Spivey[1], Joseph R. Zoeller[2], Richard D. Colberg[2], Gerald N. Choi[3], and Samuel S. Tam[4]

[1]Research Triangle Institute, P.O. Box 12194, Research Triangle Park, NC 27709-2194
[2]Eastman Chemical Company, P.O. Box 1972, Kingsport, TN 37662-5150
[3]Bechtel, P.O. Box 193965, San Francisco, CA 94119-3965
[4]Bechtel, P.O. Box 2166, Houston, TX 77252-2166

KEYWORDS: Ethylene Carbonylation, Formaldehyde Condensation, MMA.

INTRODUCTION

The most widely practiced commercial technology for the synthesis of methacrylic acid (MAA) and methyl methacrylate (MMA) is the acetone cyanohydrin (ACH) process. The ACH process requires handling of large quantities of extremely toxic and hazardous hydrogen cyanide and generates copious amounts of ammonium sulfate wastes which are either discarded or reclaimed at substantial cost. The ACH technology is thus environmentally and economically untenable for new expansions. There is a strong drive within the chemical industry for an alternate coal-based process (Gogate et al., 1997; Spivey et al., 1995a, 1996). The process proposed here (Figure 1) is based on C_2"-hydrocarbonylation reactions using CO generated from coal and C_3-Condensation reactions (Spivey et al., 1995b) and consists of three steps: Step1–ethylene carbonylation, Step 2–formaldehyde condensation, and Step 3–esterification of MAA produced in Step 2 to MMA. Steps 1 and 2 present technical challenges for successful commercial demonstration and are the focus of this paper.

The research presented in this paper on Step 1 elucidates the development of a homogeneous catalyst for propionate synthesis and research on Step 2 delineates the development of an acid-base catalyst for condensation of formaldehyde with propionates. Additionally, results of a preliminary economic analysis comparing the product value of MMA via six different commercial or near-commercial routes is presented.

EXPERIMENTAL

Ethylene Carbonylation

To allow the measurement of experimental rates of ethylene carbonylation to propionates, a 2-L Hastelloy®-C overhead stirred autoclave was fitted with a high-pressure condenser and a dip tube for removing samples during the reaction. During a typical run, 5.81 g (0.022 mol) of $Mo(CO)_6$, 15.5 g 0.040 mol) of tetrabutyl phosphonium iodide, 109.2 g (0.700 mol) ethyl iodide, 81 g (4.5 mol) of H_2O, and 450 g (7.5 mol) of acetic acid (as an internal standard and solvent) were added to the autoclave. The autoclave was then pressure-tested with nitrogen at 68.0 atm and a gas purge was established through the reactor at 3 mol/h. The nitrogen was vented, and autoclave was then pressurized to 23.8 atm with 5 percent hydrogen in carbon monoxide, and subsequently heated to 160 °C. Upon reaching the temperature, the pressure was raised to 51.0 atm using a gas mixture consisting of 6 percent hydrogen, 47 percent CO, and 47 percent ethylene, maintaining the 3 mol/h gas purge. Liquid samples were removed every 30 min from the reactor for the first 5 hours after the steady state was reached, and analyzed for ethyl iodide, ethyl propionate, acetic acid, and propionic acid, using a Hewlett Packard 5890 Gas Chromatograph (GC) containing a 25 m (0.25 - mm ID, 0.25 μm film) Quadrex 007 FFAP capillary column, with p-xylene as the internal standard. Gas samples were also removed every 60 min for first 5 h, to ensure that the gas composition was uniform. All trace materials were detected by a gas chromatograph (GC) / mass spectrometer (MS).

Condensation Catalysis

The condensation catalysts were tested in a continuous fixed-bed microreactor system. The nominal flow rates of propionic acid, formaldehyde, and nitrogen were kept at 75, 15, and 220 mmol/h. The feed was prepared by dissolving trioxane (solid trimer of formaldehyde) into propionic acid in a ca. 5:1 mole ratio, and fed into a preheater maintained at 300 °C, using a syringe pump (ATI Orion SAGE M361). The vaporized feed was passed over a catalyst charge, located centrally in a 6-mm ID x 356-mm L SS316 reactor tube. The catalyst charge (of a 16-30 mesh nominal size fraction) was held in place by glass wool and glass beads. Thermocouples mounted directly at the entrance and exit of catalyst bed provided temperature control and readout. Both the preheater and the reactor

were mounted horizontally in Lindberg furnaces (Blue M, Model #TF55035A). The product vapors containing methacrylic acid, water, propionic acid, and diethyl ketone were cooled and collected in a impinger contained in an ice bath. The product gases were collected in a Tedlar Bag. The liquid products were analyzed over a fused silica capillary column (30 m x 0.32 mm ID) with a 0.25 μm film thickness of DB-FFAP, using a flame ionization detector (FID) using a HP 5890 gas chromatograph (GC). The gas samples were analyzed using a fixed-volume loop injection onto a Poropak®T/Molecular Sieve (MS) 5 Å columns, with a column isolation sequence, using a thermal conductivity detector (TCD).

The catalysts were characterized for their surface area, pore volume, and surface acid-base properties. The surface and pore volume determinations were made on a Quantachrome NOVA 100 BET-N_2 surface area analyzer. The acid-base properties were measured on an Altamira AMI-100 catalyst characterization system. The NH_3-adsorption was carried out with a 10 percent NH_3-N_2 gas mixture (25 mL/min) for 30 min at 50 °C. The desorption was carried out from 50 to 550 °C, at 10 °C/min. The evolved gases were continuously monitored using a thermal conductivity detector (TCD). For surface basicity measurements, an identical time, temperature, and flow profile was followed, with a 10 percent CO_2-N_2 gas mixture as the treatment gas.

RESULTS AND DISCUSSION

Ethylene Carbonylation.

General Description of the Catalyst. Although homogeneous catalysts for this reaction are well known (Samel et al., 1993), commercial application has been limited to a highly toxic and volatile $Ni(CO)_4$ catalyst operating at high pressures (>180 atm) and high temperatures (>270 °C) (Bertleff, 1986; Samel et al., 1993) to produce propionic acid. Processes operating at lower pressures and temperatures generally require expensive catalysts such as Rh, Ir, or Pd and none have been employed commercially (Bertleff, 1986; Colquhoun et al., 1991; Forster et al., 1981, Mullen, 1980; Pino et al., 1977). Although Cr group metals have been used in combination with known carbonylation catalysts such as Co, Ni, Rh, and Ir, they have not been shown to have significant catalytic activity in isolation. In the study reported here, a halide-stabilized $Mo(CO)_6$ homogeneous catalyst is used at 130 to 170 °C and 350 to 750 psig.

The results of batch experiments comparing the observed order of reactivity for the Group 6 metals shows that Mo>>W>Cr and that the halide employed may be either Br or I. Substitution of bromine for iodine only leads to a small change (~25 percent decrease) in reaction rate, suggesting an electron transfer process (Huber et al., 1995). When the process is operated with a catalyst composed of Bu_4PI, $Mo(CO)_6$, and EtI, the Mo catalyzed carbonylation of ethylene to propionic anhydride at a nearly linear rate with time, until a 75- to 85-percent conversion of the propionic acid is achieved, at which point the reaction begins to slow markedly. A typical reaction profile for this process appears in Figure 2.

Effect of Temperature, Determination of Activation Parameters. The effect of temperature was measured in batch experiments between 130 and 170 °C using identical levels of gas and catalyst components throughout the full range of temperatures. The apparent activation energy (E_{act}) was 39.3 kcal/mol. The rate expression is:

$$k = \frac{\text{Rate} \cdot [P_{\tilde{T}\partial}]^{\Theta\beta\wedge}}{[Mo(CO)_\kappa]^{\eta\chi\Theta}[EtI]^{\eta\chi\Theta}[I^-]}$$

The enthalpy of activation ($\Delta H‡$) and entropy of activation ($\Delta S‡$) were determined from the Eyering plot: [ln (k/T vs. (1/T)] $\Delta H‡$ was found to be +38.4 kcal/mol and $\Delta S‡$ was estimated to be +40 cal/mol/K. These activation parameters suggest a rate-determining step involving the dissociation of the Mo-CO bond in $Mo(CO)_6$ (Ehlers and Frenking, 1993, 1994).

Kinetic Effects of Reactants. To measure kinetic effects due to ethylene, CO, and hydrogen, a continuously gas purged autoclave with a liquid sampling loop was used. Using this apparatus, the partial pressure of each reactant could be varied independently. The effects of hydrogen and ethylene were uneventful and increasing partial pressures of these two reactants did not show any discernible increase in the reaction rate. It was therefore concluded that the reaction is zero order with respect to hydrogen and ethylene. Increasing the partial pressure of CO led to a deacreased reaction rate and the measured reaction order was found to be -1.2. This inverse and complex dependence of reaction order in CO suggests that the overall mechanism involves a step which is inhibited by CO. To study the effect of $Mo(CO)_6$, EtI, and Bu_4I levels on reaction rate, the partial

pressures of CO, hydrogen, and ethylene were kept constant, with CO levels controlled very accurately at 23.8 atm. While the reaction order in Bu_4I was first order, the experimentally measured reaction orders for both $Mo(CO)_6$ and EtI were both approximately ½ order, indicating a likely free-radical type reaction mechanism. Based on these reaction order measurements, a predictive rate equation was proposed.

Condensation Catalysis

The condensation of formaldehyde with propionic acid is catalyzed by acid-base catalysts, as shown in Figure 3 (Gogate et al., 1997). The catalyst development effort has focused on developing a stable, selective, and active condensation catalyst for this reaction. Fixed-bed microreactor studies of more than 80 potential catalytic materials have shown that Group V metals (V, Nb, and Ta) are active condensation catalysts and that niobium catalysts are the most active.

The results show that the 20 percent Nb/SiO_2 is the most active catalyst. However, the catalyst deactivates. The long-term deactivation of a 10 percent Nb/SiO_2, V-Si-P 1:10:2.8, and 10 percent Ta/SiO_2 are shown in Figure 4. The deactivation of these catalysts has been correlated with the strength and distribution of the acid and base sites on the catalyst. There appears to be an optimum balance between these sites that is necessary to promote the condensation reaction. Figure 4 shows that an oxidative treatment of the deactivated catalyst partially restores the activity. Work is under way to minimize deactivation.

Economics of the Overall Process

An economic analysis was carried out by Eastman and Bechtel based on the results on the 20 percent Nb/SiO_2 catalyst at 300 °C, 2 atm, flow rates of propionic acid: formaldehyde:nitrogen 72:16:200 mmol/h, 5 g catalyst charge (0.7- to 1.1-mm size fraction), and a volume hourly space velocity of 1,080 cm^3/g cat·h. Reaction kinetics are assumed to be first order in formaldehyde, in order to remove the effects of excess nitrogen diluent and excess HOPr. This process was compared to five commercial (or, near commercial) technologies for MMA manufacture:

- Conventional ACH-based process (Rohm & Haas),
- (New) Mitsubishi Gas Chemical (MGC) ACH-based process,
- *i*-butylene oxidation process (Lucky, Japan Methacrylic),
- *t*-butanol oxidation process (Kyodo, Mitsubishi Rayon), and
- Propyne carbonylation (Shell, ICI).

A comparison of production cost (or, product value) was carried out for these six routes, based on a 250 Mlb/year plant (except for the propyne carbonylation process, for which a 100 Mlb/year capacity is assumed due to the very limited worldwide supply of propyne). To account for catalyst deactivation, the process design includes parallel fixed-bed reactors.

The product value comparison for the RTI-Eastman-Bechtel HOPr/MeOH route with five commercial routes (Figure 5) shows that the RTI-Eastman-Bechtel three-step process at 52¢/lb MMA is competitive with all commercial technologies for MMA manufacture, except propyne carbonylation (at 44¢/lb). [The current selling price for MMA is roughly 75¢/lb.] However, the propyne carbonylation technology suffers from limited raw material supply. Both the conventional ACH and MGC ACH-based processes (at 73¢/lb and 70¢/lb MMA, respectively) are more costly than the RTI-Eastman-Bechtel three-step route, as is the *i*-butylene oxidation route (at 59¢/lb). In the United States, the *i*-butylene route suffers from competing raw material demands for methyl tert-butyl ether (MTBE) plants. The *t*-Butanol oxidation process at 55¢/lb MMA appears quite competitive with the RTI-Eastman-Bechtel three-step process.

CONCLUSIONS

The carbonylation of olefins, particularly ethylene, with a halide-promoted Mo catalyst represents the efficient process using a Cr-group metal as the active catalyst. Detailed mechanistic analysis indicates that the reaction likely proceeds via a free radical mechanism, which is initiated by a rate limiting dissociation of CO from $Mo(CO)_6$. The precise propionate derivative obtained depends on the nature of the nucleophile, and the process for propionic acid uses steam. If present in too large a quantity (alcohol for methyl propionate process, or water for propionic acid process), the nucleophilic component can inhibit the reaction, by competing with the EtI for the vacant coordination site of $Mo(CO)_5$. The condensation of propionate derivatives with formaldehyde is a synthetic route to MAA and MMA. The reaction mechanism suggests that both acid and base properties are required and a definitive balance of acid and base site strengths is perhaps needed for an active, selective, and stable catalyst. As a result of screening over 80 catalytic materials, a 20%

Nb_2O_5/SiO_2 catalyst is found to give optimum performance, although catalyst deactivation is ubiquitous on this and other catalysts. Detailed XPS/ESCA/XRD studies prove that carbon deposits in nodular form on the active Nb_2O_5 sites, thereby limiting accessibility of an Nb_2O_5 site to the reactants. Based on the XPS/ESCA study of a regenerated catalyst (using oxidative regeneration), a reaction-regeneration cycle study on the 20% Nb_2O_5/SiO_2 is planned, which may alleviate the catalyst deactivation pattern. A preliminary economic evaluation of the RTI-Eastman-Bechtel three-step methanol process consisting of external formaldehyde generation, condensation of formaldehyde with propionic acid, and external esterification of resulting methacrylic acid with methanol to form MMA shows that for a 250 Mlb/yr product and 10 percent rate of return on investment, the product value of RTI-Eastman-Bechtel three-step route at 52¢/lb is cost-competitive with known commercial and near commercial technologies for MMA manufacture, except propyne carbonylation, which suffers from limited raw material supply. Further research on condensation catalysis, particularly in enhancing catalyst longevity is under way.

ACKNOWLEDGEMENTS

The authors gratefully acknowledge the support of this research, by the U.S. Department of Energy / Federal Energy Technology Center (DOE/FETC), through Contract No. DE-AC22-94PC065. The authors are also indebted to DOE Project Officer, Dr. Richard E. Tischer, for his support and guidance.

REFERENCES

Bertleff, W. 1986. Carbonylation. In: *Ullman's Encyclopedia of Industrial Chemistry*, 5th edn., Vol. A5, VCH Publishers, New York, NY, p. 223.

Colquhoun, H.M., D.J. Thompson, and M.V. Twigg. 1991. *Carbonylation-Direct Synthesis of Carbonyl Compounds*, Plenum Press, New York, NY, pp. 102-106; 119-130.

ChemSystems. 1996. Methacrylic Acid/Methacrylates, PEP Report 94/95-3.

Forster, D., A. Hershman, and D.E. Morris. 1981. *Catalysis Rev.-Sci. Eng.*, 23, p. 89.

Gogate, M.R., J.J. Spivey, and J.R. Zoeller. 1997. "Synthesis of methyl methacrylate by vapor phase condensation of formaldehyde with propionate derivatives", *Catal. Today*, 36(3), pp. 243-254.

Gogate, M.R., J.J. Spivey, J.R. Zoeller, R.D. Colberg, S.S. Tam, and G.N. Choi. 1997. "Novel Catalysts for Environmentally Friendly Synthesis of Methyl Methacrylate." *Ind. Eng. Chem. Res.*, 36, pp. 4600.

Huber, T.A., D.H. Macartney and M.C. Baird. 1995. *Organometals*, 14, p. 592.

McKetta, J.J., ed. 1989. *Encyclopedia of Chemical Processing and Design*. Vol. 30.

Mullen, A. 1980. In J. Falbe (Ed.), *New Syntheses with Carbon Monoxide*, Springer, Berlin, pp. 275-286.

Pino, P., F. Piacenti, and M. Bianchi. 1977. In: *Organic Syntheses via Metal Carbonyls*, 1st edn., Wender and P. Pino, Vol. 2, Wiley, New York, NY, pp. 233-296.

Samel, U.R., W. Kohler, A.O. Gamer, and U. Keuser. 1993. "Propionic Acid and Derivatives." In *Ullman's Encyclopedia of Industrial Chemistry*, 5th edn., Vol. A22, VCH Publishers, New York, NY, p. 223.

Spivey, J.J. M.R. Gogate, B.W.L. Jang, E.D. Middlemas, J.R. Zoeller, S.S. Tam and G.N. Choi. 1995a. "Synthesis of Methyl Methacrylate from Coal-Derived Syngas", In *Proceedings of the Contractors' Review Meeting on Coal Liquefaction and Gas Conversion*, U.S. DOE/PETC, Pittsburgh, PA, pp. 385-395.

Spivey, J.J., M.R. Gogate, B.W.L. Jang, E.D. Middlemas, J.R. Zoeller, S.S. Tam, and G.N. Choi. 1995b. "A New Route to Acrylates and Methacrylates from Syngas." Presented at the World Environmental Congress, London, Ontario.

Spivey, J.J., M.R. Gogate, J.R. Zoeller, R.D. Colberg, G.N. Choi, S.S. Tam, R.E. Tischer, R.D. Srivastara. 1996. "Novel Syngas-based Process for Methyl Methacrylate." In *Proceedings of the Thirteenth Annual International Pittsburgh Coal Conference*, Volume 1, pp. 559-564, The University of Pittsburgh, Pittsburgh, PA.

SRI. 1993. Methacrylic Acid and Esters, PEP Report 11D, Section 8.

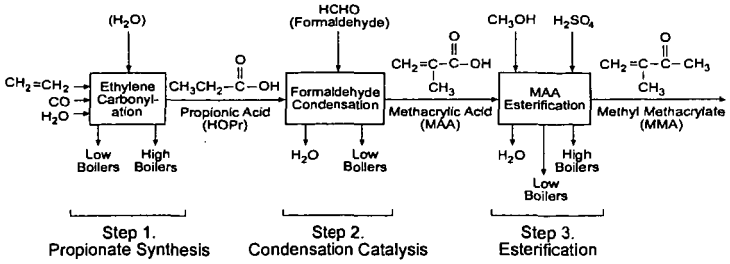

Figure 1. RTI-Eastman-Bechtel three-step HOPr/MeOH-based MMA process (with external formaldehyde feed).

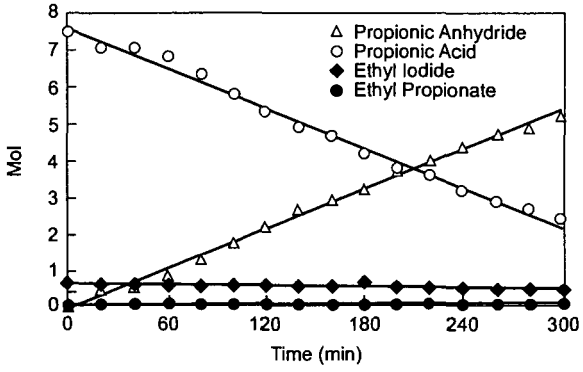

Initial composition: EtI, 0.7 mol; EtCOOH, 7.5 mol; $Mo(CO)_6$, 22 mmol; Bu_4PI, 40 mmol. Conditions: 160 °C, 55 atm. Gas compositions: 5% H_2, 50% C_2H_4, 45% CO.

Figure 2. Reaction profile for the carbonylation of ethylene to propionic anhydride.

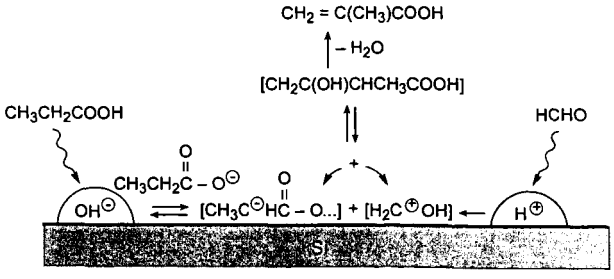

Figure 3. Representative mechanism for propionic acid and formaldehyde.

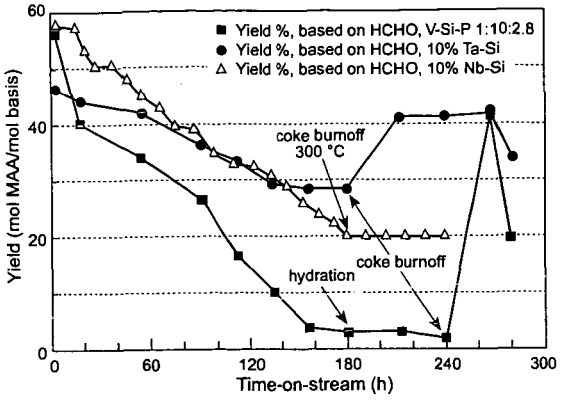

Experimental Conditions V-Si-P, Ta-Si

For V-Si-P, Ta-Si: 300 °C, 2 atm, **15 g cat. charge**, 41:17:220 mmol/h
PAA:HCHO:Nitrogen, 290 cm^3/g cat-h

For Nb/Si: 300 °C, 2 atm, **5 g cat. charge**, 72:16:220 mmol/h
PA:HCHO:Nitrogen, 1080 cm^3/g cat-h

Figure 4. Long-term activity check on V-Si-P 1:10:2.8, 10% Ta-Si, and 10% Nb-Si catalysts.

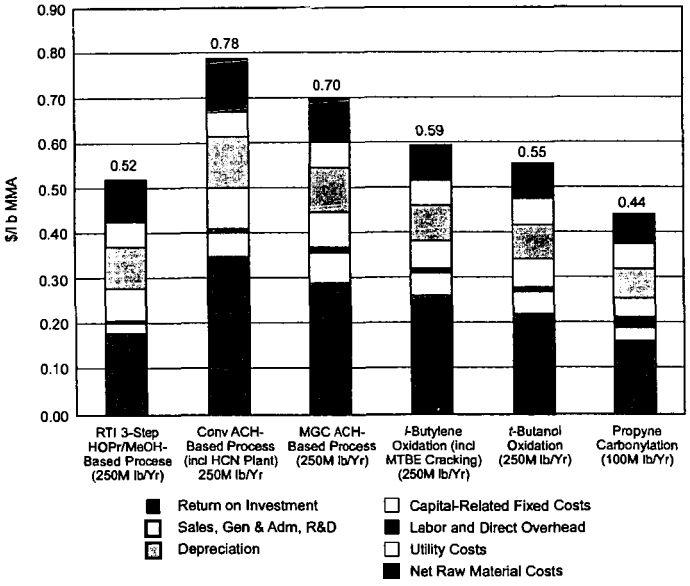

Figure 5. MMA processes, product value comparison (10% ROI).

STUDY OF PETROLEUM COKE USED AS REDUCING AGENT IN IRON ORES PROCESSING

Jun M. Lee, Jeffrey G. Rolle, James J. Baker
A. J. Edmond Co., 1530 West 16th Street, Long Beach CA 90813
Marcos de Albuquerque Contrucci, Edmar Saul Marcheze
TECNORED LTDA, Rua Georges Smirnow 305/306 Bairro Boa Vista
CEP 89206-740, Joinville, SC Brasil
James W. Ramming
Tecnored Technologies Incorporated, 100 First Stamford Place, Stamford, CT 06902

Keywords: petroleum coke, iron ores reduction

ABSTRACT

A petroleum coke with a high sulfur content (approximately 7.0 wt %) was tested as reducing agent in iron ores processing. Proprietary TECNORED pellets were prepared by blending of iron ore fines, petroleum coke fines and other additives (binders, fluxing agents, etc.) through a wet-pelletizing process. A pilot-scale reaction system was assembled for the reaction performance study with the petroleum coke and TECNORED pellets, which consists of a packed-bed Inconel reactor with temperature controller and programmer, air, argon and nitrogen gas supply system, effluent product gas sampling system, and gas analyzers. Five screening tests were recently performed and experimental results are presented.

INTRODUCTION

Production of petroleum cokes steadily increased by 51% during the past decade, expecting continuous increase in the coming years, primarily due to declining quality of crude oils [1]. Green petroleum cokes are mostly used as utility fuels (about 73% for fuel grade), and as feedstocks (about 27%) for further upgrading calcination. The calcined petroleum cokes are used in production of specialty products such as aluminum anodes, graphite electrodes, titanium oxide pigments, recarburized ductile irons, etc.

In addition green petroleum coke was often used as an additive in metallurgical coke making, depending on its availability in the market at lower prices than those of coking coals [2]. The performance of metallurgical coke, produced from coking coal blends containing petroleum coke, was successfully tested in several blast furnaces. The maximum limit of petroleum coke in a coal blend for acceptable coke quality was reported to be 5 wt % in Japan. However, elsewhere a higher limit (20 or 40 wt %) was reported. Several properties of coal blends such as particle size, rheological properties, volatile matter and total carbon content are important affecting quality of metallurgical coke. Various instrumental and analytical methods and techniques can be found in the literature to be used to characterize petroleum cokes and coal blends.

TECNORED Process Background and Description

The proprietary TECNORED process (developed by the TECNORED in Brazil) utilizes self-reducing pellets composed of tiny particles of iron ore and petroleum coke, and generating infinite reaction sites, enhances reaction rates of iron ore reduction by more than ten times (residence time 0.5 vs. 6 to 8 hours) [3]. The pellet consists of 70 to 75 wt % iron ore fines, 15 to 20 wt % coke fines and 5 to 10 wt % binders and fluxes, respectively. The process can use 100% petroleum coke without blending with coal or any blends of petroleum coke and coal.

In conventional commercial blast furnace processes [4,5,6], two main reduction steps are involved, requiring 1 to 2 hours residence time for each reduction zone, zone converting wustite ($Fe_{0.947}$) to solid iron (Fe_s) and zone converting Fe_2O_3 to Fe_3O_4 and further to $Fe_{0.947}$. Fusion and slagging zones add more residence time after completion of reaction, totaling 5 to 8 hours. Gas residence times are in the order of only 1 second and hence good gas and solid contact is required for efficient operation.

In contrast, the TECNORED process has many advantages in processing iron ores:

- Diversified low-cost raw materials and fuels
  - low-grade iron-ore fines with 60 to 64% Fe
  - low-cost reductant fines with non-coking coals, cokes, petroleum cokes, etc.
  - low-cost binders
  - low-cost solid fuels with non-coking lumps, petroleum cokes, semi-cokes, etc.

- full recycling of all dust and fines
- Low-cost and low-investment pelletizing process
  - cold curing in open air yards
  - grinding of coal fines only to minus 140 mesh
  - grinding of ores, if any, only to minus 100 mesh
  - no hot-firing of pellets
  - green pellets with enough strength to bulk handling
- High productivity and energy efficiency in TECNORED furnace
  - 30 to 40 minutes residence time against 6 to 8 hours in blast furnaces
  - no Boudouard reaction on solid fuels due to side feeders
  - CO burning in the upper shaft to heat up and pre-reduce pellets
  - pellets drying in the silos by hot-blast stack off-gases
  - low power requirements due to low shaft height (2-3 m), low-pressure blast and lower elevation of the charge
  - use of blast partially cold
  - cheap top-gas available, if desired
- Low investment TECNORED furnace
  - multi-mode atmosphere concept on a single-vessel unit
  - compact shaft-furnace design with classical units of hot blast, gas cleaning and centrifugal blowers, making even blast furnace conversion possible
  - small working volume due to high productivity
  - no dosing of charge required
  - flow of charge regulated by melting rate solely through the blast
  - simple process control

Summary of Pilot-Scale Tests

The pilot-scale plant tests were performed during July 21-22, 1997 at the Kaiser's Mead Works laboratory of an aluminum smelter, located at Spokane, Washington. Five gas sampling runs were successfully completed as planned by the A. J. Edmond Company (primary contractor - test planning and coordinator), the Kaiser laboratory (subcontractor – testing reactor set-up and operator), and the Am Test-Air Quality, LLC (subcontractor for gas sampling and analysis). Highlights of sampling activities are summarized as follows:

(1) Nitrogen oxides (NO_x) of five gas samples collected in Tedlar bags were analyzed on-site using a chemiluminescent analyzer, Thermo Environmental Instrument Model 42H, performing the EPA Method 7E. In addition, carbon dioxide (CO_2), carbon monoxide (CO) and oxygen (O_2) were analyzed on-site, performing the EPA Method 3A for CO_2 and O_2, and the EPA Method 10 for CO, respectively.

(2) Five gas samples for GC/MS analysis of CO, CO_2, H_2 (hydrogen), CH_4 (methane), C_nH_m (speciated volatile organic compounds-VOC), SO_2 (sulfur dioxide), H_2S (hydrogen sulfide), COS (carbonyl sulfide) and N_2 (nitrogen), were collected in 6-L evacuated SUMMA stainless steel canisters. The sample canisters were transported next day to the Atmospheric Analysis and Consulting, Inc. laboratory in Ventura, California, for immediate analysis of gas samples, performing the EPA Method TO-14.

(3) Five gas samples were withdrawn through a sampling probe. Analysis samples were collected passing through the sampling train device, for IC analysis of Cl_2. The collected samples were transported to the Am Test laboratory, Redmond, Washington, for immediate analysis performing the EPA Method 26.

Details of the experimental procedure for each test are described in the following sections.

RUN OBJECTIVES

The objective of this study is to perform pilot-scale process simulation and variable testing using petroleum coke as a reducing agent of iron ore under operating conditions of a commercial blast furnace process. Specific detail objectives of three Tests A, B and C performed for this study with a petroleum coke and/or iron ore pellets are listed below.

Test A: To perform a chemical analysis of volatile matter produced from petroleum coke heated at 950 °C for 10 min under non-oxidizing conditions (argon atmosphere) as defined in the ASTM Method D 3175, or equivalent.

Test B: To perform a chemical analysis of effluent gases produced from combustion of petroleum coke through the injection of air at the base of

the packed column, which is controlled at 1000 °C of the effluent gas temperature.

Test C: To perform chemical analyses of effluent gases produced at three different effluent gas temperatures (500, 900, and 1100 °C, respectively), which are resulting from operation of a column of TECNORED pellets (iron ore blended with petroleum coke) under internally self-generated reduction atmosphere. The column operation is controlled under neutral and non-pressurized argon atmosphere. In addition, to analyze solids product (sintered and clogged pellets) remained in the reactor after heating beyond 1200 °C for composition of carbon, sulfur, and residual FeO present in both metal and slag, which are separated by heating.

EXPERIMENTAL PROCEDURES

Materials Tested

Petroleum coke, a testing sample derived from a refinery located in Texas, with high sulfur content of 7.0 wt %. Approximately 5 kg of sponge/shot coke (60/40 mixture) was prepared with ¼" to ½ " (6 to 13 mm) particle sizes by A. J. Edmond Company. The volatile matter content present in this coke was 10.0 wt %.

TECNORED pellets (iron ore blended with the coke fines) were made in Joinville, Brazil and forwarded by courier to A. J. Edmond Co. Approximately 15 kg of TECNORED pellets were prepared with 7.5 wt % moisture content and 3.4-6.4 mm particle sizes.

Reaction System

A schematic diagram of the reaction system of the pilot-scale plant is shown in Figure 1. The reaction system consists of argon cylinder, compressed air supply, nitrogen cylinder, pressure regulators, gas mass flow meter and control valves, preheating zone, reactor with temperature controller and programmer, sampling probes and analyzers for Cl_2, NO_x, and other gases (CO, CO_2, H_2, CH_4, C_nH_m (VOC), SO_2, H_2S, COS and N_2). The packed column reactor was made of a 3"ϕ x 48"H Inconel tube connected at the top to the stainless-steel sampling vent tube (3"ϕ x 24"H) with three sampling ports. At the mid-point inside the reactor a nickel-chromium screen (16 mesh, #24 wire size) welded to the wall to support the loading of petroleum coke and TECNORED pellets.

Effluent Gas Analyses

The Am Test-Air Quality, LLC (a subcontract service laboratory), Preston, WA performed on-site effluent gas analyses and sampling. Total five grab samples were collected and analyzed as required in this study, employing the analytical methods as described in Section INTRODUCTION, Summary of Pilot-Scale Tests.

Run Procedures

Tests A, B and C were performed under operating conditions closely simulating commercial blast furnace processes, as required by the client, CAEMI International and TECNORED. A 3" Inconel vertical reactor tube was placed in a 3" tube furnace capable of being controlled at 1200 °C of the reaction temperature. The control thermocouple was located at the mid-point outside surface of reactor tube. The effluent gas temperature at the top of reaction zone was not determined, but estimated to be similar within several degrees of this control temperature, based on previous experience with the heating furnace used. The temperature controller was effectively programmed to reach a target temperature within an hour in order to be ready for the next test planned as soon as possible. Effluent gas stream was naturally cooled without condenser through the sampling vent tube before reaching gas sampling probes. The effluent gas temperature at the sampling probe location was periodically measured using a portable thermometer during each test, and ranged from 100 to 350 °C. During the first Run 1, pre-tests were conducted for an integrity check of the reaction system, gas sampling and instrumental analyses, and other pertinent experimental parameters such as temperature, flow rate, etc.

RUN 2 - TEST A

A representative sample of a petroleum coke with 7 wt % sulfur content (approximately 5 kg) was prepared using ASTM Practice D 346 in the range of particle size from ¼" to ½" (6 to 13 mm), and stored in an air tight sample bag until needed for the test. The moisture content of the coke was approximately 0.21 wt %. The reaction test steps were:

(1) Approximately 312.6 g of the petroleum coke sample was charged into the reactor. The packed-bed height was approximately 4-5".

(2) Initially the nitrogen gas flow was on for 30 min at 5 liter/min to purge out the reaction system. Then the gas flow switched to argon.
(3) The argon gas flow slowly increased to 17 liter/min (1000 ± 10 liter/hr). The inlet argon gas pressure to the reactor was set at 70-75 psig.
(4) The reactor heating furnace was turned on, and the reactor temperature was rapidly increased to 400 °C in 6 min. No sampling was conducted during this preheating period.
(5) Sampling began at 400 °C and continued heating-up of the reactor from 400 to 950 °C. Three sampling probes were installed and total sampling rate was set at 6.2 liter/min; 4 for NO_x analysis, 2 for Cl_2 analysis, and 0.2 liter/min for GC/MS analysis, respectively.
(6) The reactor temperature maintained at 950 °C for additional 5 min, and during this period sampling continued. Total sampling time (or reaction time) was 25 min.
(7) After completion of the gas sampling, the argon gas flow valve and reactor heating furnace were turned off, and the gas flow switched back to nitrogen. Opened the heater when the temperature lowered several hundred degrees and allowed the reactor to cool down.
(8) Solids product remained in the reactor was easily removed without any visible deposits on the wall, when the reactor was sufficiently cooled down, and the reactor was cleaned thoroughly for preparation of the next test.

The material balance showed approximately 9.3 wt % of the petroleum coke converted to volatile matter.

RUN 3 - TEST B
The reaction test steps were:

(1) Approximately 302.3 g of the petroleum coke sample was charged into the reactor. The packed-bed height was approximately 4-5".
(2) Initially the nitrogen gas flow was on for 30 min at 7.5 liter/min to purge out the reaction system. Then the gas flow switched to compressed air.
(3) The air gas flow was set at low rates, 7.5-8.3 liter/min, in order to closely observe the reactor exotherm. *Note: This lower air flow rate employed was primarily due to the safety consideration of equipment limitation, that is, the Inconel reactor should operate below 1260 °C (maximum operating temperature for Inconel material). The planned air flow rate estimated for complete combustion was 17 liter/min.*
(4) At the same time the reactor heating furnace was turned on, and the reactor temperature was slowly increased to 920 °C. No sampling was conducted during this preheating period.
(5) Sampling began at 920 °C and continued heating-up of the reactor from 920 to 1000 °C. Three sampling probes were installed and total sampling rate was set at 5.1 liter/min; 4 for NO_x analysis, 1 for Cl_2 analysis, and 0.1 liter/min for GC/MS analysis, respectively.
(6) The reactor temperature maintained at 1000-1015 °C for additional 56 min, and during this period sampling continued. The air flow rate was adjusted in the range of 6 to 9.4 liter/min in order to control the reactor exotherm during this period.
(7) After completion of the gas sampling, the air gas flow valve and reactor heating furnace were turned off, and the gas flow switched back to nitrogen. Opened the heater when the temperature lowered several hundred degrees and allowed the reactor to cool down.
(8) Solids product remained in the reactor was easily removed without any visible deposits on the wall, when the reactor was sufficiently cooled down, and the reactor was cleaned thoroughly for preparation of the next test.

The material balance showed approximately 27.5 wt % of the petroleum coke combusted and converted to various product gases. This low conversion is partly attributed to the oxygen-deficient reaction condition employed in this test with the lower air flow, 6-9.4 liter/min, than 17 liter/min (planned target and estimated stoichiometric flow for complete conversion), and/or partly attributed to possible low reactivity of petroleum coke with air. *Note: The lower oxygen flow (air flow) was employed primarily due to the equipment limitation of Inconel material as discussed in the above (3). This would significantly affect the effluent product composition, resulting in lower content of CO, CO_2, and SO_2.*

RUN 4, 5 AND 6 - TEST C

A representative sample of TECNORED pellets (iron ore blended with coke fines) with 7.5 wt % moisture content was prepared (approximately 15 kg) in the range of particle size from 3.4 to 6.4 mm, and was stored in an air tight sample container until needed for the test. The reaction test steps were:

(1) Approximately 1200 g of the TECNORED pellets sample was overnight dried in an oven at 100 °C and was charged into the reactor. The packed-bed height was approximately 4-5".
(2) Initially the nitrogen gas flow was on for 30 min at 15 liter/min to purge out the reaction system. Then the gas flow switched to argon.
(3) The argon flow was set at 6.9 liter/min. This gas flow was above the sampling rate set in the following (5), <5.1 liter/min.
(4) At the same time the reactor heating furnace was turned on, and the reactor temperature was rapidly increased to 500 °C in 12 min. No sampling was conducted during this preheating period.
(5) Sampling began at 500 °C and continued for 60 min with the reactor temperature maintained at 500 °C. Three sampling probes were installed and total sampling rate was set at <5.1 liter/min; <4 for NO_x analysis, 1 for Cl_2 analysis, and 0.1 liter/min for GC/MS analysis, respectively.
(6) After completion of the gas sampling at 500 °C, three sampling probes were reinstalled, and then the reactor temperature was again rapidly increased to 900 °C. No sampling was conducted during this second preheating period. The argon gas flow rate was set at 6.7 liter/min.
(7) Sampling began at 900 °C and continued for 30 min with the reactor temperature maintained at 900 °C. Sampling rates were the same as before at 500 °C.
(8) After completion of the gas sampling at 900 °C, three sampling probes were reinstalled, filters were replaced, and then the reactor temperature was again rapidly increased to 1100 °C. No sampling was conducted during this third preheating period (about 37 min consumed). The argon gas flow rate was set at 6.7 liter/min.
(9) Sampling began at 1100 °C and continued for 20 min with the reactor temperature maintained at 1100 °C. Sampling rates were the same as before at 900 °C.
(10) After completion of the gas sampling at 1100 °C, sampling devices were removed, sampling ports were blocked, and than the reactor temperature was again rapidly increased to 1200 °C. No sampling was conducted during this fourth preheating period. The argon gas flow rate was the same as before.
(11) Without sampling the reactor temperature was maintained at 1200 °C for 60 min before ending the Test C.
(12) The argon gas flow valve and reactor heating furnace were turned off, and the gas flow switched back to nitrogen. Opened the heater when the temperature lowered several hundred degrees and allowed the reactor to cool down.

During the heating-up period to 1200 °C for the pre-melt and slag-off test, trickling and slipping-down noise was noticed inside the reactor tube. It appeared that the wire-mesh screen welded to the reactor wall (for support of pellets and petroleum coke loading inside the reactor) was loosened and fell down to the bottom section of the reactor. The test was not successfully completed for further analysis of solids remained.

RESULTS AND DISCUSSION

Table 1 summarizes analysis results of gas samples collected for this study. Some of Runs 4 to 6 results are proprietary data. Therefore, ratio values of N_2, CO, CO_2 and H_2 compositions were calculated for comparison. Run 5 data were used as basis.

Devolatilization and Pyrolysis of Petroleum Coke under Argon Atmosphere

A study of pyrolysis of petroleum cokes under nitrogen inert atmosphere showed that the volatile matter significantly released in the plastic range of a given coal (400-500 °C) [2]. Maximum evolution of volatile matter (about 40 to 49% of total) was observed in the range of 500-750 °C, and then the volatile matter release decreased in the range of 750-1000 °C. Based on this literature information, in Run 2 - Test A gas sampling was performed for 25 min in the temperature range of 400-950 °C. The weight loss determined after the test showed 9.3 wt %,

similar to the volatile matter content (10.0 wt %) determined by ISO 562, which is equivalent to ASTM Method D 3175.

The gas analysis data for Run 2 – Test A at 400-950 °C (in Table 1) shows that the effluent product gas consists of H_2, CH_4, CO_2 and CO. In addition a significant amount of H_2S is present in the gas sample produced primarily due to the high sulfur content of the petroleum coke (7.0 wt %) tested for this study. Other trace gases are NO_x, C_nH_m (VOC), and insignificant amounts of Cl_2 and SO_2 plus COS.

Combustion of Petroleum Coke with Air Flow

During the start-up (heating-up) period in Run 3 – Test B, the oxygen deficient reaction condition was employed as mentioned in Section RUN 3 – TEST B, in order to control highly exothermic reaction (combustion), $C + O_2 \rightarrow CO_2$, occurring below 930 °C (1200 K) [4]. When the reaction temperature reaches above 930 °C, the controlling reaction changes to highly endothermic reaction (gasification), $CO_2 + C \rightarrow CO$. The low flow rates of air, 6-9.4 liter/min, coupled with slow heating-up of the reactor enabled to closely control the reactor exotherm. The estimated stoichiometric flow of air for complete conversion was 17 liter/min. Without increasing the flow rate of air for complete conversion, gas sampling started at 920 °C when the governing reaction changes from combustion to gasification and continued for 60 min at 1000-1015 °C (most of time).

The material balance showed approximately 27.5 wt % of the petroleum coke combusted and converted to various product gases. This low conversion is partly attributed to the oxygen-deficient reaction condition employed in this test with the lower flow rate of air, and/or partly attributed to possible low reactivity of petroleum coke with air. The low conversion would significantly affect the effluent gas product composition, resulting in low content of CO, CO_2, and SO_2. The on-site gas analysis data showed an insignificant amount of O_2, 0.2%, present in the gas sample, indicating most of oxygen in the air converted to oxides and depleted in the reaction zone.

The gas analysis data for Run 2 – Test B at 1000-1015 °C (in Table 1) shows that the nitrogen-free effluent product gas consists of H_2, CH_4, CO_2 and CO. A significantly reduced amount of H_2S is present in the gas sample, and the SO_2 plus COS content significantly increased by oxidation, compared to the result of Run 2 – Test A. Other trace gases are NO_x, C_nH_m (VOC), and insignificant amount of Cl_2.

The combustion reaction with air produced much higher amounts of CO_2 and CO, while reducing CH_4 composition, compared to the result of Run 2 – Test A. The high hydrogen content observed suggests a possibility of pyrolysis reaction still present under the oxygen deficient condition. The reactor temperature profile was not measured in this study, which might provide better understanding of reaction mechanism.

TECNORED Pellets Reduction under Argon Atmosphere

In Runs 4 to 6 – Test C, TECNORED pellets were processed under argon atmosphere at three different reaction temperatures, 500, 900 and 1100 °C, sequentially. Ratio values were used for comparison of proprietary data (compositions of N_2, CO, CO_2 and H_2). Other gas composition data are reported as measured (carrier gas-free basis) in Table 1.

Run 6 at 1100 °C shows the highest CO composition in the gas sample among three runs, indicating that a significant gasification reaction occurs above 930 °C with TECNORED pellets present. The CO content is several times higher than the CO_2 content at this condition. This suggests that gasification is the controlling reaction, $CO_2 + C \rightarrow CO$, and TECNORED pellets generate self-reducing environment.

In Run 5 at 900 °C, the CO content is similar to the CO_2 content. Both combustion and gasification are competing and important at this temperature. Again this indicates that TECNORED pellets generate self-reducing environment.

Relatively small, insignificant amounts of CO and CO_2 were observed at the lower reaction temperature of 500 °C. A small degree of devolatilization might be mainly happening at this temperature without presence of self-generated combustion and gasification reactions.

Other trace gases produced at 900-1100 °C are CH_4, H_2S, SO2 plus COS, NO_x, C_nH_m (VOC), and insignificant amount of Cl_2.

SUMMARY

Five screening tests with high sulfur petroleum coke and TECNORED pellets were successfully completed under process conditions of iron ores reduction. Effluent product gas analyses suggest that:

- TECORED pellets generate self-reducing environment for iron ores processing at 900-1100 °C.
- The high CO production at 1100 °C with TECNORED pellets provides an evidence of gasification reaction controlling at this temperature.
- Minimum or insignificant amounts of trace gases (H_2S, SO_2 plus COS, NO_x, C_nH_m (VOC) and Cl_2) were produced at 900-1100 °C with TECNORED pellets.
- TECNORED pellets effectively reduce sulfur compounds emission in the gas stream through internal scavenging actions with addition of additives in the pellets, even though a high-sulfur petroleum coke fines (7 wt %) was used in pelletizing.
- Reactivity of petroleum coke under combustion and gasification condition seems significant and sufficient enough in its application for iron ores processing.

ACKNOWLEDGMENT

The project was sponsored by North Star Steel and Tecnored Technologies, Stamford, Connecticut and TECNORED LTDA, Joinville-SC, Brazil. Messrs. Mark Wyborney and Randy Czikall, Kaiser laboratory, Spokane, WA, are acknowledged for their participation and efforts in testing reactor set-up at the Kaiser laboratory and successful operation of the reactor. Mrs. Karen Kumke, A. J. Edmond Company, Texas City, TX, provided the petroleum coke sample used for this study.

REFERENCES

1. J. M. Lee, J. J. Baker, R. Llerena, J. G. Rolle, 214th American Chemical Society National Meeting, Las Vegas, Preprints of Symposia, Division of Fuel Chemistry, Vol. 42, No. 3, 844-853 (1997).
2. J. A. Menendez, et. al., Energy & Fuels, Vol. 10, No. 6, 1996,1262-1268.
3. J. W. Ramming, M. Contrucci, E. Marcheze, TECNORED process data published (1997).
4. J. G. Peacey, The Iron Blast Furnace: Theory and Practice (1979).
5. McGraw-Hill Encyclopedia of Science and Technology, 7th Ed., 423 (1992).
6. Kerk-Othmer Encyclopedia of Chemical Technology, Volume 9, 7th Ed., 829 (1995).

Figure 1. SCHEMATIC DIAGRAM OF REACTION SYSTEM

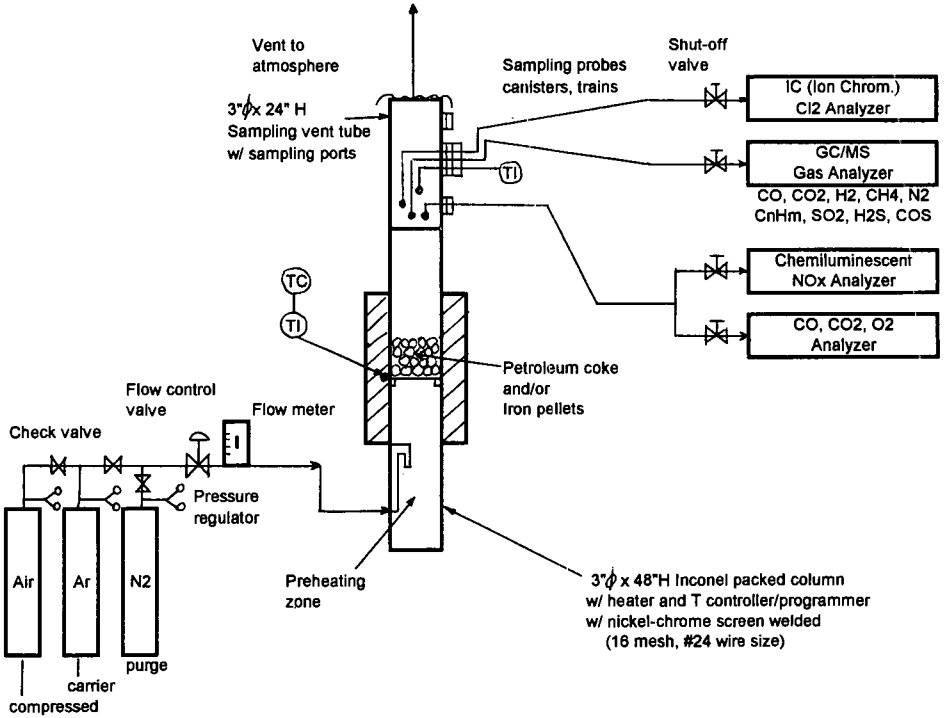

Table 1. EFFLUENT PRODUCT GAS ANALYSES
(Carrier Gas-Free Basis)

Based on argon (carrier gas)-free in Runs 2, 4 to 6, & nitrogen-free in Run 3.

	Run 2 Test A	Run 3 Test B	Run 4 Test C	Run 5 Test C	Run 6 Test C
Operating Conditions					
Reaction temperature (°C)	400-950	1000-1015	500	900	1100
Reaction/sampling time (min)	25	60	60	30	20
Raw material charge (gr)					
Petroleum coke	312.6	302.3	---	—	—
TECNORED pellets (dried)	---	—	1200[a]	1200[a]	1200[a]
Gas flow (L/min)					
Argon (carrier gas)	17	—	6.9	6.7	6.7
Air (reactant gas)	—	6-9.4	---	—	---
Effluent Gas Composition (vol %)			*Relative ratio to Run 5 data*[b]		
N_2 (nitrogen)	---	—	*2.1*	*1*	*0.7-1.0*
CO (carbon monoxide)	<0.1-1.2	8.5	*<0.01*	*1*	*2.9*
CO_2 (carbon dioxide)	<0.1-2.1	15-24	*0.0-0.5*	*1*	*0.9*
H_2 (hydrogen)	---	---	*1*	*1*	*0.6-0.8*
CH_4 (methane)					
C_nH_m (C_2-C_6 hydrocarbons)					
C_nH_m (VOC) (ppmv)	DETERMINED BUT NOT DISCLOSED				
(volatile organic compounds)	DUE TO CONTRACT AGREEMENT				
H_2S (hydrogen sulfide) (ppmv)	(HYDROGEN TO CHLORINE ANAYTICAL DATA)				
SO_2 (sulfur dioxide) plus					
COS (carbonyl sulfide) (ppmv)					
NO_x (nitrogen oxides) (ppmv)					
Cl_2 (chlorine) (ppmv)					
Undetermined (H_2O, etc.)					

NOTE: Most of data were determined using GC/MS analysis of SUMMA canister samples

a Initially charged in Run 4, and Runs 5 and 6 continued without replacement.

b Ratio values of some of Runs 4 to 6 results (proprietary) were used for comparison.

MIXING ELEMENT RADIANT TUBE (MERT) OFFERS NEW CONCEPT FOR ETHYLENE STEAM CRACKING PROCESS

T.Torigoe, H. Hamada, M. Inui, A. Yoshitake, KUBOTA CORPORATION, Hirakata-shi Osaka 573, Japan

Keywords: Ethylene, Thermal Cracking, Mixing

ABSTRACT

Mixing Element Radiant Tube (MERT) is a centrifugal cast cracking tube with a spiral element protuberate inside of it. The concept of the mixing the feed gas is introduced in the ethylene steam cracking technology for the first time. The mixing the feed gas in the tube appears to afford homogeneity in gas temperature which provides minimizing under and over cracking and consequently maximizing proper cracking volume. This means that higher yield of ethylene and/or propylene with lower coking rate can be expected. Moreover, effective heating with breaking boundary film by mixing flow provides reducing tube metal temperatures which result in extending tube life. The concept of MERT and its verification test is described.

INTRODUCTION

In a petrochemical industry, olefins such as ethylene or propylene is produced from hydrocarbon by thermal cracking process. In the process, cracking tubes are used in several types of coils. The feed gas ,typically naphtha or ethane and steam gas, flows inside of the cracking tube at high velocity. The tube is heated at high temperature from the outside of the tube - within a pyrolysis furnace. During the passage of the feed gas throughout the coils, it is thermally cracked into ethylene, propylene, and so on (see Fig. 1).

There have been a lot of developments in ethylene pyrolysis furnace to increase capacity, improve yield and thermal efficiency and reduce downtime for maintenance and decoking along with material developments [1][2] and improvement in tube size and shape[3].

MERT or mixing element radiant tube , is a centrifugal cast cracking tube with a spiral mixing element on the inside diameter(see Fig.2), and provides new concept for improving steam cracking process.

By the mixing of the feed gas:

1. Homogeneous heating can be achieved.
2. The feed gas flow inside of the tube, can be effectively heated thus breaking the boundary film which act as an insulator effecting heat transfer at the metal gas interface.

Homogeneous heating of the feed gas inside the tube can minimize both under and over cracking as well as maximizing proper cracking volume. Therefore it is reasonable to assume that a) ethylene and/or propylene yield can be increased and b) coking can be reduced.

In order to verify the effect of the mixing element, computational fluid dynamic (CFD) analysis was applied to both smooth tube (Bare Tube) and MERT using hot air. As shown in Fig. 3, homogeneous heating of the gas inside of the tube can be expected in MERT. The advantage of homogeneous heating of the feed gas is illustrated in Fig. 4.

Effective heating can provide an energy saving and reduce tube metal temperature which is normally related to coking rate. Therefore tube life can be extended, run length can be extended because of lower coking rate, and firing can be increased as much as the temperature drop as well as production increase without sacrificing tube life.

Based on this new concept of cracking tube, MERT was developed to apply to commercial ethylene cracker.

The material used for MERT is KHR45A(43Ni-31Cr-Nb,Si,Ti) which is superior grade of conventional HP alloys for the mother tube and KHR45A mod. for the element. The element in the MERT is well integrated to the mother tube, and has excellent properties of carburization resistance, thermal shock resistance, and anti-coking.

This paper mainly described the performance of the MERT both in pilot test plant and commercial plant.

EXPERIMENTAL

Experimental 1

In general, internal protrusions in the cracking tube have been considered a cause of coking due to stagnation of the feed gas where over cracking might occur[4]. The MERT element is designed in a spiral shape to produce a "swirl flow", thus eliminating stagnation of the feed gas(see Fig. 5). The visualization tests were performed to confirm the "swirl flow" in each tube size and element angle(see Fig. 6).

In the design of the element, pressure drop (delta P) and heat transfer coefficient should be taken into account. As shown in Fig. 7, the heat transfer coefficient and pressure drop was measured by air test. The air supplied from a blower is controlled in the flow rate by the air damper. And the tests were carried out within the range of the Reynolds Number between $2.5x10^4$ and $2x10^5$. The heat was supplied from hot water or well controlled electric heater from outside of the pipe. Inlet temperature and outlet temperature were measured by thermocouples. Then the heat transfer coefficients of the boundary film were calculated.

In the same way, the pressure drop was measured from the measurement of the pressure difference between inlet and outlet pressure.

These measurements were performed on both bare pipe and MERT in each test.

The pressure drop and boundary film heat transfer coefficient depend on both element angle and fluid velocity. In order to apply MERT technology practically in an ethylene furnace, these data should be made available.

Experimental 2

In order to verify the concept of MERT described in Fig. 4, pilot plant tests were performed.

As shown in Fig. 8, the tube used in this test was 2 inch O.D. and 1.5 inch I.D. and 3.6 M in length. The element angle in MERT was 30° and element height was 2.5mm. The furnace used in this test had electric heater separated in three zone which were independently controlled. The feed gas flows from top to bottom. The composition of the naphtha used is shown in Table 1. The steam to feed ratio was 0.5 for naphtha and 0.3 for ethane respectively. The system of the pilot plant was quite similar to that of commercial plant.

The product was immediately quenched just after the outlet of the tube and the product yield was analized by G.C. The coking amount was measured by the analysis of CO and CO_2 as well as the measurement of the temperature during de-coking.

Experimental 3

In order to verify the performance of the MERT tubes, they are testing in commercial plants. Fig. 9 shows an example of the result of U coil furnace. The MERT tubes were installed in one quadrant of the furnace in two types of modes, applied MERT to both inlet and outlet tubes and to only outlet.

The pressure drop , Tube Metal Temperature(TMT), and feed increase was measured throughout the run length.

RESULTS AND DISCUSSIONS

The heat transfer coefficient of MERT is ,however it is depend on tube size, the element angle and height, and velocity of the gas, normally 20 to 50 % higher than that of smooth tube (Bare tube) while its increasing of heat transfer area is only around 1%.

So it is expected that TMT must be lower than that of bare tube under the same firing condition.

In the pilot plant test using naphtha as a feedstock, when the temperature was adjusted at the same TMT, the feed rate of the MERT could be increased by 40%. And under the same TMT, coking rate of MERT was about 50% lower than that of bare tube. Moreover both ethylene and propylene yield was increased by MERT(see Table 2 - test 1).

When the feed rate was adjusted at the same, TMT of MERT was 24℃ lower than that of bare tube. In this condition, coking rate of MERT was around 50% lower and ethylene and propylene yield was also increased in MERT.(See Table 2-test 2).

The test data shown in Table 2 is under the P/E ratio of 0.45 which is severe condition. The tests were carried out in the range of P/E ratio from 0.45 to 0.70, and the same tendency, especially the increasing of the yields was observed in all tests.

In ethane test (see Table 3), when the conversion was adjusted at the same of 65%, the TMT of MERT was 56 ℃ lower than that of bare. And ethylene yield could be increased by 3%. When the selectivity was adjusted at the same level, ethane conversion of MERT should be raised up. Even in this condition, the TMT of MERT was 25℃ lower than that of bare tube.

In this case, the ethylene yield was 8% higher than that of bare. The test result also suggested that coking rate of MERT was much less than that of bare.

Based on these pilot plant tests, it can be said that the concept described in Fig. 4 was somewhat occured in actual furnace.

Because no catastrophic coking problem was reported in commercial plants where MERT tubes were preliminary installed, MERT performance tests in commercial plants were started. Firstly MERT test was performed in U coil furnace in1997. In the test operation, the TMT of MERT was found to be approximately 50F lower than that of the other bare tubes in the same furnace. This may suggest that if the firing could be increased as much as the temperature drop of MERT, the capacity could be increased by 33% without sacrificing tube life. Due to efficient heating by MERT, the feed rate of MERT section was 2 to 3% higher than the average value of Bare section under the same firing condition. The most remarkable point was that the pressure drop increasing rate of MERT was 2/3 of that of bare tubes. This may suggest the MERT has less coking rate than the bare tubes and can extend run length by 50%.

CONCLUSION

Through the above mentioned tests, it is found MERT has mixing effect and has following advantages.

Higher capacity, Extend tube life(Low TMT), Extend run length(low coking rate)

The yield improvement is now studying in commercial furnace tests and computer simulation. Because ethylene cracking tubes are used in several types of coils[2][3], several factors such as the coil arrangement, the length of MERT, the position installed should be taken into accountin the adequate application of MERT to commercial plants. The MERT has a internal protrusion which may cause for higher friction factor which is related to higher pressure drop. The higher the pressure drop, the longer the residence time which may cause for decreasing yield. The mixing effect in MERT should overcome the pressure drop effect.

It was reported that thousands of chemical reactions might be occured in the hydrocarbon thermal cracking process[5], and these decompositions might be endothermic reactions. In order to estimate the mixing effect, theoretically and experimental approach should be required.

REFERENCES

(1)Steanson B. Parks, C.M.Schillmoller, AIChE 1995 Spring Paper 24b
(2)F.W.Tsai,S.C.Che, R.G.Minet, Hydrocarbon Processing,August 1985 p41-47
(3)J.V.Albano,K.M.Sundaram,M.J.Maddock, Energy Progress, 1988 Vol.8, No.3 P160
(4)Hirata, 123rd Committee Report, JSPS, 1981,Vol 22, No.3
(5)E.Ranzi,M.Dente, S.Plerucci, G.Blardi, Ing. Eng. Fundam., 1983,22.132-139

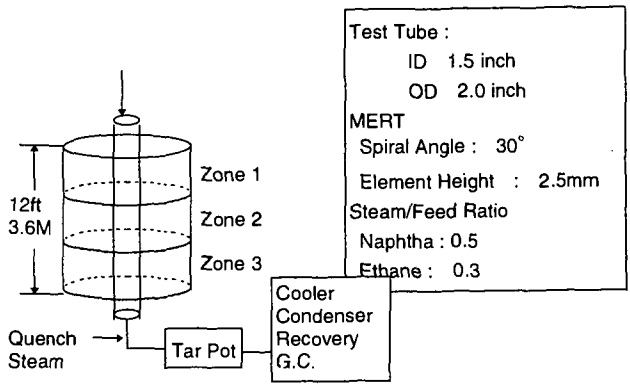

Fig. 8 Pyrolysis Pilot Plant Test

Table 1 Naphtha Composition (wt%)

Paraffins	28.06	C4's	P	0.06	C7's	P	5.36	C9's	P	0.23
Isoparaffins	34.70		I	0.07		I	8.69		I	0.29
Aromatics	11.35	C5's	P	12.24		A	5.56		A	0.00
Naphthens	23.96		I	13.21		N	11.38		N	0.03
Olefins	0.68		N	0.40		O	0.40	C10's	P	0.00
		C6's	P	9.09	C8's	P	1.07		I	0.16
			I	6.85		I	5.43		N	0.02
			A	0.75		A	5.04	C12's	N	0.00
			N	11.51		N	0.63		A	0.00
			O	0.00		O	0.28	C15's	P	0.00
									I	0.00

Table 2 Prototype Test of MERT (Naphtha) P/E : 0.45

Test 1		
	MERT	Bare
Ethylene Yield (wt%)	27.6	25.3
Propylene Yield (wt%)	12.4	11.4
Feed Rate (kg/h)	12.0	8.4
TMT (℃)	892	892
Coking Rate (g/h)	0.68	1.34

Test 2		
	MERT	Bare
Ethylene Yield (wt%)	27.6	25.5
Propylene Yield (wt%)	12.4	11.6
Feed Rate (kg/h)	12.0	12.0
TMT (℃)	892	916
Coking Rate (g/h)	0.68	1.47

Table 3 Prototype Test of MERT (Ethane)

Test 1		
	MERT	Bare
Ethylene Yield (wt%)	52	49
Ethane Conversion(%)	65	65
Ethylene Selectivity(%)	80	75
TMT (℃)	1003	1059

Test 2		
	MERT	Bare
Ethylene Yield (wt%)	57	49
Ethane Conversion(%)	75	65
Ethylene Selectivity(%)	76	75
TMT (℃)	1034	1059

Test 3		
	MERT	Bare
Coking Rate (g/h)	1.3	3.3
TMT (℃)	1034	1059

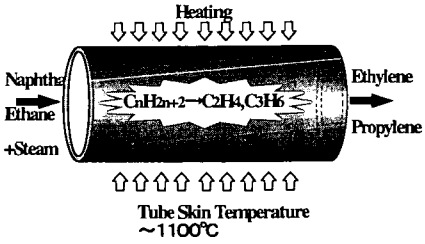

Fig. 1 Cracking Tube

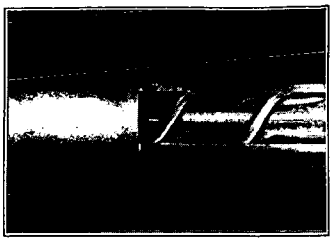

Fig. 2 Cross Sectional Overview of MERT

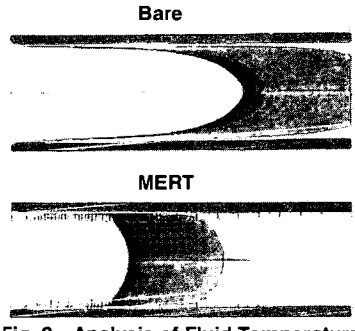

Fig. 3 Analysis of Fluid Temperature

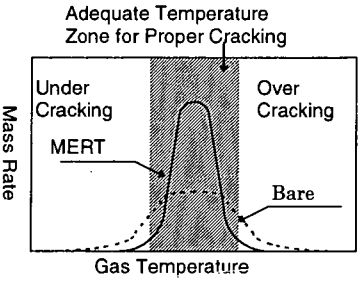

Fig. 4 Homogeneous Chemical Reaction in Tube

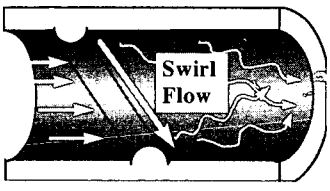

Fig. 5 Swirl Flow

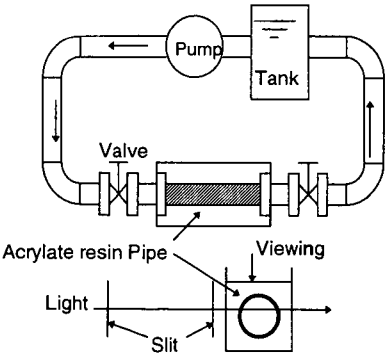

Fig. 6 Visualization Test by Water Flow

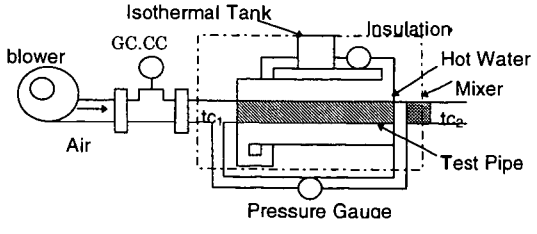

Fig. 7 Heat Transfer Coefficient and Pressure Drop Measurement Apparatus

CHARACTERIZATION OF GREEN AND CALCINED COKE PROPERTIES USED FOR ALUMINUM ANODE-GRADE CARBON

Jun M. Lee, James J. Baker, Jeffrey G. Rolle, Robert Llerena,
A. J. Edmond Co.
1530 West 16th Street, Long Beach, CA 90813

Keywords: petroleum coke, calcine, aluminum anode carbon

ABSTRACT

Various properties of green (raw) and calcined petroleum cokes were analyzed and evaluated for use in aluminum anode-grade carbon. Petroleum cokes for this characterization study include different cokes produced from several refineries in U.S. and in other regions of the world such as China, Indonesia, Brazil, Argentine and Kuwait. Coke properties evaluated are: moisture, volatile carbon matter (VCM), ash, fixed carbon (FC) (by difference), sulfur, carbon, hydrogen, nitrogen, oxygen (by difference), metals (Si, Fe, V, Al, Ca, Na, Cr), calorific value, real density (RD), vibrated bulk density (VBD), size distribution, etc. Some of recent analysis results with these petroleum cokes are compared and presented.

INTRODUCTION

Export quality of petroleum cokes was evaluated and discussed at the ACS Las Vegas Meeting (September 7-11, 1997), based on recent analysis results from calcined petroleum coke produced for aluminum anode-grade and green (raw) coke used in calcination [1]. Production of petroleum cokes steadily increased by 51% during the past decade, expecting continuous increase in the coming years, primarily due to declining quality of crude oils. Exports to foreign countries are a major market for the U. S. coking industry and were 66% of the annual production (78,430 tons/cd) in 1993 . Green petroleum cokes are mostly used as utility fuels (about 73% for fuel grade), and as feedstocks (about 27%) for further upgrading calcination. The calcined petroleum cokes are used in production of specialty products: 71% for aluminum anode-grade, 9% for graphite electrodes, needle-grade, 8% for titanium dioxide pigments, 6% for recarburized ductile iron products, and 6% for others (chlorine, phosphorous, silicon carbide, calcium carbide, etc.).

Petroleum cokes are produced at refineries using three different types of coking processes: delayed, fluid, and flexicoking. The delayed coker is mostly used at forty-nine U.S. refineries processing total 1.57 mm b/sd [2]. The other fliud coker and flexicoker are less utilized at a relatively smaller capacity (seven refineries and 0.2 mm b/sd). Coke products from a delayed coker are classified as shot, sponge, (sometimes honeycomb), or needle coke depending on their chemical and physical characteristics. Shot coke (almost always sold as fuel) is hard, having spherical form, and physically produced through precipitating asphaltenes; sponge coke (mostly used for anode-grade) is dull and black, having porous, amorphous structure, and is considered as a mixture of shot and needle cokes; and needle coke (not used in anode production) is silver-gray, having crystalline broken needle structure, and chemically produced through cross linking of condensed aromatic hydrocarbons during coking reactions [3,4]. Most of fluid coke does not enter the anode pool and flexicoke has never been used in aluminum smelting.

The objective of this study is to evaluate various properties of green (raw) and calcined petroleum cokes used in aluminum anode-grade carbon, comparing different cokes produced from several refineries in U.S. and in other countries such as China, Indonesia, Brazil, Argentine and Kuwait.

COKE, ANODE PROPERTIES, AND CARBON CONSUMPTION

Rolle and Hoang [5] investigated the impact of metal impurities, vanadium and sodium, on the air reactivity of cokes and anodes. Vanadium has less impact on air reactivity than previously published and sodium is approximately five times more leveraging than vanadium on both coke and anode air reactivity.

Casada, Rolle, et. al. [6] reported the influence of nickel on reduction cell anodes. Nickel alone does not significantly effect anode air or CO_2 reactivity, but including anode butt material increased CO_2 reactivity.

Leach, et. al. [7] evaluated calcined coke and anode core properties to predict carbon consumption and anode performance in aluminum reduction cells. Calcined cokes having a range

of properties can produce quality prebake anodes that yield low, stable carbon consumption. Their specific findings are:

- o Highly efficient modern prebake potlines can allow larger variability of carbon properties.
- o A strong correlation exists between the coke V content and anode air reactivity, while no correlation between coke air reactivity and anode air reactivity residue (ARR) was evident. To lower anode air reactivity (increase the ARR), reduce the coke V concentration.
- o A strong correlation exists between the anode Na content and anode carboxy reactivity residue (CRR), while a weaker correlation exists between the coke carboxy reactivity and anode CRR. The carboxy reactivity of the anode can be minimized by lowering the anode Na content through the use of cleaner butts and purer coke.
- o A strong correlation between coke grain stability and anode flexural strength was identified.

A desired range of calcined coke air reactivity based on the ignition temperature is 0.05-0.30 %/minute, and airburning increases near 0.30 %/minute [7]. A grain stability range of 75-85% is desirable with values below 75% causing substantially lower anode strength and thermal shock resistance. A substantial reduction in carbon consumption (a 12% decrease in eight years) was achieved and reported by de Mori by applying the correlation formula published by Fisher, et. al. that incorporates baked anode properties, potroom operations parameters, and a cell factor to predict carbon consumption.

$$PAC = C + 334/CE + 1.2\,(BT-960) - 1.5(ARR) - 1.7(CRR) + 9.3(AP) + 8(TC)$$

, where PAC is predicted anode consumption; C, cell factor; CE, current efficiency; BT, bath temperature; ARR, air reactivity residue; CRR, carboxy reactivity residue; AP, air permeability; and TC, thermal conductivity.

With 100% efficiency, the amount of carbon required would be 0.334 kg/kg of aluminum [4]. Actual net carbon consumption is in the range of 0.44 to 0.5 kg C/kg Al.

Eidet et. al. [8] studied effects of iron and sulfur on the air and CO_2 reactivity of calcined cokes. Excess carbon consumption (0.02 to 0.15 kg C/kg Al in prebake cells) in the aluminum electrolysis is caused by the oxidation of the anodes by air and CO_2, catalyzed by many different inorganic impurities present in the carbon anode materials. Iron catalyzes both O_2 combustion and CO_2 gasification of carbon. Sulfur is inactive in and do not have a significant effect on both reactions. Sulfur inhibits iron catalytic reactions.

Vogt and Ries [9] investigated the effect of anode desulfurization on baking by varying temperature and soak time. The best baking furnaces can achieve a uniform baking temperature (typically 1100-1150 deg C) with a variation of +/-25 deg C. Average anode baking temperature has been increased to near 1200 deg C with a soak time of 56 hours. Desulfurization during the baking can cause high air, CO_2 reactivities and permeability with abnormally low sulfur levels (<2.0% S as compared to >2.3% normal). Optimum baking temperature exists at a given soak time, and the porosity created by the loss of sulfur ultimately contributes to poorer reactivity behavior due to increased active sites available for oxidant molecules to attack carbon surface.

During calcining, green cokes with low sulfur less than 2% typically produce a calcined product having 90% of the green coke's sulfur level; cokes with high sulfur up to 5% calcine to about 85% of the original sulfur level. The remaining sulfur in the calcined coke is liberated during the smelting process. A critical temperature was identified in a laboratory calcining study investigating desulfurization, corresponding the initial release of sulfur and the creation of micropore volume (pore diameters <0.1 mm). The critical temperature was found to be coke specific and ranged from 1300 deg C for the high sulfur coke and 1500 deg C for the low sulfur coke.

TYPICAL PROPERTIES OF ALUMINUM ANODE-GRADE CALCINED COKE

Green (raw) petroleum coke is produced as a by-product in the refinery crude oil processing and primarily used in anode manufacture because of its low ash content. In general, coke is considered more valuable if it has low sulfur content, high bulk density, and metals content [4]. Sulfur emissions are an environmental liability in aluminum manufacturing. V and Ni (chemically bonded

to hydrocarbons) and Na (dissolved as sodium chloride in water which is entrained with the crude oil) catalyze anode oxidation accelerating anode consumption and are ingot impurities. Two other variables affecting anode performance are density and sizing. Higher density cokes enhance anode properties and most coke users desire a product which is at least 30 wt % plus No. 4 Tyler mesh.

Calcination process basically removes volatile matter, hydrogen and some of sulfur present in green cokes as a result increasing density and electrical conductivity suitable for use of carbon anodes in aluminum production. Typical ranges of calcined coke properties for aluminum anode-grade specifications are listed in the following [4,10-13]:

Property	Green	Calcined
wt% S	2.5	2.5 (1.7-3.0)
wt% ash	0.25	0.30 (0.1-0.3)
ppm V	150	200 (165-350)
ppm Ni	150	200(120-350)
wt% Si	0.02	0.02
wt% VM	10-12	<0.25
resistivity, microomega-m		950
real density, g/cu-cm		2.06
bulk density, g/cu-cm		0.80
coefficient of thermal expansion per deg C		2 x 10 to -6

SAMPLING AND PREPARATION

Representative samples of petroleum cokes for this study have been obtained from various refineries in U.S., China, Indonesia, Brazil, Argentine and Kuwait. Green (raw) cokes were produced in the delayed coking process and calcined using laboratory furnaces. Laboratory samples are prepared for coke properties analysis following the procedures and principles in handling listed in the ASTM Methods D 346, D 2013 and D 2234.

ANALYTICAL METHODS USED

Laboratory test methods using various advanced analytical instruments are described in the Quality Assurance Manual of the A. J. Edmond Company. Primary analytical methods used for this study are summarized as follows:

Purpose	ASTM Method		Instrument
metals	D5600	ICP-AES	PE Optima 3000
sulfur	D4239	LECO	LECO SC 432
CHN	D5373	LECO	LECO CHN-1000
Btu	D3286	PARR	PARR 1108, 1261, 1563
moisture	D3173		
volatile	ISO562		
ash	D4422,D3174		
VBD	D4292		
RD	D2638		Micrometrics AccuPyc 1330
sieve	D5709,D293		

RESULTS AND DISCUSSION

Table 1 summarizes analysis results of typical properties of green (raw) and calcined petroleum cokes used for aluminum anode-grade carbon. Export qualities of calcined cokes at U.S. West Coast ports are also included in the last two columns of Table 1 (Continued). Proximate, ultimate analysis, metals content, sizing, calorific value, RD and VBD were determined in this study and are compared.

Laboratory Calcination Results

Ratios of calcined to green coke property value as percentage are listed in Table 1 to evaluate laboratory calcination. Calcination basically removed VCM, hydrogen, and some of sulfur and nitrogen present in green cokes. As a result ash, FC and carbon contents increased, while calorific value decreased. Loss or gain of each coke property value after calcination are compared in the following.

Property	Loss, %	Gain, %
VCM	95.4-97.6	
Hydrogen	96.9-99.4	
Sulfur	8-13	(0-1% gain with three samples)
Nitrogen	25-46	
Ash		9-46 (0-10% loss with three samples)
FC		9-13
Carbon		5-6
Btu/lb	9-11	

Ash ratio of calcined to green coke significantly varies from 10% loss to 46% gain, showing analytical errors associated with low ash content of cokes studied (0.05-0.36 wt %).

Sulfur Content

Sulfur content of petroleum cokes analyzed for this study varies in the range of 0.46 to 3.21 wt %. Chinese, Brazilian and Indonesian cokes have a low sulfur content of 0.5 to 0.8 wt %, while cokes from Kuwait and several refineries in U.S. (USA1, USA3, USA4, LV and LB) have a high sulfur content of 2.2 to 3.2 wt %. Cokes from Argentine and a refinery in U.S. (USA2) have a medium sulfur content of 1.0 to 1.5 wt %. Aluminum smelter sulfur restrictions are regional, and locally regulated to meet environmental emission standards, depending upon industrial, urban or rural area [14]. In Europe and Scandinavia, a coke sulfur limit of 2% maximum is frequently imposed locally; and for new smelters in North America and Australia, the sulfur limit is 3% maximum. Latin America, South Asia and Africa generally have few restrictions on sulfur levels in calcined coke. To lower sulfur content of coke (which is projected to significantly increase to 5% in future), residual oil hydro-desulfurization or thermal desulfurization of petroleum coke may be become an important, viable process.

Ash and Metals Content

Ash content of petroleum cokes analyzed for this study ranges from 0.05 to 0.36 wt %. Calcined cokes from Kuwait, Brazil and several refineries in U.S. (USA1, LV and LB) show a low ash content of 0.07 to 0.13 wt %, while calcined cokes from Indonesia, USA2 and USA3 have a high ash content ranging from 0,29 to 0,35 wt %. A medium level of ash content, 0.17 to 0.19 wt %, is indicated with calcined cokes from China, Argentine and USA4.

V, Ni and Na metal impurities catalyze oxidation and gasification reactions of carbon in the aluminum smelting process resulting in a higher carbon consumption. Studies performed with various V and Na concentrations indicated a strong correlation with air and carboxy reactivity, but with Ni results were less conclusive. Other metals most likely stay with aluminum ingot as impurities and may affect coke quality parameters.

Chinese, Argentina and Indonesian calcined cokes have a low V content of 24 to 81 ppm; 228-257 ppm with Brazilian, Kuwait and USA4; and a high V content of 300 to 607 ppm is observed with calcined cokes from several refineries in U.S. (USA1, USA2, USA3, LV and LB).

A Ni content less than 200 ppm (ranging from 118 to 194 ppm) is shown with Argentina, Kuwait, USA1, USA4, LV and LB calcined cokes. Other calcined cokes have a high Ni content of 215 to 592 ppm.

Na content of calcined cokes studied varies less in the range of 21 to 140 ppm compared to V and Ni content.

Real Density and Vibrated Bulk Density

Real density of calcined cokes is in the range of 2.057 to 2.076, and all are acceptable for aluminum smelting. Vibrated bulk density of calcined cokes varies in the range of 0.672 to 0.922 g/cu-cm, indicating significant differences in size distribution among calcined cokes studied.

Size Distribution

Larger than 4 mesh size fraction of calcined cokes varies ranging from 22.9 to 53.7 wt %. Depending on buyer and producing refinery, as listed in Table 1 (Continued), export specification for this fraction can be >32% or >55%. Less than 200 mesh size fraction of these cokes is in the range of 0.2 to 0.6 wt %, meeting export specification.

SUMMARY

Various green (raw) and calcined cokes were analyzed and evaluated for application in production of aluminum anode-grade carbon. Typical coke property data are obtained from nine green and

eleven calcined cokes produced in several different regions of the world (U.S., China, Argentine, Indonesia, Brazil and Kuwait). Important coke quality parameters for these cokes are tabulated and compared, primarily focused on sulfur content, ash and metals (V, Ni, Na) content, density and size distribution. Coke quality significantly varies and is regional in nature depending upon quality specifications dictated by buyer and/or producing refinery.

ACKNOWLEDGMENT

RAIN Calcining Limited, Hydrabad, India, sponsored this project.

REFERENCES

1. J. M. Lee, J. J. Baker, R. Llerena, J. G. Rolle, 214th ACS National Meeting, Las Vegas, Preprints of Symposia, Division of Fuel Chemistry, Vol. 42, No. 3, 844-853 (1997).
2. E. J. Swain, Oil & Gas Journal, Jan. 2, 1995, 33-39; Jan. 9, 1995, 37-42.
3. N. P. Lieberman, Oil & Gas Journal, Mar. 27, 1989, 67-69.
4. R. E. Dymond and B. H. Spector, Light Metal Age, Feb. , 1992, 34-38.
5. J. G. Rolle and Y. K. Hoang, Light Metals 1995, 741-744, 124th TMS Annual Meeting, Las Vegas, Feb. 12-16.
6. M. R. Casada, J. G. Rolle, et. al., Light Metals 1997, 489-495, 126th TMS Annual Meeting, Orlando, FL, Feb. 9-13.
7. C. T. Leach, et. al., Light Metals 1997, 481-488, 126th TMS Annual Meeting, Orlando, FL, Feb. 9-13.
8. T. Eidet, et. al., Light Metals 1997, 511-517, 126th TMS Annual Meeting, Orlando, FL, Feb. 9-13.
9. F. Vogt and K. Ries, Light Metals 1995, 691-700, 124th TMS Annual Meeting, Las Vegas, Feb. 12-16.
10. W. M. Goldberger, et. al., Petroleum Derived-Carbons, ACS Symposium Series 303, 1986, Ch. 15, 200-214, (Edited by J. D. Bacha, et. al.).
11. Ullmann's Encyclopedia of Industrial Chemistry, Volume A20 and A27 (1986).
12. E. J. Swain, Oil & Gas Journal, May 20, 1991, 49-52.
13. Kerk-Othmer Encyclopedia of Chemical Technology, Volume 4, 4th Ed., Carbon, 956 (1992).
14. M. F. Vogt, et. al., JOM, July 1990, 33-35.

Table 1. TYPICAL PROPERTIES OF GREEN AND CALCINED COKES USED FOR ALUMINUM ANODE-GRADE CARBON

Origin	China		Argentine		Indonesia		Brazil		Kuwait	
Type	*Green*	*Calcine*	*Green*	*Calcine*	*Green*	*Calcine*	*Green*	*Calcine*	*Green*	*Calcine*
(as-received)										
Moisture, wt%	1.2		7.2		5.7		5.1		0.9	
(dry-basis)										
Proximate, wt%										
VCM	9.90	0.27	11.74	0.28	11.07	0.28	10.09	0.29	8.46	0.28
Ash	0.15	0.17	0.21	0.19	0.36	0.33	0.11	0.11	0.05	0.07
FC	89.95	99.56	88.05	99.53	88.57	99.39	89.80	99.60	91.37	99.65
Ultimate, wt%										
Sulfur	0.68	0.66	1.45	1.46	0.53	0.46	0.79	0.73	3.21	3.14
Carbon	92.10	97.52	91.09	96.89	92.22	97.87	91.95	97.46	91.55	96.05
Hydrogen	3.73	0.10	3.61	0.09	3.94	0.11	3.63	0.05	3.43	0.08
Nitrogen	2.30	1.55	2.08	1.37	1.63	1.23	2.63	1.65	1.05	0.66
Oxygen	1.04	0.00	1.56	0.00	1.32	0.00	0.89	0.00	0.59	0.00
Metals, ppm										
Silicon	87	124	98	73	472	579	42	20	7	9
Iron	98	106	256	268	93	184	197	99	18	51
Vanadium	31	34	91	81	5	24	201	257	184	257
Nickel	256	279	117	134	144	238	176	215	86	118
Aluminum	88	85	43	83	48	95	13	9	3	15
Calcium	87	95	123	130	48	73	8	9	5	3
Sodium	63	59	110	96	91	124	51	61	15	21
Chromium	1.1	1.2	0.5	1.4	0	0.8	1.5	1.5	0.3	0.3
Btu/lb	15603	14089	15660	13997	15666	14156	15454	14087	15664	13889
RD, g/cm3		2.066		2.068		2.070		2.071		2.075
VBD, g/cm3		0.823		0.765		0.672		0.810		0.792
Size, wt%										
+20 mm	21.2		10.3		10.3		13.7		38.0	
-6 mm	51.1		70.6		72.5		65.7		24.7	
+4 mesh		37.7		28.2		31.8		22.9		53.7
+8 mesh		52.6		44.7		49.8		35.7		68.0
-50 mesh		6.4		6.5		3.4		11.8		5.3
-70 mesh		1.4		3.9		1.7		7.3		3.1
-200 mesh		0.3		0.5		0.3		0.6		0.3
Ratio of Calcine to Green, %										
VCM		2.7		2.4		2.5		2.9		3.3
Ash		109		90		92		100		140
FC		109		113		112		111		109
Sulfur		100		101		87		92		98
Carbon		105		106		106		106		105
Hydrogen		0.6		2.5		2.8		1.4		2.3
Nitrogen		60		66		75		63		64
Btu/lb		90		89		90		91		89

Table 1 (Continued). TYPICAL PROPERTIES OF GREEN AND CALCINED COKES USED FOR ALUMINUM ANODE-GRADE CARBON

Origin	USA1-CA		USA2-CA		USA3-CA		USA4-LA		LV-WA	LB-CA
Type	*Green*	*Calcine*	*Green*	*Calcine*	*Green*	*Calcine*	*Green*	*Calcine*	*Calcine*	*Calcine*
(as-received)										
Moisture, wt%	4.2		2.6		9.2		6.4		0.03	0.1
(dry-basis)										
Proximate, wt%										
VCM	8.90	0.26	11.02	0.29	11.18	0.51	10.54	0.27	0.1	0.1
Ash	0.11	0.12	0.28	0.35	0.22	0.29	0.13	0.19	0.1	0.13
FC	90.99	99.62	88.70	99.36	88.60	99.20	89.33	99.54	99.8	99.77
Ultimate, wt%										
Sulfur	2.96	2.95	1.10	1.02	2.42	2.20	2.81	2.65	2.8	2.85
Carbon	91.20	96.03	91.27	96.59	90.68	96.32	91.02	96.22		
Hydrogen	3.56	0.02	3.83	0.12	3.79	0.04	3.70	0.04		
Nitrogen	1.47	0.88	3.39	1.92	1.80	1.15	1.67	0.90		
Oxygen	0.70	0.00	0.13	0.00	1.09	0.00	0.67	0.00		
Metals, ppm										
Silicon	23	22	60	87	156	130	22	20	30	20
Iron	28	45	202	272	211	291	83	105	50	75
Vanadium	321	365	504	607	264	338	229	228	300	385
Nickel	137	158	488	592	238	300	190	194	125	160
Aluminum	10	18	28	61	131	211	14	27		
Calcium	18	13	127	140	44	52	89	156	15	30
Sodium	32	31	133	140	37	67	79	89	30	35
Chromium	0.5	0.5	1.9	1.9	0.7	0.7	0.1	0.1		
Btu/lb	15600	13991	15539	13929	15612	14030	15633	13946		
RD, g/cm3		2.068		2.065		2.057		2.076	2.07	2.07
VBD, g/cm3		0.823		0.922		0.758		0.744	0.89	0.87
Size, wt%										
+20 mm	20.5		33.0		19.2		6.2			
-6 mm	50.1		34.3		53.7		65.5			
+4 mesh		44.7		29.1		32.0		33.4	32	55
+8 mesh		58.2		46.3		50.0		47.9	-	70
-50 mesh		8.0		1.8		5.1		10.9	8	-
-70 mesh		4.8		0.9		2.7		7.1	-	3.3
-200 mesh		0.3		0.2		0.4		0.6	0.6	0.3
Ratio of Calcine to Green, %										
VCM		2.9		2.6		4.6		2.6		
Ash		109		125		132		146		
FC		109		112		112		111		
Sulfur		100		93		91		94		
Carbon		105		106		106		106		
Hydrogen		0.6		3.1		1.1		1.1		
Nitrogen		60		57		64		54		
Btu/lb		90		90		90		89		

ALKYLATION OF ISOBUTANE AND BUTENES OVER ANION-MODIFIED ZIRCONIUM OXIDE CATALYSTS.

Xin Xiao, Jianmin Chen†, Shuguang Zhang, John W. Tierney and Irving Wender*
Department of Chemical and Petroleum Engineering, 1249 Benedum Hall,
University of Pittsburgh, Pittsburgh, PA 15261

Keywords: alkylation, solid acid catalyst, anion-modified zirconium oxide

Introduction Alkylation of isobutane with butenes is an important industrial process for the production of isooctane and its isomers, i.e., trimethylpentanes (TMPs). The product, called alkylate, has a high octane number (90-94 RON), low vapor pressure (RVP), no aromatics or olefins. It is a preferred blending stock for reformulated gasoline. The production of alkylate in the US should exhibit steady growth through the year 2000 [1] and will top 900,000 b/d in 1997 [1], about 13 vol% of the US gasoline pool [2]. Two types of commercial processes are now in operation: one based on HF, the other on H_2SO_4. There are considerable environmental concerns about the use of the toxic HF and sulfuric acid presents problems of corrosion and disposal of spent catalysts. Efforts are being made to use HF in a way to reduce its volatility [3]. It is recognized that alkylate production by use of an environmentally benign solid acid catalyst is highly desirable [4-8]. Work on the chemistry and technology of C_4 alkylation before 1993 has been reviewed [9]. A recent symposium was held on the use of solid acid catalysts and processes[10]; none have been commercialized as yet. Major problems for solid catalyst alkylation are short catalyst life time and low selectivity to TMP.

Rao [2] has written a reaction pathway for the isobutane-isobutene alkylation:

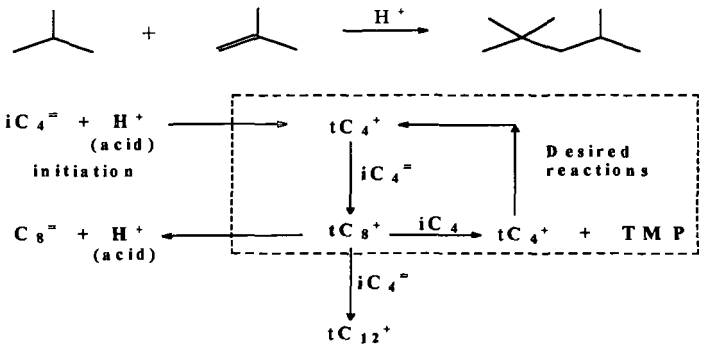

Two major undesirable reactions usually occur: competitive side reactions leading to formation of octenes rather than TMPs; and consecutive side reactions leading to higher (C_{12} and C_{16}) hydrocarbons. To obtain a high selectivity to alkylate, a low olefin concentration must be maintained in the reaction zone; high isobutane to olefin feed ratios and high olefin conversions are necessary. In commercial alkylation processes, the feed isobutane/butenes ratios (external ratio) are typically 5-8 for the H_2SO_4 process and 10-14 for the HF process. Due to high olefin conversion inside the reactor, the internal isobutane/butenes ratios are much higher. However, this ratio is difficult to maintain on a solid catalyst surface because olefin adsorption is much stronger than paraffin adsorption. This may explain a difficulty of the alkylation process over solid catalysts.

Recently, new types of anion-modified metal oxides have drawn increasing attention[11-13]. Metal-promoted ZrO_2/SO_4 and ZrO_2/WO_3 are strong solid acids with activity for hydrocracking and hydroisomerization of hexadecane, polyethylene and Fischer-Tropsch waxes at relatively mild reaction conditions [14-16]. Initial activity has been demonstrated over ZrO_2/SO_4 catalyst for alkylation reaction [7, 17]. In this work we investigated the alkylation chemistry and deactivation behavior over two Pt-promoted anion-modified metal oxide catalysts, $Pt/ZrO_2/SO_4$ (PtSZ) and $PtZrO_2/WO_3$ on Al_2O_3 support (PtWZ-Al_2O_3).

Experimental Section

Feed mixture preparation. Isobutane (i-C_4H_{10}, 99.7%; C_3H_8, 0.3%) was obtained from Praxair. A mixture containing isobutene (i-C_4H_8, 8%; i-C_4H_{10}, 91%; C_2H_6, 1%) and a mixture containing cis-2-butene (cis-2-C_4H_8, 20%; i-C_4H_{10}, 80%) were obtained from Air Products. All three are in steel cylinders with dip tubes. Various ratios of isobutane/butene were made by mixing into a

*Correspondence author. †Current address: Department of Environmental Science & Engineering, Fudan University, Shanghai 200433, China.

500ml steel container kept at dry ice temperature. Before loading of each component, connecting tubes were purged with the feed component to remove air. The steel container with its contents was weighed each time after a component was put in. The final composition of the mixture was calculated and verified by GC.

Catalyst Synthesis. The solid catalysts PtSZ and PtWZ-Al_2O_3 were synthesized following a similar method described elsewhere [15]. $ZrCl_4$ was dissolved in 1500 ml of distilled water and hydrolyzed at room temperature by slowly adding 28-30% NH_4OH with vigorous agitation until pH = 9 was reached. The mixture was stirred for another 30 min and left to settle overnight. The precipitate [$Zr(OH)_4$] was filtered and washed with distilled water until no chloride ions were detected. The solid was then dried at 110 °C overnight and ground to below 100 mesh. Sulfation was carried out by treating 10.0 g of the resultant $Zr(OH)_4$ with 150 ml of 0.5 M H_2SO_4 solution for 30 min with constant stirring. The solid was separated from the liquid by filtration, rinsed with ~150 ml of water and dried at 110 °C overnight. The sample was loaded with 0.5 wt% Pt by incipient wetness impregnation of an H_2PtCl_6 aqueous solution, dried at 110 °C overnight and calcined at 650 °C for 3 hr. Tungsten [$WO_3/(ZrO_2 + WO_3)$ was 8.3 wt%] was loaded on $Zr(OH)_4$ by incipient wetness impregnation of a $(NH_4)_6H_2W_{12}O_{40}$ solution. The sample was dried at 110 °C overnight, mixed with γ-Al_2O_3 (ZrO_2:Al_2O_3 = 1:1 by wt), and impregnated with 0.5 wt% Pt (based on total solid) using an H_2PtCl_6 aqueous solution. The sample was dried at 110 °C overnight and calcined at 700 °C for 3 hr.

Reactor. A continuous up-flow fixed bed reactor equipped with on-line GC analysis was employed. The isobutane/butene mixture was maintained in liquid phase under He pressure, and fed to the reactor by a piston-type pump. The reactor temperature was controlled by a computer in the range of 30 - 750 °C; pressure was controlled by a back-pressure regulator in the range of ambient to 1000 psig. Various gases, air, He, N_2 and H_2, could be fed into the reactor and the flow rate controlled by a mass flow meter.

Experimental Procedure. Catalysts were formed into pellets and then crushed to 40-60 mesh particles. The catalyst was then mixed with the same weight of 50-70 mesh quartz sand and packed into a 3/8" o.d. stainless steel tubular reactor. Quartz sand was packed before and after the catalyst bed. Before a reaction, the reactor system was purged with He and pressurized. Liquid isobutane was pumped into the reactor and heating started. The feed was switched from an isobutane to isobutane/butene mixture at least 10 min after a stable reaction temperature was reached. Time-on-stream (TOS) was recorded as zero min at the moment of the feed switch. On-line GC analysis (FID detector) was used periodically to analyze product composition. Liquid products condensed by dry ice were kept in a refrigerator (4 °C). After evaporation of isobutane, the remaining liquid products were identified by GC/MS and compared with literature data [18], pure compounds, and boiling points of the species.

Results and Discussion

Alkylation of isobutane and 2-butene. Figure 1 shows liquid product obtained from alkylation of isobutane and 2-butene over a Pt/ZrO_2/SO_4 catalyst at a whsv of 2.0 h^{-1}. The main peak was 2,2,4-TMP, accompanied by 2,3,4- and 2,3,3-TMPs. Dimethylhexanes (DMHs), branched C_8 olefins, C_9 and higher paraffins and olefins as well as C_5-C_7 cracking products were also found. At a lower whsv, 0.25 h^{-1}, under otherwise identical conditions, the catalyst life time was extended and TMP selectivity increased (Table 1). GC analysis revealed that the increase in TMP selectivity at the lower whsv was mainly due to an increase of 2,3,4- and 2,3,3-TMPs (Figure 2). However, fractions higher than C_8 also increased. At prolonged reaction times (1.5 and 5 hr, respectively) TMPs were diminished but selectivities to C_8 olefins and higher hydrocarbons increased in both runs.

Deactivation and regeneration of the catalyst. TMP selectivity was highest at low TOS; C_8 olefins appeared a few minutes later, and gradually replaced TMP as the main peak during alkylation of isobutane and 2-butene over a PtSZ catalyst. At high TOS, C_8, C_{12} and C_{16} branched olefins were the main products, as shown in the following sequence:

$$i\text{-}C_4 + C_4^{=} \xrightarrow{\text{solid catalyst in i-}C_4} \text{TMP (isooctane and isomers)}$$

$$\boxed{\text{TMP} + C_8^{=}} \quad \boxed{C_8^{=}} \quad \boxed{C_8^{=} + C_{12}^{=}} \quad \boxed{C_{12}^{=} + C_{16}^{=}} \longrightarrow$$

Time On Stream

Conversion of 2-butene remained almost unchanged in the first few hours. The shift in product composition was probably due to adsorption phenomena on the catalyst surface. The catalyst surface was originally covered only by isobutane. When the isobutane/2-butene mixture passed through the catalyst bed, 2-butene first reacted with surface isobutane to yield TMP. The more strongly adsorbed 2-butene then started to replace isobutane from the catalyst surface. After

the concentration of 2-butene reached a certain level, C_8 olefins formed by dimerization of adsorbed 2-butene were the main product. The C_8 olefins reacted further with 2-butene to give C_{12} and C_{16} olefins. TMPs as the main product indicated predominant adsorption of isobutane on the catalyst surface, and C_8 olefins as the main product indicated adsorption of 2-butene, and C_{12} olefins indicated C_8 olefin adsorption. Jong et al. indicated that these side reactions contribute to catalyst deactivation [19]. Low butene concentration is crucial in alkylation to keep good TMP selectivity.

To verify the surface adsorption hypothesis, a series of regeneration experiments on the same catalyst were performed. Since solid alkylation catalysts could be regenerated by air, H_2 stripping [20] and solvent extraction [21], the catalyst deactivation is probably caused by carbonaceous deposits.

Full regeneration was indicated when TMPs appeared as the main product at the beginning of a run. The run was continued until C_{16} olefins appeared. Without regeneration, only C_8 and higher olefins were observed. As seen in Table 2, the catalyst was successfully regenerated by H_2 accompanied by liquid isobutane flow (400 psig) at 110 °C for 30 min. It can be explained by assuming that the surface was saturated with adsorbed 2-butene and C_8 olefins which were replaced by an excess of isobutane. The catalyst was also successfully regenerated at 71 °C for 2 hr in H_2 and isobutane. However, when the temperature was lowered to 24 °C, the catalyst was only partially regenerated as indicated by both TMP and C_8 olefin peaks at the initial TOS. The catalyst was also regenerated by air at 450 °C and 690 °C. If deactivation of the catalyst were caused by surface lay down of olefins, removal of olefins by desorption would regenerate the catalyst. To test this, He was passed through the reactor which was gradually heated to 450 °C and kept at that temperature for 3 hr, a procedure similar to TPD; the following alkylation reaction showed initial activity to TMPs. Repeated regeneration by He at 450 °C was also successful. The experiments indicated that degradation of the catalyst was caused by strong adsorption of certain species, probably olefins, which covered active sites responsible for alkylation, but the active sites were never destroyed.

Alkylation of isobutane and isobutene. In order to weaken the adsorption of olefins and enhance the adsorption of isobutane on the catalyst surface, the following modifications were made: (1) PtWZ (on a γ-Al_2O_3 support) , which has higher hydrogen transfer activity than PtSZ [22,23], was used as catalyst; (2) reaction temperature was increased to 150 °C; and (3) H_2 was used along with the feed. It was found that low H_2 amounts (less than 1 mol% of total feed) was not enough to suppress polymerization reactions while H_2 amounts greater than 100 mol% of isobutene stopped the alkylation reaction by hydrogenation of isobutene. By comparing runs with and without H_2, and other process variables, suitable reaction conditions and product compositions were obtained (Table 3). At 150 °C and 780 psig (supercritical), isobutene conversions reached 100.0% and 2,2,4-TMP selectivity was between 65.1 to 83.2 %. On-line GC analysis of this run at 4.0 hr is shown in Figure 3. The run was stopped after 6.8 hr. No deactivation was observed. TMP selectivity had a tendency to increase with TOS; selectivities were 65.1 % at 1.7 hr and 83.2 % at 6.8 hr. C_8 components other than 2,2,4-TMP were TMP isomers and DMHs. No olefins were observed. All by-products were in trace amounts except C_{12} branched paraffins, which was about 20 wt%. Total gasoline boiling fractions (C_5-C_{12}) were over to 99 % in all TOS. A run with a lower H_2 to isobutene ratio, i.e., H_2 : isobutene = 1 : 5 (mol), was also made for a longer run time, i.e., 8.3 hr (Table 3). Similar results were observed. The H_2 to isobutene molar ratio was varied from 1:5 to 1:3. Larger amounts of H_2 hydrogenated olefins and decreased the TMP yield dramatically. If the amount of H_2 was lower, TMP selectivity could not be maintained, eventually being replaced by C_8 and higher olefins.

Acknowledgment. The research was supported by the U.S. Department of Energy through the Consortium for Fossil Fuel Liquefaction Science (Grant No. DE-FC22-93PC93053).

REFERENCES

(1) Gonzalez, R. G., editor, *Fuel Reformulation*, January/February, **1995**, 37-41.
(2) Rao, P.; Vatcha, S. R., *Oil & Gas Journal*, September 9, **1996**, 56-61.
(3) Del Rossi, K. J. US Patent 5,220,096 **1993**.
(4) Garwood, W. E.; Leaman, W. K.; Myers, C. G.; Plank, C. J. US Patent 3,251,902 **1966**.
(5) Yang, C.; Ossining, N. Y. US Patent 3,851,004 **1974**.
(6) Chu, Y. F.; Chester, A. W. *Zeolites*, **1986**, 6, 195-200.
(7) Corma, A.; Juan-Rajadell, M. I.; Lopez-Nieto, J. M.; Martinez, A.; Martinez, C. *Applied Catalysis A: General*, **1994**, 111, 175-189.
(8) Taylor, R. J.; Sherwood, D. E. Jr. *Applied Catalysis A: General*, **1997**, 155, 195-215.
(9) Corma, A.; Martinez, A. *Catalysis Reviews-Science & Engineering*, **1993**, 35(4), 483-570.
(10) *Symposium on New Chemistry with Solid-Acid Catalysts in the Alkylation of Isobutane with Olefins, Division of Petroleum Chemistry*, 212th ACS National Meeting, Orlando, FL, August 25-29, **1996**, 668-724.

(11) Song, X.; Sayari, A. *Catalysis Reviews-Science & Engineering*, **1996**, 38, 329-412.
(12) Arata, K. *Applied Catalysis A: General*, **1996**, 146, 3-32.
(13) Misono, M; Okuhara, T. *CHEMTECH*, November, **1993**, 23-29.
(14) Wen, M. Y.; Wender, I.; Tierney, J. W. *Energy & Fuels*, **1990**, 4, 372.
(15) Venkatesh, K. R.; Hu, J.; Wang, W.; Holder, G. D.; Tierney, J. W.; Wender, I. *Energy & Fuels*, **1996**, 10, 1163-1170.
(16) Shabtai, J.; Xiao, X.; Zmierczak, W. J. *Energy & Fuels*, **1997**, 11, 76-87.
(17) Guo, C.; Yao, S.; Cao, J.; Qian, Z. *Applied Catalysis A: General*, **1994**, 107, 229-238.
(18) Durrett, L. R.; Taylor, L. M.; Wantland, C. F.; Dvoretzky, I. *Analytical Chemistry*, **1963**, 35(6), 637-641.
(19) de Jong, K. P.; Mesters, C. M. A. M.; Peferoen, D. G. R..; van Brugge, P. T. M.; de Groot, C. *Chemical Engineering Science*, **1996**, 51(10), 2053-2060.
(20) Zhang, S. Y.; Gosling, C. D.; Sechrist, P. A.; Funk, G. A. US Patent 5,489,732 **1996**.
(21) Cooper, M. D.; Rao, P.; King, D. L.; Lopez, R. R. US Patent 5,326,923 **1994**.
(22) Iglesia, E.; Barton, D. G.; Soled, S. L.; Miseo, S.; Baumgartner, J. E.; Gates, W. E.; Fuentes, G. A.; Meitzner,G. D. *11th International Congress on Catalysis - 40th Anniversary Studies in Surface Science and Catalysis*, **1996**, 101, 533-542.
(23) Iglesia, E.; Soled, S. L.; Kramer, G. M. *Journal of Catalysis*, **1993**, 144, 238-253.

Table 1. Liquid Product Composition after Evaporation of isobutane

TOS range min	whsv, h^{-1}	C_5-C_7	C_8			C_{9+}
			TMPs	other paraffins	olefins	
20 - 70	2.00	4.2	24.6	0.7	17.4	53.1
138 - 285	0.25	2.3	32.7	7.0	7.5	50.5

Catalyst: PtSZ, 40-60 mesh, mixed with the same weight of 50-70 mesh quartz sand. Reaction temperature, 30 °C; liquid pressure, 400 psig (no H_2); i-C_4:2-$C_4^=$ = 20.

Table 2. Various Successful Regeneration Conditions for a PtSZ catalyst for Alkylation of Isobutane with 2-Butene[a]

110 °C	**30 min**	**H_2/i-C_4H_{10}**
71 °C	**2 hr**	**H_2/i-C_4H_{10}**
690 °C	**3 hr**	**air**
450 °C	**3 hr**	**air**
450 °C	**3 hr**	**He**

[a] The same catalyst was used.

Table 3. Alkylate Compositions from On-line GC Analysis

TOS, hr	Product Composition				
Run No. 1 (a)	C_5-C_7	2,2,4-TMP	other C_8	C_9-C_{12}	C_{13+}
0.9	2.8	73.7	2.6	20.5	0.4
1.7	1.5	65.1	4.5	28.6	0.3
3.1	0.0	74.4	0.9	24.8	0.0
4.0*	0.3	79.4	2.3	18.0	0.0
4.6	0.0	78.3	1.0	20.6	0.1
6.3	0.0	80.3	1.2	18.1	0.4
6.8	0.0	83.2	0.9	15.9	0.0
Run No. 2 (b)	C_5-C_7	2,2,4-TMP	other C_8	C_9-C_{12}	C_{13+}
5.2	4.7	67.4	7.9	20.0	0.0
5.7	3.4	72.2	7.1	17.3	0.0
6.8	3.1	79.4	6.8	10.7	0.0
8.3	5.1	77.2	11.3	6.4	0.0

Conditions: 150 °C; 780 psig; PtWZ-Al_2O_3 catalyst; (a) whsv, 0.5 h^{-1}; H_2:i-C_4:i-$C_4^=$ = 0.3:16.3:1(mol), (b) whsv, 1.5 h^{-1}; H_2:i-C_4:i-$C_4^=$ = 0.2:16.3:1 (mol). * See Figure 3.

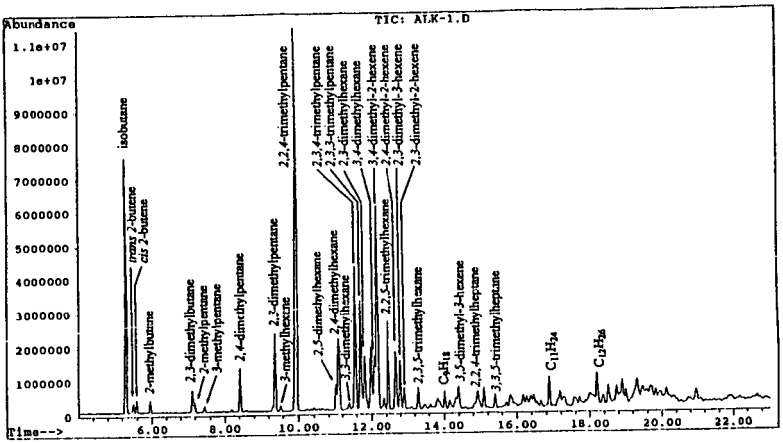

Figure 1. Liquid Products from Alkylation of Isobutane and 2-Butene (fixed bed reactor; isobutane/butene ratio, 20; 30 °C; 400 psig; WHSV, 2.0 h^{-1}; catalyst, PtSZ).

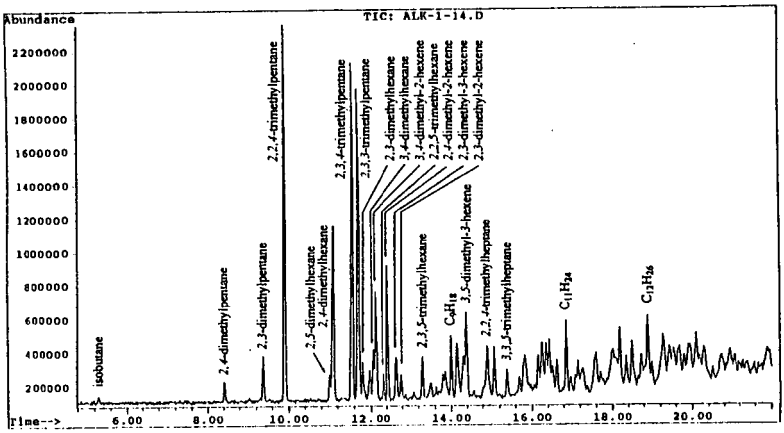

Figure 2. Liquid Products from Alkylation of Isobutane and 2-Butene (fixed bed reactor; isobutane/butene ratio, 20; 30 °C; 400 psig; WHSV, 0.25 h^{-1}; catalyst, PtSZ).

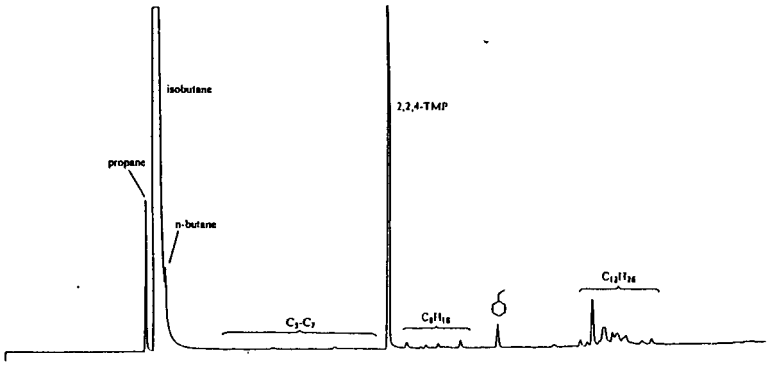

Figure 3. On-line GC Analysis of Alkylate from Isobutane and Isobutene at 242 min TOS (fixed bed reactor; H_2 : i-C_4 : i-$C_4^=$ = 0.3 : 16.3 : 1; 150 °C; 780 psig; WHSV, 0.5 h^{-1}; Pt\WZ-Al_2O_3).

THE OXIDATION STATE OF GALLIUM IN Ga/HZSM-5 LIGHT ALKANE AROMATIZATION CATALYSTS

Z.X. Gao, C.R. Chang and C.Y. Tan

Institute of Coal Chemistry,
Chinese Academy of Sciences,
Taiyuan 030001,P.R.China

Key Words: Ga/HZSM-5, aromatization, gallium state

ABSTRACT:

Gallium modified ZSM-5 catalysts were prepared and the transformations of propane were studied. The influences of catalyst pretreated with H_2 at different temperatures and addition of a small amount of O_2 and H_2 on propane aromatization were investigated. The reduction behavior and physical properties as well as the state and distribution of gallium species of the prepared catalysts were characterized by XPS, H_2-TPR and NH_3-TPD techniques. Considering the catalyst evaluation results and the characterization results, it was suggested that the gallium species existed as oxides and did not occupy the exchangeable ion position in the zeolite. Gallium oxides well dispersed on the zoelite and could be easily reduced might be the active species. It was suggested that the probable active oxidation state of gallium was less than +3 but greater than +1.

1.Introduction

Gallium modified HZSM-5 catalysts have been shown to exhibit increased activity and product selectivity for aromatizaton of light hydrocarbons such as propane and butane[1]. In recent years, much work has been done on the role of gallium species and the reaction mechanism. It has shown that gallium species is effective not only for dehydrocyclization of oligmers, but also for the direct dehydrogenation of alkanes to corresponding olefins. However the reactoin mechanism concerning gallium, especially about the active state of gallium remains unclear[1]. N.S.Gnep et al proposed Ga^{+3} may be the active state, and the active species may be gallium oxide Ga_2O_3 highly dispersed in the zeolites[2]. By H_2-TPR study along with catalytic testing, G.L.Price et al came to the conclusion that the active species was probably Ga^{+1} as a zeolitic cation and was not incorporated in the zeolite lattice[3]. Yuan et al also suggested that the higher aromatization activities were more likely to be related with the Ga^{+1} species[4]. Further more, L.Petit et al had shown that at lower conversion level, Ga_2O_3 partially reduced by H_2 produced during propane aromatization had higher dehydrogenation activity than Ga_2O_3 that was further reduced at higher conversion level[5]. This suggested that the active valence of Ga should be less than +3.

According to our previous study, Ga neither entered into the zeolitic framework nor occupied any exchangeable cation position, it probably existed as highly dispersed Ga_2O_3 on the surface of HZSM-5[6]. A further study had shown that Ga components can be divided into two parts:active gallium species and free Ga_2O_3, the former having a strong surface interaction with HZSM-5. The active gallium species could be easily reduced by H_2 at lower temperatures[7].So it was difficult to determine the active valence of Ga in the reaction process since H_2 was one of the products.

In this paper, conversion of propane to aromatic hydrocarbons over Ga/HZSM-5 zeolite catalyst was tested as a model reaction. The influence of catalyst pretreatment with H_2 at different temperatures and the influences of H_2 and O_2 on propane conversion were studied. We report here our results about the active valence state of Ga in Ga/HZSM-5 catalysts.

2.Experimental

2.1 **Catalyst Preparation:** The catalyst Ga/HZSM-5 (I) was prepared by ion-exchange of HZSM-5 (with SiO_2/Al_2O_3 ratio about 56)with gallium nitrate solution. The obtained product then washed with water,dryed, and activated for 4hrs at 540 ℃ in air. The Ga/HZSM-5(M) was obtaoned by mixing HZSM-5 with gallium oxide, and then calcinated at 570 ℃ in air.

2.2 **Catalytic test:** propane aromatization reactions were carried out at atmospheric pressure in a microflow reactor using 1.2g catalyst. In all case, the concentration of propane in Ar was 20%

by volume, and in some other cases a small amount of oxygen or hydrogen was added in the feeding gas. Reaction temperatures were varied among 520-550 ℃. After 1h time on stream, the reaction products were analyzed by gas chromatography.

2.3 **Catalyst Characterization:** NH_3-TPD Method was used to measure the surface acidity of catalyst samples pretreated at different conditions[8]. XPS spectra were recorded with a PHI 5300 ESCA SYSTEM as in ref.7. TG technique was applied for the catalyst reduction process.

3. Results and discussion

3.1 Catalytic activity

As we had noticed before, the catalytic activity of propane conversion over Ga/HZSM-5 varied with catalyst pretreatment conditions. After the regeneration process, the conversion level changed compared to that of freshly activated catalyst. The activity leveled off upon several reaction regeneration performances. So in this paper, the catalyst had been subjected to several reaction-regeneration performances before the following data were obtained.

The catalytic reactions for propane aromatization were studied. Results shown that catalyst Ga/HZSM-5(I) had higher catalytic activity than Ga/HZSM-5(M) catalyst. Ga/HZSM-5 pretreated with various conditons were tested for propane conversion and the results are listed in table 1. Compared to the catalytic activity of the oxidized catalyst, the activity changed little with catalysts treated by 5% H_2 at 540 ℃ for 1h. Much activity decrease was obtained when the catalyst was reduced in 5% H_2 at 600 ℃ for 1h.The catalytic activity was largely restored after the catalyst was re-oxidized.

In order to obtain more information about the active state of gallium species, the effects of O_2 and H_2 addition to the feed on propane aromatization were also tested. The results are listed in table 2. As one can see in this table, a small amount of O_2 addition in the propane feed caused a suprising decrease of propane conversion and BTX selectivity. On the other hand, the influence of H_2 was small, the conversion of propane and the BTX selectivity changed slightly despite a higher yield of methane.

3.2 Characterization of the catalyst

Using IR technique, we had found that there was a little change of acidity before and after the introduction of gallium[9]. Here conventional NH_3-TPD method was applied to study the acidic properties of Ga/HZSM-5. Upon pretreatment by 5% H_2 at 540 ℃ for 1h, the total acidity did not change. Even pretreated at 600 ℃ the total acidity decreased only 3.2%, and most of acidic centers and their distribution remained unchanged. This further convinced that there was no exchange of Gallium with Bronsted acid site in the zeolite upon reduction at higher temperatures, and thus gallium existed as oxides dispersed into the zeolites.

Using TG technique, we calculated the Oxidation states of gallium, in the presence of H_2, up to 540 ℃ the oxidation state of Ga appeared to about +2, up to 600 ℃ less than +1.The results were inconsistent with that of G.L.Price[10]. The oxidation states of Ga before and after H_2 reduction were also studied by XPS technique. As one can see in fig. 1, after pretreatment in H_2 at 540 ℃, an additional peak appeared on the lower binding energy side of Ga 2p,which indicated that gallium species existed in several oxidation states. Because the reduced sample was stored for several days before XPS measurement, it was likely that the above result did not reflect the true oxidation state in the sample. Unfortunately we were not able to perform reduction experiment directly in the preparation chamber of the XPS device. However the XPS revealed that at least Ga/HZSM-5 can be reduced in 5% H_2. Since H_2 is one of the products in propane aromatization process, we propose that Ga species can be reduced during propane aromatization as was proposed by L.Petit[5].

3.3 The active state of gallium species

In the present investigation, our main aim is to determine the active state of gallium species that is still disputed in the literature. Considering the above results, we come to the following conclusions. As is known in the literature, acidic property of Ga/HZSM-5 catalysts is of great importance for propane aromatization. After the catalyst was pretreated at 600 ℃ in the presence of H_2, the acidity did not change much but the Ga oxidation state change to lower oxidation state less than +1. So in table 1 the activity decease can be attributed to the gallium state change. This is to say that lower oxidation state of Ga can not be the active state. If we assume the higher oxidation state be the active state, thus after the catalyst was pretreated in H_2, the

Table1. Aromatization of propane over Ga/HZSM-5 pretreated at different condition [a]

No	Catalyst pretreatment[b] conditionb	C_3^0 conv. (%)	BTX yield (%)	Product selectivity(%)				
				C_1	C_2	$C^=_3$	C_{4-7}	BTX
1	Oxidized at 540 ℃	43.3	31.4	7.8	9.7	7.1	2.7	72.6
2	Reduced at 540 ℃	42.3	30.3	7.8	10.4	7.1	3.0	71.6
3	Reduced at 600 ℃	32.8	22.0	7.6	12.5	8.8	3.9	67.1
4	Re-0xidized at 540	40.6	29.5	8.4	9.7	6.4	2.9	72.6

a. Reaction temperature 535 ℃, WHSV of propane 1.84.

b. The catalyst was regenerated by air in Ar in all cases.

Table2. Effects of O_2 and H_2 on propane aromatization over Ga/HZSM-5[a]

Composition of feed				C_3 conv.	BTX yield	Product selectivity(%)					
C^0_3	Ar	O_2	H_2	(%)	(%)	C_1	C_2	$C^=_3$	C_{4-7}	BTX	COx
20	80	--	--	60.3	43.2	9.8	9.9	5.3	3.4	71.6	--
20	75.8	4.2	--	48.0	27.8	9.4	11.1	6.6	2.2	57.9	12.9
20	72.5	--	7.5	59.1	41.7	11.6	10.8	5.4	1.7	70.6	--

a. Reaction temperature 545 ℃, WHSV of propane 2.0

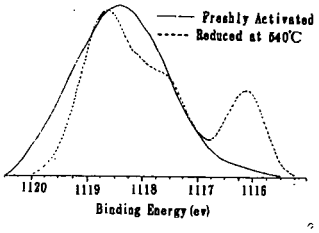

Fig.1 XPS spectra of Ga/HZSM-5 catalyst

catalytic activity would decrease due to the fact that the gallium was reduced to lower oxidation state. However this was not the case, after the catalyst was pretreated by 5%H_2 at 540 ℃ for 1h, the state of Ga changed, but the activity did not change much. Further more, the addition of a small amount of O_2 in the feeding gas caused a decrease of propane conversion level and the BTX selectivity also decreased. In theory, O_2 reacts with H_2 and thus accelerates the propane aromatization as in the case of using HZSM-5 as catalysts[11]; the negative effects on Ga modified HZSM-5 may due to the fact that presence of O_2 maintained Ga in its higher oxidation state. These results suggested that the higher oxidation state of Ga not be the active state.

With mild reduction at 540 ℃ for 1h, the activity did not change much compared to that of oxidized catalyst. Since in this case, Ga exists as +1 —+2, we presume that this should be the active valence state. This is further convinced by introducing a small amount of H_2 into the reaction system. The effect of H_2 on propane aromatization could be divided into two parts: on chemical equilibrium H_2 did not favor the propane conversion, but on the other hand, the presence of additional H_2 caused gallium in its active state; the first effect was balanced by the second one. So in this case, the activity did not change much.

Recently, P. Meriau deau et al[12] has studied the adsorption properties of Ga_2O_3 by FIIR technique,and found that with H_2 as adsorbate,the number of Ga^{+y}-H function group was higher when Ga was in +1 ~ +2 oxidation state.Our suggestion of gallium active state is strongly supported by Meriaudeau ' s findings.

References

[1] M.Guisnet N.S.Gnep and F.Alario, Appl. Catal.A:General, 89(1992)1.

[2] N.S.Gnep,J.Y.Doyemet, et al, Appl. Catal.,43(1988)155-166.

[3] G.L.Price and V.KanaziRev, J.Catal. 126(1990)267-278

[4]S.B.Yuan,L.Q.She,X.Y.Liu, X.W.Li, P.li, H.Z.Huang and Y.Zhou,Chinese J.Catal.9(1988)25

[5] L.Petit, J.P.Burnonville and F.Raatz, in P.A.Jacobs and R. Van Santen(eds.)Stud. Surf. Sci. Catal." Vol.44,PartB, Elesivier, Amsterdam, 1989, P1163.

[6]C.Y.Tan, C.R.Cheng L.X.Zhou and S.Y.Peng, C1-C3Hydrocarbons Workshop Meeting, 1991.9, Krasnoyarsk,USSR

[7] Z.X.Gao, C.Y.Tan C.R.Cheng, J. Fuel Chem. and Tech.(Chinese),1995,23(3)300

[8]C.Y.Tan, C.R.Cheng, L.X.Zhou and S.Y.Peng. in" Proceedings 9th international Congress on Catalysis (editors: M.J.Phillips and M.Ternan)", Calagary,1988, The Chem.Institute.of Canada,Ottawa,1988,P.445.

[9] Z.X. Gao, MS Thesis of ICC, 1992.

[10] G.L.Price and V.KanaziRev, J. Mol. Catal.66(1991)115-120

[11] G.Centi,G.Golinelli, J.Catal.,115(1989)452

[12] P.Merideau, and M.Primet, J. Mol. Catal. 61(1990)227-234

HYDROCARBON FUEL PROCESS ANALYSIS BY ACOUSTO OPTIC TUNABLE FILTER NEAR INFRA-RED SPECTROSCOPY

Don Muller
Bran+Luebbe, Inc.
1025 Busch Parkway
Buffalo Grove, IL 60089
telephone 847-520-0700

Keywords: near infra-red spectroscopy, acousto optic tunable filter, on-line fuel analysis

ABSTRACT

Octane and other properties of gasoline have been measured by near infra-red (NIR) spectroscopy since the laboratory trials at Technicon in the early 1980s. Over the past decade, systems have been developed for industrial process analysis. Acousto optic tunable filter (AOTF) is one of the NIR instrument technologies which has survived as appropriate for petrochemical process service. NIR spectroscopy is often the process analysis method of choice because of the speed of results and AOTF is one of the fastest NIR methods.

NIR spectroscopy is used for gasoline, diesel, and other hydrocarbon fuels as well as chemical and polymer process lines. One NIR sensor and instrument measures multiple properties -- octane, aromatics, vapor pressure, boiling points, and others of interest. The instrument is connected to sampling probes and cell at remote sites with fiber optics which can be used in the NIR. We have learned from experience which probes and sampling systems give good results. A double fiber optic and probe system provides the benefits of stable double beam spectroscopy.

Several chemometric systems have been used to develop the calibration equations required for NIR analysis. Those providing robust transferable calibrations will be presented.

INTRODUCTION

Because the ASTM research octane number (RON) and motor octane number (MON) knock engines (1,2) are lengthy procedures not usually done at-line and have poor precision, they are not the best for refinery process control. NIR spectroscopy is more appropriate for process monitoring and control measurements.

Whether in a laboratory, near a process line, at-line, or on-line; NIR is a process analysis and control technology. Calibration development from samples of known composition is required. Once the calibration equation(s) are established, spectroscopic answers are provided in seconds

Electronic transitions in the visible and ultraviolet spectral region and molecular vibrational transitions in the infra-red (IR) region absorb so much energy that dilutions or very thin samples are required. This means that sample preparation and handling are required as part of any spectroscopic procedure, The NIR transitions are overtones and combination bands of the fundamentals IR vibrational transitions. They are thus much weaker and reasonably convenient pathlengths can be used with no sample preparation.

NIR spectroscopy measures absorbance at more than one wavelength. One or more can be used as a constant reference signal. This provides the stability and precision for NIR which is either lacking or has to be achieved in some other way for other on-line instrumental technologies.

EXPERIMENTAL

Instrumentation

There are several different technologies for producing NIR spectra for instrumental analysis. The heart of an AOTF spectrometer is the tellurium dioxide crystal shown in

Figure 1. The incident beam is from a quartz halogen source lamp. The lithium niobate transducer converts a radio frequency (RF) signal into untrasonic waves in the AOTF crystal. The frequency (wavelength) of the resultant tuned spectral beams depends on the wavelength of these ultrasonic waves (the acousto optic effect). Hence, as quickly and as accurately as the RF signal can be changed produces tuned beams of changed wavelength with no moving parts.

These tuned beams are sent through glass fiber optics to a sample probe up to hundreds of feet away and back to matched detectors in the instrument. One beam goes through the sample and the other is used as a reference beam. This provides the stable signal of double beam spectrophotometry. Flow through cells are provided on bypass lines or probes can be inserted into the main piping or vessel depending on the particular installation..

Calibration & Chemometrics

For calibration development, full spectra are taken as shown in Figure 2. For our example of MON, the knock engine reference measurements for the same samples are required. Software is used to drive the instrument for spectra collection and data regression to product calibration equations. Principle component regression (PCR) or partial least squares (PLS) calibrations use all or part of the full spectrum of usually several hundred data points. Multiple linear regression (MLR) selects the best few (usually 2 to 6) wavelengths from the spectra.

For almost all of the applications mentioned below, MLR provided the calibrations most robust for analyzing samples once the calibration has been established. This is because the selected wavelengths are the ones due to the components being measured. Interferences and variations due to other factors in other parts of the spectra do not influence the predicted answer.

Applications

The Bran+Luebbe InfraPrime was designed as an industrial environment system for liquid measurement in the refining and petrochemical industry. The most common installations are to measure those properties used to control motor fuel refineries: RON, MON, RVP, density, and characteristic distillation points. NIR nicely provides all these analyses from one spectrum. One calibration equation is used for each property measured. Several sites have added aromatics and PONA as measured properties.

Cetane number, boiling points, cloud point, freezing point, flash point, and CFPP are being measured for diesel fuel and kerosene production. Some of the calibration statistics are not as good for some of these properties because of the less precise nature of the reference analysis methods.

Sulfur, viscosity, and heat content are being measured at heavy fuel operations.

A wide range of applications are being used In polymer and chemical industries,. Less than 0.1 % additives are measured and controlled in high pressure and temperature extruders. Major components in polymerization reactors are being controlled. Physical properties such as viscosity are regularly being measured.

RESULTS AND DISCUSSION

The prediction plot (Figure 3) shows how well the resulting NIR calibration and instrument agree with the reference knock engine for measuring MON. For this particular example, the standard error of the calibration samples was 0.18 MON and a standard error on predicting samples not in the calibration set of 0.22 MON. These are well within the variability of the MON knock engine method. NIR is often more precise than the reference method which generated the calibration set data.

The installation has been monitoring MON with on-line answers at this accuracy every 1.25 seconds continuously since August 1993. Several systems have been functioning for over 30,000 hours. With years of on-line design, installation, and evaluation experience; AOTF NIR spectroscopic systems have lived to their exciting promise as a technology for the on-line quality and process control of hydrocarbon fuels.

REFERENCES

(1) ASTM *Annual Book of ASTM Standards* **1995,** *05.02,* D2699 *Standard test Method for Knock Characteristics of Motor Fuels by the Research Method*
(2) ASTM *Annual Book of ASTM Standards* **1995,** *05.02,* D2700 *Standard test Method for Knock Characteristics of Motor Fuels by the Motor Method*
(3) Tran, C.D.*Anal. Chem.* **1992,** *64,* 971A-981A

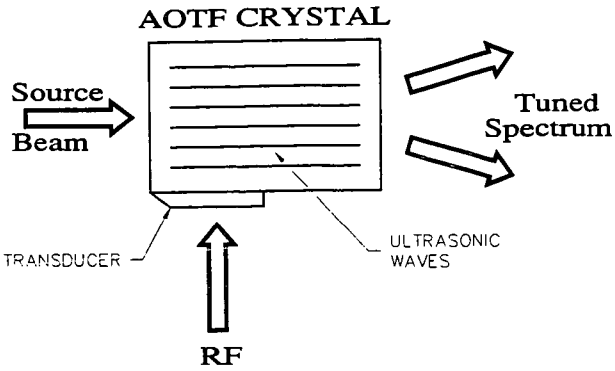

Figure 1. AOTF: acousto optic tunable filter crystal spectroscopy

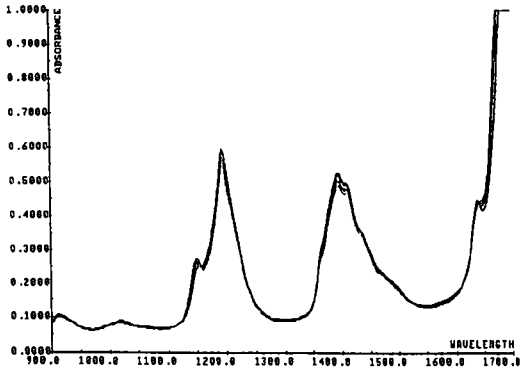

Figure 2. AOTF spectra of gasoline after the "naptha cracker" in a European refinery

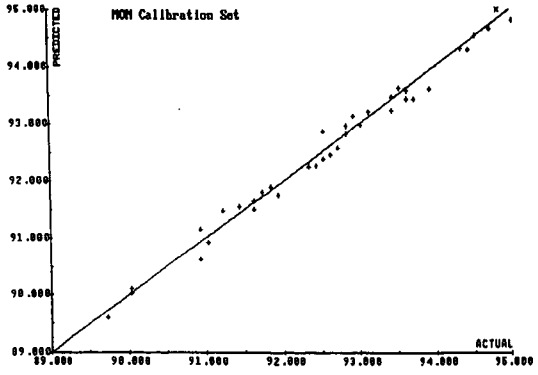

Figure 3. Prediction plot of MON precidcted by the NIR calibration model versus acual knock engine measured MON

NEAR INFRARED SPECTROSCOPY FOR ON-LINE ANALYSIS OF ALKYLATION PROCESS ACIDS

Bruce B. Randolph, Senior Research Chemist, Process Support/Light Ends, CT Unit;
Alan D. Eastman, Senior Research Chemist, Molecular Structure Team, CT Unit;
Randall L. Heald, Special Problems Chemist, Refinery Laboratory, Borger Complex;

Phillips Petroleum Company, Bartlesville, OK 74004.

INTRODUCTION

Alkylate, formed by the acid-catalyzed reaction of isobutane with C3-C5 olefins, is a key component for motor fuel blending. In the United States, current production is about $1x10^6$ bbl/day, and represents 11-15% of the gasoline pool (somewhat higher in California).[1] Alkylate is comprised essentially of highly branched isoparaffins and has very high octane values, often in the 94-97 range for RON. It has low vapor pressure, narrow distillation range, and is essentially devoid of olefins, aromatics, and sulfur, making it the preferred blending component for reformulated gasolines (RFG). The demand for alkylate in the US is expected to lead to capacity expansions of 10-35%.[2]

HF alkylation is an important and widely-used process for making high-quality alkylate. Although the HF process has been used around the world for >50 years, efforts to optimize individual unit performance are always underway. Optimization can lead to significant economic advantage, since US capacity utilization is already 90%.[2]

The generally recognized advantages of on-line process monitoring, such as tighter process control, higher productivity, and improved product quality has led to much recent interest in this area. Continuous and immediate feedback of quantitative information is critical for optimized operation. These features are ideally suited for the alkylation process, where changes in the acid composition can occur more rapidly than can be observed with samples taken at normal intervals. Acid composition is important for optimal product quality, but until recently no on-line method existed for the determination of total acid composition.[3,4] Acid, water, and acid-soluble oil (ASO) concentrations are usually determined on intermittent samples taken to a laboratory. We have recently demonstrated the feasibility of using Near Infrared (NIR) spectroscopy for the on-line determination of HF, water, and ASO,[3] and here report application of those methods under continuous alkylation conditions.

EXPERIMENTAL

The laboratory scale alkylation unit used in this work has been described previously.[3] The unit consists of a riser reactor, feed dispersion device, acid settler, acid recirculation pump, and product collection equipment.

The NIR data were collected with a flow cell mounted between the acid heat exchanger and acid pump; all of the acid inventory flows through the cell during each pass around the reactor. The cell was constructed of Hastelloy C alloy, using sapphire windows. For each run, a pre-blended feed of olefins and isobutane was introduced to the reactor. Starting acid was 98% HF and 2% water by weight. The acid/hydrocarbon emulsion from the reactor is routed to the settler, where the acid phases out to the bottom and is recirculated to the reactor. Product hydrocarbon is withdrawn from the top of the settler, scrubbed to remove any HF, and collected for analysis. Acid samples were withdrawn intermittently for HF and ASO determination to provide a comparison for NIR values. All spectral data were collected using an Applied Automation Advance FT-IR. The instrument was coupled to the cell using 600 μm low-OH silica optical fiber. The data were processed using a partial least squares model developed from a calibration dataset described earlier.[3]

RESULTS AND DISCUSSION

Selected results for Run #1 are given in Table 1. The feed was a blend of refinery-supplied olefins and isobutane, and a feed introduction device was chosen in order to increase the amount of ASO produced over that normally observed. This allowed enough ASO to be generated for a good comparison between NIR and standard techniques.

Standard HF titrations (dilution and titration to phenolpthalein endpoint) gave values within 2-3 wt% of the NIR values. The ASO concentrations determined by extraction (after neutralization) were usually only 50-70% of the NIR values. This was expected because the NIR measures total ASO, while the extraction measures mostly heavier ASO (*vide infra*). Water was not analyzed by an independent method; however the concentrations determined by NIR varied within a fairly narrow range (1.8 and 2.2 wt%). Figure 1 shows the trend lines associated with HF, ASO, and water at increasing times on stream.

After 92 hours, the feed was spiked with 570 ppm MTBE (or ~7000 ppm based on olefin only). MTBE is commonly produced upstream of the alkylation unit as an oxygenate for RFG. Under normal operation the concentration of MTBE in the alkylation feed is nil, but under upset conditions, levels of 1000-5000 ppm can have rapid, deleterious consequences for acid purity due to accelerated ASO production. Table 2 gives the results for the acid analysis at selected times on stream. Again the HF values from NIR are within 1-2 wt% of the titration values. Note the 70% increase in ASO concentration between 92 hours (table 1) and 113 hours (table 2), reflecting the high propensity for ASO production from MTBE. The increase in ASO based on traditional data was only ~33%. Both the NIR and traditional data show an increase in ASO with time, but again with traditional tests we observed only ~50-65% of the total ASO determined by NIR. Water remained relatively constant until purity was increased after 167 hours. At this time, the catalyst was nearly deactivated, necessitating a reduction of ASO and water and an increase in HF concentration. Figure 2 shows the trend lines for HF, ASO, and water with the MTBE-containing feeds.

One of the key advantages of NIR is the fast response time; in the present work spectra were taken every six minutes (times as short as 1 minute are possible). The inherent precision of NIR is another significant advantage, showing a 30- to 50- fold improvement in repeatability when compared to the traditional laboratory test methods for HF, water, and ASO. The current technique allows the rapid determination of HF, ASO, and water *directly* and *independently* of each other, in the presence of other dissolved/dispersed non-ASO hydrocarbons (C3, iC4, nC4, C5+ alkylate, etc.). This is a result of the method in which the training set data was collected. The NIR results add to 94% since the raw data was normalized to reflect the usual rule of 6% hydrocarbon dissolved/dispersed in the acid phase. In all cases, the sum of the raw data for HF, ASO, and water was between 99.6 and 100.1%, even though the model was *not* constrained to give that result. In traditional analyses, the difference between 94% and the sum of the acid components is taken as an indication of light ASO. As these data show, the traditional tests gave an indication of ~1-3% light ASO (the titration value of 93% at 44 hours is likely an outlier). The NIR technique is set up (by design) to measure both light and heavy ASO. This is the reason for the discrepancy between NIR and extraction measurements. Lighter ASO components are frequently lost during sample preparation for traditional tests.

The "spikes" present in Figures 1 and 2 occurred when acid was either added to or withdrawn from the reactor. These spikes in the trend lines result from the formation of gas/vapor bubbles which form inside the cell. Nitrogen is used as a pressure source for acid addition and to maintain constant unit pressure. As acid is withdrawn or added, a pressure differential results. The cell, which is located between the acid cooler and the magnetically driven acid recirculation gear pump, is susceptible to N2 gas bubble formation in the acid line. If bubbles develop, they can easily be trapped in the cell, since all of the acid in the system is routed through the cell. The gas bubbles cause rapid changes in the optical pathlength, resulting in wildly fluctuating values. The bubbles could be removed from the system by manipulation of the acid flow rate. Gas/vapor bubble formation is a phenomenon related to the experimental set-up in the laboratory, and proprietary equipment has been designed to eliminate their formation.

CONCLUSIONS

NIR appears to be ideally suited for on-line analysis of circulating acid in alkylation units. The fast response times, improved repeatability, and ability to provide quantitative information on HF, ASO, and water directly and independently in circulating acid represents a significant improvement over traditional methods of analysis.

ACKNOWLEDGEMENTS

The authors wish to express their sincere thanks to Applied Automation, Inc. for providing the process analyzer used in this study and expert technical assistance. Jim Nye and Don Renfro of Phillips Corporate Technology prepared the feed and catalyst blends, operated the lab unit, and collected spectral data and provided the final results.

REFERENCES

1. Rao, P., Vatcha, S.R., *Oil & Gas Journal*, 94(37), 56 (1996).

2. Rhodes, A., *Oil & Gas Journal*, 92(34), 49 (1994).

3. Heald, R.L., Randolph, B.B., Eastman, A.D., "NPRA National Meeting", March 16-18, 1997, San Antonio, TX, paper AM-97-57.

4. Ramamoorthy, P., US Patent 5,681,749, October 28, 1997.

Table 1. NIR and Traditional Acid Test Results: MTBE-Free Feed

TOS (Hours)	20	44	68	92
%HF (titration)	89.3	93.0	86.6	88.4
%ASO (extn)	0.85	1.25	2.09	2.52
%H2O (NIR)	1.80	2.0	2.19	2.16
TOTAL	92.0	96.3	90.9	93.0
%HF (NIR)	91.81	90.22	88.69	88.02
%ASO (NIR)	0.391	1.78	3.12	3.92
%H2O (NIR)	1.80	2.00	2.19	2.06
TOTAL	94.0	94.0	94.0	94.0

Table 2. NIR and Traditional Acid Test Results: 570 ppm MTBE In Feed

TOS (Hours)	113	143	167	191
%HF (titration)	87.3	86.4	84.2	86.0
%ASO (extn)	3.35	4.0	4.7	4.7
%H2O (NIR)	2.01	2.08	2.01	1.78
TOTAL	92.7	92.5	90.9	92.5
%HF (NIR)	85.3	84.4	83.3	85.0
%ASO (NIR)	6.71	7.51	8.73	7.28
%H2O (NIR)	2.01	2.08	2.01	1.78
TOTAL	94.0	94.0	94.0	94.0

PLANAR LIQUID AND GAS VISUALIZATION*

Lynn A. Melton
Department of Chemistry
University of Texas at Dallas
Richardson, TX 75083-0688

keywords: hydrocarbon fuel sprays and droplets, fluorescent diagnostics, temperature and mixing

INTRODUCTION

Over the past decade, a variety of fluorescent diagnostic systems, based on the photophysics of organic molecules and intended for use in planar laser induced fluorescence (PLIF) measurements of heating, evaporation, mixing, and flow visualization in hydrocarbon liquids and vapors, have been developed. These organic dopants interact with their surroundings, either through concentration-dependent effects such as quenching or through physical effects such as temperature and polarity, and reveal information about the surroundings through their fluorescence. The intent in this paper is to describe the photophysical principles on which the systems are based, to describe engineering applications (currently within the combustion/mechanical engineering community), and to explore applications of these and related diagnostics within the chemical process industry. While there exist many applications of fluorescence within the diagnostic community, this paper is restricted to a review of the photophysics and applications of these four novel systems, which have are not yet widely known in the chemical process area.

The fluorescent diagnostic systems make use of PLIF measurements of intensity and/or fluorescent lifetimes; they fall into five broad categories:

(1) **exciplex-based vapor/liquid visualization** (EBVLV) systems, which are now available for automotive as well as for diesel and gas turbine fuels, make use of the photophysics of organic exciplexes in order to provide spectrally-separated emissions from the vapor and liquid phases.[1-4]

(2) **fluorescence shift thermometry** (FST) systems also make use of the photophysics of organic molecules; these systems use either the ratio of the emissions from the exciplex to that from the excited monomer or the shift of the fluorescence band, both of which are temperature-dependent, as an optical liquid phase thermometer.[5-6] Such thermometers have been used to track the temperature of falling, sub-millimeter diameter droplets in experiments directed toward understanding heat transfer from a hot gas to cold droplets.

(3) **streamlines by oxygen quenching** (SOQ), a technique which exploits the efficient quenching of the fluorescence of organic molecules by oxygen has been used in connection with **droplet slicing imaging** (DSI) to provide dramatic qualitative evidence of the existence of internal circulation patterns within falling, sub-millimeter diameter droplets.[7]

(4) **fluorescence lifetime imaging** (FLI) requires the use of fast dual gated image intensifiers to obtain two PLIF images, one a few nanoseconds after the first. Quenching results in a reduction of the fluorescence intensity **and** a reduction of the fluorescence lifetime. The two images make it possible, in principle, to obtain a lifetime image and, after appropriate calculations, an intensity image, completely corrected for quenching.[8] To date, the technique has been applied (a) to fuel/oxygen equivalence ratio imaging (ERI),[9] and (b) to vapor phase temperature imaging (VTI)[10].

(5) **film thickness imaging** (FTI)

Fluorescent thickness imaging is under development. In this method the fluorescence of a molecule which has almost the same volatility as automotive gasoline will be used to track the evaporation of films of automotive gasolines. The system is used in an optically thin configuration, and the fluorescence intensity in a pixel is thus proportional to the film thickness.

PHOTOPHYSICS OF FLUORESCENT DIAGNOSTICS

A. processes

A recent review article discusses the photophysics of these combustion-related fluorescent diagnostics, and their fundamental limitations (volatility, quenching, etc.), in detail.[11]

B. excited state complexes

An exciplex or excimer [excited state complex or excited state dimer, denoted E* and called exciplex, unless the distinction is required] is formed in the reaction of an electronically excited molecule M* with an appropriate ground state molecule G (for excimers G = M), as shown in eqn. 1.[12]

$$M^* + G(M) \leftrightarrows E^* \qquad (1)$$

E* may be bound by as much as 20-40 kJ/mole with respect to separated M* and G(M). Since there is no significant chemical binding of the ground state components of E*, and there may even be significant repulsion at the distance at which E* is most strongly bound, the fluorescence from E* is necessarily red-shifted with respect to the fluorescence of the excited monomer M*. The concentrations of M and G in the liquid can be adjusted to that the E* emission dominates in the liquid. The exciplex is unstable in the vapor phase, and thus the M* emission dominates in the vapor. Consequently, filters which isolate the E* and M* emission allow separate PLIF visualization of the liquid and vapor phases, respectively.

The reaction shown in equation (1) is temperature dependent, and the temperature dependence of the E*/M* intensity ratio can be exploited to make exciplex thermometers, which allow PLIF imaging of liquid phase temperatures within a few degrees over the temperature range 20 - 400 ^{o}C.

C. apparatus for PLIF

Most PLIF experiments make use of a pulsed laser (in order to provide time resolution of the flow phenomena under study) whose beam is formed, via cylindrical lenses, into a sheet which is a fraction of a millimeter thick and 5-10 cm wide. Typically the fluorescence from the flow is imaged onto a CCD array camera which is placed at 90^{o} to the plane of the exciting laser sheet. The choice of laser is determined by the wavelengths required for excitation of the fluorescent dopants. Most studies have used nitrogen lasers (337 nm) or Nd:YAG lasers (third harmonic at 355 nm or fourth harmonic at 266 nm). This apparatus is generic and the specificity of the diagnostic is gained through choice of the fluorescent dopant system(s).

APPLICATIONS OF FLUORESCENT DIAGNOSTICS

A. exciplex-based vapor/liquid visualization

The best characterized, and most often applied, EBVLV system uses 0.5-1% (w/w) N,N,N',N'-tetramethyl-p-phenylenediamine (TMPD), nbp = 265 ^{o}C/10% (w/w) naphthalene, nbp = 218 ^{o}C/balance alkane (decane, tetradecane, or hexadecane). The liquid phase emission is dominated by the E* emission (peak at 480 nm), and the vapor phase emission is dominated by the M* emission (peak at 390 nm). Thus it is possible, by use of relatively broad-band filters to obtain separate images of the liquid or vapor phases in an evaporating fuel spray.

Most of the current applications of EBVLV have been in research automotive engines. Two examples are particularly noteworthy. Bardsley et al. acquired images for "diesel" and "automotive" sprays in a research engine, which was motored on nitrogen.[13-14] Shimizu et al. achieved near-quantitative use of an EBVLV system by using the E* emission to show that the liquid had completely evaporated. They were then able to calibrate the vapor phase emission as a function of the mixture fuel/oxygen ratio and crank angle in their automotive test engine. As a result, the spatial dependence of the equivalence ratio in the

precombustion portion of the engine cycle was displayed quantitatively.[15]

B. fluorescence shift thermometry

Fluorescence thermometry has been used with bulk liquids and droplets falling into heated nitrogen. Stufflebeam showed that, in sealed, bulk liquids, spatial resolution of less than 1 mm and temperature errors of less than 1 ^{o}C could be achieved over the range 20 - 100 ^{o}C.[16] "Proof of concept" measurements of the temperature of decane or hexadecane droplets falling into heated nitrogen have been carried out with illumination of (1) the entire cross section of an optically thick droplet ("whole droplet, skin temperature"),[17] (2) the entire cross section of an optically thin droplet ("whole droplet, volume averaged temperature"),[18] and (3) a central slice of the droplet ("droplet slicing, temperature field").[19] In more recent work, the evaporation of a fuel which had been sprayed onto a hot steel plate was followed through images of the temperature of the remaining liquid at intervals of a 0-100 msec after the injector was pulsed.[20]

C. streamlines by oxygen quenching

The techniques of streamlines by oxygen quenching and droplet slicing imaging were developed for the purpose of testing whether aerodynamic drag on droplets of sizes typical of fuel sprays could induce internal circulation within the droplet, which circulation can dramatically alter the time required for the droplet to heat sufficiently for evaporation rates to become significant.[7] For SOQ, the droplet is formed from a solution which contains a dopant whose fluorescence is easily quenched by oxygen (typically naphthalene in decane) and which solution has been purged of oxygen. The droplet falls into an oxygen containing atmosphere, and oxygen contacts and diffuses into the surface liquid. For DSI, the laser beam is formed into a sheet which is narrow compared to the droplet diameter and which illuminates an equatorial plane of the droplet. SOQ/DSI measurements on droplets which have internal circulation show dark (oxygen containing, fluorescence quenched) streaks curving into the light droplet disk.[7]

D. fluorescence lifetime imaging

In FLI, a rapid lifetime determination algorithm, which relies on two gated intensity images and the assumption that the fluorescence decay is a single exponential, allows the subsequent calculation of the fluorescence lifetime image.[21] The fluorescence image was split, and each portion passed through a fast gated imaged intensifier (off/on/off time selectable from 1 to 12 nsec, intensifiers and high voltage pulser system supplied by Grant Applied Physics, Berkeley, CA) and an appropriate filter. The two gated fluorescence signals were finally focused onto two halves of a single CCD camera (Photometrics Star-1).

The equivalence ratio (phi) is the ratio of the fuel vapor concentration to the oxygen concentration, normalized so that the equivalence ratio is unity when there is just sufficient oxygen present to burn all the fuel to water and carbon dioxide. phi < 1 is "fuel lean", and phi > 1 is "fuel rich".

For equivalence ratio imaging (ERI), further processing is required. As shown in equations (2a) and (2b), the Stern-Volmer equations for intensity and for lifetimes have the same right hand side.

$$I_o/I = 1 + K'[O_2] \qquad (2a)$$

$$tau_o/tau = 1 + K'[O_2] \qquad (2b)$$

where the "o" subscript denotes the quantity measured in the absence of the quencher, which here is O_2. In a non-homogeneous mixture of fuel with air, variations in intensity may arise either from variations in the distribution of the fuel (and with it the fluorescent dopant which was mixed into the fuel), or from variations in the amount of oxygen (and consequent variations in the amount of quenching), or both. One needs to determine the unquenched intensity image (I_o) in order to determine the

distribution of fuel, however, only the intensity image with quenching (I) is experimentally accessible. With prior knowledge of the fluorescence lifetime in the absence of quenching, and measurement, pixel-by-pixel, of the mixture lifetime, the right hand side of equations (2a) and (2b) can be determined, and thus the unquenched intensity image, in which the intensity is directly proportional to the fluorescent dopant concentration, can be obtained. With further knowledge that quenching by oxygen is the only significant means of shortening the fluorescence lifetime in the system under study and with measurement of the rate of quenching of the fluorescence by oxygen, the oxygen concentration image can be obtained. If the system has been prepared in such a fashion that the concentration of the fluorescent dopant is in a fixed and known ratio to the fuel vapor concentration, then pixel-by-pixel ratioing and subsequent scaling of the ratio yields an image of the fuel/oxygen equivalence ratio. This technique has been demonstrated in fluoranthene doped jets of methane into air; typical results are shown in Figure 7.[9]

For vapor temperature imaging, a fluorescent dopant whose lifetime is temperature sensitive is used. In this case a calibration curve of the fluorescence lifetime versus temperature is used to convert the fluorescence lifetime image to a vapor temperature image. The temperatures are obtained solely from lifetime data and do not depend upon the concentration of the fluorescent dopant so long as sufficient signal is obtained for accurate measurements. Since oxygen, particularly, also shortens the fluorescence lifetimes, it must be rigorously excluded in the VTI experiments. This technique has been demonstrated for a heated jet of naphthalene doped nitrogen at the center of a cold coflow of naphthalene doped nitrogen.[10]

POTENTIAL APPLICATIONS IN THE CHEMICAL PROCESS INDUSTRY

A significant drawback to the utilization of such fluorescent diagnostics in the chemical process industry is the sensitivity of the fluorescent dopants to quenching by molecules in the environment. It may be possible to show that the process stream does not contain significant quenchers, but this must be established on a case-by-case basis.

As described in the discussions of exciplex-based vapor/liquid visualization, exciplex fluorescence thermometry, streamlines by oxygen quenching, and fluorescence lifetime imaging, fluorescence measurements can also be generated under planar illumination conditions, and thus two-dimensional maps of a property field can be obtained. Thus fluorescence imaging is particularly useful for situations, such as studies of two phase flow or mixing, where such 2-D information is critical.

ACKNOWLEDGEMENTS

This work has been supported by the U.S. Army Research Office through grants DAAL03-91-G-0033 and DAAL03-91-G-0148 and by the Texas Higher Education Coordinating Board, Energy Research Applications Program through contract #27. Continuing technical management through Dr. David Mann (ARO) and Dr. Julian Tishkoff (AFOSR) is gratefully acknowledged.

REFERENCES

1. Melton, L.A., "Fluorescent Additives for Determination of Condensed and Vapor Phases in Multiphase Systems", U.S. Patent 4,515,896, issued May 7, 1985, assigned to United Technologies Corporation.

2. Melton, L.A., "Spectrally Separated Fluorescence Emissions for Diesel Fuel Droplets and Vapor," *Appl. Opt.* **1983**, *22*, 2224.

3. L.A. and Verdieck, J.F., "Vapor/Liquid Visualization for Fuel Sprays", *Combust. Sci. and Tech.* **1985**, *42*, 217.

4. Melton, L.A., "Exciplex-Based Vapor/Liquid Visualization Systems Appropriate for Automotive Gasolines", *Appl. Spectrosc.* **1993**, 47, 782.

5. Melton, L.A., "Method for Determining the Temperature of a Fluid," U. S. Patent 4,613,237; issued September 23, 1986; assigned to United Technologies Corporation.

6. Murray, A.M. and Melton, L.a., "Fluorescence Methods for Determination of Temperature in Fuel Sprays," *Appl. Opt.* **1984**, *24*, 2783.

7. Winter. M. and Melton, L.A., "Measurement of Internal Circulation in Droplets Using Laser-Induced Fluorescence", *Appl. Opt.* **1990**, *29*, 4574.

8. Ni, T.Q. and Melton, L.A., "Fluorescence Lifetime Imaging: An Approach for Fuel Equivalence Ratio Imaging", *Appl. Spectrosc.* **1991** *45*, 938

9. Ni, T.Q. and Melton, L.A., "Fuel Equivalence Ratio Imaging for Methane Jets", *Appl. Spectrosc.* **1993**, *47*, 773.

10. Ni, T.Q., and Melton, L.A., "2-D Gas Phase Temperature Measurement Using Fluorescence Lifetime Imaging", *Appl. Spectrosc.* **1996**, *50*, 1112.

11. Melton, L.A., "Planar Laser and Gas Visualization", *Ber. Bunsenges. Phys. Chem.* **1993**, *97*, 1560.

12. Birks, J.B., "Excimer Fluorescence in Organic Compounds," in Progress in Reaction Kinetics, G. Porter, Ed., **5**, (Pergamon, London, 1969).

13. Bardsley, M.E.A., Felton, P.G., and Bracco, F.V., "2-D Visualization of Liquid Fuel Injection in an IC Engine", SAE Int. Congress and Exp., Feb. 29 - Mar. 4, 1988, paper 880521, (1988).

14. Bardsley, M.E.A., Felton, P.G., and Bracco, F.V., "2-D Visualization of a Hollow-Cone Spray in a Cup-in-Head, Ported I.C. Engine", SAE Int. Congress and Exp., Feb. 27 - Mar. 3, 1989, paper 890315, (1989).

15. Shimizu, R., Matumoto, S., Furuno, S., Murayama, M. and Kojima, S., "Measurement of Air-Fuel Mixture Distribution in a Gasoline Engine Using LIEF Technique", SAE Fuels and Lubricants Meeting, October 21-23, 1992, paper 922356, (1992).

16. Stufflebeam, J.H., "Exciplex Fluorescence Thermometry of Liquid Fuel", *Appl. Spectrosc.* **1989**, *43*, 274.

17. Wells, M.R., and Melton, L.A., "Temperature Measurement of Falling Droplets", *Trans. ASME: Journal of Heat Transfer* **1990**, *112*, 1008.

18. Hanlon, T.R., and Melton, L.A., "Exciplex Fluorescence Thermometry of Falling Hexadecane Droplets", *Trans. ASME: Journal of Heat Transfer* **1992**, *114*, 450.

19. Winter, M., "Measurement of the Temperature Field Inside a Falling Droplet", ILASS-Americas, 4th annual conference, Extended Abstracts, Hartford, CT (1990).

20. Ni, T.Q., and Melton, L.a., in preparation.

21. Ballew, R.M., and Demas, J.N., "An Error Analysis of the Rapid Lifetime Determination Method for the Evaluation of Single Exponential Decays", *Anal. Chem.* **1989**, *61*, 30.

*Adapted from a presentation at Eighth International Forum on Process Analytical Chemistry, January 24-26, 1994 Houston (Montgomery), Texas ["Planar Liquid and Gas Visualization", *AT-Process, Journal of Process Analytical Chemistry* 1996, 227]

SENSOR SELECTION AND PLACEMENT FOR PROCESS CONTROL

Charles F. Moore, Arlene A. Garrison, Paul D. Hall
Measurement and Control Engineering Center
102 Estabrook Hall
University of Tennessee
Knoxville, TN 37996-2350

Keywords: Measurements, Process Control, Distillation

ABSTRACT

Effective application of sensor technology in industrial processes requires careful attention to the optimal placement of the sensor. Available locations must be analyzed based upon potential leverage in a control scheme. After location is determined, the measurement need is clearly defined and the most appropriate sensor can be selected. Tools have been developed to assist in appropriate sensor placement. The use of the tools in distillation column applications will be discussed.

INTRODUCTION

Raman spectroscopy provides a useful alternative for in-process vibrational spectroscopic analysis. Instrument vendors originally designed spectrometers for laboratory use, and recently systems have become available with NEMA enclosures and remote optical fiber capability. There are many potential process applications for these stable, easy to use instruments. Raman spectroscopy is highly suited to analysis of aqueous samples.

The Department of Energy has funded research at the Measurement and Control Center to establish the utility of Raman spectroscopy for on-line composition analysis in distillation columns. The Fourier Transform instrument selected employs an air-cooled laser and a thermoelectrically cooled detector. The device is mounted on a three by three foot cart for convenient location in control rooms. Current fiber optic extension cables allow for analysis in a cell thirty five meters from the instrument.

Application of the device to an acid recovery column at Eastman Chemical Company in Kingsport, Tennessee will be discussed. Sensor placement is critical to optimal application of any on-line device. Potential energy savings and product throughput increase will be outlined.

EXPERIMENTAL

During the project a multiple point measurement system was constructed and tested.[1-5] This was accomplished by routing the excitation light from a diode pumped YAG laser to the measurement points with optical fibers and returning the Raman scattered light to the spectrometer with optical fibers. An optical multiplexer was designed to time-share the light in both paths. The excitation light wavelength was in the near infrared range, thereby reducing the possible fluorescence of the samples to be analyzed.

The spectrum of the Raman-scattered light was measured by use of an interferometer-based spectrometer, a Perkin-Elmer 1700 adapted for Raman use. The system was controlled by an INTEL based computer. The computer initiated a scan of the spectrum of the chemical stream, gathered the spectral data from the spectrometer and estimated the composition of the constituents. The calibration of the system was accomplished by a process in which multiple samples with different typical concentrations of the constituents of the chemical stream were analyzed and their spectra stored. Next, the unique set of orthogonal functions making up the experimental data were found. Finally an empirical mathematical model of the relation between spectral features and composition was formed based on multiple linear regression of the weights of the orthogonal functions against the known concentrations of the constituents. The accuracy goal of the project was a measurement of composition of each constituent of a process chemical stream within 3 minutes with a root-mean-square (rms) uncertainty of less than 2%. The final system achieved an error of about 1% rms in 3 minutes for the constituents composing the chemical stream in the field trial test site, Eastman Chemical Company of Kingsport, Tennessee.

Various composition analysis methods have been considered for use in column process control. Many methods have been utilized with varying degrees of success due to inherent limitations in these techniques. A critical concern in determining potential energy savings utilizing comp-

osition control is the universality of the on-line analyzer. Raman spectroscopy was chosen for this development effort as highly appropriate for the control of a broad range of distillation separations. Of the three common optical spectroscopic methods in use today, fluorescence spectroscopy, absorption spectroscopy, and Raman spectroscopy, Raman was selected because of its narrow, distinct spectral features and relative insensitivity to the presence of water in the sample.

One important aspect of composition based control systems is the relationship between the composition measurement location and the required measurement resolution. One feature of the Raman based composition analyzer is that it can be used to measure compositions internal to the distillation column. (Conventional process analyzers are typically applied to product streams). This offers several advantages for addressing the control and energy reduction problems. The first advantage is demonstrated in Figure 1, where the sensitivity of the composition profiles to changes in the reflux and steam is plotted against the height in the column. Note that product ends (where conventional analyzers are applied) have very little sensitivity. The leverage in controlling composition is orders of magnitude greater if the measurement is made inside the column. This is a characteristic of the Eastman column, but it is also a general characteristic of most distillation processes. If composition information is to be used in stabilizing a column, it needs to be well selected internal composition and not product compositions.

RESULTS AND DISCUSSION

The projected economic analysis quantified the improvements in the Eastman column control that would be possible if the control system were based on composition measurements instead of temperature as was the prior practice. This preliminary study was conducted on a simulation of the proposed field test column and included two relatively simple composition control strategies. The results of the study indicate that there is a clear advantage to composition based control.[6] Both composition control schemes significantly reduced the variation in the product composition. Reducing variation saves energy by allowing operation of the column much closer to the minimum energy requirement without jeopardizing the product specification.

The cost of the analyzer vs. the anticipated energy savings was not specifically addressed in the economic analysis. The general feeling is that the cost of the components in the prototype system does not accurately reflect the price for an industrially hardened, commercial unit.

This study demonstrates that the high resolution and mechanical sampling requirements placed on present industrial analyzers are not necessary. High resolution and sampling both contribute to the capital as well as the maintenance costs of current process analyzers. A commercial Raman based analyzer should compete quite favorably with these existing technologies in both price and maintenance. Also, it should yield much higher control performance. The control performance advantage offered by the Raman based analyzer is that it can be applied with relatively little difficulty to determine the internal composition of the column.

ACKNOWLEDGMENTS

The Measurement and Control Engineering Center was founded as a joint program of the University of Tennessee and the Oak Ridge National Laboratory. Additional support for the Center from the National Science Foundation, the Department of Energy and numerous industrial sponsors is gratefully acknowledged.

REFERENCES

1. M.J. Roberts, A.A. Garrison, S.W. Kercel, D.S. Trimble, C.F. Moore and E.C. Muly, "Development and Application of a Raman Spectroscopy Based Instrument for Multi-Point Composition Analysis and Control of a Distillation Column", ISA 90, New Orleans, LA, pp. 463-468, October 1990.

2. A.A. Garrison, D.S. Trimble, E.C. Muly, M.J. Roberts and S.W. Kercel, "On-Line Chemical Analysis Applied to Distillation Control - A Status Report", American Laboratory, pp. 19-27, February 1990.

3. A.A. Garrison, C.F. Moore, M.J. Roberts and P.D. Hall, Distillation Process Control using FT-Raman Spectroscopy, Process Control and Quality, 3 (1992) 57-63.

4. M.Z. Martin, A.A. Garrison, M.J. Roberts, P.D. Hall, and C.F. Moore, Composition Monitoring by On-Line Remote Raman Spectroscopy, Process Control and Quality, 5 (1993) 187-192.

5. A.A. Garrison and M.Z. Martin, Fourier Transform Raman Spectroscopy for Process Analysis, Proceedings of the Fourteenth International Conference on Raman Spectroscopy, Hong Kong, August, 1994, N.-T. Yu and X.-Y. Li, editors, 804-805.

6. Paul D. Hall, *Distillation SISO Control System Design and Analysis Using Internal Composition Measurements*, University of Tennessee Dissertation, 1994.

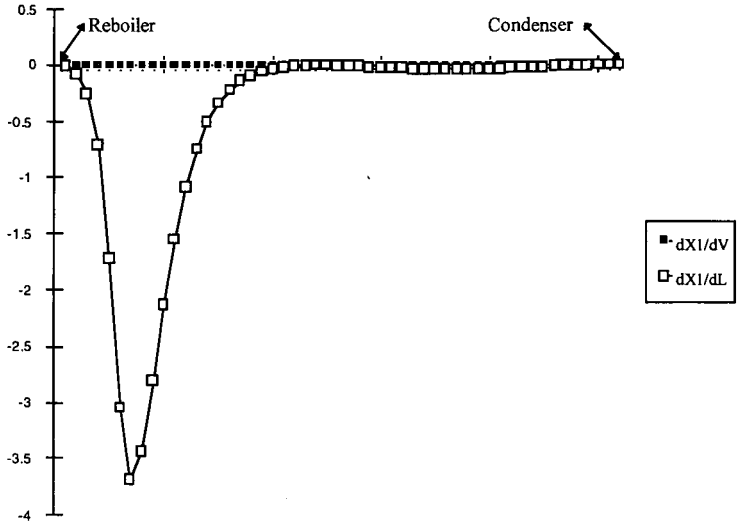

dX1/dV = the change in acid composition with respect to the change in the vapor rate
dX1/dL = the change in acid composition with respect to the change in the liquid rate

Figure 1
Acid Composition Sensitivity vs. Column height

FIBER-OPTIC ARRAY SENSORS

Paul Pantano,* Anna A. Panova† and David R. Walt†
*Department of Chemistry, University of Texas at Dallas, Richardson, TX 75083
†and Department of Chemistry, Tufts University, Medford, MA 02155

Keywords: fiber-optic sensors, remote digital imaging, corrosion.

ABSTRACT

Despite many innovations and developments in the field of fiber-optic chemical sensors, optical fibers have not been employed to both view a sample and concurrently detect an analyte of interest. While chemical sensors employing a single optical fiber or a non-coherent fiber-optic bundle have been applied to a wide variety of analytical determinations, they cannot be used for imaging. Similarly, coherent imaging fibers have been employed only for their originally intended purpose, image transmission. Recently, we have used coherent imaging fibers to make fiber-optic chemical sensors. First, imaging fibers can be used to fabricate array sensors that can concurrently view a sample and detect a single analyte. Second, sensors can be made with spatially-discrete sensing sites for multianalyte determinations. Applications will include studying corrosion processes from remote locations.

INTRODUCTION

An imaging fiber is comprised of thousands of individual 2-μm-diameter optical fibers that are melted and drawn together in a coherent manner such that an image can be transmitted from one end of the fiber to the other. These imaging fibers (200-500 μm in diameter) have been utilized to construct several types of novel chemical sensors.[1]

In one approach, we have demonstrated the ability to combine two types of useful measurements (visual and chemical) using a single imaging fiber.[2] A pH-sensitive fluorescent dye was incorporated into a porous polymer layer after it was spin-coated directly onto the distal surface of an imaging fiber. When the pH-sensitive layer was sufficiently thin (≤2 μm), the fiber's imaging capabilities were not compromised. By combining the distinct optical pathways of the imaging fiber with a charge coupled device, visual (white light) and chemical (fluorescence) measurements could be acquired concurrently with 4-μm-spatial resolution. This technique has many potential applications for remote in situ analyses. For example, recent work has involved imaging a copper/aluminum corrosion cell with a pH-sensitive imaging fiber.[3]

In another approach, discrete arrays of micrometer-sized sensing regions have been photodeposited onto the distal tip of a single imaging fiber.[4] Using a charge coupled device, the fluorescence from each of the different sensing regions immobilized on the imaging fiber could be spatially resolved. The creation of spatially discrete sensing sites on a single optical sensor solves many of the problems associated with designing multianalyte optical sensors such as spectral overlap of multiple indicators and the need to use individual optical fibers for each analyte. Simultaneous measurements are especially important in a number of environmental applications, especially when the dynamics of different analytes are closely interrelated (e.g., pH, pCO_2, and pO_2). This technique has many potential applications since numerous indicating chemistries (including those for metal ions) can be co-immobilized on a single imaging fiber to form compact multianalyte sensor arrays.

EXPERIMENTAL

Approach #1: pH-sensor fabrication begins by successive polishing of the distal and proximal faces of a 350-μm-diameter imaging fiber (Sumitomo Electric Industries, Torrance, CA) with 30-μm, 15-μm, 3-μm and 0.3-μm lapping films (General Fiber Optics, Fairfield, NJ). Residual polishing material was removed by wiping the faces of the imaging fiber with an acetone-soaked cotton swab. The polished distal face of the imaging fiber required treatment to activate the glass surface with a polymerizable double bond. Surface activation was achieved by silanizing the fiber surface for 2 h using a 10% solution of 3-trimethoxysilylpropyl methacrylate in acetone. After rinsing the fiber with acetone, the surface-bound acrylate was cured at room temperature for a minimum of 30 min. This procedure functionalizes the surface with a polymerizable acrylate to facilitate adhesion of a photopolymer to the glass surface of the optical fiber. A thin layer of polyHEMA/N-fluoresceinylacrylamide was then polymerized at the distal tip using photochemical polymerization in conjunction with

spin coating methods. The stock photochemical polymerization solution consisted of 10 mL HEMA, 200 µL ethyleneglycol dimethacrylate, and 1 mL of dye solution (50 mg N-fluoresceinyl-acrylamide (synthesized from fluoresceinamine isomer I and acryloyl chloride) in 10 mL *n*-propanol). Individual solutions were prepared with 0.5-mL stock polymerization solution and 30 mg benzoin ethyl ether. Deoxygenated stock polymerization solution (100 mL) was stirred in a 6 x 50 mm test tube and prepolymerized with 366-nm light for 45 s. The resulting viscous oligomer was spread uniformly across the imaging fiber surface by placing a drop of it (approximately 1 mL) on the distal tip of a functionalized imaging fiber (held vertically in a Servodyne mixer head (Cole Parmer, Chicago, IL)) and spinning the fiber at 2000 RPM for 20 s. After spin coating, the polyHEMA/ fluorescein-modified imaging fiber was illuminated with 366-nm light for 1.5 min to complete the polymerization and bond formation. The modified epifluorescence microscope used for fluorescence measurements and imaging has been described previously.[2] The system is capable of making continuous ratiometric measurements through the use of a CCD camera and computer-controlled filter wheels and shutters. During fluorescence measurements, the filter wheels are positioned at the dye's excitation and emission maxima with the fluorescence images being captured by the CCD camera.

RESULTS AND DISCUSSION

The main objective of this work is to create a planar array of thousands of optical sensors in a unitary, flexible fiber format. This approach benefits from the commercial availability of coherent imaging fibers comprised of thousands of micron-sized optical fibers fused together in a fixed arrangement. By coating one end of the imaging fiber with an analyte-sensitive material, we obtain thousands of microsensors capable of simultaneously measuring chemical concentrations with 4-µm spatial resolution over tens of thousands of square microns. In addition, the image carrying capabilities of the fiber are preserved allowing the operator both to position the sensor and to couple the chemical measurements to visual information.

Recent work has involved imaging a copper/aluminum corrosion cell with a pH-sensitive imaging fiber (Figure 1). In these experiments, the electrodes were placed in aqueous buffer and the distal end of the pH-sensitive imaging fiber was brought into contact with the metal surface. Fluorescence images were taken before and after the surface was exposed to a buffer solution with the change in fluorescence being attributed to the generation of hydroxide ion from the reduction of water that accompanies the anodic dissolution of a metal (Figure 2). Such studies provide information regarding the chemical and physical changes during the initial stages of corrosion.

ACKNOWLEDGMENTS

The authors are grateful to the Robert A. Welch Foundation (P.P.), the National Institutes of Health (D.R.W.) and the Office of Naval Research (D.R.W.) for financial support of this work.

REFERENCES

[1] Pantano, P. and Walt, D. R. *Anal. Chem.* 1995, *67*, 481A-487A.
[2] Bronk, K. S.; Michael, K. L.; Pantano, P. and Walt, D. R. *Anal. Chem.* 1995, *67*, 2750-2757.
[3] Panova, A. A., Pantano, P. and Walt, D. R. *Anal. Chem.* 1997, *69*, 1635-1641.
[4] Healey, B. G.; Foran, S. E. and Walt, D. R. *Science* 1995, *269*, 1078-1080.

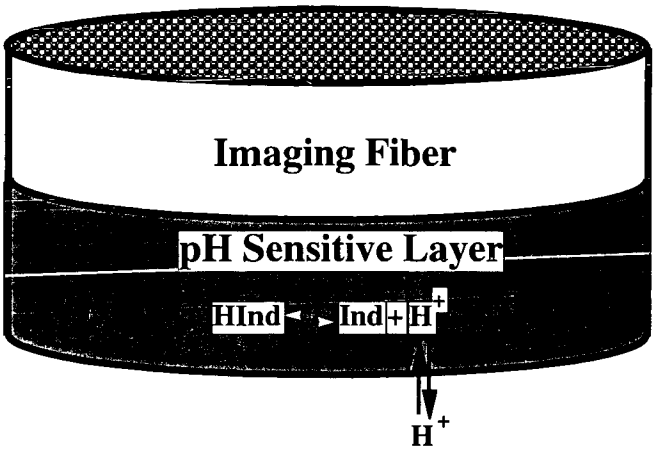

Figure 1. Schematic diagram of a pH-sensitive indicator immobilized to an imaging fiber's distal face.

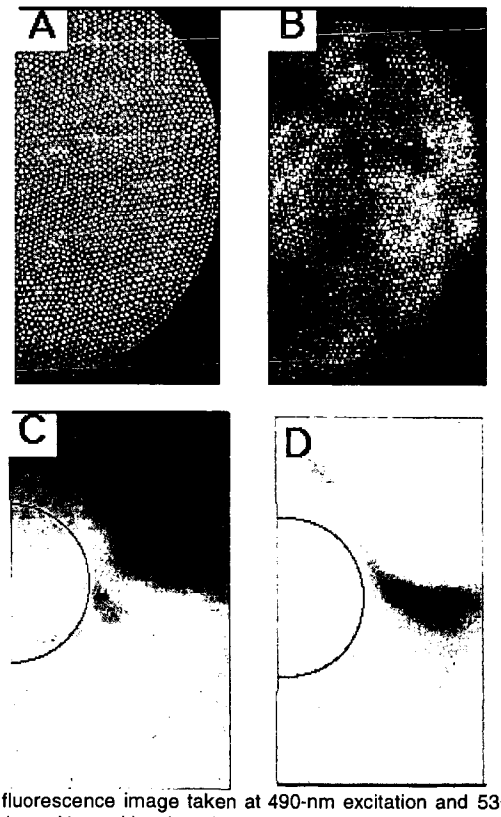

Figure 2. (A) fluorescence image taken at 490-nm excitation and 530-nm emission acquired through a pH-sensitive imaging fiber placed in contact with buffer. **(B-D)** images acquired through a pH-sensitive imaging fiber placed in contact a polished aluminum-clad copper wire (the image corresponds to half of the wire surface). **(B)** white light image, **(C)** fluorescence image after 1-min exposure of the metal surface to buffer, **(D)** background-subtracted fluorescence image taken after 5-min exposure. High fluorescence intensities (high pH) are denoted by white. The black half-circle denotes the Al/Cu border.

CAN SOOT PRIMARY PARTICLE SIZE BE DETERMINED USING LASER-INDUCED INCANDESCENCE?

Thomas M. Ticich, A. Brock Stephens, Department of Chemistry,
Centenary College of Louisiana, Shreveport, Louisiana, 71134

Randy L. VanderWal, Nyma@NASA-Lewis Research Center,
Cleveland, Ohio 44315

laser-induced incandescence, soot, primary particle size

ABSTRACT

We have obtained temporally-resolved laser-induced incandescence (LII) signals from different size primary particles produced by diffusion flames of methane, ethane, ethylene, and acetylene. These results represent the first direct comparison between primary particle sizes based on optical measurements and those directly measured through TEM. Two measures of the temporal decay of the LII signal reveal a correlation with primary particle size. Comparison between primary particle sizes based on the calibrations using the temporal analysis of the LII signal and TEM measurements reveal agreement within the growth region and very late in the oxidation region within an ethylene gas-jet diffusion flame. Significant differences exist at intermediate positions which likely represent the effects of cluster-cluster aggregation within the oxidation region.

INTRODUCTION

Soot surface growth rather than nucleation has been found to dominate soot mass yield (*1-4*). Essential in characterizing the rate of soot growth and assessing theoretical models is the soot surface area. For example, soot mass proceeds via hydrogen abstraction creating a surface radical site in preparation for acetylene addition to the site (*5*). In such a process, the mass addition rate will depend upon total surface area in addition to the number of potential reactive sites (*6*).

Several parameters characterizing soot mass growth can be readily measured optically, such as soot volume fraction (f_v), velocity and temperature. Optical measurements are advantageous because they are non-intrusive and take place in real time. Optical, in-situ determination of primary particle size would further facilitate measuring soot mass growth and oxidation rates per unit surface area. The current methodology for primary particle size determination is through analysis of transmission electron microscopy (TEM) micrographs of thermophoretically sampled soot, an intrusive and time-intensive process (*1-4*).

Largely due to its high temporal and spatial resolution, laser-induced incandescence (LII) has advanced f_v measurements to a wide range of combustion processes. Theoretical models of LII predict that the temporal evolution of the signal after the excitation laser pulse is dependent upon primary particle size (*7-11*). This is physically sensible given that the temporal evolution of the LII signal is dependent upon the cooling of the primary particles predominantly through conduction and convection, processes dependent upon surface area. Thus the work presented here seeks to explore the potential of LII for determining primary particle size. Given the number of assumptions utilized in present LII theoretical models regarding the physical and structural properties of the laser-heated soot (*7-11*), we adopted an empirical approach to seek a correlation between the temporal decay rate of the LII signal and primary particle size as determined from analysis of transmission electron micrographs of thermophoretically sampled soot.

EXPERIMENTAL

A variety of laminar gas-jet diffusion flames produced by different fuels and flowrates were used to produce a wide range of primary particle sizes at similar temperatures and near the maximum in their growth history. Table 1 lists the different fuels, flow conditions, sampling heights above the burner, primary particle sizes and local temperatures for each of the four flames studied. The flame temperatures reported were measured by thermocouples employing rapid

insertion (*12*) with subsequent radiation correction (*13*). Each gas-jet diffusion flame was supported on a 10.5 mm I.D. nozzle surrounded by an air coflow through a 101 mm diameter honeycomb. A chimney with windows for optical access served to stabilize the flame and provide shielding from room drafts.

For LII measurements, the 1064 nm light from a pulsed Nd:YAG laser was formed into a 500 μm-wide sheet and directed through the flame. LII signals were relayed through a quartz optical fiber to a monochromator fitted with a photomultiplier tube (PMT) as the detector. The signal collection system has a spectral bandwidth of 12 nm and a transverse spatial resolution of 1 mm. Time-resolved PMT signals were sampled using a 500 MHz digital oscilloscope which also coaveraged 200 individual temporal scans.

Thermophoretic sampling provided soot samples for transmission electron microscopy. Probe residence times within the flames ranged from 30-60 ms depending on the soot volume fraction. TEM grids with ultrathin substrates aided visualization of the sampled soot. TEM micrographs were analyzed for primary particle size using commercial image processing software.

RESULTS AND DISCUSSION

Calibration Development

Figure 1 shows the time-resolved LII signal for three flames at the longest detection wavelength studied, 600 nm. Qualitatively similar data were obtained at shorter detection wavelengths but the largest observed variation in the temporal evolution of the LII signal occurred at 600 nm. Two analysis methods based on a theoretical model of the LII signal have been reported recently for extracting primary particle size from LII data (*10,11*). The first method uses the ratio of signal intensity (integrated over a specified time duration after the excitation laser pulse) at two detection wavelengths (*10*). An advantage of this method, according to the theoretical model, is reduced sensitivity to differences in ambient flame temperature. Analysis of our data in this manner, however, gave a nonmonotonic relationship between the ratio and primary particle size, which would result in a given signal ratio indicating two different particle sizes.

The second method of analysis is based on the ratio of signal intensity at a single detection wavelength with the signal integrated over selected electronic gate durations (*11*). Figure 2 shows the results of this method of analysis applied to the time-resolved LII signals from the different primary particle sizes. Because the method uses a limited portion of the experimental data, we also sought to utilize all the experimental data by fitting the signal decay to a mathematical function. Our analysis showed significant disagreement between the decaying portion of the time-resolved data and a single exponential fit. Far better agreement was observed using a double exponential fit. The double exponential curve fits were applied between data points where the signal intensity was 10% and 90% of the peak value. The cooling process of the laser-heated soot reflects the concurrent contributions of radiation, conduction, and convention that vary with time after the excitation laser pulse (*7-12*). Thus, the dual time constants may reflect different timescales associated with the different cooling mechanisms. Using the fast decay rate did not give a monotonic relation with increasing primary particle size. Figure 2 plots the second decay rate value (obtained by fitting the time-resolved LII signals for the various diffusion flames) against their primary particle size. The dynamic range and monotonic relationship exhibited by the analysis methods whose results are plotted in Figure 2 give each potential as an empirical calibration curve for inferring primary particle size based on the temporal decay rate of the LII signal in other systems.

Application

Motivated by the need for measuring primary particle size to determine soot mass growth and oxidation rates per unit surface area (*1-6*), we tested the utility of the calibration curve for determining primary particle size. Time-resolved LII data were obtained at different heights above the burner along the axial streamline within the

ethylene flame and subsequently fit to a double exponential and also analyzed using the method of gate ratios. Using the calibration curves presented in Figure 2, the measured long-time decay rates were translated into primary particle sizes.

The trend exhibited in both calibration plots is similar to the predicted results published in reference 10. Although the acetylene point is consistent with this trend, it was not used because of the different flame temperature which will affect the cooling processes (see Table 1). Given the uncertainty in the functional form of a curve-fit, line segments connecting the calibration points were used for interpolation. The ethane-ethylene segment was extrapolated to obtain primary particle sizes from points beyond the ethylene calibration point.

Figure 3 presents the results. In order to test the accuracy of the predictions, thermophoretic sampling measurements were performed followed by TEM microscopy and subsequent primary particle size analysis. These results are also plotted in Figure 3. While good agreement is observed at heights above the burner (HAB) of 40, 45, 80, and 85 mm, pronounced differences exist between 55 and 75 mm HAB, where the values measured from the TEM micrographs are significantly below the predicted values. Note that the agreement observed at 50 mm reflects its being used as a calibration point.

The deviations observed in the oxidation regions likely result from the aerosol process of cluster-cluster aggregation (*14*). Soon after the formation of aggregates within the growth region, clustering of aggregates can begin. This process will continue to occur throughout the growth and well into the oxidation regions of the flame. TEM images in the annular region of the flame show that as the aggregates cluster, they not only become larger but also more dense and compact (*15,16*). This is consistent with our own observations along the axial streamline. TEM images of soot aggregates collected at 40, 60, and 80 mm HAB show that the open branched chain appearance of aggregates within the growth region do qualitatively change to a more densely-packed, less open structure in the oxidation region. Such a structure could decrease the rate of cooling of individual primary particles (or fused units) through self-absorption of emitted thermal radiation and inhibition of conductive and convective cooling. Hence the optical measurement, which reflects the rate of temperature decrease of the laser-heated soot, would also be affected. Upon sufficient oxidation, the aggregates eventually crumble, so that the primary particles within the fragments return to a more open structure similar to that at their initial coalescence early within the growth region. At this stage, good agreement between the optical and TEM measurements would be expected, as observed. It could be argued that the oxidation process itself could slow the rate of cooling of the laser-heated soot. Localized burning of the soot could contribute to locally elevated temperatures of the particles. Given the agreement between temperatures within sooting flames measured via optical pyrommetry and thermocouples, however, this appears to be a minor contribution.

Another soot particle property that could affect the cooling process is the degree of primary particle connectivity. The degree of connectivity is a maximum at the peak of the soot growth region. Increasing primary particle connectivity would increase the effective primary particle size thus decreasing the cooling rate. Since our calibration points are at the peak of the growth region where the connectivity effects are maximum, this would underpredict primary particle sizes at other heights. The observed agreement between the predicted and experimental results within the soot growth region and the fact that the predicted results lie above the TEM measured values indicate that primary particle connectivity does not significantly impact the results presented here. The overprediction of the primary particle size relative to the TEM values within the oxidation region is also consistent with this postulate.

CONCLUSIONS

Our results suggest that LII can be used to predict primary particle size under certain conditions. Local flame temperatures will affect the cooling rate of the particle and thus the optical signal. Therefore, the flame temperature in the calibration system and the system to which it is applied must be similar in this empirical approach. Cluster-cluster aggregation will also affect the cooling rate

and the predicted primary particle sizes if it differs between the two systems. Particle-particle connectivity does not appear to be a significant factor in the results presented here.

These results represent the first direct comparison between primary particle sizes based on optical measurements and those directly measured through TEM. Predictions based on the temporal decay rate of the LII signal produce better agreement than those based on the gate ratio method.

ACKNOWLEDGEMENTS

This work was supported through NASA contract NAS3-27186 with Nyma Inc. Dr. Ticich and Mr. Stephens gratefully acknowledge support through the Ohio Aerospace Institute ASEE summer faculty fellowship and accompanying student program.

REFERENCES

1. Harris, S.J.; Weiner, A.M. *Combust. Sci. and Technol.* **1984**, *38*, 75.
2. Megardis, C.M. *Combust. Sci. and Technol.* **1989**, *66*, 1.
3. Sunderland, P.B.; Faeth, G.M. *Combust. and Flame* **1996**, *105*, 132.
4. Sunderland, P.B.; Koylu, U.O.; Faeth, G.M. *Combust. and Flame* **1995**, *100*, 310.
5. Frenklach, M.; Wang, H. 23rd Symposium (International) on Combustion, The Combustion Institute, Pittsburgh, PA. 1990; 1559.
6. Howard, J.B.; 23rd Symposium (International) on Combustion, The Combustion Institute, Pittsburgh, PA. 1990; 1107.
7. Melton, L.A. *Appl. Opt.* **1984**, *23*, 2201.
8. Hofeldt, D.L. Society of Automotive Engineers, Warrendale, PA, 1993; SAE Tech. Paper 930079.
9. Dasch, C.J. *Appl. Opt.* **1984**, *23*, 2209.
10. Mewes, B.; and Seitzman, J.M. *Appl. Opt*, **1997**, *36*, 709.
11. Will, S.; Schraml, S.; and Leipertz, A. 23rd Symposium (International) on Combustion, The Combustion Institute, Pittsburgh, PA. 1996; 2277.
12. Eisner, D.A.; Rosner, D.E. *Combust. and Flame*, **1985**, *61*, 153.
13. Smyth, K.C.; Miller, J.H.; Dorfman, R.C.; Mallard, W.G.; Santoro, R.J. *Combust. and Flame*, **1985**, *62*, 157.
14. Puri, R.; Richardson, T.F.; Santoro, R.J.; *Combust. and Flame*, **1993**, *92*, 320.
15. Dobbins, R.A.; Megaridis, C.M. *Langmuir* **1987**, *3*, 254.
16. Koylu, U.O.; Faeth, G.M.; Farias, T.L.; Caravalho, M.G. *Combust. and Flame*, **1995**, *100*, 621.

Fuel	Flow Rate (sccm)	Axial Height (mm)	Primary Size TEM (nm)	Temperature (K)
Methane	350	50	13.4+/- 1.6	1750
Ethane	255	61	24.4+/- 2.1	1700
Ethylene	231	50	33.3+/- 3.5	1600
Acetylene	200	50	59.7+/- 3.9	1200

Table 1. Summary of experimental conditions and primary particle sizes.

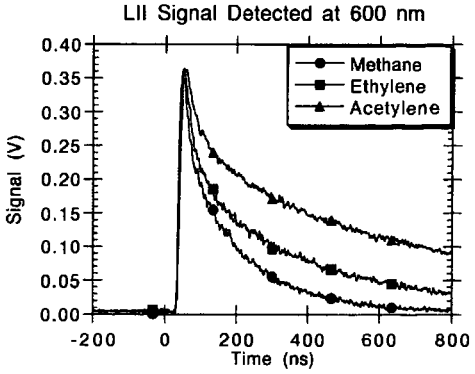

Figure 1. Time-resolved LII signals produced by the different size primary particles in the various flames.

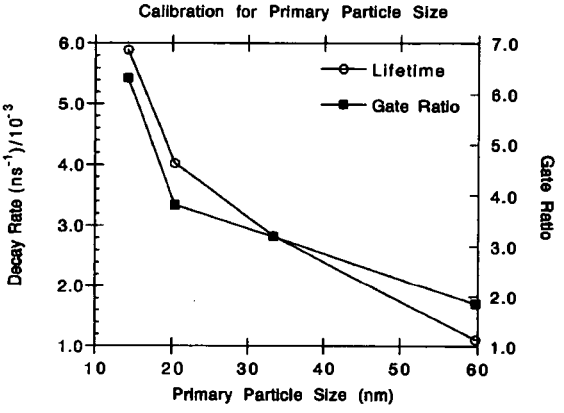

Figure 2. Correlation between measured primary particle size and the second decay rate and gate ratio describing the temporally resolved LII signal.

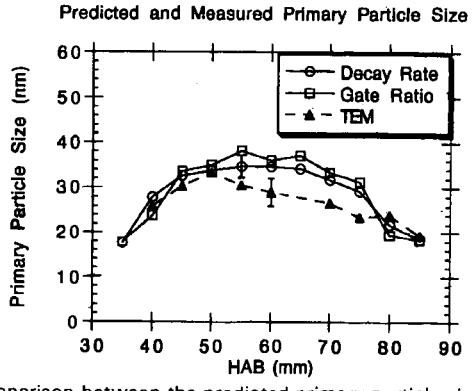

Figure 3. Comparison between the predicted primary particle size based on the optical measurements and interpreted using the calibration curves in Figure 2 and direct measurements from TEM micrographs.

OPTIMIZATION OF THERMAL CRACKING UNIT WITH AUTOMATIC HEAVY FUEL OIL STABILITY ANALYZER

Olli Pilvio[1] , Juha Vilhunen [2] ,Jouni Tummavuori[3]
[1] Neste Oy, Corporate Technology, PO Box 310, FIN 06101 Porvoo, Finland
[2] Finnish Measurement Systems FMS Ltd, Tekniikantie 21 A, FIN-02150 Espoo, Finland
[3] University of Jyväskylä, Dept. of Chemistry, PO Box 35, FIN 40351 Jyväskylä, Finland

Keywords: heavy fuel oils, stability, analyzer

ABSTRACT

The main target in optimizing the thermal cracking unit is to maximize the yield of the valuable lighter intermediate distillates. The cracking process is then running as near as possible but still on the safe side of the severity limit resulting stable fuel oil. Stability or long storage life is an important factor demanded of heavy fuel oils refined in the thermal cracking/visbreaking production units. The stability figure for heavy fuel oils indicates the precipitation tendency of asphaltene molecules in the oil. The stability parameters (P-value, toluene or xylene equivalents) are usually determined by the manual spot test method using visual detection. However, these tedious manual methods take up to hours to perform.

PORLA, an automatic stability analyzer for heavy fuel oils[1,2] was developed and has been used for several years by a Finnish oil company Neste Oy. The stability analyzer performs the same stability measurement procedure (determination of P-value) as the manual method only in few minutes. The laboratory model of the instrument is now commercially available and it has also been tested in the laboratories of other oil companies. There is a good correlation between the results obtained by the analyzer and those by the manual method. The automatic stability analyzer brings with a cost-effective and reliable tool for optimization of thermal cracking processes and blending of heavy fuel oil components.

INTRODUCTION

An important prerequisite for the hassle-free use of heavy fuel oils is that there exist no precipitate formation during their storage and use. The formation of the precipitates in oils is a consequence of flocculation of the asphaltenes present in the oil. The amount and quality of asphaltene particles in the oil and the production conditions determine the tendency for asphaltene precipitation. The stability figure is depending on quality of the feed stock, the reactor temperature and reactor residence time. Stability figures (P-value, peptization value, xylene or toluene equivalent) all describe the precipitation tendency of the asphaltenes. One of the stability figures p value is an abstract real number varying between 1 and 6.

In oil refining, the thermal cracking processes are adjusted such a way that the bottom products are always stable. The optimal temperature of thermal cracker unit is decisive. The profitability of thermal cracking unit improves as the quantity of valuable middle-distillates such as light fuel oil and diesel fuel components increase. The yield of these components is maximized by control of process temperature. If the process temperature is too low, part of the middle-distillates remain in the heavy fuel oils and production is not optimal. If again the process temperature is too high, that results in unstable products, which will sedimentate during storage or upon mixing with other oils.

In general, when the stability figure is about two the production economics is optimized; the yield of the valuable light and middle-distillate components are maximized and the heavy fuel oil is still stable without any remarkable addition of expensive "solvents" (light gas oil components). P values near 1 mean unstable products.

However, the optimal P-value for each process varies, because the products can be used for different applications. For some applications, however, a sufficient P- value for the product is even 1.5 and in some applications it must be near 2, it depends on the blending. In case of e.g. marine applications, where wide range of blending may take place, the sedimentation of aphaltenes may result in engine problems due to clogging of ship's fuel system (separators and filters). To prevent asphaltene precipitation in oil products refined at too high temperature, "solvents" have to be added. Solvents are however expensive and production economy suffers. Therefore, the range between 1.5 and 2 is the area where the optimization of the process and the product with help of the P-value determination can bring huge amounts of money to oil refining companies. 0.5 P-value units may mean millions of US dollars annually, depending on the capacity and feed stock of the refinery. The P-values above two mean "too good" products which will seldom cause any stability problems, but that is at the expense of the production economy.

In practice, the optimal process temperature of thermal cracker unit is set at safe distance from, but as close to the upper temperature limit as possible. The automatic stability analyzer method, which gives the stability figure in few minutes, will be presented. The instrument was developed to replace the tedious manual methods in order to regulate the optimal process temperature especially when changing the feed stock in the production.

EXPERIMENTAL

Determination of stability figures

The stability parameter is usually determined by manual spot test method using visual detection. In order to adjust the viscosity of the heavy fuel oil sample be aromatic solvent likc xylene or toluene is added. The asphaltenes in the heavy oil sample are precipitated by gradual addition of paraffinic solvent like n-heptane, decane or iso-octane. When subsequent amount of paraffinic solvent is added the oil becomes unstable and asphaltenes precipitate. After each addition of paraffinic solvent a droplet of the solution is placed on a filter paper and the visual detection of the two dark rings within each other formed in the spot indicate the precipitation. The stability parameter is determined from the amounts of oil, paraffinic and aromatic solvents. This manual test procedure takes from one to two hours to perform.

The function of an automatic computer controlled analyzer is based on the same procedure as the manual method, and the optical detection of precipitation point of asphaltenes during the measurement procedure is based on the scattering of visible light. At the precipitation point the intensity of scattered light rapidly increases. The analyzer gradually adds the selected paraffinic solvent in the prediluted heavy fuel oil sample, detects optically the precipitation point of asphaltenes and finally calculates the stability figure (P-value) on the basis of mass of the oil and the volume of aromatic solvent and paraffinic solvent consumption. To calibrate the instrument, three different dilutions from a heavy fuel oil with known P-value are first run by the instrument. Typical oil/aromatic solvent ratios are 4/1, 4/2, 4/3. The stability figures of these three solutions are applied in extrapolation procedure, where the impact of aromatic solvent to the solubility of asphaltenes is eliminated.

When all three solutions have been run by the analyzer the consumption of paraffinic solvent e.g. heptane of the undiluted heavy fuel oil sample X_0 can be extrapolated with the following way[3]:

Y = xylene (ml) / [xylene (ml) + n-heptane (ml)]

X = oil (g) / [xylene (ml) + n-heptane (ml)]

Figure 1 schematically illustrates the extrapolation procedure based on the titration of the three dilutions resulting paraffinic solvent consumption of an undiluted oil sample. Consequently, the stability figure P-value is calculated from the following equation:

$$P = 1 + 1/X_0,$$

where X_0 is the intersection of x axis and the straight line extrapolated via the three data points.

Correlation of P-value and toluene/xylene equivalents

In addition to the P-value, other methods like toluene and xylene equivalents are used to determine the stability of heavy fuel oils. Toluene and xylene equivalents are equal, the only difference between these two methods is the solvent (toluene/xylene). Toluene equivalent is determined by a method where the heavy fuel oil sample is first mixed with toluene typically in the proportion of one to five. Paraffinic solvent is gradually added in the mixture. After every paraffinic solvent addition a droplet of the mixture is taken and placed on a filter paper until separation of the spots appear. The toluene equivalent is the lowest toluene concentration (expressed in vol-%) of the solution where the asphaltenes are not precipitated[3]. The toluene/xylene equivalent is calculated in the following way:

Tol-eq. ={toluene (ml) / [toluene (ml) + n-heptane (ml)]}*100 %

When comparing the equation for the calculation of toluene equivalent and that one for the Y axis of the P-value determination the correlation between P-value and toluene equivalent can be seen. Figure 2 illustrates this linear correlation.

RESULTS

In an eight months laboratory monitoring test carried out by Scanraff refinery in Sweden[4] almost one hundred heavy visbreaker fuel (Vistar) oil samples with same origin were analyzed both manually and automatically with the analyzer. One objective of this test was to check correlation between the analyzer and the manual spot test method in the oil quality control laboratory use. The original values of this test period can be seen in Table 1. Fig 3 shows the stability figures for product "Vistar" obtained by PORLA and the deviations from the manual method during the monitoring period. 73 samples of 93 gave exactly the same stability figure by both methods, 8 samples gave 0.1 P-value unit higher value and 12 samples 0.1 P-value unit lower value by the analyzer than by the manual method. The statistical testing of the analyzer during over decade's constant use in refinery laboratories has proven the repeatability of the analyzer to be ±0.05 P-value unit. The test run result confirmed our repeatability results.

The results obtained by manual and automated methods did not significantly differ from each others. This is shown on the basis of the statistical tests carried out from the original data of Table1. The statistical tests done were F-test (Two-Sample for Variances), t-test (Paired Two-Sample for Means) and Friedman test (Repeated Measures Analysis of Variance on Ranks).

Probability value 0.40 of F-test shows variances to be equal. Paired t-test of which critical t-value was $1.98_{0.05}$ gave t-value 0.61 and probability 0.53. To confirm the test results obtained by F-test and t-test the Friedman test (Repeated Measures Analysis of Variance on Ranks) was performed. Table 2 shows and figure 4 illustrates the result of Friedman test. The differences in the median values among the treatment groups are not great enough to exclude the possibility that the difference is due to random sampling variability; there is not a statistically significant difference between manually and automatically obtained results of P-values.

Especially the process temperature affects the formation and precipitation tendency of asphaltene particles. It is essential to control the reactor temperature of a thermal cracker production unit to such a level, where the heavy oil produced is still stable and there is no coke formation in the reactor tubes. A typical correlation between the temperature of thermal cracker reactor and the stability figure (P-value) for certain crude oil feed stock is illustrated in figure 5. The optimum reactor temperature, however, may vary according to the feed stock material and therefore it is important to detect for every feed stock the stability limit, which corresponds the highest temperature, where the production is on the safe side, where the product is stable and as near as possible to the severity limit in order to optimize the yield of the valuable lighter products and to avoid coke formation, which may lead to interruption of the production.

CONCLUSIONS

The optimization of thermal cracker units and the quality control of heavy fuel oil production can be improved as minimized off-spec production by an automated stability analyzer. Additionally, the use of an automatic analyzer brings with remarkable labor cost savings in an oil quality control laboratory compared to the tedious manual methods. Besides, the automated analyzer minimizes the errors due to differences in individual human capabilities for visual detection of spot test.

An automated stability analyzer developed at Neste oil refinery in Finland is based on this manual test method, but it performs the same procedure automatically in few minutes. It has been developed in order to save oil refinery laboratories' labor costs and to improve the handling of heavy oil stability and quality control.

It is known that the wider the dissimilarity between the blend components, the greater is the risk of incompatibility and possible often significant economical consequences. This automated method can be used also for detecting the stability figure of heavy fuel oil blends i.e. binary or ternary systems. Some stable products may form an unstable blend. Therefore, it could be reasonable to check beforehand the stability of such blends by making stable/unstable maps for binary or ternary heavy fuel oils systems.

Statistical calculations of the Scanraff's test run results indicate that there are not statistically significant differences between the result obtained by the manual and automated method. The small differences in the results is if anything due to random sampling variability. Therefore, the automatic method offers an fast, cost-effective and reliable tool to replace the tedious manual methods for analyzing the stability figure of heavy fuel oils.

REFERENCES

1. O.Pilviö, "Automatic Stability Analyzer of Heavy Fuel Oils", IASH '94, the 5th International Conference on Stability and Handling of Liquid Fuels, October 3-7, 1994, Rotterdam, the Netherlands
2. O.Pilviö, J.K.Vilhunen and L.-Å. Larsson., "Experiences in Use of Automatic Heavy Fuel Oil Stability Analyzer", IASH '97, the 6th International Conference on Stability and Handling of Liquid Fuels, October 12-17, 1997, Vancouver, B.C., Canada
3. R.Kassinger, "Fuel Blending - How to Minimize Risk of Incompatibility", IASH '97, the International Conference on Stability and Handling of Liquid Fuels, October 12-17, 1997, Vancouver, B.C., Canada
4. L.-Å.Larsson, Test run report of Porla analyzer January 1997, Scanraff, Lysekil, Sweden

TABLE 1. Stability figures P-values obtained manually and by automated PORLA analyzer during eight months test period at Scanraff, Sweden.

Manual	Automat	Manual	Automat	Manual	Automat	Manual	Automat
1.7	1.7	2.0	2.0	2.0	2.0	2.0	2.0
1.9	1.9	2.1	2.0	2.0	2.0	2.1	2.1
1.9	2.0	2.4	2.3	2.0	2.0	2.0	2.0
1.8	1.8	1.9	1.9	2.0	2.0	2.0	2.0
1.8	1.8	2.5	2.5	2.0	2.1	2.1	2.1
1.9	1.9	2.1	2.1	2.0	2.0	2.1	2.1
1.9	2.0	2.6	2.6	1.8	1.8	2.1	2.0
2.0	1.9	2.0	2.0	2.0	2.0	2.2	2.2
2.1	2.0	2.0	2.0	1.8	1.8	2.3	2.4
1.7	1.6	2.0	2.0	2.0	2.0	2.0	2.0
1.6	1.6	2.0	2.0	2.1	2.1	1.9	1.9
1.6	1.6	2.1	2.1	2.0	2.0	2.1	2.1
2.3	2.2	1.8	1.7	1.9	1.9	2.1	2.1
1.6	1.6	1.8	1.7	1.9	1.9	2.0	2.1
1.6	1.6	1.9	1.9	1.7	1.8	2.1	2.1
2.2	2.1	1.8	1.8	1.9	1.9	2.1	2.1
2.2	2.2	1.8	1.8	1.9	1.9	2.1	2.1
1.9	1.9	2.0	2.1	1.7	1.7	2.0	2.0
2.1	2.1	2.2	2.1	2.0	2.0	2.1	2.1
2.1	2.1	1.9	1.9	2.0	2.1	2.0	2.0
1.9	1.8	1.8	1.8	2.3	2.3	2.1	2.1
2.2	2.2	1.8	1.8	2.0	2.0		
2.1	2.1	2.1	2.1	2.0	2.0		
2.2	2.2	2.0	1.9	2.0	2.0		

TABLE 2. The results of Friedman test from the values of table 1.

Group	Median	25 %	75 %
Manually	2.0	1.9	2.1
Automatic	2.0	1.9	2.1
Chi-square = 0.667 with 1 degrees of freedom. (P = 0.4142)			

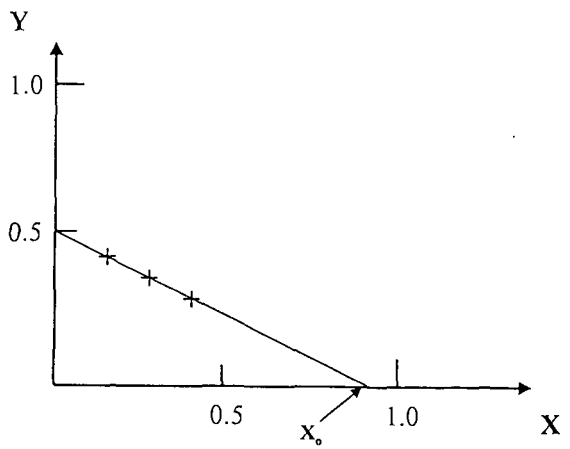

FIGURE 1. Determination of paraffinic solvent consumption for an undiluted heavy fuel oil sample X_0 by extrapolation.

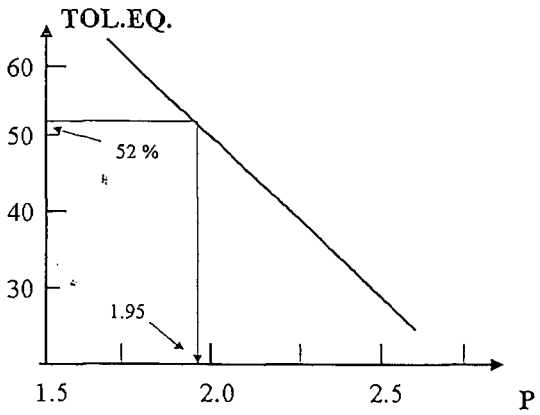

Figure 2. Linear correlation between toluene equivalent and P-value for heavy fuel oils.

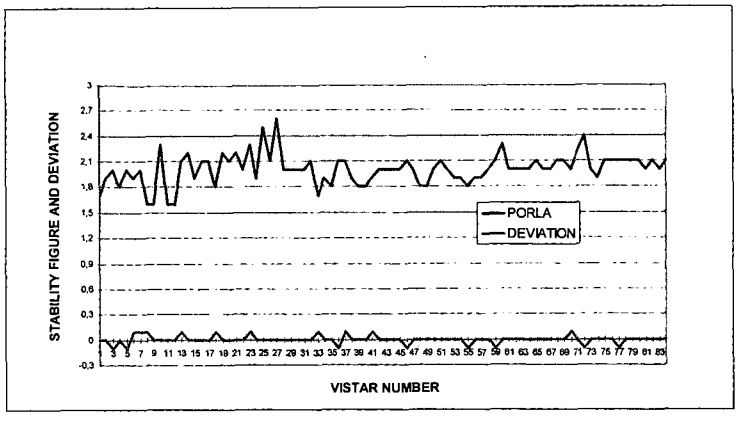

FIGURE 3. Stability figures of Vistar heavy fuel oil product obtained by PORLA analyzer and deviation of each value from the manually obtained value.

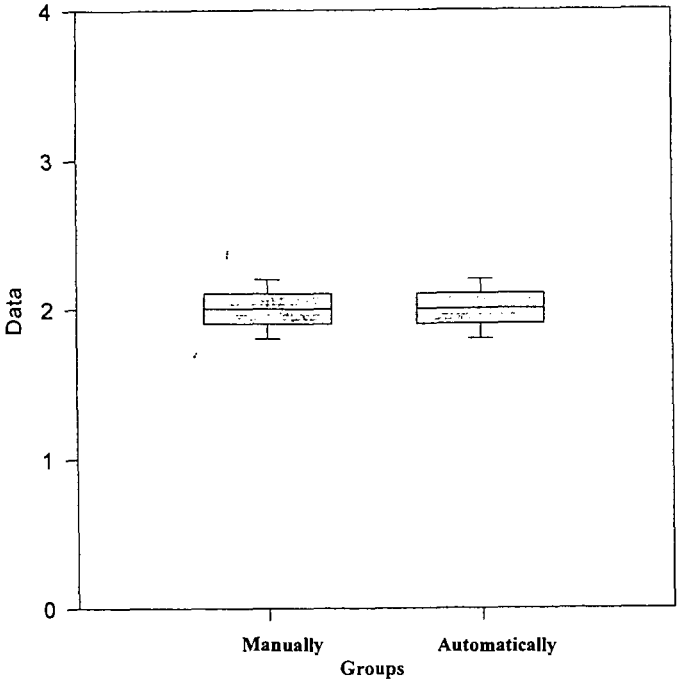

FIGURE 4. A graphical illustration of the result of Friedman test carried out from the data of table 1.

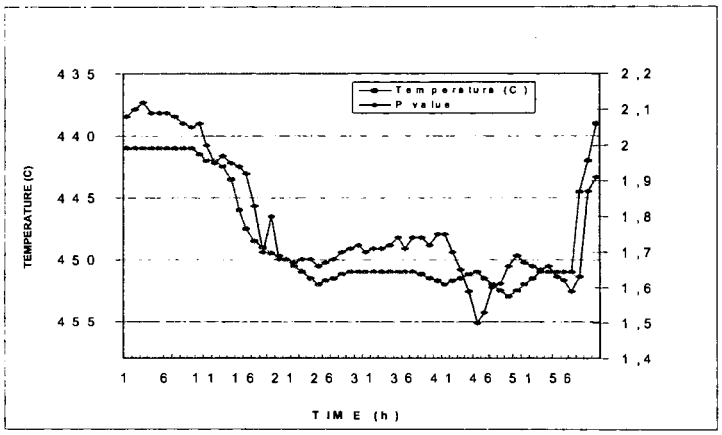

FIGURE 5. Correlation between stability figure and thermal cracking process for certain feed stock material.

CONVERSION OF OXO AND THIOMOLYBDATES TO ACTIVE DISPERSED CATALYSTS

Xiaodong Zhan, Mike Dieterle, Anthony Lucas
Howard Van Woert, and Edwin N. Givens

Center for Applied Energy Research
University of Kentucky
2540 Research Park Drive
Lexington, KY 40511-8410

Keywords: Molybdenum catalyst, Coal Liquefaction

ABSTRACT

Oxomolybdates impregnated on coal are excellent catalyst precursors in the liquefaction of Wyodak coal, especially when sulfur is added during the reaction. It has been suggested that the active catalysts are oxothiomolybdates. This paper discusses two approaches toward converting oxomolybdates into active catalysts and identifying the types of Mo-S bonding that contribute toward their activity. In the first, several oxothiomolybdates having different forms of Mo-S bonds were prepared in our laboratory and impregnated onto Wyodak coal. THF dissolution and resid conversion for these precursors were determined both in the presence and absence of added H_2S. In the second approach, ammonium heptamolybdate was treated in flowing H_2S in H_2 at temperatures to permit slow conversion of the oxomolybdate into its active form. The effect of this pretreatment on the activities of these catalyst impregnated coals were determined.

INTRODUCTION

A vast amount of observations has indicated that the presence of sulfur is important to coal liquefaction. For molybdenum based catalyst, it is generally agreed that the predominant active species for the primary coal liquefaction is some form of molybdenum sulfide, e.g., MoS_2. The active species may be produced by the decomposition of molybdenum precursors under liquefaction condition. When metal sulfide catalysts are used, a source of sulfur such as hydrogen sulfide, carbon disulfide, or elemental sulfur is introduced to the reactor to maintain the catalysts in a sulfided form. If the precursor contains no sulfur, external sulfur participates in forming the highly active phase. If excess sulfur is present in a sulfur containing precursor, some must diffuse out to allow transformation into the active phase to occur.[1] The importance of the correct stoichiometry of Mo sulfide has also been emphasized by Montano. [2]

The type of catalyst precursor and its activation conditions are important factors influencing the function of the molybdenum catalyst. Utz et al.[3] compared the effects of ammonium tetrathiomolybdate (ATTM), MoS_3, and ammonium heptamolybdate (AHM) on the liquefaction yields of coals. Two activation methods employed were rapidly heating up the reactor to 450°C in 1-2 minutes and slowly heating up in 45-60 minutes. Their results showed greater activities of ATTM and MoS_3 when they were heated rapidly, while slow heating favored AHM. They suggested that since ATTM and MoS_3 were already in a sulfided form, they could decompose more rapidly to a highly dispersed active phase. The transition of AHM to MoS_2 having a high surface area was slow because an external sulfur source was required. By studying the temperature and pressure profiles in a batch reactor, Bockrath et al.[4] found that the molybdenum sulfide was able to participate in liquefaction reactions at low temperature, e.g., 350°C, in contrast to the conventional 400-465°C. They concluded that the dispersed catalyst should be present in an already active form rather than allowing a precursor to undergo transformation during liquefaction. The influence of catalyst precursor on coal conversion also was investigated by Hirschon and Wilson,[1,5] who used Illinois #6 coal with various molybdenum precursors. They found that much higher toluene solubles could be obtained with organometallic complexes than with aqueous metal salts. They suggested that the higher activity of the molybdenum sulfide complex could be attributed to its better dispersion and already being present in highly active form. Subsequent activation during liquefaction was unnecessary. Our recent studies indicate that low-cost water-soluble oxomolybdate salts can be transformed into liquefaction catalysts having activity comparable to more expensive oil soluble precursors.[6]

Although oxomolybdates have demonstrated substantial activity toward coal liquefaction in the presence of H_2S, we suspect that their transformation into active phase can be achieved in situ. The objective of this study is to investigate approaches for improving the activity of dispersed catalysts generated from oxomolybdates. A series of Mo based compounds with various sulfur content were prepared from H_2S and oxomolybdate before impregnating them on coal. Another approach that was also tested was to pretreat the oxomolybdate impregnated coal slurry with H_2S in H_2 to convert the precursor to oxothiomolybdate prior to reaction. This method has been reported to form an active catalyst or close intermediate to an active species. [7,8]

EXPERIMENTAL

Materials Elemental analysis of the Black Thunder Wyodak coal are presented in Table 1. The as-received coal was impregnated with an aqueous solution containing various concentrations of catalyst precursors at the level of 0.5 g solution/g coal. The concentration of the aqueous solution was varied so that desired Mo loadings on coal could be achieved. In all of the cases, the coal paste was dried at 125 Torr and 100°C for two days to completely remove water. Solvent used in this study comprised mixtures of heavy distillate and deashed resid from Run 262e made at the Advanced Coal Liquefaction R&D Facilities at Wilsonville, AL. The properties of these materials, which were produced when the plant was operated with the same coal, are also summarized in Table 1. Ammonium heptamolybdate (AHM, Aldrich, A.C.S. reagent) and tetrahydrofuran (THF, Aldrich) were used as received. Ammonium dioxodithiomolybdate (ADOM), ammonium tetrathiomolybdate (ATTM), and three types of ammonium polythiomolybdate having different sulfur contents were prepared in our lab from AHM and H_2S. ATTM was prepared by the method of Naumann and Behan[9], AOTM was prepared by the method of McDonald et al.,[10] APTM-1A and APTM-2A ($(NH_4)_2[Mo_2{}^VS_{12}]\cdot 2H_2O$) were prepared by the method of Müller and Krickemeyer,[11] and APTM-P ($(NH_4)_2\cdot Mo_3S(S_2)_6\cdot 2H_2O$) was prepared by the method of Kurtak and Hartzog.[12] The compositions of these material are summarized in Table 2. In all experiments, catalyst loadings were reported as mg Mo per kg dry coal.

Catalyst Pretreatment In some of the experiment, the oxomolybdate impregnated coal slurry was pretreated prior to reaction with H_2 containing 8 vol% H_2S. In a typical run, the reactor was loaded with coal slurry and placed horizontally in a furnace after purging with H_2 to remove air. The pretreatment was conducted at 300 psig and a gas flowrate of 200 ml/min (STP). The furnace was heated to 120 °C and held for 30 min after which it was successively heated to 250 and 360 °C while holding for 30 minutes at each temperature. After pretreating at 360 °C, the reactor was cooled, vented and subjected to regular reaction procedures described in the following section.

Coal Liquefaction Reaction Procedures All of the experiments were conducted in a 65 ml microreactor which was agitated at 400 rpm in a fluidized sand bath (Techne, SBL-2D) maintained at 440°C with an Omega CN4600 temperature controller. In every run, 3 g dry coal, 1.8 g heavy distillate, and 3.6 g deashed resid were added to the reactor which was then pressurized to 1000 psig at room temperature with H_2 containing 3 vol% H_2S. Except in some runs when the reactor was charged with pure H_2 only, all reactions were performed at the above baseline reaction conditions. After 30 minutes reaction time, the reactor was removed and quenched in ice water. The liquid and solid products were scraped from the reactor using THF and subjected to Soxhlet extraction for 18 hours. The THF soluble material was distilled at 1 Torr and an atmospheric equivalent cut point of 566°C according to ASTM method D-1160 . This cut point corresponds to that used in the pilot plant where the solvent was generated. All experiments were replicated at least twice to assure the reproducibility.

THF coal conversion and resid conversion were defined below as a measure of catalyst activity on an maf coal basis.

$$Coal\ Conv. = 100\times\left(1-\frac{[IOM]_{product}}{Coal(maf)}\right) \quad (1)$$

$$Resid\ Conv. = 100\times\left(\frac{[Coal(maf)+Resid]_{feed}-[IOM+Resid]_{product}}{Coal(maf)}\right) \quad (2)$$

RESULTS AND DISCUSSION

Effect of Oxothiomolybdates on Coal Liquefaction In this study, several sulfur containing molybdenum compounds including AOTM, ATTM, and three types of APTM were used as catalyst precursors to examine the effect of sulfur content in precursors on liquefaction. Conversions with these precursors at Mo loading of both 100 and 300 ppm are shown in Figures 1 and 2.

In the presence of H_2S, coal conversion was almost unchanged at both catalyst loadings. However, in the absence of added H_2S, coal conversions increased significantly for precursors having S/Mo ratios ≥ 4. Another sizable increase was observed for APTM-1A which contains a S/Mo ratio of 10.9. This material had been extracted with CS_2 to remove free sulfur and probably contained a large fraction of polysulfide bonds. As shown in Figure 2, resid conversion increased slowly as the S/Mo ratio increased, whether in the presence or absence of H_2S. Because of the wide variations observed in the resid conversion values, however, the data do not show a statistically significant difference between precursors having S/Mo ratios from 2 to 6. Overall, the presence of sulfur is important to both coal and resid conversions whether sulfur is supplied externally or is present in the catalyst precursor. Lower conversions observed in the absence of H_2S may be due to insufficient sulfur in the reactor to sulfide the precursors and to protect the active phase from being oxidized by

the water. Since the fraction of converted precursor apparently increased as sulfur increased, coal conversion also increased as the S/Mo ratio in the precursor increased. When H_2S was introduced to the reactor, the amount of sulfur carried in by the precursor became negligible compared to the total sulfur available, thus coal conversion became independent of the S/Mo ratio.

Since coal solubilization takes place very early during liquefaction, without added H_2S, the small amount of sulfur associated with the precursors may be sufficient to transform and stabilize an active phase for a short period. Within that period when conversion is occurring, THF solubilization showed an increase as the S/Mo ratio in the precursor increased. Since resid conversion progresses over a longer period, the active phase may lose sulfur through oxidation by water causing the catalyst to deactivate. Thus, an added source of sulfur is necessary to maintain the catalyst in an active form. Clearly, an external sulfur source is necessary for precursors already containing a significant concentration of sulfur.

In coal liquefaction with impregnated catalyst, it is generally assumed that catalyst precursor converts to sulfided active phase *in situ*. There is evidence showing that the activity of the final catalyst depends upon the conditions employed during its preparation.[7] At high temperatures typical of coal liquefaction, an oxomolybdate catalyst precursor such as AHM experiences two type of competition reactions, i.e., thiosubstitution and decomposition. When the rate of ammonia loss due to decomposition is greater than the rate of thiosubstitution, the intermediate Mo compounds are more difficult to sulfide. Therefore, complete sulfidation of ammonium oxomolybdate by H_2S under liquefaction conditions may not occur. By contrast, in oxothiomolybdates, the loss of ammonia is not critical since the catalysts are already in their sulfided forms. Complete conversion of these precursors to an active catalyst is more likely through reaction with the H_2S or intramolecular rearrangement transfer of the sulfur in precursors. For different sulfur-containing precursors, there may be differences in their decomposition mechanisms and kinetics. The chemical form and the number of active sites may also differ as reflected by the different activities towards resid conversion.

Another factor that affects the formation of active catalyst is the presence of water. Although the impregnated coal was dried before reaction, inevitably, some water will be present in the reactor as a result of deoxygenation reactions. At high temperatures and in the presence of water, the Mo catalyst will deactivate as it gains oxygen from water. Also, water may cause removal of sulfur, thus deactivating the catalyst. The observation that resid conversion increases with the S/Mo ratio in the presence of H_2S may also be attributed to the fact that the oxothiomolybdate catalyst may remain the active phase as excess sulfur is lost in the presence of water.

Pretreatment of oxomolybdate impregnated coal slurry with H_2S/H_2 Sulfur is obviously important for the transformation of these oxo and thiomolybdate precursors into an active catalytic phase. In order to have a better understanding of this transformation, a series of tests were made in which AHM impregnated coal slurries were pretreated with H_2S. In every run, the catalyst impregnated coal was dried, slurried with solvent, and pretreated in a stream of H_2S/H_2 at a series of temperatures at 300 psig.

A blank run was made to determine the effect that pretreating coal for 90 minutes at a sequence of temperatures up to 360°C would have on conversions at 440°C. THF and resid conversions for a coal impregnated with AHM to a Mo loading of 100 ppm were quite small, i.e., 3.6% and 2.4%, respectively. Therefore, conversions observed at 440 °C are not significantly influenced by the 90 minutes pretreatments at ≤ 360°C and 300 psig.

For coals impregnated with 100 and 300 ppm Mo, THF coal conversions were not affected by the pretreatment, as shown in Figure 3. The most noticeable effect is an increase in resid conversion for the coal loaded with 100 ppm Mo. The resulting resid conversion is the same as that achieved with the coal loaded with 300 ppm Mo. This result suggests that the pretreatment converts a large fraction of the precursor to an active phase. At the 300 ppm Mo loading, no apparent advantage was gained from pretreating.

It appears that pretreating the coal slurry with H_2S/H_2 improves resid conversion. Also, high resid conversions can be obtained by using an oversulfided Mo substrate such as APTM-1A. Note that the following two 100 ppm Mo impregnated coals were as active as the 300 ppm Mo impregnated coals.

	Resid Conv, maf coal
100 ppm Mo as AHM+treatment with H_2S/H_2	82.3±1.7
100 ppm Mo as APTM-1A	82.3±2.9
300 ppm Mo as AHM+treatment with H_2S/H_2	82.2±1.6
300 ppm Mo as AHM	80.3±0.4

CONCLUSIONS

When non-sulfur containing oxomolybdate was used as catalyst precursor for coal liquefaction, complete transformation to active catalyst in situ apparently does not occur under

reaction conditions. Upon recycle, the Mo-catalysts have been observed to be far more active. The inevitable presence of water in the reaction system at the high reaction temperature affects this transformation. If oxothiomolybdate is used as precursor or if oxomolybdate impregnated coal is presulfided prior to reaction, activity for resid conversion improves substantially and is retained for a longer period. In these cases, the catalyst is more active and more resistant to water oxidation. An external sulfur is still necessary with oxothiomolybdate precursors.

ACKNOWLEDGMENTS

This research project was supported by the U.S. Depart of Energy under contract number of DE-AC22-91PC91040.

REFERENCES

1. Hirschon, A.S., and Wilson, R.B., ACS Fuel Chem. Prepr., 34(3), p881-885, 1989.
2. Montano, P.A., Stenberg, V.I., and Sweeny, P., J. Phys. Chem., 90, 156-159, 1986.
3. Utz, B.R., Cugini, A.V., and Frommell, E.A., ACS Fuel Chem. Prepr., 34(4), 1423-1430, 1989.
4. Bockrath, B.C., Illig, E.G., and Keller, M.J., ACS Fuel Chem. Prepr., 37(1), 133-140, 1992.
5. Hirschon, A.S., and Wilson, R.B., ACS Fuel Chem. Prepr., 36(1), 103-107, 1991.
6. Zhan, X, Shabel, M., Cash, R., and Givens, E.N., ACS Petro Chem. Prepr., 42(4),639-642, 1997.
7. Lopez, J., and Pasek, E.A., Process for Preparing Heavy Oil Hydroprocessing Slurry Catalyst, US Patent 4,710,486, 1987.
8. Lopez, J., McKinney, J.D., and Pasek, E.A., Heavy Oil Hydrotreating, US Patent 4,557,821, 1985.
9. Naumann, A. W. and Behan, A. S. Production of improved molybdenum disulfide catalysts. U. S. Patent 4,243,553. Jan. 6, 1981.
10. McDonald, J. W., Friesen, G. D., Rosenhein, L. D., and Newton, W. E., Inorganica Chimica Acta 1983, 72, p 205-210.
11. Muller, A. and Krickemeyer, E, Inorganic Synthesis 1990, 27, 47-51.
12. Kurtak, C. R. and Hartzog, L. D., Preparation of ammonium polythiomolybdate. U. S. Patent 3876755, Apr. 8, 1975.

Table 1. Properties of Wyodak Coal and Feed Solvent

	Coal	Solvent	
	Ultimate Analysis	Heavy Distillate	Deashed Resid
<566°C	-	96.9	14.7
Composition (wt%)			
Carbon	70.62	88.86	89.79
Hydrogen	5.03	9.91	7.26
Nitrogen	1.13	0.44	0.86
Sulfur	0.52	<0.03	0.03
Oxygen (diff)	16.38	0.79	1.33
Ash	6.32		0.73
Ash, SO_3-free	5.46		

Table 2. Composition of Mo-Based Oxothiomolybdates (wt%)

	AHM	AOTM	ATTM	APTM-P	APTM-2A	APTM-1A
H	2.59	3.58	3.08	1.30		1.16
N	6.80	11.7	10.77	3.76		3.0
S	0	28.28	49.23	55.05	60.23	72.16
Mo	54.37	43.97	36.92	36.76	31.05	19.91
O (diff)	36.24	12.47	-	3.13		3.77
S/Mo (atomic)	-	1.93	4.00	4.49	5.82	10.87

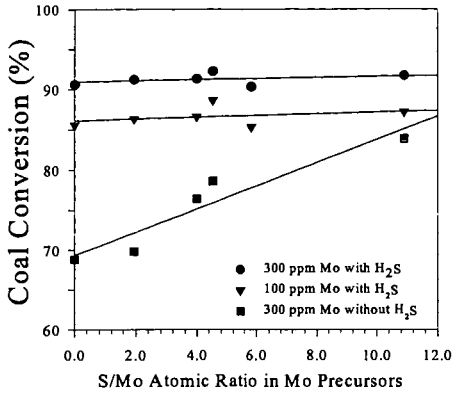

Figure 1. Effect of S/Mo ratio in precursors on coal conversion in the presence/absence of external H_2S

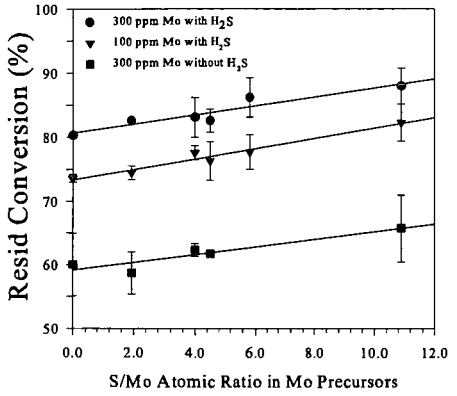

Figure 2 Effect of S/Mo ratio in precursors on resid conversion in the presence/absence of external H_2S.

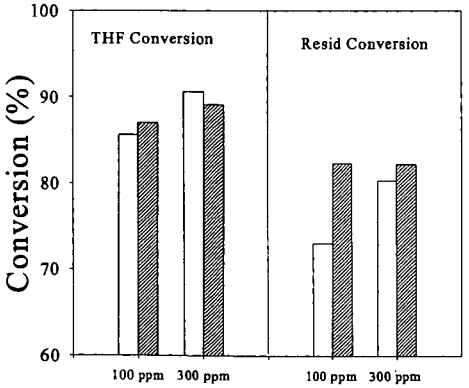

Figure 3. Effect of H_2S/H_2 pretreatment on coal liquefaction with AHM as catalyst precursor. ▭ --- no pretreatment, ▨ --- H_2S/H_2 pretreatment.

ASSESSMENT OF BIMETALLIC AND PARTIALLY-SULFIDED PHOSPHOMOLYBDATES FOR LIQUEFACTION OF WYODAK COAL

Belma Demirel, Chad M. Adams and Edwin N. Givens
University of Kentucky Center for Applied Energy Research
2540 Research Park Drive, Lexington, KY 40511-8410

Keywords: Coal conversion, phosphomolybdic acid, sulfided catalysts

ABSTRACT

Phosphomolybdic acid (PMA) is an excellent catalyst precursor for direct liquefaction of Wyodak coal when well dispersed within the reaction system by impregnating onto the feed coal. Addition of sulfur during the reaction significantly increased the activity of the catalyst. Several partially sulfided phosphomolybdates were prepared and characterized by a variety of analytical techniques. THF and resid conversions with these partially converted precursors were determined when added as particulate material directly to the reaction mixture and when impregnated onto Wyodak coal. The effectiveness of these partially converted intermediates will be related to their physical characteristics and elemental and structural compositions. Nickel and cobalt bimetallic phosphomolybdates were prepared and impregnated on coal. The effect of the co-metal on the activity for solubilizing coal and conversion of coal-derived resid will be compared with other active Mo precursors.

INTRODUCTION

Development of catalysts is important for more efficient coal liquefaction to produce liquid fuels. Dispersed catalyst is understood as the catalytic material employed as particles dispersed on coal or in the reaction media. It provides intimate contact with the surface of coal particles which influence reactions and break the coal structure to gas and liquid products. Many reports have been published on liquefaction using dispersed catalysts, particularly molybdenum and iron sulfide. Molybdenum is often added to liquefaction processes either as the oxide or thiolate water-soluble salts or as molybdenum naphthanate.[1] The active form of molybdenum is not well-known, although it is considered to be molybdenum disulfide. Our studies indicate that intermediate molybdenum oxysulfides may be the active catalyst.[2,3] Lopcz et al. reported that the atomic S/Mo ratio was less than two in the active catalysts isolated from processing heavy petroleum fractions with ammonium molybdate and thiomolybdate.[4]

Most active catalysts are insoluble in common solvents and one method of increasing dispersion is to introduce the catalyst as a soluble precursor.[5-8] Phosphomolybdic acid (PMA) and most bimetallic phosphomolybdates are soluble in water and provide good dispersion.[9] When PMA was impregnated onto coal, THF and resid conversions are comparable to those obtained from various molybdenum salts.[3, 10-12]

The addition of a second metal, such as Ni and Co, can increase hydrogenation and hydrodesulfurization activity. Chiantelli et al. used bimetallic complexes to study the promotional effects of Ni and Co for MoS_2.[13] Garg and Givens reinvestigated the catalytic activity of several impregnated transition metals in coal liquefaction and showed that addition of Ni, Co and Mo salts was effective.[2] Eccless and de Vaux reported that Ni-Mo or Co-Mo gives a very high yield of light oil fractions.[14]

The first objective of this work is to show the performance of sulfided catalysts produced from PMA for coal liquefaction. The second objective is to show the catalytic activities of bimetallic phosphomolybdates for coal liquefaction and to compare them to PMA.

EXPERIMENTAL

Wyodak coal from the Black Thunder Mine in Wright, Wyoming was supplied by Hydrocarbon Technologies, Inc. Proximate and ultimate analysis of the coal are given in Table 1. The recycle solvents were obtained from the Advanced Coal Liquefaction R&D Facilities at Wilsonville, Alabama. Phosphomolybdic acid (PMA) was supplied by Aldrich Chemicals Inc. $Co_3(PMo_{12}O_{40})_2 \cdot xH_2O$ (CoPM), $Ni_3(PMo_{12}O_{40})_2 \cdot xH_2O$ (NiPM) and $K_3PMo_{12}O_{40} \cdot xH_2O$ (KPM) were synthesized in our laboratory.

Sulfidation of PMA was carried out in a 9" x 2" tubular quartz reactor equipped with a furnace, thermocouple and temperature controller. A stream of nitrogen or 8 vol% hydrogen sulfide in hydrogen flowed into the reactor through flowmeters. The exhaust gases from the reactor were passed through a H_2S scrubber filled with NaOH solution and vented to a hood. About one gram of PMA in a porcelain boat was placed into the reactor for sulfidation experiments. After the reactor was purged with nitrogen at ambient temperature to remove air, a stream of 8 vol% H_2S in H_2 was

passed over the sample and the reactor heated to 125, 150, 200, 300 or 450°C. The samples remained at the specified temperature for 4 h at a H_2S-H_2 flow rate of 80 ml/min. In each experiment, a total of 19.2 liters of H_2S-H_2 was passed over the sample. The reactor was subsequently cooled to ambient temperature under nitrogen, and sulfided catalysts (PMA125, PMA150, PMA200, PMA300 and PMA450) were ground to fine powder before use.

Sulfided PMA materials were added to the reaction media in two ways: direct addition of sulfided PMA materials to the reaction mixture and impregnating sulfided PMA materials onto coal. The apparent water solubility of the sulfided PMA materials decreased as the temperature of preparation increased. Coals were prepared by slowly adding in a dropwise manner the water solutions containing the sulfided materials, and any undissolved material, which was normally quite small, was washed onto coal with additional water. Total amount of water used for impregnating the sulfided PMA materials was about 0.5 g per g dry coal. Coals were then dried in a vacuum oven at 96°C and 33 kPa overnight to remove essentially all of the moisture.

The Ni, Co and K salts of PMA were impregnated onto coal from aqueous solutions. The patassium salt was soluble only after adding a few drops of KOH to the water. Coals were impregnated by adding aqueous solutions (0.03 g solution/g dry coal) that contained the appropriate concentration of the individual metal salts to provide a final loading of 300 mg Mo/kg dry coal. During addition, the powdered coal was continually stirred to assure even dispersion. Impregnated coals were used without being dried and contained 11.9 wt% moisture.

Activity tests were carried out in a 50-cc micro autoclave at 440°C and 1350 psig for 30 minutes. The reactor was equipped with a thermocouple, and connected to pressure transducer for monitoring temperature and pressure during the reaction. Experiments were duplicated at least 2 times to confirm the reproducibility. In a typical experiment, 1.75 g of 524°C-distillate (Wilsonville Run 258 period B), 2.8 g of deashed resid (Wilsonville Run 258 period A) and 2.45 g of metals impregnated coal were added to the reactor and pressurized with H_2S/H_2 (3 wt% H_2S in H_2). The reactor was submerged in a fluidized sand bath and agitated continuously at the rate of 400 cycles per minute at the specified temperature. After quenching, solid and liquid products were removed from the reactor using tetrahydrofuran (THF) and the mixture was extracted in a Soxhlet extractor overnight. The THF insoluble fraction was dried in a vacuum oven and weighed. The soluble fraction was distilled under vacuum (modified ASTM D-1160-87) to atmospheric equivalent end point of 524°C to determine the resid and coal conversions.

$$\text{Resid Conv} = \left(1 - \frac{(\text{IOM} + 524\,^{\circ}\text{C}^{+}\ \text{Resid (af)})_{\text{Products}}}{(\text{coal (rnaf)})_{\text{Feed}}}\right) \times 100$$

RESULTS AND DISCUSSION

Molybdenum compounds are widely used in coal liquefaction because of their hydrogenation activity and the case which they can be dispersed in the reaction system or impregnated onto coal. Sulfur or sulfided catalysts are generally added to the reaction mixture to convert them to the sulfided forms under reaction conditions.[15]

PMA was sulfided at elevated temperatures in order to understand the form of the catalyst derived from the precursors.[16] Elemental analysis of presulfided materials are given in Table 2. The activities of these materials were determined by adding these particulate solids to the reaction mixture and by impregnating them from an aqueous solution onto coal. The activity resulting from adding the particulate presulfided materials directly to the reaction mixture was much less than observed by impregnating untreated PMA onto coal (Figure 1). THF conversions decreased as the treatment temperatures increased. They were about 62% for materials treated between 125 and 200°C and decreased to about 57% for materials prepared at 300 and 450 °C. The THF conversion for untreated particulate PMA was 80.7%. Resid conversions (maf) for the sulfided materials varied between 43-48% while untreated particulate PMA gave 42.7%.

Good dispersion of the catalyst on the surface of the coal particles improves conversion by increasing the amount of active surface area in the reaction phase. An approach to achieving catalyst dispersion is to employ a solvent for dispersing the catalyst. Unfortunately, liquefaction catalysts such as pyrhotite, pyrite and molybdenum sulfide are insoluble in all common solvents. Although the soluble precursors may not be catalytically active they transform into active catalysts at elevated temperatures. As an example, the water soluble PMA, which decomposes to intermediate molybdenum oxysulfides at typical liquefaction temperatures, has been used as a precursor to obtain a good dispersion.[7]

Because of the partial solubility of the sulfided PMA materials in water, they were impregnated onto coal from aqueous solutions. The activity of the impregnated coals was higher than observed for the particulate addition of the sulfided materials but not as high as observed for PMA impregnated coal (Figure 2). Both THF and resid conversions were higher for those materials

prepared at the lower temperatures. THF conversion for PMA125 is only slightly less than the PMA impregnated coal, i.e., 89.2 and 92.3%, respectively. Resid conversions varied from 65 to 42% with PMA125 and PMA150 giving essentially the same resid conversion as PMA impregnated coal (64.5%). Higher treatment temperatures resulted in a significant decrease in resid conversions. Although the data indicate that the sulfided materials prepared at lower temperatures are as active as PMA, they do not show any improvement over impregnated untreated PMA.

Activities of metal impregnated coals were compared in Figure 3. Nickel phosphomolybdate (NiPM) and cobalt phosphomolybdate (CoPM) gave almost the same average THF conversions, which was somewhat higher than the average conversion for potassium phosphomolybdate (KPM). The THF conversion for PMA (92.3%) was slightly higher than the Co and Ni salts. The standard deviations for the salts showed significant overlap in the values suggesting no significant difference in these conversions, although the PMA value appears to have statistical significance. The resid conversion of NiPM was higher than the Co and K salts although standard deviations again indicated significant overlap in the values. The NiPM resid conversion is also greater than observed for the PMA impregnated coal (64.5%).

CONCLUSION

Sulfided PMA materials did not show higher catalytic activity than PMA when added directly to the reaction media, and gave lower THF conversion than the non-catalyzed thermal case. The activities of impregnated sulfided PMA materials prepared at 125 and 150°C was comparable to PMA. Conversions decreased for sulfided materials produced at higher temperatures. Apparently, materials prepared at the higher temperatures are not as well dispersed due to their decreasing solubility in water. None of the bimetallic phosphomolybdates (CoPM, NiPM and KPM) improved THF conversion, however resid conversion was higher for NiPM than for the other bimetallic salts or untreated PMA. Resid conversion for CoPM was comparable PMA.

ACKNOWLEDGEMENT

This project was supported by the U.S. Energy of Department under the contract number DE-AC22-91PC91040.

REFERENCES

1. Gates, B. C., Katzer, J. R. and Schuit, G. C. S. in 'Chemistry of Catalytic Processes' McGraw-Hill, New York, 1979, 411
2. Garg, D. and Givens, E. N., Fuel Processing Technology, 1984, 8, 123
3. Demirel, B. and Givens, E. N. Liquefaction of Wyodak coal with phosphomolybdic acid, Submitted to Energy Fuels, 1997
4. Lopez, J., McKinney, J. D. and Pasek, E. A., Heavy oil processing, U. S. Patent 4,557,821, Dec. 10, 1985
5. Hisrchon, A. S. and Wilson, R. B. Jr, Fuel, 1992, 71, 1025.
6. Derbyshire, F. J., Catalysis in Coal Liquefaction, IEACR/08, IEA Coal Research, London, 1988.
7. Herrick, D. E., Tierney, J. W., Wender, I. Huffman, G. P. and Higgins, F. E. Energy Fuels, 1990, 4, 231
8. Song, C., Parfitt, D. S. and Schobert, H. H., Energy Fuels, 1994, 8, 313
9. Okura, T., Mizuno, N. and Mosono, M, in Advances in Catalysis, Eds. D. D. Eley, W. O. Haag, B. C. Gates, Academic Press, Inc., San Diego, CA, 1996, Vol. 41, 113
10. Givens, E. N., Anderson, R., Demirel, B., Derbyshire, F., van Woert, H., Zhan, X., Winschel, R., Robbins, G., Burke, F., Peluso, M., Hu, J and Lee, T. Bench-scale testing of advanced concepts for direct coal liquefaction:
evaluation of dispersed Mo catalysts, paper presented to the 1997 Coal Liquefaction and Solid Fuels Contractors Review Conference, Pittsburgh, PA, Sept. 4, 1997
11. Southern Electric International, Inc., Run 262 with Black Thunder mine subbituminous coal and dispersed molybdenum catalysts, U. S. DOE Report, DOE/PC/90033-22, Wilsonville, AL, 1992
12. Southern Electric International, Inc., Run 263 with Black Thunder mine subbituminous coal and dispersed molybdenum catalysts, U. S. DOE Report, DOE/PC/90033-23, Wilsonville, AL, 1992
13. Chianelli, R. R. Daage, M., Halbert, T. R., Ho, T. C. and Stiefel, E. I., Prepr.-Am. Chem. Soc., Div. Petr. Chem., 1990, 35(2), 227
14. Eccless, R. M. and de Vaux, G. R., Chem. Eng. Progr. May 1981, 80
15. Rahimi, P. M., Fouda, S. A. and Kelly, J. F., Prepr.-Am. Chem. Soc., Div. Fuel Chem., 1986, 31(4), 192
16. Demirel, B. and Givens, E. N., Transformation of phosphomolybdic acid into an active catalyst for coal liquefaction, Submitted to Catalysis Today, 1997

Table 1. Analysis of Wyodak Black Thunder Coal.

Proximate Analysis	w%	Ultimate Analysis	w%(dry)	Sulfur Analysis	w%
Moisture	8.89	Carbon	70.62	Total	1.94
Ash	5.76	Hydrogen	5.03	Pyritic	0.80
Volatile matter	39.88	Nitrogen	1.13	Sulfate	0.80
Fixed carbon	45.47	Sulfur	0.52	Organic	0.34
		Oxygen (diff)	16.38		
		Ash	6.32		
		Ash, SO_3-free	5.47		

Table 2. Elemental analysis of PMA and the sulfided samples.
S/Mo atomic ratio in feed = 12.3
Sulfidation time = 4 h

	Composition, wt%				Formula
	P	Mo	S	O (diff)[a]	$P_xMo_{12}S_yO_z$
PMA	3.52	49.65	0.00	46.83[b]	$H_{45.6}P_{2.6}Mo_{12}O_{65.8}$ $(H_3PMo_{12}O_{40}\cdot 20H_2O)$
PMA125	4.26	59.50	4.95	31.29	$P_{2.7}Mo_{12}S_{3.0}O_{37.8}$
PMA150	4.57	60.97	5.40	29.06	$P_{2.8}Mo_{12}S_{3.2}O_{34.3}$
PMA200	4.74	65.60	4.79	24.87	$P_{2.7}Mo_{12}S_{2.6}O_{27.3}$
PMA300	5.48	66.49	4.93	23.10	$P_{3.1}Mo_{12}S_{2.7}O_{25.0}$
PMA450	5.31	70.11	20.60	3.98	$P_{2.8}Mo_{12}S_{10.6}O_{4.1}$

a. Difference includes oxygen and hydrogen b. Includes 3 wt% hydrogen

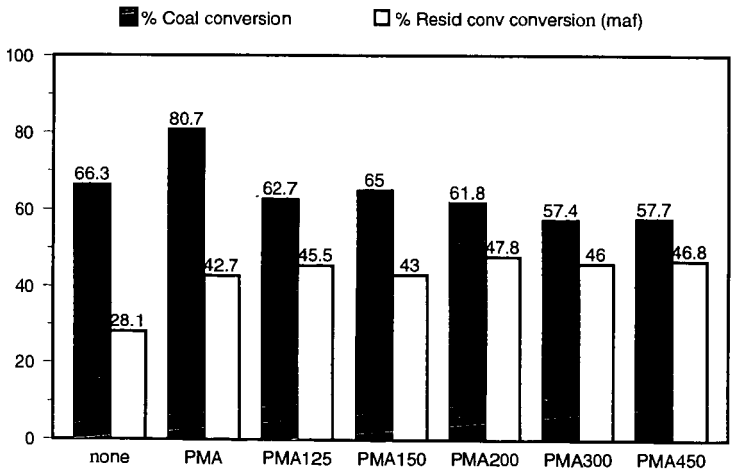

Figure 1. Activity tests from direct addition of PMA and the sulfided PMA materials to reaction mixture.

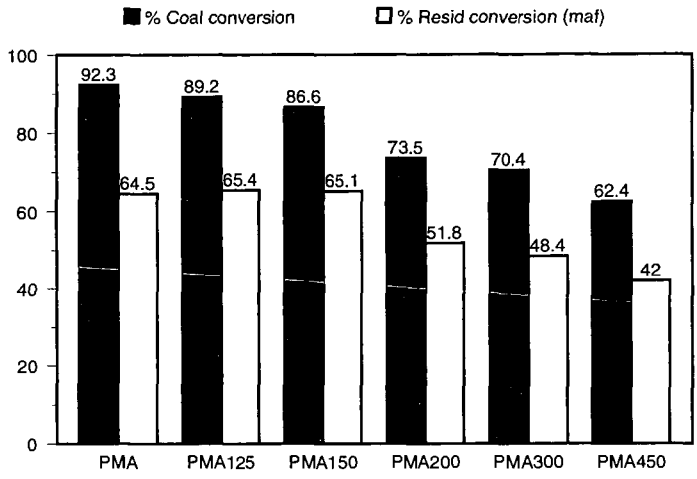

Figure 2. Activities of coal impregnated with PMA and the sulfided PMA materials.

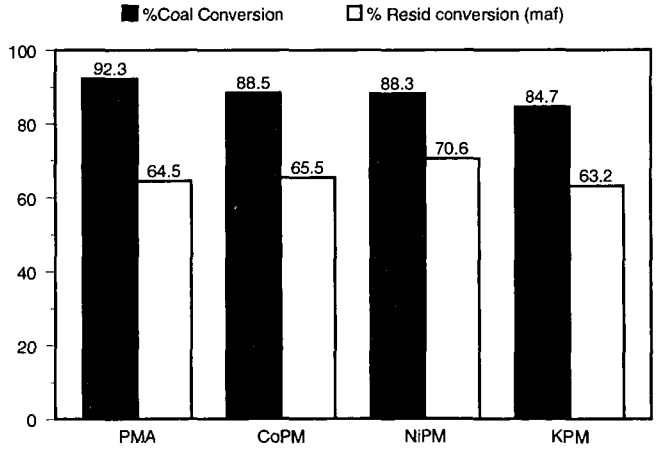

Figure 3. Activities of coal impregnated with PMA, CoPM, NiPM and KPM.

COAL CONVERSION TECHNOLOGIES ON THE NEW SUNSHINE PROGRAM IN JAPAN

Akira Sugawara[1], Shigeru Kurosawa[1], Hiroaki Hatori[1], Kazufumi Saito[1], Yasuhide Yamada[1], Makoto Sugihara[1], Sadao Wasaka[2] Haruhiko Yoshida[2], Tomoyuki Seo[2], Takakazu Susuki[2], Mikiya Inoguchi[2] and Makoto Sohnai[2]

1) New Sunshine Program Promotion Headquarters, Agency of Industrial Science and Technology (AIST), Ministry of International Trade and Industry (MITI), 1-3-1 Kasumigaseki, Chiyoda, Tokyo 100, Japan.
2) Clean Coal Technology Center (CCTC), New Energy and Industrial Technology Development Organization (NEDO), 1-1-3 Higashi-Ikebukuro, Toshima 170, Japan.

Keywords: New Sunshine Program, coal gasification technologies, coal liquefaction technologies

ABSTRACT

Agency of Industrial Science and Technology (AIST) has been conducting R&D on coal conversion technologies in Japan. New Energy and Industrial Technology Development Organization (NEDO) has been carrying out some R&D projects on coal conversion technologies as a part of "New Sunshine Program" lead by AIST. Coal gasification technologies and liquefaction technologies are major concern for NEDO and the overview of the R&D projects updated is presented in this paper. In addition, a new project on coal hydrogasification technology are also outlined.

INTRODUCTION

AIST initiated the "**Sunshine Project**" to develop technologies associated with new energy in 1974 after the first oil crisis in 1973. In 1978, the "**Moonlight Project**" for energy conversion was started followed by the R&D Project on environmental technology in 1989. These projects were consolidated into the "**New Sunshine Program**" in 1993, aiming to develop the innovative technologies that could support the sustainable economical growth while solving energy and environmental issues. The R&D schedules of coal conversion technologies in the New Sunshine Program are shown in Table 1 [1, 2].

Both R&D of gasification and liquefaction started under the "**Sunshine Project**" have a long history (from 1974 for gasification and 1976 for liquefaction). By now, an integrated coal gasification combined cycle (IGCC) pilot plant with a capacity of 200 t/d demonstrated its capability in giving high thermal efficiency and environmental acceptability, while the operation of an 150 t/d coal liquefaction pilot plant is being carried out. Basic researches on coal liquefaction have been constantly conducted at national institutes and universities. The R&D of refining coal-derived liquids is still on the stage of laboratory scale. The project on coal hydrogasification started in 1996. This process produces methane directly from coal and hydrogen with BTX as co-products and is expected to have high efficiency, coal adaptability, environmental adaptability and cost competitiveness. The final target is to commercialize in 2010's [3].

Coal gasification technologies

In 1986, operation of a hybrid gasification pilot plant which employed a pressurized fluidized-bed gasifier feeding coal and heavy oil mixture was finished. The project demonstrated production of high calorific gas containing a high concentration of methane together with high energy efficiency comparable to other processes. Following the results of the hybrid gasification, a coal-based hydrogen production project (HYCOL) started in 1984. Pulverized coal is gasified into hydrogen and carbon monoxide in a gasifier under the condition of a pressure of 30atm and a temperature 1500℃ or above. Gasification is carried out in oxygen-blow one chamber and two-step spiral flow system. High purity hydrogen is then produced after processing carbon monoxide with shift-reaction and other processes. A pilot plant with a capacity of 20 t/d for

HYCOL was constructed in 1990. The operating research has been completed in 1993.

The history of R&D of IGCC is follows: In 1996, the 200 t/d pilot plant was disassembled after 5 years' operation test, and all data obtained is accumulated to discuss the possibility of construction of a demonstration plant. The organization which lead the R&D was reunified and is now working for the feasibility study of the demonstration plant. The study will continue for two years to conclude whether we should go further or not.

A feasibility study was started on coal hydrogasification technology that employs hydrogen as the gasifying agent and produces high calorific gases with high concentrations of methane in FY1990. A elemental study started in 1996.

Coal liquefaction technologies

There are two streams for R&D of coal liquefaction in Japan. One is the project for brown coal liquefaction which was conducted in Victoria, Australia from 1981 to 1990. The present work is to improve the liquefaction process to make it feasible for a commercial use [4]. The other is on bituminous coal liquefaction of which process is named as "**NEDOL Process**". After 4 years of construction, the pilot plant has started its official operation [5-7]. Some results of the operation will be presented at the ACS meeting. Seven runs of the plant are scheduled over two years and "**Technology Package of the NEDOL Process**" will be documented afterward. "**NEDOL Process**" is also being verified at process supporting unit (PSU) facilities in Kimitsu [8]. It still takes one year or so to start the operation of a 40 b/d PDU, which is now under construction to demonstrate the refining of coal-derived liquids so that it meets the requirements of petroleum market. Meanwhile, basic studies are pursuing the optimization of the hydrotreatment of coal-derived liquids in and the prevention of plugging during refining. We focus on the NEDOL process for coal liquefaction in this presentation.

EXPERIMENTAL

NEDO has been promoting a development of a coal liquefaction technology, since 1980, under "New Sunshine Program" and developed the "NEDOL" process that can attain high light oil yields under relatively mild conditions. The NEDOL process was realized in the 1 t/d PSU based on research and development work through autoclaves, bench scale plants and PDU scale plants. In the PSU, comprehensive experiments have been conducted with several kinds of coals and operating conditions and lots of significant data have been acquired. In parallel with the research and development in the PSU, the 150 t/d pilot plant (PP) was constructed for collecting scale-up data to demonstration and commercial plants. The construction of the PP was finished on July, 1996 and the operation was commenced.

The NEDOL process, shown in Figure 1, consists of four primary units, such as coal preparation unit, coal liquefaction unit, solvent distillation unit and solvent hydrogenation unit. The NEDOL process can attain high oil yield even in relatively low severity condition as shown in Table 2. It has been concluded that ultra fine iron catalyst and hydrogenated solvent bring this high oil yield. In the PSU operation, several kinds of coals have been liquefied and the efficacy of the NEDOL process has been demonstrated. Based on the results of the PSU, a standard coal for the PP operation was determined. Table 3 indicates the analytical data of the standard coal for the PP. The operation of the PP has been conducted in the conditions shown in Table 2 and with the standard coal shown in Table 3 and the results were compared with the results of the PSU conducted in the same conditions and with the same coal.

RESULTS AND DISCUSSION

The results of the PP operation were compared with the results of the PSU operation and the comparison result is indicated in Table 4. Although the results of the PP are not results on 100 % plant load, yields of the PP have a good correlation with the results of the PSU. The yields of the 80 % load in the PP imply that the yields of 100 % load in the PP can attain same yields as the PSU on the same liquefaction conditions. This indicates that scale up data for larger plant will be able to be acquired in comparison of the data between the PSU and PP.

REFERENCES

1. S. Kurosawa, in *Guidebook of New Energy Technologies* (Y. Adachi ed.), Ohm Press, Tokyo (1997) chapter 3.
2. S. Kurosawa, K. Saito and A. Sugawara, *Proceedings of 14th Japan-US Joint Technical Meeting on Coal Liquefaction & 9th Materials for Coal Liquefaction*, **1997**, 1-7.
3. T. Seo and K. Itoh, *ibid*, **1997**, 159-165.
4. K. Shimasaki, T. Okui, T. Kaneko, N. Komatsu and Y. Kageyama, *ibid*, **1997**, 55-65.
5. H. Yoshida, Z. Kamio and S. Wasaka, *ibid*, **1997**, 8-20.
6. Y. Namiki, H. Ishibashi, T. Takagi and M. Kobayashi, *ibid*, **1997**, 45-54.
7. H. Matsubara, M. Uchiyama, M. Miyake and T. Nishibayashi, *ibid*, **1997**, 150-158.
8. H. Kakebayashi, Y. Nogami, K. Inokuchi, M. Mochizuki and K. Imada, *ibid*, **1997**, 55-63.

Table 1. R&D schedule of coal conversion technologies on the New Sunshine Program

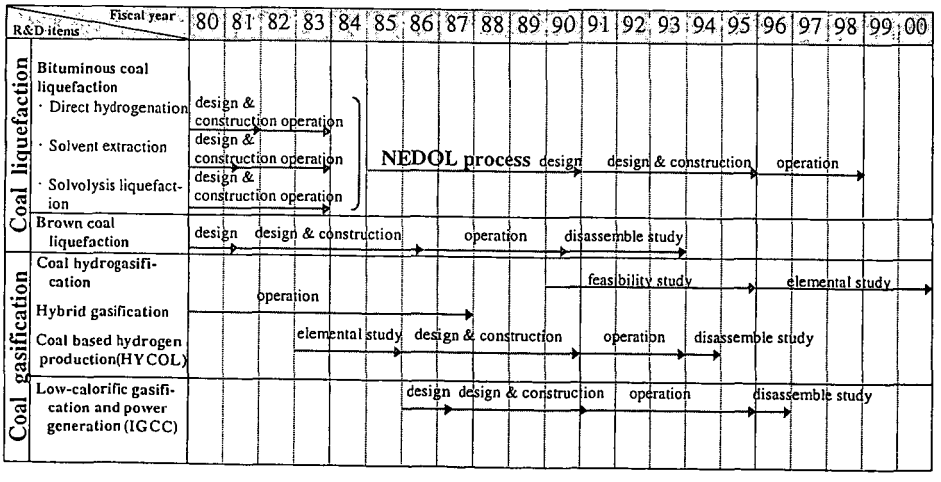

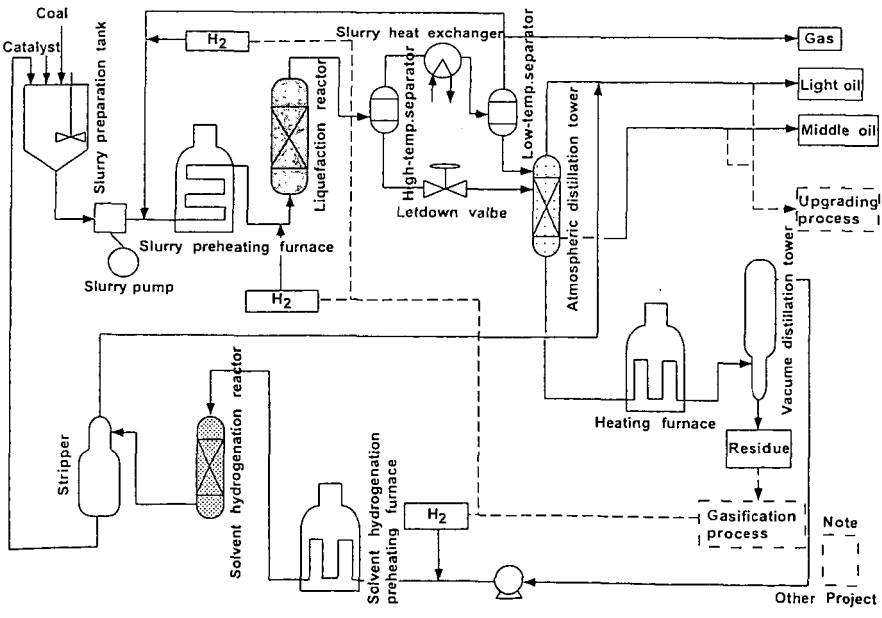

Figure 1. Diagram of NEDOL Process

Table 2. Typical liquefaction conditions

	Typical condition
Temperature	430 - 465 ℃
Pressure	150 - 190 kg/cm^{2}G
Catalyst	Ultra fine iron sulfide 2 - 3 wt%
Slurry concentration	40 - 50 wt% (dry coal)
Slurry residence time	1 hr
Gas/slurry ratio	500 - 700 Nm^3/t
Hydrogen conc. in recycle gas	85 vol %

Table 3. Typical coal analytical data for the PP operation

Proximate analysis (wt %)		Ultimate analysis (wt % daf)	
Moisture	3.8	C	76.4
Volatile matter	47.4	H	5.8
Fixed carbon	47.7	N	1.8
Ash	4.9	TS	0.3
		O	15.7

Table 4. Comparison of the yields between the PP and the PSU

	150 t/d PP		1 t/d PSU		
Plant load [%]	60	80	100	100	100
Temperature [℃]	450	450	450	465	465
Pressure [kg/cm^{2}G]	170	170	170	170	190
G/L [Nm^3/t]	700	700	700	700	900
Catalyst addition [wt %]	3	3	3	3	4
Residence time [hr]	1.67	1.25	1.0	1.0	1.0
Yields [wt % daf]					
Water	12	11	10.8	11.5	11.4
Gas	18	17	19.7	25.5	26.5
Oil	54	52	51.7	55.5	59.4
Residue	22	26	23.3	14.4	9.9
H_2 consumption	5.9	5.4	5.5	6.9	7.2
Total	105.9	105.4	105.5	106.9	107.2

CONVERSION OF LOW-RANK COALS AND LIGNINS TO PHENOLIC PRODUCTS BY CATALYTIC HYDROGENOLYSIS IN AQUEOUS BASE

Caroline E. Burgess*, J. Michael Robinson*, Kevin O'Hara, Jeremy Rashidi, Ernesto H. Sanchez, and Paul F. Greenwood†, The University of Texas of the Permian Basin, 4901 E. University Blvd., Dept. of Chemistry, Odessa, TX 79762, †Commonwealth Scientific and Industrial Research Organisation (CSIRO), Division of Petroleum Resources and Australian Petroleum Cooperative Research Centre (APCRC), PO Box 136, North Ryde, NSW, 2113, Australia.

KEYWORDS: low-rank coal, lignin, base hydrogenolysis, proton nmr, pyrolysis-gc/ms

INTRODUCTION

Direct methods of coal conversion to liquids have been studied in depth since the initial experiments were conducted in the late 19th century; however, the identification of methods to lower reaction severity has been slow. Earlier work, as discussed by Schobert,[1] successfully achieved conversion to liquids using very high reaction temperatures and hydrogen pressures (>450 °C and >5000 psi). Reactions at somewhat lower severity (i.e., lower temperature and pressure) were achieved by the use of various catalysts and solvents. These catalyzed reactions can occur at ~ 400-425 °C and hydrogen pressures (initial) of ~900-1000 psi (2500-3000 psi at temperature) in 30-60 minutes. Even under these reaction conditions, economic viability in today's petroleum market still has not been achieved. Researchers continue to seek avenues to further reduce reaction severity.

Some research has shown that for lower rank coals, particularly lignites, reaction severity can be reduced.[2-6] It is thought that the mechanism that drives coal reactions in the 350-450 °C range is the thermolysis of C-C bonds and particularly C-O bonds; lower rank coals contain more oxygen functionality, and therefore, these coals tend to react at the lower end of this temperature region because C-O bonds are weaker than C-C bonds. Derbyshire, *et al.*[2,3] and Jackson, *et al.*[7,8] have achieved conversions of ~ 90 % for low rank coals when using various hydrogenation catalysts (Ni/Mo) at lower reaction temperatures of ~ 400 °C and reaction times of 30-60 min. Understanding the complexity of the macromolecular structure and the mechanisms of liquefaction of low-rank coals is important in order to optimize the production of valuable liquid products. The main limitation to lowering the reaction severity of coal liquefaction processes is identifying a reaction method that is not completely dependent on the thermolysis of C-C and C-O bonds for depolymerization.[2-6] Lewis acids (e.g., $SnCl_2$, $ZnCl_2$) do accomplish coal cleavage at slightly lower temperatures (~ 350 °C and 1 h reaction time).[9-14] Unfortunately, large quantities of catalyst must be used and the chlorides in these compounds cause significant reactor corrosion.[9-14]

The present primary energy project at UTPB relates to the reductive depolymerization of biomass polysaccharides to C_5 and C_6 hydrocarbons.[15] Since coal essentially represents a degraded biomass, it is envisioned that the reactions used to fractionate biomass into polyols and lignins, and to further react the latter, might be equally successful when applied to low rank coals. The reaction conditions initially employed were based on Russian reports of sequential catalytic hydrogenolyses in acid and base. This was done to first convert carbohydrates to C_5 and C_6 polyols at 185 °C and 700 psi (initial) and then lignin into phenolic materials at 280-320 °C and 700-900 psi hydrogen (initial), respectively.[16] Because of the very high conversions of raw biomass by the "biomass-to-polyol" process and because of some similarities in the structures of lignin and lignites, we expected similar sequential reactions could have a significant effect on the conversion of low rank coals to liquids. We chose to focus on the base hydrogenolysis omitting a prior acid hydrogenolysis, as this step had the greatest effect on the lignin in biomass.[16] This paper focuses on reacting DECS-1 coal and lignin at 240, 270, and 300 °C, 700 psi (initial) for 6 h in NaOH solution and subsequent characterization of the products by solution NMR and pyrolysis-GC/MS.

EXPERIMENTAL

The coal was obtained from the Pennsylvania State University Coal Sample Bank (COPL), denoted by DECS-1. The coal rank of DECS-1 as determined by the COPL is subbituminous C. Elemental analysis for the coal and the solids (acids) from the NaOH-solubles was done by Galbraith. For the coal, the elemental analysis was carbon % (C) - 58.7 , hydrogen % (H) - 4.7 , nitrogen % (N) - 1.0, sulfur % (S) - 1.2, and oxygen % (O) (by difference) - 18.1. The ash content is 16.3 %. The lignin used is a commercial hydrolytic lignin obtained from Aldrich Chemical Company.

Reactions of coal with NaOH were carried out in a 1-gallon Parr stirred autoclave. The reactions were run at 240, 270, and ~300 °C under 700 psi hydrogen (initial) atmosphere using a carbon-supported ruthenium catalyst (Ru/C) purchased from Aldrich (5 % Ru). About 20 g of coal or lignin was loaded with 2 g of catalyst (Ru/C) and 2 L of 1.5 % (wt) NaOH. Reactions were run at the designated temperature for ~6 h although initial heating and final cooling of the reactor could take

several hours depending on the final temperature. The contents of the reactor were filtered and the solid washed with water to remove all of the base (until pH ~7).

Figures 1 and 2 are schematics of the procedure used to extract all of the soluble organic products resulting from the reaction. Neutral oils were obtained by washing the initial solids and aqueous layer (including rinse water) with methylene chloride CH_2Cl_2 (see Figure 1). The NaOH-solubles were acidified with concentrated H_2SO_4 to pH ~2 and heated to ~ 80°C to promote coagulation and filterability; the precipitated solids (acids) were then filtered (see Figure 2). All the solids from the initial filtration procedure and the acidic solids were extracted (using sonication) with CH_2Cl_2 followed by extraction (using sonication) with tetrahydrofuran (THF). The percent conversion was determined from the difference between the initial weight of the dry coal and catalyst and the final dry weight of solid residue and catalyst, per initial amounts.

All organic products were analyzed by ^1H and ^{13}C solution NMR. Samples were dissolved/filtered in chloroform ($CDCl_3$) or dimethyl sulfoxide (DMSO-d_6) and spectra obtained by a Bruker 250 MHz Avance DPX NMR.

Pyrolysis-GC/MS was performed with a Hewlett Packard (HP) 18580A pyroprobe interfaced to a (HP 5890/5970) GC/MS. Chromatography was carried out on a 25 m x 0.22 mm i.d. x 1.0 µm film thickness column coated with a BPX5 phase (modified to 5% phenyl siloxane). The GC oven temperature was programmed to increase from 40°C, initially held for 2 min., at a rate of 4° C/min to 300 °C (maintained for a further 30 min). The samples pyrolyzed were the DECS-1 raw coal and the solids (acids). On pyrolysis at 850 °C about 55-60 % of both samples was vaporized.

RESULTS AND DISCUSSION

Percent of Coal Extracted

Figure 1 is a schematic of the initial treatment of reactor contents, whilst Table 1 shows the total conversion and the material balance information. For all reactions, > 90% of the organic matter from DECS-1 was extracted and/or dissolved. About 85-95 % of the coal was extracted into the aqueous base solution. As the temperature increases, then the amount of coal extracted into the aqueous base slightly decreases. For reactions at 240 and 270 °C, the other materials extracted from the remaining catalyst/organic/ash residue (CH_2Cl_2- and THF-soluble compounds) amounted to about 4-5 %. However, at 300 °C, the CH_2Cl_2- and THF-soluble compounds increase to 15 %. This suggests the reaction chemistry is indeed changing with increasing temperature and this may account for the higher proportion of neutral compounds and less of the acidic compounds at higher temperature, i.e., more thermolytic reduction (see Table 1).

Figure 2 is a schematic of the product work-up of the NaOH-solubles. Table 2 shows a breakdown of the product into fractions. The NaOH-solubles were acidified with H_2SO_4 to a pH of ~2. The solution then formed a dark brown precipitate that was briefly digested (to coagulate solids) at 80 °C before filtering. The remaining filtrate was a clear, pale yellow solution with a strong phenolic odor. The 240 °C reaction had the highest percent NaOH-solubles, 95 %, with 49.7% solids and 45.8 % (determined by difference) of material either left in solution or gaseous reaction products. At 270 °C, a lower amount of coal was solubilized by the base, 87.5 %, but a much greater proportion, 72.7 %, were solids. At 300 °C, only 84.5 % of the coal was solubilized by the base, but only 34.9 % precipitated out. Since the majority of the coal was extracted into the base solution, determining the product character of this fraction is important in understanding the reaction chemistry. However, elucidation of the composition of both the solid and water-soluble materials has proved to be complicated and is to-date not complete. Clearly, phenols (A2 acids) and carboxylic acids (A1 acids) would be expected to be dissolved into aqueous base but polyfunctional compounds remain in the water layer even after neutralization. The variability in the ratio of precipitated acids versus water-soluble compounds is also being addressed. Results from the present methods of analysis are outlined below.

NaOH-soluble Products

Most of the work completed has been done on the 240 °C reaction solids from the acidification of the base solution. The elemental analysis of the NaOH-soluble solids from the 240 °C reaction is 64.7 % C, 5.4 % H, 1.4 % N, 1.2 % S, 1.1 % ash, and 26.2 % O (by difference). The H/C ratio is 1.0 and the O/C ratio is 0.3, compared to the coal H/C, 0.98 and the O/C, 0.23. The H/C of the product is essentially the same as the coal whilst the O/C ratio is significantly higher than that of the coal, suggesting at 240 °C hydrolysis mostly accounts for the strong oxygen increase and not much hydrogenation has occurred. In fact, more hydrogen is consumed at higher temperature.

None of the solids (acids) proved soluble in CH_2Cl_2 or other less polar solvents. The material is therefore thought to be very polar and possibly also of very high molecular weight, albeit a reduction of the large macromolecules in the coal to smaller oligomers is anticipated. Solution GC/MS analysis revealed little molecular information from the solid NaOH-soluble product. This material did prove soluble to varying degrees in THF, DMSO, and pyridine. Solution ^1H NMR was obtained using the

polar solvent DMSO-d_6. The ^{1}H NMR is shown in Figure 3 (a). The main feature of the proton NMR is the noticeable -OH or -CH-O- functionality. Unfortunately, the concentration of this solution was not high enough for ^{13}C NMR detection.

Figure 3 (b) and (c) shows the pyrolysis-GC/MS of DECS-1 coal and of the solid product from the NaOH-solubles. Significantly fewer aliphatic and large aromatic compounds are detected from the NaOH- solubles than from the parent coal. These compounds may be present in a different fraction obtained by extraction with other solvents. The compounds in the pyrolysis-GC/MS of the NaOH-soluble product have been identified as predominantly alkylated aromatic compounds with or without -OH functionality. Work will be continued to more accurately determine the structure and/or molecular weight of the NaOH-soluble solid products and will likely include direct MS of the solids with chemical ionization and gel chromatography for polymer size distributions.

The liquids that remain in the water have not yet been completely isolated. Following exhaustive extraction with CH_2Cl_2, some color and odor remained in the water indicating that not all of the organic was extracted. Work continues to more efficiently extract the compounds from the water so as to complete the material balance. Once released these products will also be analyzed by GC/MS. Organic acids and alcohols will first be derivatized to less polar and more volatile esters. Several derivative methods are being screened, e.g., acetylation according to Thring *et al.*[17]

Comparative Reactions

As stated earlier, these reactions of coal were suggested as an extension of lignin reactions in the literature, so a comparative reaction with lignin was done under these conditions. In our case, however, as noted in Tables 1 and 2, less lignin reacted than the coal reaction at 240 °C. Lignin reactions are higher temperatures are also planned.

The amount of coal extracted under these reaction conditions is remarkable as most reactions at these temperatures produce little if any product. For example, Garcia and Schobert[18] showed with coals of high organic sulfur content that about 8.8 % THF-soluble material could be extracted at 250 °C. This increases up to ~50 % at 325-350 °C when using a molybdenum catalyst in a hydrogen atmosphere (the reactor used in this case was a "tubing bomb" type and caution in comparing this to a stirred autoclave must be noted). Most coal liquefaction reactions produce high conversions at 400-450 °C, and most of the product is composed of lighter molecular weight materials than produced in the reactions reported here. One research group, Hulston *et al.*,[7,8] used NaOH or $NaAlO_2$ combined with a hydrogenation catalyst (Ni/Mo) at 365 °C to produce significantly higher conversions to CH_2Cl_2-soluble products than when using the Ni/Mo catalyst alone, but the increase in conversion is noted with low-rank coals only. It is also expected for our reaction conditions that coals of rank higher than subbituminous will not convert as easily because of the significantly lower oxygen content of bituminous and anthracite coals. While the ultimate goal of high conversion efficiency of coal into small phenolic liquids has not yet been achieved, a significant amount of liquefaction and a remarkably high conversion to more soluble/extractable products (with little mineral matter left in the organic material) has been realized. Further analytical data are required to show the extent of conversion to small (liquid) molecules.

REFERENCES

1. Schobert, H.H., *Coal: The Energy Source of the Past and Future*, Amer. Chem. Soc., Washington, DC, **1987**, Ch. 11, p 235.
2. Derbyshire, F. J. *Catalysis in Coal Liquefaction: New Directions for Research,* IEA Report CR/08, IEA Coal Research, London, **1988**, p 16.
3. Derbyshire, F.J. and Stansberry, P.G., *Fuel*, **1987**, *66*, 1741.
4. Schobert, H.H., *Lignites of North America*, Elsevier: Amsterdam, **1995**, Ch. 4, pp 139-217.
5. Snape, C.E., Derbyshire, F.J., and Stephens, H.P., *Fuel Processing Technology*, **1990**, *24*, 119.
6. Solomon, P.R., Serio, M.A., Deshpande, G.V., Kroo,E., Schobert, H.H., and Burgess, C.E., "Chemistry of Catalytic Preliquefaction," in *Coal Science II*, Ed. H.H. Schobert, K.D. Bartle, and Lynch, L.J., American Chemical Society Symposium Series 461, Washington, DC, **1991**, Ch. 15, p 193.
7. Hulston, C.K.J., Redlich, P.J., Jackson, .W.R., Larkins, F.P., and Marshall, M., *Fuel*, **1996**, *75*, 1387.
8. Burgess, C.E., Hulston, C.K.J., Redlich, P.J., Marshall, M., and Jackson, W.R., *Amer. Chem. Soc. Fuel Chem Div. Preprints*, **1995**, *40* (3), 564.
9. Schobert, H.H., *The Chemistry of Hydrocarbon Fuels*, Butterworths, London, **1990**, pp 224-226.
10. Olah, G.A., Bruce, M.R., Edelson, E.H., and Husain, A., *Fuel*, **1984**, *63*, 1130.
11. Olah, G.A. and Husain, A., *Fuel*, **1984**, *63*, 1427.
12. Song, C., Nomura, M., and Miyake, M., *Fuel*, **1986**, *65*, 922.

13. Song, C. and Nomura, M., *Fuel*, **1987**, *66*,1225.
14. Song, C. and Nomura, M., *Bull. Chem. Soc. Japan*, **1986**, *59*, 3643.
15. a) Robinson, J.M., *Amer. Chem. Soc. Fuel Chem Div. Preprints*, **1995**, *40* (3), 729,
b) Robinson, J.M., Burgess, C.E., Mandal, H.D., Brasher, C.D., O'Hara, K.O., and Holland, P., *Amer. Chem. Soc. Fuel Chem Div. Preprints*, **1996**, *41* (3), 1090,
c) Robinson, J.M., *U.S. Patent* **#5,516,960**, May 14, 1996.
16. Sharkov, V.I., *Angew. Chem. I.E.E.*, **1963**, *2* (8), 405 and reference therein.
17. Thring, R.W., Chornet, E. and Overend, R.P., *J. of Chromatography*, **1989**, *467*, 441.
18. Garcia, A.B. and Schobert, H.H., "Liquefaction Behavior of High-Sulfur Lignites" in *Coal Science II*, Ed. H.H. Schobert, K.D. Bartle, and Lynch, L.J., American Chemical Society Symposium Series 461, Washington, DC, **1991**, Ch. 16, p 213.

Table 1: Conversion information for reactions of DECS-1 and lignin.

Temp °C[a]	Feed	Reactor Load (g)	% NaOH-solubles[b]	% Other[c]	Total	Psi
240	DECS-1	20	95.5	4.7	100	700
270	DECS-1	20	87.5	5.7	93.4	700
306	DECS-1	20	84.2	15.8	100	500
240	Lignin	20	78.9	9.0	87.9	700

a All reactions were 6 h at temperature shown; does not include ramp times.
b Includes any gas that may have been generated because this is determined by difference.
c Methylene chloride-solubles + tetrahydrofuran-solubles.

Table 2: Yield information for the NaOH-soluble portion of the coal. This fraction was acidified with H_2SO_4 to a pH of about 2 and solids filtered out (see Figure 2 for flow diagram).

Temp °C[a]	Feed	% NaOH-solubles[b]	% Solids	% H_2O-solubles[c]	Total
240	DECS-1	95.5	49.7	45.8	100
270	DECS-1	87.5	72.7	14.8	93.4
306	DECS-1	84.2	34.9	49.3	100
240	Lignin	78.9	31.5	47.4	87.9

a All reactions were 6 h at temperature shown; does not include ramp times.
b Includes any gas that may have been generated because this is determined by difference.
c H_2O-solubles are the compounds that remain in solution but also includes any gas that may have been generated.

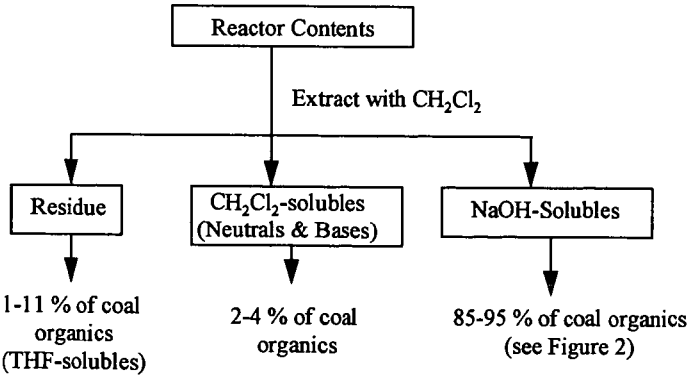

Figure 1: Initial product work-up of coal from reactor. The residue also contains ash and recovered Ru/C catalyst.

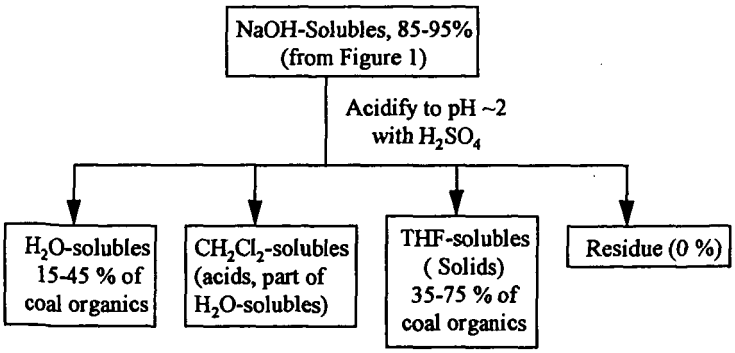

Figure 2: Schematic of product work-up of the aqueous NaOH fraction, the major portion of the coal.

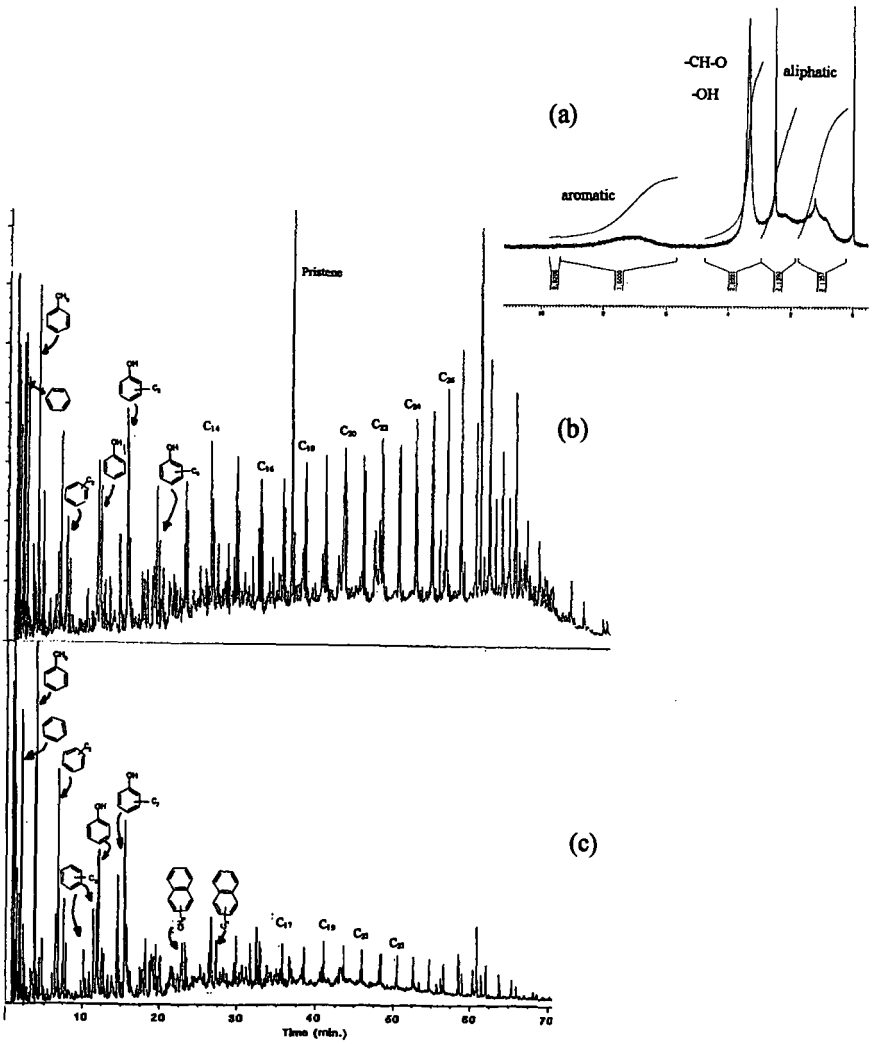

Figure 3: Spectra for: (a) ^{1}H NMR of NaOH-soluble solids (acids), (b) pyrolysis-GC/MS of DECS-1, and (c) pyrolysis-GC/MS of NaOH-soluble solids (acids).

EFFECT OF OXYGEN COMPOUNDS ADDITION ON THE HYDROCRACKING OF ALKYLPHENOLS

Y.Sato, Y.Kodera, T.Kamo and S.Kushiyama

National Institute for Resources and Environment
16-3 Onogawa, Tsukuba, Ibaraki 305, Japan

Keywords : Alkylphenol, Hydrocracking, Dimethylcarbonate

ABSTRACT

To produce and purify useful compounds in tar from coking and from low temperature pyrolysis of coal, hydrocracking of alkylphenol mixture is very important reaction. In this study, the effect of oxygen compounds such as dimethylcarbonate(DMC) addition on the hydrocracking of alkylphenols was investigated to decrease hydrogen loss by the production of water. Hydrocracking of three dimethylphenols(DMP) was carried out using atmospheric flow apparatus with quarts reactor at 700°C, residence time of 3-10 sec and hydrogen to reactant mole ratio of about 10. From the hydrocracking of 3,5-DMP without DMC, m-xylene and m-cresol were produced with the production ratio of 1:1.8. However the dehydroxylation to produce m-xylene was decreased by the addition of 10% DMC with the production ratio of 1:2.7. Similar reaction behavior was observed in the hydrocracking of 2,5-DMP. These are considered due to the strong interaction between DMC and hydroxyl group. Relationship between reaction behavior and molecular structure would be also discussed.

INTRODUCTION

Mild gasification and low temperature pyrolysis are considered to be the most promising process for high-moisture, subbituminous and lignite coal to produce upgraded solid fuel with high heating value and low sulfur, and to produce a useful liquid fuel. However these liquid products contain considerable amounts of oxygen, and are rich in alkylphenols with alkylbenzenes and alkylnaphthalenes.[1] Gas phase thermal demethylation of a series of methyl substituted benzenes under a excess hydrogen stream has been a subject of many investigators. Reaction behavior, including kinetics, and product distribution for toluene and methylbenzenes can be accounted for by the following free radical mechanism. [2]

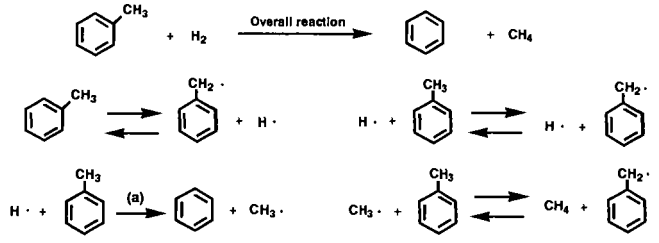

In the above chain scheme, the propagation rate is effectively controlled by reaction (a). This reaction can be pictured as a perpendicular approach to hydrogen atom to phenyl carbon atom, to which methyl group is attached. We have found the same mechanism can be applied for the demethylation of methylnaphthalenes, and the relative reactivities of both methylbenzenes and methylnaphthalenes have been correlated with the reactivity indices, theoretically calculated by molecular orbital method. [3,4] According to the results for methyl substituted aromatic compounds and the reaction behavior for the other alkyl aromatic compounds, demethylation rates for methylnapthalenes are generally higher than that for methylbenzenes, and the removal of higher alkylgroup takes place competitively with demethylation. In this reaction, aromatic structure does not cracked, and simple aromatic compounds, without having alkyl substituents, are produced with high selectively in the presence of excess hydrogen.

On the other hand, kinetic studies of the thermal hydrocracking of cresols, and 2,4,6-trimethylphenol have been discussed in terms of the reaction mechanism by Davies et al [5], Kawase et al [6], and Moghul et al [7]. The same type of kinetic equation with dimethylation, and the following concurrent reaction scheme have been proposed to account for the experimental measurement of the reaction rate, and the product distribution.

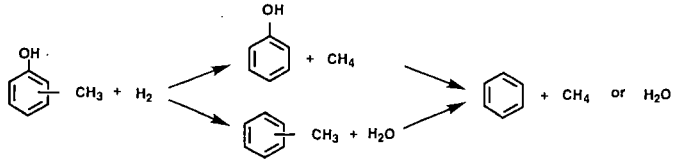

However the relationship between molecular structure and kinetic observations has not yet been explained satisfactory. In this reaction, hydrogen was consumed to produce water by dehydroxylation.

In this study, the effect of oxygen compounds addition on the hydrocracking of alkylphenols was investigated to decrease hydrogen consumption due to the production of water.

EXPERIMENTAL

Commercial reagent grade dimethylphenols(DMP), dimethylcarbonate(DMC) and diethylcarbonate(DEC) were used as received. Thermal hydrocracking of DMP was carried out using a small atmospheric flow apparatus at temperatures of 700°C with residence times of 3-10 sec, and hydrogen-to-reactant molar ratio of more than 10. The reactor was made of a quartz tubing, 21.5 mm in inside diameter and 120 mm in length, and was equipped with a thermo-sheath placed along its central axis. Annular space of the vessel was filled with 10-20 mesh quartz tips, resulting in a free volume of about 18.3 ml. DMP were introduced into the reactor quantitatively by using a small liquid feeding pump, and hydrogen stream was supplied by using a mass flow controller. DMP was mixed with an adequate amount of toluene as a standard reference and 10% DMC or DEC in some of the experimental runs. Gaseous and liquid products were subjected to a conventional gas chromatographic analysis.

RESULTS AND DISCUSSIONS

Reaction behavior of DMP

From the hydrocracking of 3.5-DMP mixed with toluene, benzene from toluene, m-xylene and m-cresol with trace of phenol from DMP were mainly produced with methane. The conversion of toluene and 3,5-DMP with and without DMC were illustrated in Fig.1. These show good fittings of first-order kinetic equation with respect to both toluene and 3,5-DMP. Similar reaction behavior was also observed for 2,5- and 2,6-DMP, however, the conversion ratio of DMP to toluene calculated by first-order rate low was same in all three cases with and without DMC. Products distribution at 700°C from 3,5-DMP are shown in Fig.2 and Table 1. 63.5 mol % m-cresol and 34.5 mol % m-xylene were produced with production ratio of 1.8 from the hydrocracking of 3,5-DMP at 700°C with residence time of 5sec without DMC. This result indicates the rate of demethylation is faster than that of dehydroxylation. From the overall relative first-order cracking rate and the product distribution, the rate per one equivalent methyl and hydroxyl groups for three DMP's were calculated as shown in Fig. 3. The specific rates of demethylation and dehydroxylation are affected by both number and position of substituents of the reactant molecule. Removal of the substituent at ortho position of DMP is quite definitely easier than that of toluene.

Effect of DMC addition on the hydrocracking of DMP

From the hydrocracking of 3,5- DMP mixed with toluene and DMC, observed conversion for both toluene and 3,5-DMP with 10% DMC was higher than that without DMC as shown in Fig.1. The production of m-cresol increased and that of m-xylene decreased by the addition of 10% DMC as shown in Fig.2 and Table 1. The production ratio of m-cresol to m-xylene changed drastically from 1.8 to 2.7 by the addition of DMC. This indicates the dehydroxylation, caused by the attacking hydrogen atom to the phenyl carbon adjacent to hydroxyl group, was prevented by the strong interaction between DMC and

hydroxyl group in 3,5-DMP. Similar effect was observed by the addition of DEC. Contrary to these, demethylation was accelerated probably by the indirect electronic effect of DMC. However, in the case of 2,5-DMP, the effect of DMC addition on the products distribution was not strong, and the production ratio of cresols to p-xylene changed only from 3.0 to 3.6, as shown in Table 1. The decrease of p-xylene and the increase of cresols in the products distribution was less than 12 mol%. It was thought that the interaction between DMC and hydroxyl group in 2,5-DMP was slightly hindered by the neighboring methyl group at ortho position. Therefore the effect of DMC on the dehydroxylation was weakened by the steric hindrance.

On the other hand, there were no differences in the product distribution and the conversion from the hydrocracking of 2,6-DMP, as shown in Table 1. It was very clear that the interaction between DMC and hydroxyl group was almost completely disappeared by the neighboring two methyl groups at ortho position.

CONCLUSION

The strong effect of DMC addition on the products distribution was observed from the hydrocracking of 3,5-DMP at 700°C. The production ratio of m-cresol to m-xylene changed drastically from 1.8 to 2.7 by the addition of DMC. These are considered due to the strong interaction between DMC and hydroxyl group in 3,5-DMP. Similar reaction behavior was observed for the case of 2,5-DMP, however, the production ratio of cresols to p-xylene increased only 20% from 3.0 to 3.6. Moreover, there were no differences in the products distribution and the conversion for the case of 2,6-DMP. These indicate that the interaction between DMC and hydroxyl group in 2,5- and 2,6-DMP is slightly and strongly hindered by the neighboring methyl group in the molecule. These findings suggest that the addition of DMC can decrease hydrogen consumption on the hydrocracking of alkylphenols. These are also very valid to concentrate and purify phenol and cresols economically by the hydrocracking of coal derived tar.

REFERENCES

[1] Y.Sato, Y.Kodera, T.Kamo, M.Kameyama, K.Tatsumoto and D.W.Coolidge, *Preprint, 14th Int. Pittsburgh Coal Conf.*, paper No.28-1 (1997)

[2] A.Amano, H.Tominaga and H.Tokuhisa, *Bull. Japan Petrol. Inst.*, **7**,59 (1965)

[3] Y.Sato, *Petrotech*, **19(8)**, 638 (1996)

[4] Y.Sato, Y.Yamamoto and K. Miki, *Sekiyu Gakkaishi*, **35(3)**, 274 (1992)

[5] G.A.Davies and R.Long, *J.Appl.Chem.*, **15**,117 (1965)

[6] T.Kawase, H.Arai, H.Tominaga and T.Kunugi, *Kogyo Kagaku Zasshi*, **73(5)**,959 (1970)

[7] K.A.Moghul, Y.Yamazaki and T.Kawai, *Sekiyu Gakkaishi*, **14(8)**, 594 (1971)

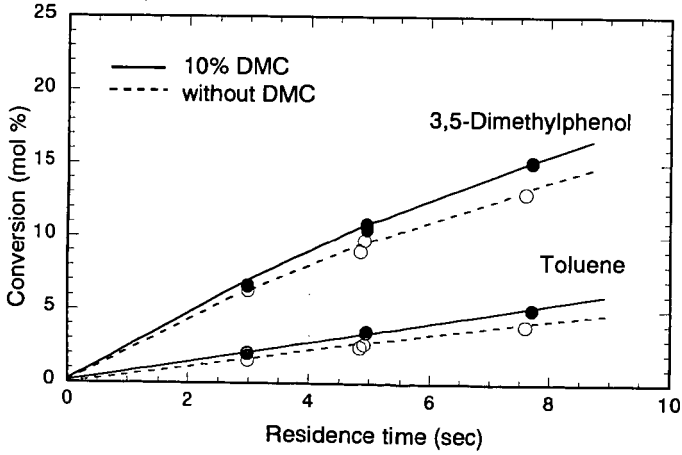

Fig. 1 Hydrocracking of 3,5-Dimethylphenol at 700°C

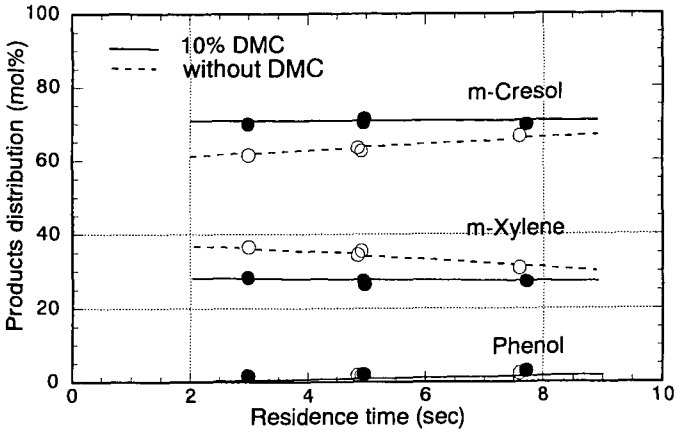

Fig. 2 Products Distribution from the Hydrocracking of 3,5-Dimethylphenol at 700°C

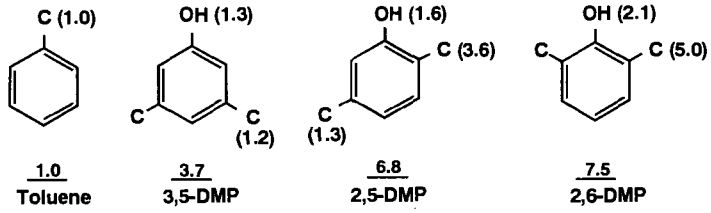

Fig. 3 Relative Rates of Demethylation and Dehydroxylation at 700°C

Table 1 Products Dstribution at 700℃, 5sec.

	3,5-DMP			2,5-DMP		2,6-DMP	
Additive	non	DMC	DEC	non	DMC	non	DMC
Conversion (mol%)							
DMP	9.0	10.5	8.8	20.3	20.9	23.3	23.9
Toluene	2.5	3.5	2.9	3.3	4.0	3.5	3.9
Product distribution (mol%)							
m-Xylene	34.5	26.5	26.4			28.0	28.0
p-Xylene				24.2	21.2		
Phenol	2.0	2.1	1.6	2.7	3.0	4.7	4.9
o-Cresol				19.7	20.8	67.3	67.1
m-Cresol	63.5	71.4	72.0	53.4	55.0		
Cresols/Xylene	1.8	2.7	2.7	3.0	3.6	2.4	2.4

COPROCESSING REACTIONS OF ILLINOIS #6 COAL WITH HONDO PETROLEUM RESID

Yanlong Shi, Thomas A. Cutler and Edward M. Eyring
Department of Chemistry, University of Utah, Salt Lake City, UT 84112

Anthony V. Cugini
Federal Energy Technology Center, Pittsburgh, PA 15236-0940

KEY WORDS: Petroleum Resid, Coprocessing, Illinois # 6 Coal, and Hondo Resid

INTRODUCTION

Petroleum crude is becoming heavier and the amount of vacuum tower resids produced in refining has been steadily increasing. Many have suggested that the combination of coal liquefaction and heavy resid upgrading has economic and processing advantages over the direct liquefaction of coal.[1-12] Because petroleum resids are still hydrogen rich materials (H/C ≈ 1.5) when compared to coal (H/C = 0.8), the amount of hydrogen required in a combined process should, in principle, be less than that required to produce the same quality products from a stand-alone coal liquefaction facility. It is generally believed that the petroleum resid in coprocessing serves as hydrogen transfer agents for coal conversion; in essence the resid replaces the donor solvent in direct coliquefaction. On the other hand, coprocessing can also improve the quality of the petroleum resid used by the removal of the vanadium and nickel complexes since the undissolved coal could act as a trap for the metal removed from the resid.[13] Thus, coprocesing is beneficial in reducing the deposition of coke and trace metals on a hydroliquefaction catalyst.[2-3, 14-15] The liquids produced by combined processing may also be more amenable to downstream processing and further refining via existing technology and equipment, than liquids from a purely coal fed plant would be. It seemed appropriate to investigate the reaction pathways and explore the conditions for the maximum conversion of both coal and resid to a liquid fuel precursor.

Vanadium and nickel, the principal metals in petroleum resid, are present in structures such as porphyrins and the more condensed asphaltenes in concentrations ranging up to 1300 ppm by weight.[16] During catalytic hydroprocessing for sulfur and nitrogen removal, these metal-bearing molecules undergo hydrodemetallation (HDM) reactions leading to metal deposition and catalyst poisoning. The removal of vanadium and nickel has been investigated widely for this purpose. However, most researchers only selected model compounds of vanadium and nickel porphyrins as subjects for study because of the complication of real petroleum resid systems.[2-3, 16-21]

The objectives of the present study are: (1) to identify conditions for maximum removal of metals, mainly Ni and V, present in petroleum resid using coal with the resultant product becoming a feed to catalytic desulfurization and cracking that does not severely shorten catalyst life; (2) to optimize conditions for the conversion of both coal and resid to a liquid fuel precursor. The catalytic coprocessing of Illinois #6 coal with Hondo resid (850 °F$^+$ or whole resid) was carried out using $(NH_4)_2MoS_4$ as catalyst at different temperatures and at 1000 psig of H_2 (cold). The influence of reaction time, and the ratio of resid to coal on the reactivity and product distribution from coprocessing were investigated. The effect on the coprocessing of hydrogenating Hondo resid in a pretreatment step was also studied. The effects of catalysts on coprocessing were studied using $(NH_4)_2MoS_4$, presulfidized $CoMo/Al_2O_3$, $Mo/Fe_2O_3/SO_4^{2-}$ and no catalyst. Ni and V removal was quantified by ICP measurements.

EXPERIMENTAL

The Hondo resid (whole resid: Anal. %C, 83.87; %H, 10.19; %N, 1.01; %S, 4.07; Ni, 78 ppm; V, 150 ppm and hexane insolubles, 25.6% or 850 °F$^+$ resid: Anal. %C, 83.60; %H, 10.11; %N, 1.00; %S, 4.23; Ni, 150 ppm; V, 290 ppm and hexane insolubles, 29.5%) obtained from the Federal Energy Technology Center at Pittsburgh and was stored under ambient conditions. The resid is semisolid at room temperature so that it was necessary to heat it to about 100 °C to make it fluid enough to pour into the reactor. Illinois #6 coal was selected for the coprocessing because it has the best demetallation effect.[13] Illinois #6 coal (~60 mesh) was obtained from the Pennsylvania State Coal Sample Bank. The hydrogenation catalyst $NiMo/Al_2O_3$ (Katalco, 6.7% NiO% and 27.0% MoO_3) was presulfided at 350 °C for two hours. The hydrogenation experiments were completed using 27 cm^3

tubing reactors at 1500 psig of H_2 (cold) for 1 h at 350 °C. Coprocessing experiments were carried out in the same tubing reactors as for the hydrogenation. Reactants were brought to the set-point temperature, usually within 10 min, by immersing the reactor in a preheated, fluidized sand bath. The reactor was shaken horizontally (3 times/s) to ensure adequate mixing. At the end of a 1 h reaction time, the reactor was removed from the sand bath and allowed to cool at room temperature for 5 mins, and was then quenched in cold water. Reaction products and solids were removed and extracted with THF, and then the solvent was removed with a rotary evaporator. The THF soluble portion was dried under vacuum for two hours and weighed. The THF insoluble residue remaining in the Soxhlet extractor thimble was also dried for two hours under vacuum. Next the dried THF solubles were extracted with cyclohexane. The cyclohexane was removed from the oil sample using a rotary evaporator. The cyclohexane insoluble residue is referred to as asphaltenes. The cyclohexane soluble portion is referred to as oil. $(NH_4)_2MoS_4$ (Aldrich) was used as received to impregnate the coal from aqueous solution by the incipient wetness technique. The coprocessing catalyst was added to the coal before coprocessing based on 300 ppm of Mo. The ICP analyses were completed by DataChem Laboratories and American West Analytical Laboratories, Salt Lake City, UT. Elemental analyses were completed by Atlantic Microlabs, Norcross, Georgia. Total conversion of coal, asphltenes conversion and conversions to product fractions were defined on an ash-free basis as follows :

total coal conversion: $Y_T = 100(1-Y)$; $Y = (W_I - W_C - W_{ash})/W_{maf}$

asphaltenes conversion (from coal and resid): $Y_{AC} = 100[1- (W_A + W_{ash})/(W_{maf} + W_{RA})]$

coal conversion to asphaltenes: $Y_{CCA} = 100[W_A - W_{RA}(1-Y_{AC})]/W_{maf}$

coal conversion to oils and gases: $Y_{O+G} = 100(Y_T - Y_{CCA})$

where W_I, W_C, W_{ash}, W_A, W_{maf} and W_{RA} are masses of THF insoluble products, catalyst, ash, asphaltenes (cyclohexane insolubles), moisture- and ash-free coal and asphltenes from resid respectively; Y_T, Y_{AC}, $Y_{CCA}$and Y_{O+G} denote the yields of total conversion, asphaltenes conversion (from coal and resid), coal conversion to asphaltenes and coal conversion to gas + oil, respectively.

RESULTS AND DISCUSSION

Effect of Hydrogenation of Petroleum Resid on the Coprocessing. Table 1 shows the effects of a hydrogenation pretreatment of the Hondo resid (whole or 850 °F$^+$) on the catalytic coprocessing of Hondo resid with Illinois #6 coal. After hydrogenation pretreatment of Hondo resid (whole or 850 °F$^+$) using presulfidized $NiMo/Al_2O_3$, the coal conversions from the coprocessing were increased from 84.3% and 82.9% to 96.6% and 91.4%, respectively for whole and 850 °F$^+$ resids. These results clearly demonstrate that the hydrogenated Hondo resid (whole or 850 °F$^+$) is a better coprocessing solvent than unhydrogenated Hondo resid. The difference is probably attributable to the formation of hydropolyaromatics in the hydrogenated Hondo resid. This trend has been observed by other investigators[7, 8] and our previous work on the coprocessing of coal and hydrogenated vacuum pyrolyzed tire oil.[22] The difference of the coal conversion between the whole and 850 °F$^+$ resid is very small because the 850 °F$^+$ resid represents 91% of the whole resid. It seems that the asphaltenes conversion from both resid and coal to gas and oil is independent of the hydrogenation pretreatment.

The ICP analyses for Ni and V of the coprocessing products from Illinois #6 with Hondo resid and hydrogenated Hondo resid are summarized in Table 2. After coprocessing, the Ni and V in oil (cyclohexane solubles) were not detected above the limit of detection for the coprocessing of whole resid or hydrogenated whole resid with the coal. Most of the Ni and V was trapped in the ash/char. There was more Ni than V in asphaltenes even though the concentration of V was larger than Ni in the original resid samples.

Effect of the Coprocessing Reaction Time. Table 3 shows the results of the coprocessing of Hondo resid (850 °F$^+$) with Illinois #6 coal at different reaction times. The asphaltenes conversion from both resid and coal to gas and oil was increased from 46.1% at 10 min to 71.7% at 80 min. Parallel with the asphaltenes conversion, the asphaltenes for maf coal was decreased from 29.0% at 10 min to 8.75% at 8.7 min, and the gas and oil increased from 49.7% at 10 min to 77.0% at 80 min. In contrast, the total coal conversion did not change much with increasing reaction time. The ICP analyses of Ni and V shown in Table 5 indicate that for most cases the Ni and V in oil were below the detection limits and most of the Ni and V were trapped in the ash/char. It seems that Ni in asphaltenes and in ash/char is independent of reaction time; however, V in asphaltenes decreases with increasing reaction time and V in ash/char increases with increasing reaction time. Hung and Wei observed the same phenomenon when they investigated the hydrodemetallation kinetics of vanadyl

etioporphyrin (VO-Etio) and Nickel etioporphyrin (Ni-Etio).[17]

Dependence on Resid/Coal. The results of changing the resid/coal ratio on the coprocessing of Hondo resid (850 °F⁺) and Illinois #6 coal are given in Table 4. When the amount of coal was fixed at 1 g, the asphaltenes conversion from both resid and coal to gas and oil was decreased from 64.9% at 1 g of resid to 55.4% at 3 g of resid. Correspondingly, the total coal conversion was decreased from 93.0% to 70.5%, asphaltenes from maf coal increased from 4.9% to 25.2%, and the gas and oil decreased from 88.1% to 45.3%. These trends are related to the limited hydrogen gas available since we used the same amount of hydrogen gas at 1000 psig (cold). When the resid was raised to 5 g, the total coal conversion dropped to only 6%, the asphaltenes conversion came mainly from the resid and was increased to 71.7%. When coal/resid was 0.2 g/1.8 g, no coal conversion was observed and a 60.4% asphaltenes conversion was totally dominated by the resid. When the ratio of coal to resid was adjusted to 1.6 g/0.4 g and 1.8 g/0.2 g, the total coal conversions were 23.1% and 20.1%, respectively. Table 5 shows that higher coal/resid ratios favor the V and Ni removal from resid.

CONCLUSIONS

Hydrogenated Hondo resid (whole or 850 °F⁺) prepared using a presulfidized $NiMo/Al_2O_3$ is a better coal liquefaction solvent than unhydrogenated Hondo resid. However, the asphaltenes conversion from both resid and coal to gas and oil is independent of the hydrogenation pretreatment. vanadium removal by Illinois #6 coal is dependent on the reaction time, but nickel removal is independent of the reaction time. Higher coal/resid ratios favor the V and Ni removal from resid.

ACKNOWLEDGMENTS

Helpful discussions with Ted Simpson, U.S. Department of Energy, Germantown, MD are acknowledged. Financial support by the U.S. Department of Energy, Fossil Energy Division, through the Consortium for Fossil Fuel Liquefaction Sciences, Contract No. UKRF-4-21033-86-24, is also gratefully acknowledged.

REFERENCES

(1) Moschopedis, S. E.; Hepler, L. G. *Fuel Sci. Technol. Int.* **1987**, *5*, 1.
(2) Hajdu, P. E.; Tierney, J. W.; Wender, I. *Energy & Fuels* **1996**, *10*, 493.
(3) Cugini, A. V.; Lett, R. G.; Wender, I. *Energy & Fuels* **1989**, *3*, 120.
(4) Ternan, M.; Rahimi, P.; Liu, D.; Clugston, D. M. *Energy & Fuels* **1995**, *9*, 1011.
(5) Ettinger, M. D.; Stock, L. M. *Energy & Fuels* **1994**, *8*, 960.
(6) Ceylan, K.; Stock, L. M. *Energy & Fuels* **1991**, *5*, 582
(7) Joo, H. K.; Curtis, C. W. *Energy & Fuels* **1996**, *10*, 603.
(8) Sato, Y.; Yamamoto, Y.; Kamo, T.; Inaba, A.; Miki, K.; Satio, I. *Energy & Fuels* **1991**, *5*, 98.
(9) Joo, H. K.; Curtis, C. W. *Energy & Fuels* **1997**,11, 801.
(10) Bengoa, C.; Font, J.; Moros, A.; Fortuny, A.; Fabregat, A.; Giralt, F. Fuel **1996**, 75, 1327
(11) Eamsiri, A.; Larkins, F. P.; Jackson, W. R. *Fuel Processing Technol.* **1991**, *27*, 161.
(12) Fouda, A.; Rahimi, P. M.; Kelly, J. F.; Lenz, U.; Beaton, W. I. *Prepr. Pap. Am. Chem. Soc., Div. Pet. Chem.* **1993**, *38*, 351.
(13) Orr, E. C.; Shao, L.; Eyring, E. M. *Prepr. Pap. Am. Chem. Soc., Div. Fuel Chem.* **1996**, *41*, 724
(14) Font, J.; Fabregat, A.; Salvadó, J.; Moros, A.; Bengoa, C.; Giralt, F. *Fuel* **1992**, *71*, 1169;
(15) Font, J.; Fabregat, A.; Salvadó, J.; Moros, A.; Bengoa, C.; Giralt, F. *Fuel Processing Technol.* **1994**, *37*, 163.
(16) Ware, R. A.; Wei, J. *J. Catal.* **1985**, *93*, 100.
(17) Hung, C-W.; Wei, *J. Ind. Eng. Chem. Process Des. Dev.* **1980**, *19*, 257.
(18) Dailey, K. K.; Rauchfuss, T. B. *Polyhedron* **1997**, *16*, 3129.
(19) Chen, H-J.; Massoth, F. E. *Ind. Eng. Chem. Res.* **1988**, *27*, 1629.
(20) Bonné, R. L. C.; van Steendern, P.; van Diepen, A. E.; Moulijn, J. *A. Appl. Catal.* **1994**, *108*, 171.
(21) Kim, C., *Ph. D. Dissertation*, University of Utah, **1993**.
(22) Shi, Y.; Shao, L.; Olson, W. F.; Eyring, E. M. *Prepr. Pap. Am. Chem. Soc., Div. Fuel Chem.* **1997**, 42, 1039.

Table 1. Coal and Asphaltenes Conversions of the Coprocessing of Illinois #6 Coal with Hondo Resid and Hydrogenated Hondo Resid (Reaction Conditions: (Resid/Coal) = 2g/1g, 430 °C, 1000 psig of H_2 (cold), 1 h and 300 ppm Mo loaded to coal using $(NH_4)_2MoS_4$)

Hondo Resid	Asphaltenes Conv. % from resid and coal	Total coal conv. % for maf coal	Asphaltenes. % for maf coal	Gas + Oil % for maf coal
whole	72.5	84.3	8.3	76.0
850 °F$^+$	59.6	82.9	6.4	76.5
whole (Hydro.)[a]	71.8	96.6	11.2	85.4
850 °F$^+$ (Hydro.)[b]	65.5	91.4	15.2	76.2

a: The hydrogenation conditions: presulfidized $NiMo/Al_2O_3$, 350 °C, 1 h, 1500 psig of H_2 (cold), and resid: catalyst = 5.5g:1g (the presulfidation was carried out at 350 °C for 2 hrs);

b: The same hydrogenation conditions as in a;

Table 2. ICP Analyses of Ni and V from the Coprocessing of Illinois #6 Coal with Hondo Resid and Hydrogenated Hondo Resid (Coprocessing Conditions: Resid/Coal = 2g/1g, 430 °C, 1000 psig of H_2 (cold) and 1h)

Reaction System	Oil		Asphaltenes		Ash/Char	
	Ni ppm	V ppm	Ni ppm	V ppm	Ni ppm	V pm
Whole resid	78	150	----	----	----	----
Hondo resid (850 °F$^+$)	150	290	----	----	----	----
Whole resid + Coal	*	*	150	36	1700	1200
850 °F$^+$ resid + Coal	*	0.62	320	150	2500	980
Hydrogenated whole resid[a] + Coal	*	*	84	19	4100	440
Hydrogenated 850 °F$^+$ resid[a] + Coal	*	0.45	150	53	2,100	250

a: The hydrogenation conditions: see Table 1;

*: Parameter not detected above limit of detection (Limits of detection: Ni: 2.3 ppm; V: 0.40ppm)

Table 3. Results from Catalytic Coprocessing of Illinois #6 Coal with Hondo resid (850 °F$^+$) at Different Reaction Time (Reaction Conditions: Coal/Resid = 1g/2g, 430 °C, 1000 psig of H_2 (cold) and 300 ppm Mo Loaded to Coal Using $(NH_4)_2MoS_4$)

Reaction Time min	Asphaltenes conv., % (from resid and coal)	Total conv., % (for maf coal)	Asphaltenes, % (for maf coal)	Gas + Oil, % for maf coal
10	46.1	78.7	29.0	49.7
20	49.2	82.3	31.6	50.7
40	59.8	88.3	20.9	67.4
60	59.6	82.9	6.4	76.5
80	71.7	85.7	8.7	77.0
120	61.3	84.7	19.4	65.3

Table 4. Results from Catalytic Coprocessing of Illinois #6 Coal with Hondo Resid (850 °F+) at Different Ratios of Coal/Resid (Reaction Conditions: 1 h, 430 °C, 1000 psig of H_2 (cold) and 300 ppm Mo Loaded to Coal Using $(NH_4)_2MoS_4$)

Coal/Resid	Asphaltenes conv., % (from resid and coal)	Total conv., % (for maf coal)	Asphaltenes, % (for maf coal)	Gas + Oil, % (for maf coal)
1g/1g	64.9	93.0	4.9	88.1
1g/2g	59.6	82.9	6.4	76.5
1g/3g	55.4	70.5	25.2	45.3
1g/5g	71.6	6.0	8.4	-2.4
0.2g/1.8g	60.4	0.0	0.0	0.0
0.4g/1.6g	55.5	50.7	25.5	25.2
1.6g/0.4g	65.3	23.1	1.7	21.4
1.8g/0.2g	56.6	24.1	-3.6	20.5

Table 5. ICP Analyses of Ni and V from the Coprocessing of Illinois #6 Coal with Hondo Resid (850 °F+) Under Different Conditions at 430 °C, 1000 psig of H_2 (cold) and 300 ppm Mo loaded to coal using $(NH_4)_2MoS_4$

Coal/ Resid g/g	Time min.	Oil		Asphaltenes		Ash/Char	
		Ni ppm	V ppm	Ni ppm	V ppm	Ni ppm	V pm
1.0/2.0	10	*	*	370	520	310	510
1.0/2.0	20	*	65	240	450	2000	190
1.0/2.0	40	24	23	240	320	2100	610
1.0/2.0	60	*	0.6	320	150	2500	980
1.0/2.0	80	*	*	310	99	1400	1400
1.0/2.0	120	*	*	49	27	1700	1400
1.0/1.0	60	*	*	180	51	1400	820
1.0/3.0	60	*	*	310	350	710	970
1.0/5.0	60	*	*	130	120	800	980
0.2/1.8	60	*	*	240	100	8500	1500
0.4/1.6	60	*	*	130	*	1700	1500
1.6/0.4	60	*	*	*	*	420	200
1.8/0.2	60	*	*	*	*	630	120

*: Parameter not detected above limit of detection (Limits of detection: Ni: 5 ppm; V: 0.5 ppm)

SOME IMPORTANT REACTION SEQUENCES IN THE WOMBAT PROCESS FOR CONVERTING SCRAP TIRES TO A HIGH CARBON GEL.

Richard C. Cummings and David L.Wertz
Department of Chemistry & Biochemistry
University of Southern Mississippi
Hattiesburg, MS 39406 USA

INTRODUCTION

The WOMBAT (Wertz Oxidative Molecular Bombardment at Ambient Temperature) process has been developed and refined in this laboratory over the past several years. The objective of this project is to convert scrap tires into a low polluting fuel via technology which is environmentally friendly and economically useful. The process has a high chemical oxygen demand but no external energy requirements.

RESULTS AND DISCUSSION

The WOMBAT process is initiated by introducing both the whole scrap tires and concentrated nitric acid into a closed reactor (see Figure One). Although the scrap tires are chemically inert to normal solvation processes and other types of chemical reactions using mild conditions, in the WOMBAT reactor the tires react to form a gel which is characterized by very low ash and sulfur contents. The production of greenhouse gases from combustion of the WOMBAT solid is slightly lower than that produced from typical bituminous coals.

The thermodynamic products of the WOMBAT process include steel belts (with surface corrosion), polymeric fibers, a solvent-swelled gel which may be processed into the high carbon WOMBAT solid partially described above, a solution containing several inorganic species extracted from the tires, and large quantities of $NO_x(g)$. The WOMBAT reactions appear to take place in the liquid phase, where at least three specific reaction processes occur. However, it is unclear at this time which liquid phase species present in concentrated nitric acid participate in these reactions. Consequently, in the reaction schemes presented below, HNO_3 represents a generic description of the reactants from the solution-phase nitric acid present at very high concentrations. Several of the more important reaction schemes are presented below. Although presented in a sequence, it appears that each of these (and perhaps other) reactions is occurring simultaneously in the reactor. In each of these reaction sequences, the thermodynamic products include $NO_x(g)$, and both $NO(g)$ and $NO_2(g)$ have been identified in the vapor phase within the WOMBAT reactor by FTIR. Of these, however, $NO_2(g)$ is the dominant species, while $NO(g)$ appears to occur only in trace amounts. In the discussions presented below, $NO_2(g)$ is used generically to represent the various NO_x species present in the vapor phase in the WOMBAT reactor.

The processes which occur in our reactor have a high chemical oxygen demand, as shown in Figure Two. The presence of high abundances of $NO_2(g)$ and $H^+(aq)$ in the reactor indicates that the very concentrated nitric acid, which serves as the source of the reactant(s) and also represents the principal continuing operational expense, is being comsumed in the WOMBAT process. Its escape into the atmosphere is not an environmentally acceptable process. For these two important reasons, the $NO_2(g)$ generated within the reactor, which approximates a closed adiabatic system, is catalytically recycled into reactant, as shown in the following reaction:

$$O_2(g) + 2\,NO_2(g) + 2\,H^+(aq) = 2\,HNO_3(g). \qquad (1)$$

Evidence of this reaction is provided by the gas chromatographic measurements $O_2(g)$ in the WOMBAT reactor. The disappearance of the atmospheric $O_2(g)$ within the WOMBAT reactor parallels the reduction in efficiency in the WOMBAT reaction processes within the reactor. Adding either $O_2(g)$ or air to the WOMBAT reactor causes the reaction to "froth"; suggesting that the addition of $O_2(g)$, even in small amounts, invigorates the reaction by causing an *in situ* increase in the abundance of the reactant $HNO_3(g)$. Thus, the environmentally unacceptable $NO_2(g)$ is converted via an equilibrium reaction to the economically important reactant, $HNO_3(g)$.

There is no evidence of nitration reactions or of any separation of the organic species (i.e., the separation of carbon black from the styrene-butadiene co-polymer, etc.) in the gelatinous solid material which is produced by our process.

The large abundances of $NO_2(g)$ produced in the reactor are thought to be due to several distinct reaction processes which occur, at least to some extent, similtaneously. These processes include the cleavage of the metal-rubber adhesion between the brass-coated steel belts and the vulcanized styrene-butadience (**SBR**) co-polymer portion of the tire, the extensive oxidation of the vulcanized **SBR**, the extraction of the organo-sulfur from the rubbery polymer, and the acid hydrolysis of the zinc and calcium salts from the **SBR** during its conversion to a gel

$$2\ NO_2(g) + 2\ H^+(aq). \qquad (2)$$

The presence of the oxidized (corroded) surfaces of the steel belts has been identified by environmental electron microscopy.

While step one is occurring, the vulcanized styrene-butadiene rubber (**SBR**) is further oxidized by a reaction scheme which may be represented as:

$$\mathbf{SBR}(s) + n\ HNO_3(aq) \rightarrow O_n\text{--}\mathbf{SBR}(s) + n\ NO_2(g) + n\ H^+(aq). \qquad (3)$$

In this process, the high carbon **SBR** material (~85%) is converted from a rigidly shaped solid to a gel which has a significant oxygen content (*ca.* 13.5%) with a concomitant reduction in the carbon abundance to *ca* 73%. Mass spectral studies indicate that much of the added oxygen is in the form of carboxylates.

Accompanying the oxidation of the **SBR** is the removal of the organo-sulfur from the **SBR** the vulcanized sulfur (from 1.5% in the original styrene-butadiene impregnated rubber to *ca.* 0.7% -- or less -- in the gel). The decrease in the organo-sulfur abundance has been verified both by x-ray spectroscopy and by gas chromatography. The sulfur from the impregnated tire is converted to aqueous sulfate in the WOMBAT reactor,i.e.,

$$S\text{-}R + 4\ HNO_3(aq) \rightarrow R + SO_4^{-2}(aq) + 4\ NO_2(g) + 4\ H^+(aq). \qquad (4)$$

The aqueous sulfate has been precipitated from the reactor solution and then identified by x-ray diffraction and x-ray spectroscopy.

In addition, the zinc (*ca.* 2% is added in the construction of modern tires to improve their structural stability) is extracted by acid hydrolysis into the nitric acid solution during the reactor processes by an acid hydrolysis reaction such as:

$$Zn + HNO_3(aq) = ZnO_a(H_2O)_b + NO_2(g) + a\ H^+(aq). \qquad (5)$$

The absence of zinc in the resulting gel and its presence in the reactor solution have been verified by x-ray spectroscopy, although the specific coordination complex(es) containing the zinc have not been identified. The low ash content of the WOMBAT gel (~0.7%) is additional evidence of the successful extraction of the zinc (and other metals) from the tires. The zinc may be extracted from the WOMBAT reactor solution by chelation, as verified by x-ray spectroscopy and by x-ray diffraction, and recovered.

Some important characteristics of the WOMBAT solids are compared to several of the Argonne Premium Coals in Table I. Shown in Table II are some environmentally important fuel factors presented as ratio per million BTU's for these fuels.

CONCLUSIONS

Although the reaction schemes presented above are simplistic, taken together they account for the thermodynamic products involved in the conversion of scrap tires to useful materials.

ACKNOWLEDGEMENTS. Financial support from the Mississippi department of Environmental Quality and from the University of Southern Mississippi via an Aubrey K. and Ella Ginn Lucas Faculty Excellence Award is gratefully acknowledged.

REFERENCES.

1. Cummings, R. C., Smithhart, C. B., Quin, J. L., and Wertz, D. L., **Amer. Chem. Soc., Fuel Chem. Div., 1995,** 40, 879-883.

2. Wertz, D. L., Eschette, R., Cummings, R. C., and Quin, J. L., **Amer. Chem. Soc., Fuel Chem. Div., 1997,** 42, 741-743.

TABLE I. PROPERTIES OF SEVERAL SOLID STATE FUELS.

A. MEASURED FUEL VALUES

FUEL	BTU's/TON	C/TON	ASH/TON	SO_2/TON
Beulah Zap	14.9 M	1000 pds	132 pds	64 pds
Illinois # 6	22.0 M	1210 pds	285 pds	319 pds
Pittsburgh #8	26.8 M	1485 pds	182 pds	86 pds
WOMBAT	27.5 M	1083 pds	29 pds	28 pds

TABLE II. SOME IMPORTANT COMBUSTION PRODUCT RATIOS.

RATIO	FUEL			
	BZ	IL	PIT	WOMBAT
PDS CO_2/ 1 M BTU	246	201	203	196
PDS SO_2/ 1 M BTU	4.3	14.5	3.2	1.1
PDS ASH/ 1 M BTU	8.9	13.0	6.8	1.1

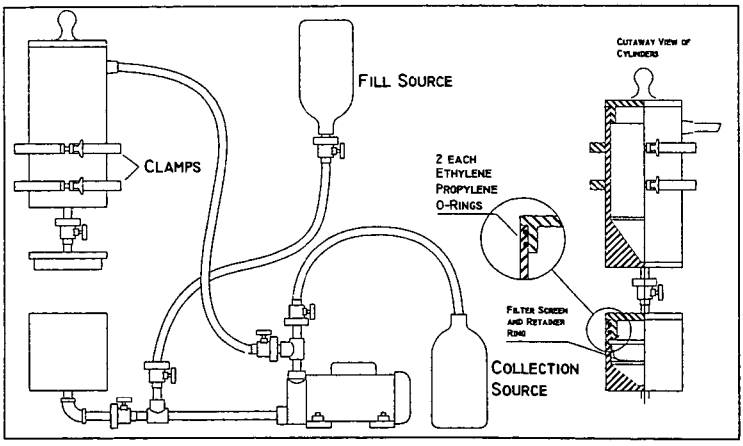

FIGURE ONE. SIMPLIFIED SCHEMATIC OF THE WOMBAT REACTOR.

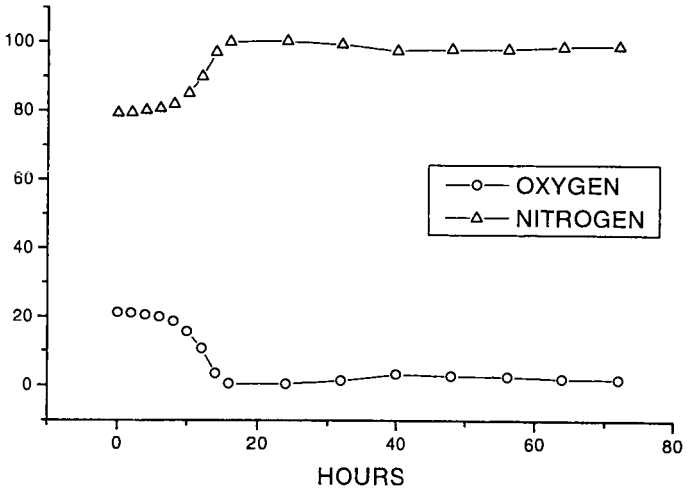

FIGURE TWO. GAS CHROMATOGRAPH OF THE OXYGEN ABUNDANCE IN THE WOMBAT REACTOR.

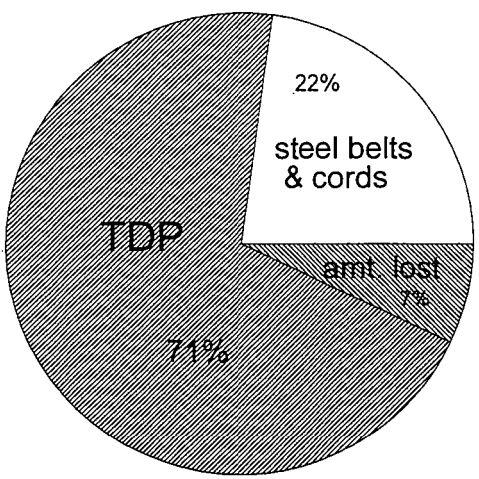

FIGURE THREE. COMPOSITION OF THE RECOVERED PARTS OF THE TIRE.

AUTHOR INDEX, VOLUME 43, (ISSUE NUMBER) PAGE NUMBER